

UC Berkeley

UC Berkeley Electronic Theses and Dissertations

Title

Employing Synthetic Modularity in Organic Molecules as a Tool for Optimizing Molecular Recognition and Polymerization Dynamics

Permalink

<https://escholarship.org/uc/item/6pd1f0b2>

Author

Bours, Justin Alan

Publication Date

2016

Peer reviewed|Thesis/dissertation

Employing Synthetic Modularity in Organic Molecules as a Tool for
Optimizing Molecular Recognition and Polymerization
Dynamics

By

Justin Alan Bours

A dissertation submitted in partial satisfaction of the

requirements for the degree of

Doctor of Philosophy

in

Chemistry

in the

Graduate Division

of the

University of California, Berkeley

Committee in charge:

Professor Felix Raoul Fischer, Chair
Professor Matt Francis
Professor Alex Zettl

Fall 2016

© Copyright 2016
Justin Alan Bours
All rights reserved

Abstract

Employing Synthetic Modularity in Organic Molecules as a Tool for Optimizing Molecular Recognition and Polymerization Dynamics

by

Justin Alan Bours

Doctor of Philosophy in Chemistry

University of California, Berkeley

Professor Felix Raul Fischer, Chair

Employing synthetic modularity in organic molecules is an under-utilized tool for tuning the intricately connected reaction dynamics and/or characteristics of a chemical application of intended practice. Two applications in which the synthetic modularity of the respective substrates is ripe for exploitation are ring-opening alkene and alkyne polymerization (ROMP and ROAMP, respectively), and molecular recognition of carboxylates and nitro-compounds.

Living ROMP and ROAMP have the potential to create polyphenylenevinylenes (PPVs) and polyphenyleneethynylenes (PPEs) with well-defined, structurally predictable, defect-free properties—polymer attributes that are not as feasible *via* other polymerization methods. These types of polymers are useful for important electronic applications and mimicking the dynamics of biological polymers. However, in order for ROMP and ROAMP to become viable methods for accessing these polymers, a better understanding of their respective mechanisms and a greater substrate scope is required. Obtaining access to monomers with tunable electronic and structural properties opens this possibility of illuminating mechanistic characteristics and delivering a library of new conjugated polymers.

Synthesis of (2Z,5Z,8Z)-1⁵,4⁵,7⁵-tribromo-1,4,7(1,3)-tribenzenacyclononaphane-2,5,8-triene (**89**), a template molecule for a library of ROMP and ROAMP monomers, was achieved in only 5 steps with 4 % overall yield. From this template molecule, two trienes, alkyl-substituted **107** and amide-substituted **108**, were synthesized for ROMP and one triyne, alkyl-substituted **113**, synthesized for ROAMP. ROMP of **107** and **108** with Grubb's II (**70**) and Grubb's III (**71**) catalysts resulted in both cyclic and linear PPVs of $n = 3$. After long reaction times, the polymerizations with Grubb's III resulted in a cyclic dimer that is also a potential precursor toward nanographenes.

ROAMP of **113** with molybdenum catalyst **78** was a much more selective polymerization resulting in linear conjugated PPEs. Kinetic studies revealed that the $[\text{SEP}]^{\ddagger}$ propagating species emerging from catalyst **78** underwent some termination processes toward the end of the polymerization, but PDIs were still quite low (< 1.15) and in the absence of monomer, the molybdenum catalyst attached to the propagating polymer chain remained active and continued to incorporate equivalents of monomer added sequentially to the reaction mixture. The ring-opening alkyne metathesis polymerization with **78** has most of the characteristics of a living polymerization and enables, for the first time, a near-living polymerization toward conjugated PPEs. UV-Vis studies revealed that with the sequential addition of guest molecule, RDX, the PPE polymers underwent a secondary structural transition to a helical formation – a transition characteristic of biological polymers.

Enhancing the molecular recognition of carboxylates and nitro groups is vital for sensing of biological molecules and explosives, respectively. Current methods for recognition of explosives rely on π - π interactions or indirect methodologies that preclude the sensitive and specific sensing of non-aromatic explosives like RDX. Hydrogen-bond recognition of bidentate nitro-compounds has the potential to allow for specific sensing *via* a method that detects RDX or other non-aromatic explosives for their unique structural properties. Thus we designed a synthetically modular molecular receptor with tunable electronics, flexibility and hydrogen-bond donating ability in order to optimize binding to bidentate guests such as isophthalate and RDX.

Five sensors of varied flexibility, electronics and hydrogen-bond donors were synthesized. In order to optimize binding to RDX, binding studies were first conducted with isophthalate, a likely stronger binding partner than RDX, to probe the right set of characteristics for optimal sensing. Sensor **R-EW-S** exhibited the strongest binding, according to NMR titration experiments, to isophthalate ($K_a \sim 10^6 \text{ M}^{-1}$) – binding comparable to the best sensors for isophthalate. Comparison to the four other sensors, accessed from a modular synthetic route, revealed that this is likely due to its rigid preorganization, its thiourea hydrogen-bond donor, and electron-withdrawing nature. Binding experiments to RDX resulted in weaker binding to the array of sensors; NMR studies with **F-EW-S** demonstrated the strongest binding ($\sim 400 \text{ M}^{-1}$) to RDX, perhaps due to its ability to create an induced fit to RDX (which is more structurally fluxional than isophthalate). However, fluorescence titration studies of sensor **R-ED-O** with RDX led to an estimate of $K_a \sim 4000 \text{ M}^{-1}$. This was the first example of a sensor exhibiting any appreciable binding *via* hydrogen-bonding to RDX.

Table of contents

Abstract	1
Table of contents	i
Acknowledgments	iv
1 Introduction: Designing Strained Cyclic Alkynes and Alkenes for ROAMP and ROMP	1
1.1 Background and Motivation	2
1.2 Incorporating and Exploiting Strain in Organic Molecules for Orthogonal Reactivity	5
1.2.1 The nature of strain in organic molecules and important examples	5
1.2.2 Synthetic approaches toward strained cyclic alkenes and alkynes	12
1.2.3 Orthogonal reactivity of cyclic alkenes and alkynes	16
1.3 Progress Toward Controlled, Living ROAMP and ROMP of Strained Conjugated Monomers	19
1.3.1 Background and defining examples in the development of ROMP and ROAMP	19
1.3.2 ROAMP of dibenzocyclooctenyne	21
1.3.3 Living ROAMP of Strained Alkynes with a Highly-Selective Molybdenum ONO Pincer Complex	22
1.3.4 ROAMP of Dibenzocyclooctadiyne Toward Conjugated Polymers	27
1.3.5 Soluble poly(<i>p</i> -phenylenevinylene) through ring-opening metathesis polymerization	28
1.3.6 Ring-opening alkene metathesis polymerization of [2.2.2]Paracyclophane-Trienes ...	29
1.4 Conclusion and Outlook	30
2 Synthesis and Polymer Studies of an Array of Monomers for Morphologically Well-Controlled Ring Opening Alkyne and Alkene Metathesis Polymerizations Via a Single Progenitor Triene Macrocyclic	32
2.1 Background and Motivation	33
2.2 Modular synthesis of substituted conjugated monomers for ROMP and ROAMP	33
2.2.1 Design of a suitable monomer library for ROMP and ROAMP	33
2.2.2 Initial synthesis of [2.2.2]metacyclophane-1,9-17-triyne and its ROAMP by [ToIC≡Mo(ONO)(OR)]•KOR (R = CCH ₃ (CF ₃) ₂ , ONO = 6,6'-(pyridine-2,6-diyl)bis(2,4-di-tert-butylphenolate))	34
2.2.3 Step-wise synthesis toward (2Z,5Z,8Z)-15,45,75-tribromo-1,4,7(1,3)-tribenzenacyclononaphane-2,5,8-triene for modular synthesis of differently substituted triene and triyne derivatives	35
2.2.4 One-pot macrocyclization toward (2Z,5Z,8Z)-15,45,75-tribromo-1,4,7(1,3)-tribenzenacyclononaphane-2,5,8-triene	38

2.2.5 Grignard cross-coupling toward tris-alkyl triene 110 and palladium-catalyzed carbonylation toward tris-amide triene 111	39
2.2.6 Bromination and elimination of substituted triene macrocycles toward triyne monomers	40
2.3 Ring-Opening Alkene Metathesis of Substituted (2Z,5Z,8Z)-1,4,7(1,3)-Tribenzenacyclononaphane-2,5,8-triene Monomers	42
2.3.1 ROMP of 108 with Grubbs II Catalyst, 70	42
2.3.2 ROMP of 107 with Grubbs II Catalyst, 70	44
2.3.3 ROMP of 107 with Grubbs III Catalyst, 71	46
2.3.4 Future Directions	50
2.4 Ring-Opening Alkyne Metathesis of Substituted [2.2.2]Metacyclophane-1,9,17-triyne Monomers.....	50
2.4.1 ROAMP of 113 by -ate complex, 78	50
2.4.2 Kinetic Studies of the Rate of ROAMP Propagation of 113 by 78 Over Time.....	52
2.4.3 Post-Polymerization Addition of Monomer as a Living Polymerization Test	55
2.4.4 UV-Vis Studies on Solvent and Small-Molecule Guest Dependence on Secondary Structure of poly- 113	56
2.4.5 Future Directions	61
2.5 Conclusion.....	63
3 Introduction: Molecular Recognition of Carboxylates and Nitro Compounds Via Hydrogen-Bonding to (Thio)Ureas.....	65
3.1 Background and Motivation	66
3.2 Introduction: Principles of Molecular Recognition and Supramolecular Interaction.....	67
3.2.1 The thermodynamics of binding and the role of cooperativity and complementarity..	67
3.2.2 The binding isotherm and methods for monitoring complexation in supramolecular chemistry and stoichiometry of binding	70
3.2.3 Important considerations when devising a titration experiment.....	72
3.3 Methodologies for the detection of explosives containing nitro-groups	73
3.3.1 Detection of nitroaromatic compounds by conducting polymers.....	73
3.3.2 Detection of nitroaromatic compounds by molecular cavities, dendrimers, oligomers and small molecules	75
3.3.3 COFs, MOFs and nanoparticle detection of aromatic nitro compounds	77
3.3.4 Indirect and “direct” detection methodologies for detection of RDX and other non-aromatic explosives	81
3.4 Ureas and thioureas as hydrogen bond donors for carboxylate and nitro-groups	83
3.4.1 Factors dictating the hydrogen-bond donor ability of ureas and thiourea	83

3.4.2 Examples and challenges of multi-site binding of compounds containing more than one nitro-group or carboxylate	86
3.5 Conclusion and Outlook	91
4 Modulating the Lock to Fit the Key: Extensible Host Molecular Clefts for Multi-Site Binding of Bidentate Nitro and Carboxylate Compounds.....	92
4.1 Background and Motivation	93
4.2 Design of a molecular cleft for bidentate intercalation of carboxylates and nitro compounds	93
4.2.1 Modular synthesis of molecular clefts for recognition of nitro- and carboxylate- analytes	97
4.2.2 Determination and comparison of binding of receptors with isophthalate	102
4.2.3 Determination and comparison of binding of receptors with RDX.....	114
4.2.4 Future Directions	118
4.3 Conclusion.....	119
5 Experimental	121
5.1 Synthetic Details.....	121
5.2 Kinetics Experiment Set-Up.....	139
6 References	140

Acknowledgments

I have always wanted to be a part of the scientific process toward the discovery and promotion of ideas that are capable of changing the world for the better. I never imagined that by actually participating in that process I would encounter so many fundamental impediments toward progress and challenges to my trust in the academic system. However, a few individuals have made the experience worthwhile, have turned around my impression of research, and even reignited my passion for basic science as a tool for changing the world.

First of all, my PhD advisor has been a relentless advocate for my success and consistently and passionately promoted my ability to achieve progress after initial disappointments. He has allowed me significant freedom and independence to pursue the subjects I cared about and always provided the support and inspiration to overcome the hurdles in my research. As an untenured professor, this approach was especially refreshing – given his incredibly busy schedule he still had the time and diligence to fully prepare his students inside and outside the lab. I would not have been able to complete my PhD without him and am incredibly grateful to have had Felix as my PI.

I am also thankful for my other mentors, Professors Martin Mulvihill, Megan Schwarzmann and Tom McKeag. They illuminated the issues in chemistry I most care about – to prevent harm from synthetic chemicals and promote responsibility in creating a sustainable future for the chemical industry. I must thank Professors Matt Francis, Alex Zettl, Richmond Sarpong, and Omar Yaghi for kindly agreeing to be a part of my qualifying exam committee and to Matt and Alex for being a part of my dissertation committee. Matt has displayed unique generosity as my qualifying exam chair and has been fully supportive of my progress and accomplishments. Alex has been notable for his incredible flexibility; were it not for him, I would not have been able to complete my qualifying exam on its intended day due to my original outside member not following through with his commitment.

I could not have accomplished my graduate career without the incredible and invaluable support of chemistry administration – especially from Chona DeMesa and Lynn Keithlin. They have both been able to circumscribe my path to graduation despite the logistical and financial challenges associated with obtaining a degree at a public institution.

A lot of my PhD has been in the company of others going through the same challenging, sometimes harrowing path as myself. My labmates Patrick Gorman and Donatella Bellone provided incredibly valuable camaraderie to endure the process – they have become not just colleagues, but close friends and mentors that have always encouraged mutual progress and provided generous support. I must also thank my other colleagues in the Fischer Group, especially Stephen Von Kugelgan, for their help and guidance in intellectual and experimental challenges alike.

Finally, I couldn't have gotten through this process without the support of my family. My mother has been my emotional rock – firmly grounding me and reminding me why I am where I am and consistently encouraging me to fulfill the potential she has always seen in me. My father has given me all of the support I could ever ask from someone. His commitment and dedication to my success is unparalleled – he has never once wavered in his belief in me. My sister has been an inspiration by showing me how to succeed in the face of incredible adversity and for her utmost tenacity – she has been incredibly wise and I have no better role model.

1 Introduction: Designing Strained Cyclic Alkynes and Alkenes for ROAMP and ROMP

1.1 Background and Motivation

The importance of conducting polymers containing double and triple bonds in their backbone has increased in recent years due to their application in organic light-emitting diodes, organic photovoltaic devices (OPVs), thin-film transistors (TFT), foldamers and sensors. Polyphenylenevinylene (PPV) and polyphenyleneethynylene (PPE) polymers, which are constituted of respective vinylic or acetylenic links between aromatic groups in a π -conjugated system, have been especially intensely examined due to their potential as semiconductors. Both types of polymers are moderately fluorescent and display high quantum yields in both films and solution. Moreover, these optical properties are highly dependent on, and are excellent indicators of, the formation of supramolecular structures called helical foldamers.^{1,2} Helical foldamers are conformationally ordered synthetic oligomers and have been used to mimic the structure and function of biopolymers for sensing guest molecules.³ As a result, the foldameric properties of certain types of PPEs and PPVs have been extensively studied toward a better understanding of dynamic helical formation in addition to being manipulated toward optimization of their emissive or absorptive properties for electronic, solar or sensor applications.^{4,5} Studying these foldameric properties has also notably illuminated an understanding of the biological facets of self-organization, and a means for generating architectures that rival biopolymers in their complexity and functionality.⁴

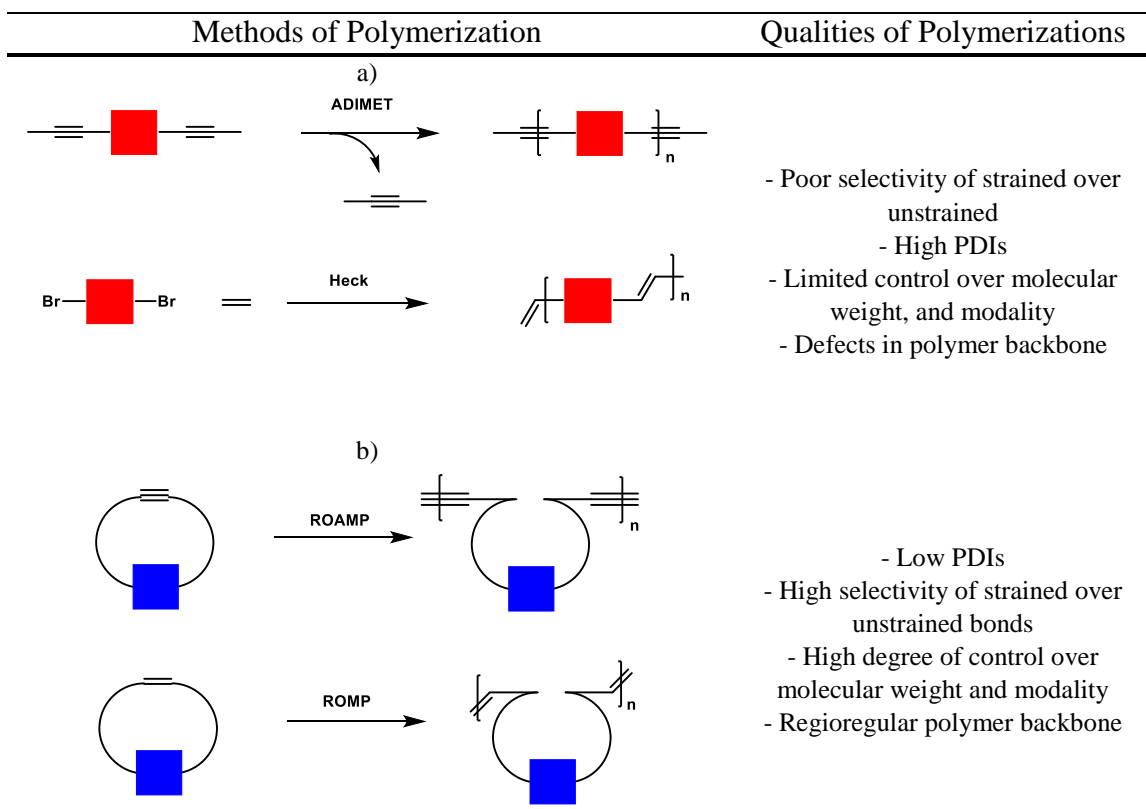
Although these facets of PPVs and PPEs have led to a burgeoning expanse of studies, the utility, integrity and repeatability of the studies of such polymers have been limited by polymerizations that lack precise control of molecular weight and the polydispersity index (PDI) which follows the equation:

$$PDI = \frac{M_w}{M_n} = 1 + \frac{1}{DP} \quad (E1)$$

where M_w is the weight-averaged molecular weight, M_n is the number-averaged molecular weight, and DP is the degree of polymerization (i.e. the average number of monomer units per polymer chain).⁶ Indeed, most reactions lead to structural defects along the polymer backbone. For example, poly(arylene ethynylenes)s have oft been synthesized by Pd-Cu-catalyzed coupling and Heck-Cassar Sonogashira-Hagihara reaction of diethynylbenzenes and dihaloarenes.^{1,7-9} Some complications associated with such reactions are the low control over the molecular weight dependent on solvent, formation of back-to-back ethynyl moieties even under strict air-free conditions, several termination reactions, dehalogenation, ill-defined end-groups, and the presence of phosphorus and palladium impurities. Gilch-type, Pd-catalyzed (Heck, Suzuki) and other methods for PPV synthesis have similar issues.¹⁰⁻¹² The groups of Swager, Bunz, and Moore have recently demonstrated accomplishments in acyclic diyne metathesis (ADIMET) polymerization. ADIMET is a better alternative to Pd-coupling methodologies to make PPEs because it facilitates the synthesis of high molecular weight polymers.¹³⁻¹⁶ However, ADIMET still lacks precise control over molecular weight and regioselectivity of PPE polymers due to

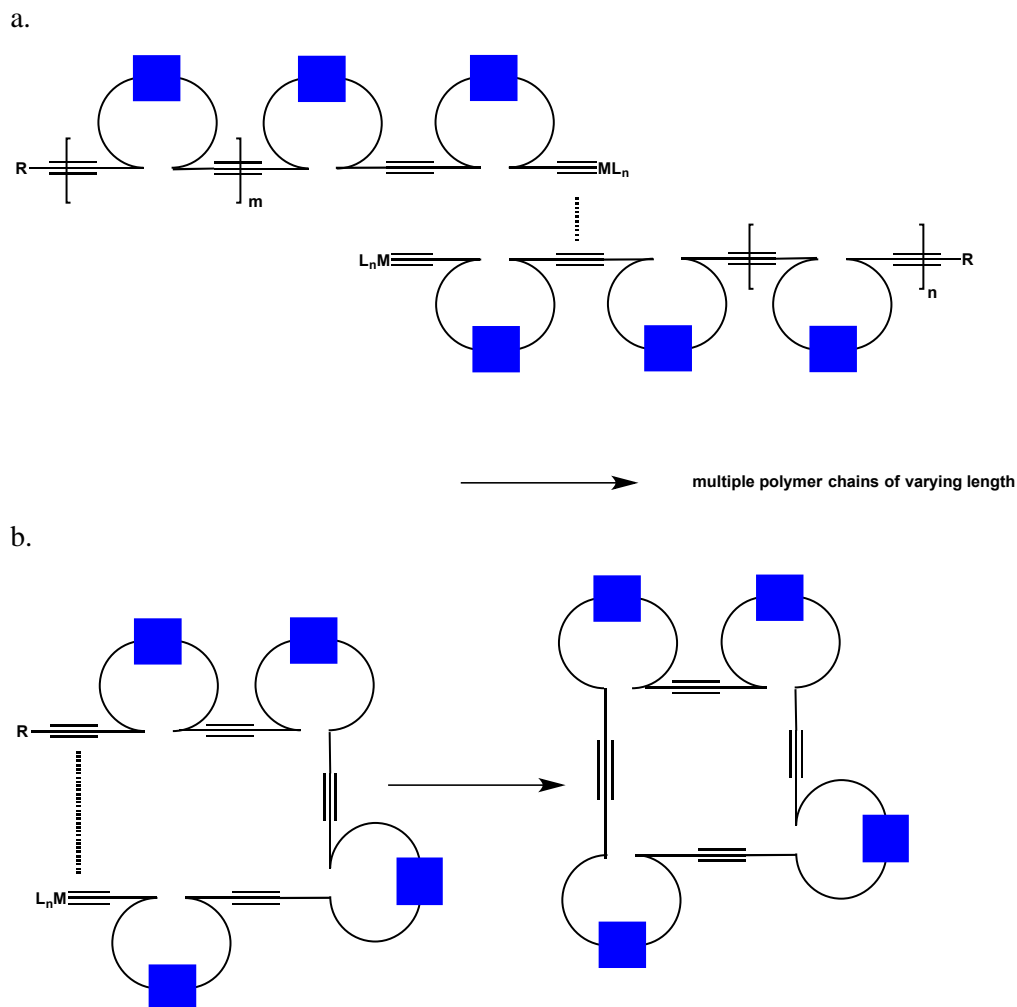
the inability of the catalyst to distinguish energetically between monomer alkynes and alkynes in the polymer backbone (Scheme 1.1a).

Living ring-opening alkene metathesis polymerizations (ROMP) and ring-opening alkyne metathesis polymerizations (ROAMP) have the potential to eliminate many of these issues (Scheme 1.1b).



Scheme 1.1 Synthesis of polymers containing alkenes or alkynes in their backbone by a) acyclic diyne metathesis (ADIMET) polymerization, b) Heck palladium coupling, c) ring-opening alkyne metathesis polymerization (ROAMP) and d) ring-opening alkene metathesis polymerization (ROMP).

A controlled, living polymerization is one in which contributions of chain breaking processes are insignificant compared to chain propagation – this characteristic allows for synthesis of polymers with predetermined molecular weights, low polydispersity and site-specific functionalities.⁶ In ROAMP, an optimal catalyst for a living polymerization will be able to distinguish between ring-strained alkynes in the monomers and unstrained alkynes in the polymer chain. Such selectivity will prevent undesired termination *via* intermolecular chain-transfer or intramolecular chain transfer (Scheme 1.2).



Scheme 1.2 a. Example of intermolecular chain-transfer termination (i.e. chain-transfer), b. example of intramolecular chain-transfer termination (i.e. back-biting).

Until recently, though, PPE or PPV polymers had not been synthesized *via* ROAMP or ROMP catalysis because of the scarcity of catalysts, the lack of synthetically accessible monomer substrates and/or a poor understanding of the catalytic mechanism. Only in the last ten years, the groups of Bunz and Turner developed monomers for living ROMP toward defect-free PPVs utilizing Grubbs 2nd Generation Catalyst.¹⁷⁻²¹ Although the studies of these mechanisms of these ROMP reactions are detailed and noteworthy, the difficulty in synthesis of monomers diminishes commercial utility.

Like PPV synthesis *via* ROMP, interest in the synthesis of PPEs *via* ROAMP has only reemerged in the last several years. A report by Fischer et al. details the living ROAMP studies of 3,8-dihexyloxy-5,6-dihydro-11,12-didehydridibenzo[*a,e*]annulene with a molybdenum catalyst activated by the addition of an alcohol.²² More recently, Bellone et al. demonstrated living ROAMP of the same monomer with a discrete molybdenum catalyst. These two instances were significant advances toward optimal living ROAMP.²³ However, living ROAMP utilizing these or similar catalysts toward conjugated PPEs has

not been fruitful. Kugelgen et al. demonstrated the synthesis of conjugated PPEs via ROAMP, but the polymers formed had high PDIs indicating undesirable termination or chain-transfer reactions.²⁴

In order to improve upon these methodologies, current catalysts must undergo thoughtful alteration. Additionally, access to a larger library of potential monomers must be opened. Accessing this library of monomers requires a better understanding of the synthesis and properties of strained conjugated molecules. In this chapter, we will first discuss the principles of incorporating and exploiting strain in organic molecules for orthogonal reactivity. We will then explore some of these strained molecules in the context of recent examples of living ROMP and ROAMP.

1.2 Incorporating and Exploiting Strain in Organic Molecules for Orthogonal Reactivity

1.2.1. *The nature of strain in organic molecules and important examples*





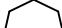
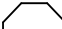
Organic chemists have strived to create orthogonal chemistries that are comparable to biological reactivity: highly complementary interactions, mild conditions, high yield and excellent selectivity.²⁵ To reach optimal reactivity, organic chemists have recently been looking toward modulation of the strain-energy of molecules instead of the traditional approach of functional group discovery. However, modulating strain for desired reactivity requires an understanding of its origin and discovering chemistries capable of creating molecules of such high energy.

As chemists were unraveling the more typical structural characteristics of organic molecules toward the late 19th century, it was the more anomalous chemical structures that were piquing the interest of Adolf Von Bayer. Only 10 years after van't Hoff and LaBel independently proposed that a four-coordinate carbon has a tetrahedral geometry and 20 years after Kekule suggested that carbon chains could form rings, William Henry Perkin, a student in Von Baeyer's laboratory, synthesized cyclopropane and cyclobutane.²⁶ One year later von Baeyer correctly conceptualized that three- and four-membered rings would be less stable due to aberrant bond angles typical of tetrahedral geometrical values.²⁷ Various ways have been used to quantify strain, including observing differences in heats of formation between strained and unstrained isomers. Recently, strain has been discussed in terms of a) bond length, b) bond angle distortions, c) torsional interactions and d) non-bonded interactions.²⁸

The series of homologous cycloalkanes ranging from three to eight carbons are an informative set of these balances in structural characteristics that lead to each respective destabilizing strain energy value. The simplest approach to determining strain energy is to use Franklin's group equivalents.²⁹ For example, cyclohexane, which is thought of as "strain-free" has a heat of formation of -29.5 kcal/mol. This is equivalent to -4.92 kcal/mol per methylene group. According to this method, cyclopropane, consisting of three methylene carbons, would have a heat of formation of -14.75 kcal/mol (3×-4.92 kcal/mol) if it was completely unstrained. However, the experimental heat of formation of

cyclopropane is -12.73 kcal/mol. The difference between the predicted value based on an unstrained structure and the experimental heat of formation leads to the value for strain energy.

Table 1.1 Contributions to strain for examples of cyclic alkanes and their respective strain energies. Values obtained from Wiberg et al.²⁸



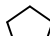
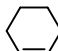
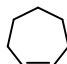
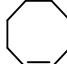
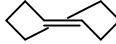

Cyclic Carbon Species	Strain Energy (kcal/mol)
 1	27.5
 2	26.5
 3	6.2
 4	0
 5	6.3
 6	9.7

Cyclopropane and cyclobutane have notably similar high strain energies due to significant torsional and angle strain. One might expect cyclopropane to have greater strain, but unlike cyclobutane and cycloalkane, cyclopropane does not have any destabilizing 1,3-nonbonded interactions. Cyclopropane also compensates for weaker C–C bonds by increasing the strength of its C–H bonds (BDEs for C–H in cyclopropane is 8 kcal/mol greater than that for open-chain methylene groups).²⁸ Larger ring systems such as cycloheptane and cyclooctane have different destabilizing interactions. These larger ring systems have to compensate for highly destabilizing internal H–H steric interactions by increasing the overall strain of the ring system.

Another source of strain in ring-systems is olefinic strain (Table 1.2). Olefinic strain (OS) is the difference in strain energy between the cycloalkene and the corresponding cycloalkane. Some cycloalkanes have considerable olefinic strain, whereas some of the strain in certain ring systems is mollified with the introduction of a double bond.³⁰ Cyclopropane and cyclobutane have significant OS. Cyclopropane is destabilized by a huge increase in angle strain; the normal angle for an sp^2 carbon is 120° and in cyclopropane the angle would be significantly smaller. Although this effect is smaller for cyclobutane, it is still significant. Larger cycloalkenes are somewhat more stable than their

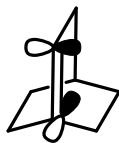
respective cycloalkanes. Removal of two hydrogens to form an alkene results in strain-relief due to a decrease in torsional interactions.

Table 1.2 Contributions to strain and the respective strain energies and olefinic strain energies of various cyclic alkenes. Values obtained from Wiberg et al.²⁸

Cyclic Alkene	Strain Energy (SE) (kcal/mol)	Olefinic Strain Energy (OS) (kcal/mol)
 7	55.2	27.7
 8	28.4	1.9
 9	4.1	-2.1
 10	-0.3	-0.3
 11	3.6	-2.7
 12	4.2	-5.5
 13	16.4	6.7
 14	19.2	4.8

There is a source of significant strain in larger ring systems, though, when a *trans*-alkene is introduced. In fact, a *trans*-cycloalkene has not even been observed for a ring system less than eight carbons. This is because, unlike the *cis*-alkenes in smaller rings where the strain is largely associated with σ bonds, the alkene in large-ring *trans*-alkene systems is deformed due to significant twisting. *trans*-Cyclooctene presents an important example of bond-twisting – electron diffraction evidence shows a twist out of planarity by a significant 44° . The twisting deformation here leads to a 11 kcal/mol energy difference between the *cis*- and *trans*-Cyclooctene, as determined from heats of formation.³¹ Twisting distortion of alkenes is also found in bicyclic systems where the alkene is placed at the bridgehead.³² This twisting deformation is so severe that bridge-head bicyclic ring systems with less than eight carbons are non-isolable and only realized as reactive intermediates.³³ Bicyclic alkenes with bridgehead double bonds are known as alkenes that violate Bredt's rule.²⁸ It is clear why these compounds are so unstable by examining bicyclo[2.2.2]oct-1-

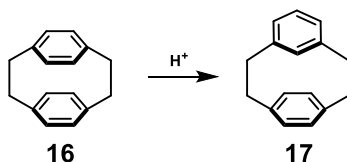
ene (**15**). The σ -system must be strongly twisted in order to achieve any appreciable π -overlap



15

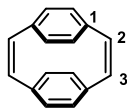
Scheme 1.3 p-Orbital diagram of bicycle[2.2.2]oct-1-ene showing the requisite destabilizing twisting required to form a double bond.

Another form of olefinic strain comes in the form of bending distortions. This form of distortion is found in norbornene.³⁴ Although this distortion is often less extreme than the twisting distortion in *trans*-cyclooctene, the 5° bending distortion in norbornene's case is enough to lead to similarly high olefinic strain ~ 5 kcal/mol. This bending strain is oft cited as the reason for norbornene's well-known anomalous reactivity. More extreme forms of bending are exemplified by cyclophane systems. Cyclophane **1**, corroborated by X-ray data, indicates a 12–13° deviation from coplanarity, benzene rings 3.4 to 3.5 Å closer than the sum of van der Waals radii would predict, and significant bending or skewing of the rings to relieve coulombic repulsion. This leads to a very high strain energy of 31–33 kcal/mol.³⁵ Cyclophane **16** is so strained that acid-catalyzed conversion to *metapara*-substituted cyclophane **17** proceeds readily (**17** only has a strain energy of 23 kcal/mol).^{36,37} **17** exhibits significantly less eclipsing of aromatic rings, and much less bending distortion in the meta-substituted ring.



Scheme 1.4 Strongly favored acid-catalyzed reaction of cyclophane **16** to **17** showing the large difference in stability of **16** and **17**.

“Classically conjugated, but orbitally unconjugated” cyclophane **18** exhibits greater bending distortion in its aromatic rings, but also maintains greater non-bonded distances between aromatic rings due to the larger allowable C₁–C₂–C₃ bond angle with the introduction of the alkene.³⁸ Cyclophanes **16**–**18** are evidence of the contribution of multitudinous physical constraints that are responsible for large differences in strain energy with minimal structural changes.



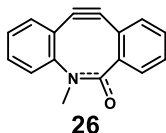
18

Scheme 1.5 Cyclophane **18** – a compound that is limited in its conjugation due to geometric constraints.

Unlike strained alkenes, the deformation in strained cyclic alkynes are largely similar in nature.³⁹ Strained cyclic alkynes are characterized by a weak, reactive π -bond formed by orbital perpendicular to a normal π -system. Bending deformation is allowed by the mixing of s character into these reactive π -bonds. Because bending is the primary source of deformation, it is also a very good predictor of reactivity (or thermodynamic stability). For example, cycloheptyne (**19**), which has a predicted bond angle between 145–150°, has only been observed as a reactive intermediate.⁴⁰

Table 1.3 Respective strain energies and alkyne bond angles of various cycloalkynes.

Cycloalkyne	Ref.	Strain energy (kcal/mol)	Alkyne Bond Angle
19	[40]	~30	145–150°
20	[41]	~20	158.5°
21	[42]	29	159.3°
22	[23]	Not reported	154.4°
23	[43]	Not reported	155.9°
24	[43]	Not reported	154°
25	[31]	31	145.8°



[44]

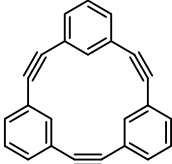
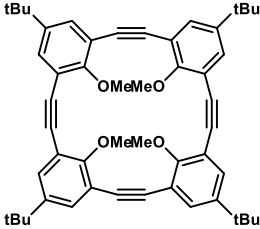
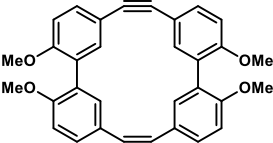
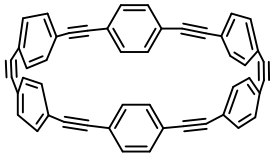
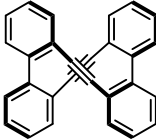
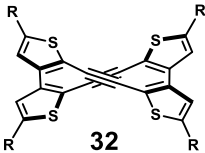
Not reported

153°

Cyclooctyne (**20**) and cyclooctadiyne (**21**) are the smallest cyclic alkynes that are isolable compounds. Cyclooctyne is a unique cyclic alkyne: it is stable at room temperature, yet highly reactive toward cycloadditions. Cyclononyne and higher order cyclic alkynes are too stable for appreciable reactivity and cycloheptyne and smaller ring cyclic alkynes are too reactive to be isolated. Bertozzi and coworkers recognized the unique reactivity profile of cyclooctyne and sought to develop other alkynes from the cyclooctyne template for their potential in bioconjugation reactions.⁴⁵ This intuition led to the development of strained alkynes in the vein of **26** – highly reactive to cycloaddition with organic azides, but thermodynamically stable at room temperature. Since then, researchers have conducted computational studies and experiments to ascertain how to enhance the reactivity of these cyclooctynes. Computational and experimental evidence suggests that there is a strong correlation between alkyne bond angle and reactivity for certain reactions. Indeed, biarylcyclooctynone **26** reacts 375 times faster than cyclooctyne with organic azides, and its alkyne bond angle of 153° is 6 degrees smaller than that of cyclooctyne.⁴⁴ The reasons for the high reactivity, but relative bench-stability of **26** may be illuminated by comparing it to analogous highly unstable (but isolable) dibenzocyclooctenyne **24**. **26** and **24** share structural similarities, but **26** has some structural flexibility due to the rehybridization allotted to the amide nitrogen in **26**. Usually deviation from sp² hybridization in amides is disfavored, but in this case some distortion allows for conformational relief of strain.

Cyclic alkynes **22-25** represent alkynes with very high strain, but greater kinetic stability due to either electronic structure or steric constraints. The unsubstituted analog of **22** is a transient species at room temperature, but transition state of **22** is higher due to the electron rich nature of the compound. **25** is stabilized kinetically because of the large steric environment around the alkyne that raises the transition state to any reaction product. The longer sulfur-carbon bonds also provide some strain relief. **23** has some steric stabilization due to the phenyl rings adjacent to the triple bonds. However, the molecule is geometrically restricted to planarity and is thus antiaromatic in nature (contains 8 electrons in conjugation in the central ring). These steric and antiaromatic contributions balance, making **23** relatively bench stable without exposure to light.

Table 1.4 Respective bond angles and sources of other strains for large strained alkyne cyclophanes.

Cycloalkyne	Ref.	Alkyne Bond Angle	Other Sources of Strain
 27	[46,47]	159°	Bent benzene bonds
 28	[47,48]	166.9°	-Steric and electronic repulsion of inner methoxy groups -Bent benzene bonds
 29	[49,50]	163°	Twisted biphenyl angle (30–39°)
 30	[47,51,52]	167.8°	Bent benzene bonds
 31	[53]	171–175°	Twisted biphenyl angle (52–58°)
 32 R = SiMe ₂ tBu	[54]	171–175°	Twisted di-thienyl dihedral angle (30–32°)

Cyclophanes containing multiple alkynes present other compelling phenomena characterizing strained alkyne systems; they often have additional sources of strain which lead to other anomalous reactivity and are also fascinatingly complex molecules that can be exploited to create pathways to complex molecular architectures. Cyclophanes **27** and **28** represent strained cyclic alkynes substituted in the *meta* position. Both molecules are

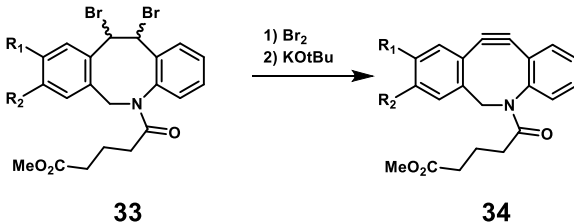
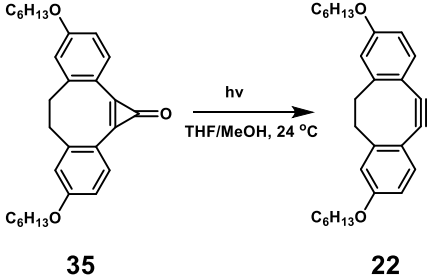
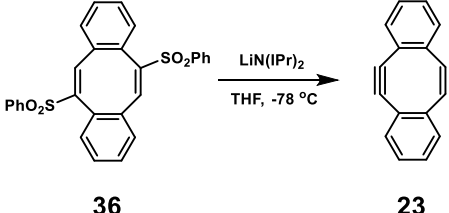
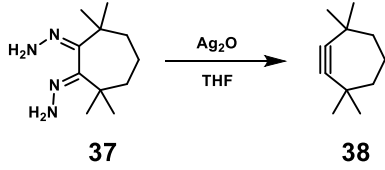
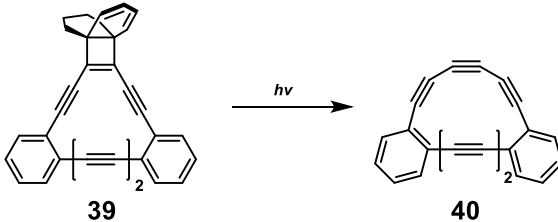
planar and exhibit significantly bent alkyne bond angles, but also have significant bending of the benzene rings. These deformations are subdued, though, because of the ability of these symmetric molecules to disperse this strain evenly throughout the entire molecule.⁴⁷ **28** has additional distortion energy garnered from forced planarity; the inner part of the ring is significantly sterically encumbered by the internal methoxy groups (which also make **28** a great ionophore).⁴⁸ Cyclophane **30** has similar attributes that include bent alkyne bonds and benzene rings. It has received a lot of attention due to its similarity to other curved π -conjugated molecules of high interest like fullerene and carbon nanotubes.^{47,52} Additionally, its large π -conjugated rigid cavity makes it an excellent host for other small organic molecules. Cyclophanes **29** and **31** represent cyclic alkynes that deviate from other strained alkynes – the biphenyl units introduce additional twisting strain up to almost 60° from the normal biphenyl dihedral angle.^{50,53} **31** and its thiophene analogue **32** also demonstrate anomalous chiral attributes and reactivity toward 2+2 type cyclization.

1.2.2 Synthetic approaches toward strained cyclic alkenes and alkynes

Strained cyclic alkenes and alkynes present a unique synthetic challenge – their high energy nature requires favorable kinetics to synthesize them. Additionally, every reaction toward a cyclic alkene or alkyne requires cyclization, and thus this intramolecular cyclization must be made more favorable than undesired intermolecular reactions.

Highly strained cyclic alkynes usually require cyclization to occur before formation of alkynes in the molecule. Thereafter, a few different synthetic techniques are used to transform a less strained cyclic molecule into the desired cycloalkyne. The most commonly used synthetic transformation of this type is the elimination of a vicinal dibromide, which is derived from the bromination of an alkene. The elimination reactions converting **33(a-e)** to **34(a-e)** reported by Debets et al. demonstrates the limitations of this strategy in creating strained cyclic alkynes.⁵⁵ The elimination was successful in forming **34a,c**, and **e**, but all attempted eliminations, using a variety of bases, to form **34b** and **c** were unsuccessful and instead the respective alkenes are formed. The authors do not attempt to explain the reason for this discrepancy, instead citing other examples of such phenomena. However, they do note that **33b** and **33c**, containing two halogens and a nitro group respectively, are more electron-withdrawing. Additionally, the author found that the more electron-withdrawing alkynes they were able to synthesize, namely **33a**, were also the more reactive alkynes toward cycloaddition. Perhaps, then, there is a limit to how electron-withdrawing the substituents must be to allow for appreciable kinetic stability at room temperature.

Table 1.5 Examples of noteworthy reactions to synthesize strained cyclic alkynes from other cyclic species

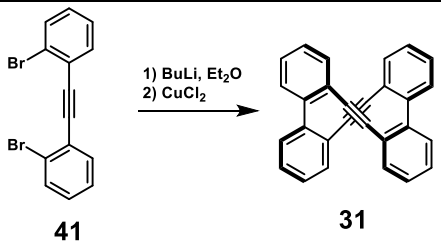
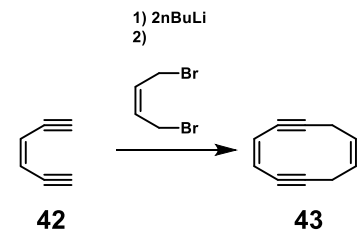
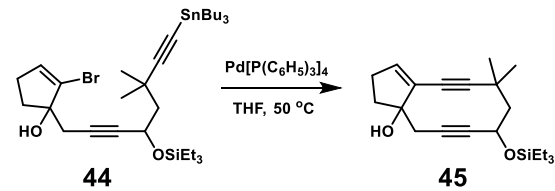
Reaction Type	Example	Reference
Elimination from vicinal dibromides	 <p>33</p> <p>34</p> <p>a) R¹ = Cl, R² = H b) R¹ = Cl, R² = Br c) R¹ = H, R² = Br d) R¹ = H, R² = NO₂ e) R¹ = OMe, R² = H</p>	[56]
Photolytic cleavage of cyclopropanones	 <p>35</p> <p>22</p>	[22]
Elimination from phenyl sulfones	 <p>36</p> <p>23</p>	[24,57]
Oxidative decomposition of dihydrazones	 <p>37</p> <p>38</p>	[58]
Photochemical [2+2] cycloreversion	 <p>39</p> <p>40</p>	[59]

Two other common and more successful strategies in forming dibenzocyclooctynes include photolytic cleavage of a cyclopropanone and elimination of phenylsulfones. Photolytic cleavage of cyclopropanone is particularly advantageous because of high conversion, fast kinetics due to the extrusion of gaseous CO, and the mild conditions. The elimination of phenyl sulfones has been used extensively to synthesize substituted

derivatives of dibenzocyclooctadiynes like **23**. Xu et al. studied the elimination of variously substituted derivatives of **23** and found similar results to that of Debets et al. with derivatives of **24**. That is, they were unable to isolate the more electron-withdrawing strained-alkynes from the reaction.⁵⁷ However Xu et al. were successful in isolating **23** in much higher yields (61%) than the bromination-elimination synthetic pathway. Oxidative decomposition of dihydrazones and photochemical [2+2] cycloreversions represent two more exotic, but useful, pathways for the formation of strained alkynes. Dihydrazone **37** is an attractive target being derived from a synthetically accessible 1,2-diketone derivative. Synthesis of strained alkyne **40** would seem difficult *via* another synthetic pathway, but is facilitated in this synthetic pathway due to energetically favorable cycloreversion.

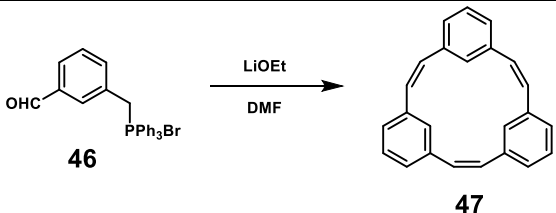
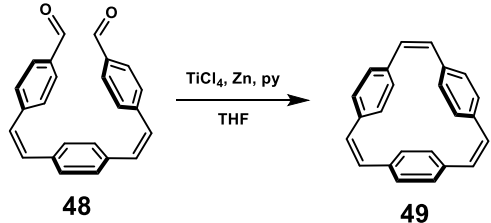
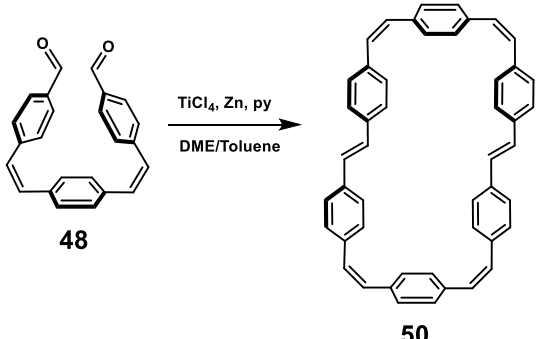
Strained cyclic alkyne synthesis *via* macrocyclization mechanisms are not generally found, but there are a few notable exceptions. The synthesis of **31** is highly unconventional – in this case the internal alkyne is already formed and macrocyclization occurs through bi-aryl organocuprate coupling. The yield here is quite small (< 15%), but the thiophene derivative of **41** undergoes the same reaction to form **32** in over 50% yield. Nucleophilic addition and palladium-catalyzed reactions, like reaction to form **45**, have also been used to create strained alkyne cyclophanes, but these strategies are not utilized commonly for more highly strained cyclic alkynes.

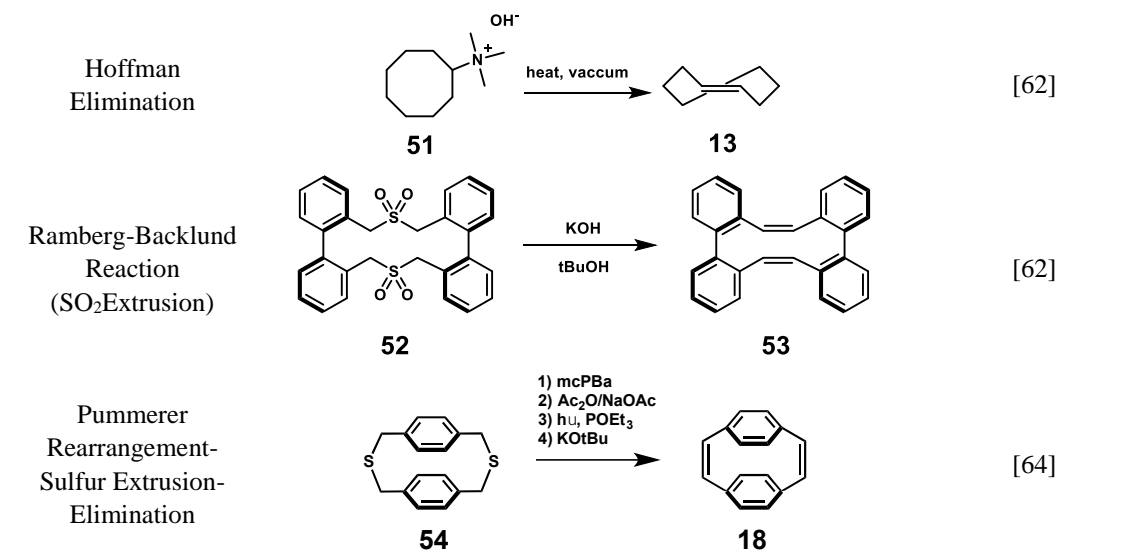
Table 1.6 Examples of noteworthy reactions to synthesize strained cyclic alkynes via macrocyclization.

Reaction Type	Examples	Reference
Cu-Catalyzed Coupling	 <p style="text-align: center;">41 31</p>	[53]
Nucleophilic Addition	 <p style="text-align: center;">42 43</p>	[60]
Palladium Catalyzed Reactions	 <p style="text-align: center;">44 45</p>	[60]

Unlike strained cyclic alkynes, macrocyclizations to synthesize strained alkenes are more common. The Wittig reaction has been used extensively for alkene macrocycle formation. A notable example is exhibited by Tanner et. al; **46** undergoes three self-Wittig reactions to form macrocycle **47** isolated as both the ZZZ and ZZE isomer. The yield here was quite high despite the possibility of polymer formation enabled by the formation of E-alkenes. This strategy has also been employed by Esser et. al to form the hexamethyl-substituted derivative of **47** which is a precursor to [6,8]₃Cyclacene, a conjugated belt molecule that serves as a model for an unusual type of carbon nanotube.⁶¹ Perhaps the most commonly utilized method for macrocyclic alkene formation is the McMurry reaction. The intramolecular kinetics for this reaction are so favorable, that even flexible long aliphatic diketones are able to form macrocycles in significant yields. In addition, intermolecular reactions can be made more favorable just by changing the solvent polarity and the concentration of reactants. Bodwell et al. demonstrated that either **49** or **50** could be synthesized from dialdehyde **48**.⁶² **49** was synthesized in high dilution conditions in THF and **50** was formed in a higher concentration solution of toluene and DME.⁶²

Table 1.7 Examples of noteworthy reactions to synthesize strained cyclic alkenes.

Reaction Types	Examples	Reference
Wittig Reaction		[63]
		
McMurry Reaction		[62]



Two other methods for forming very strained alkenes involve an elimination in violation of Zaitsev's rule and extrusion of sulfur from a pre-formed macrocycle. Transcyclooctene is routinely synthesized from **51** via the Hoffman elimination synthetic methodology. Unlike traditional elimination reactions to form alkenes, the less thermodynamically favored product is the main product. Dialkene macrocycle **53** and **18** are both formed from sulfur extrusion reactions. In the case of **53**, the Ramberg-Bäcklund reaction is utilized; a base deprotonates the carbon adjacent to the sulfur forming an unstable thiirane dioxide which spontaneously eliminates SO₂ to form the respective alkene. The synthesis of **18** from sulfur macrocycle **54** involves additional steps, but **18** is readily formed from a double nucleophilic addition reaction.

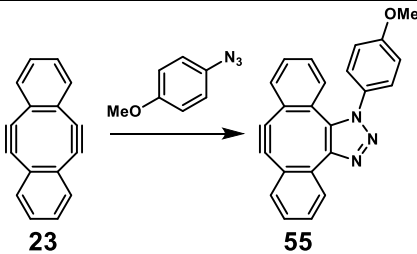
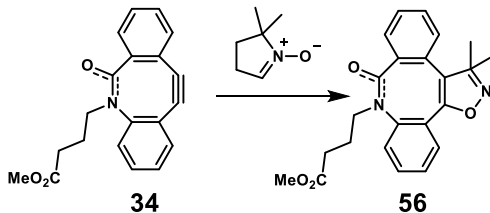
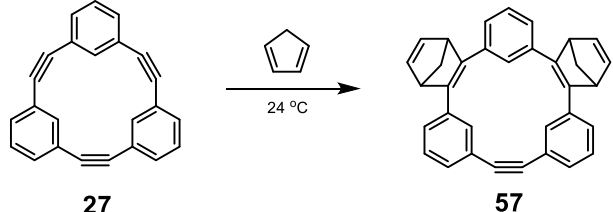
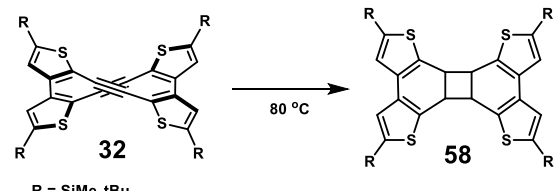
1.2.3 Orthogonal reactivity of cyclic alkenes and alkynes

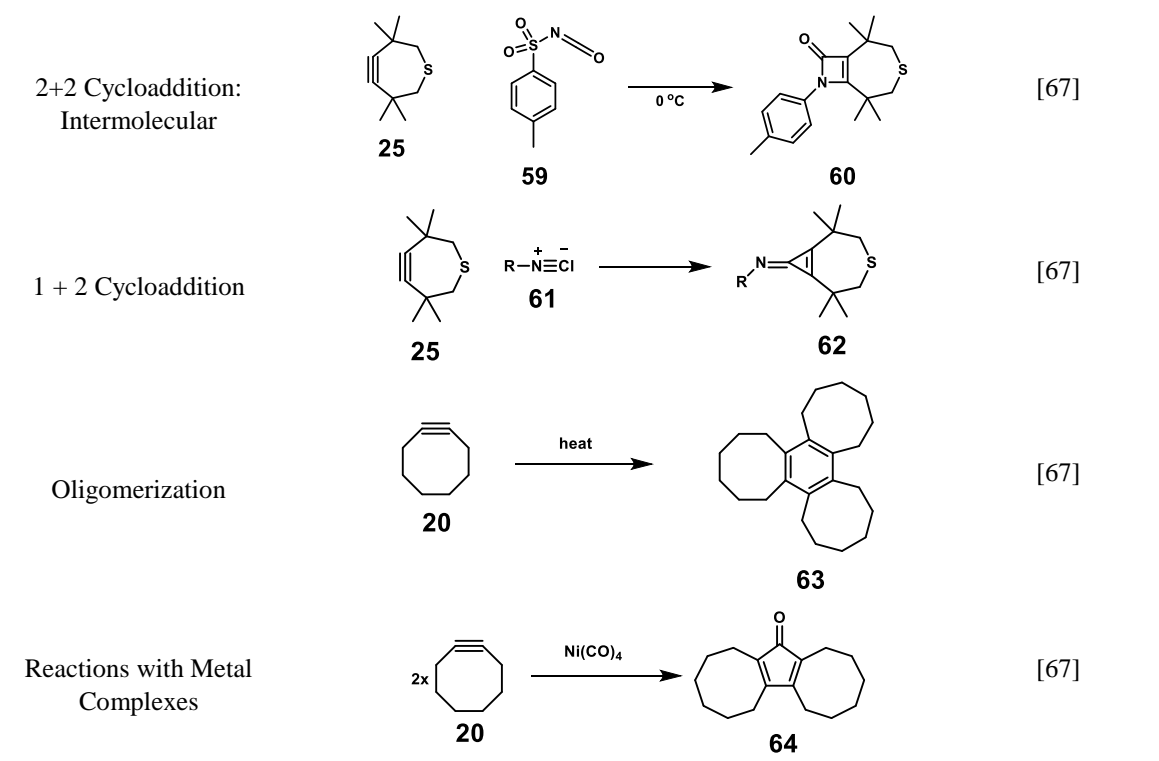
Although many strained alkenes and alkynes were discovered in the early part of the 20th century, exploiting the reactivity of strained cyclic alkenes and alkynes has only recently been reignited due to intense interest in ROMP and bioconjugation reactions. Many strained cyclic alkenes and alkynes are only reactive toward very specific substrates and can often undergo reactions that unstrained alkenes and alkynes undergo without additional reagents or high energy input. However, an increase in strain does not necessarily lead to increase in reactivity with every substrate. The location of the activated complex along the reaction coordinate for a particular reaction, and the strain energy of the product or reaction intermediate are also important. Thus in order to optimize orthogonal reactivity, researchers have had to manipulate the structural contributions that change the energy of the reactant, transition state, and product.

3+2 cycloadditions with strained cyclic alkynes, like azide and nitrene addition exhibited by the reaction toward **55** and **56** have perhaps undergone the most modulation toward optimal reactivity because of their utility in biorthogonal conjugation, a reaction that allows for monitoring of biomolecules in living systems in real time without toxic

effects. After all, these reactions must be able to occur without interfering with native biochemical processes. Debets et al. has found that the substituents on the phenyl rings have a profound effect on reactivity – electron-withdrawing substituents result in much faster reactions by lowering the energy of the transition state.⁵⁵ Gordon et al. revealed that angle strain is also highly correlated with reactivity; the smaller or more distorted the triple bond angle, the more reactive the alkyne.⁴⁴ Unfortunately, reactivity and room-temperature stability are also well-correlated. Reactions to form more highly electron-withdrawing and very highly strained cyclic alkynes are often futile.^{55,65} In order to obtain smaller alkyne angles without compromising room-temperature stability, other strategies have been employed. As mentioned earlier, **26** is an example of one of these strategies. **26** has one of the smallest alkyne angles of any cyclooctyne, but it is stable at room temperature because of the ability of amide bond contained in the ring to rehybridize. The trans-isomer of **26** is 9.6 kcal/mol more stable, but the cis-isomer is much more reactive toward cycloaddition. This reactivity profile allows for the anomalously high reactivity with azides, but relative stability at room temperature.

Table 1.8 Noteworthy reactions of strained cyclic alkynes.

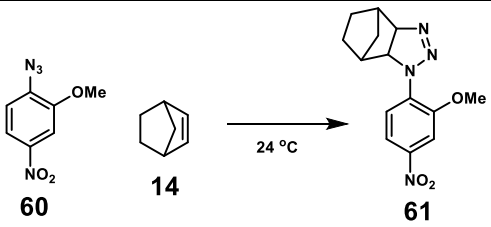
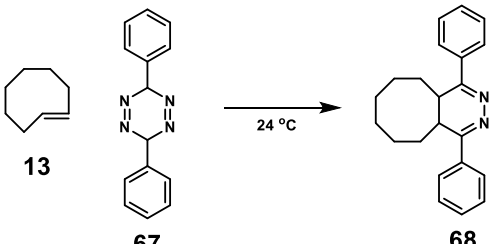
Reaction Types	Examples	Reference
3+2 Cycloaddition: Azides	 <p>23 → 55</p>	[65]
3+2 Cycloaddition: Nitrones	 <p>34 → 56</p>	[66]
4+2 Cycloaddition: Diels-Alder	 <p>27 → 57</p>	[46]
2+2 Cycloaddition: Intramolecular	 <p>32 → 58</p> <p>80 °C</p> <p>R = SiMe₂tBu</p>	[54]



Cycloalkynes are not limited to 3+2 cycloadditions; 4+2, 2+2 and 1+2 cycloadditions are all well-realized under mild conditions (Table 1.8). Triyne **27** readily undergoes two 4+2 cycloadditions with cyclopentadiene at room temperature.⁴⁶ Curiously, products corresponding to one and three cycloadditions are not isolated. Kawase et al. attributes this to the computationally derived smaller alkyne bond angle of 152° exhibited by the mono-adduct; this small alkyne bond angle correspondingly primes the product toward a second addition of cyclopentadiene. Additionally, the resultant bis-adduct has an alkyne bond angle of 162°; too large of an alkyne bond angle to make it reactive toward a third cyclopentadiene at room temperature. Intramolecular 2+2 cycloaddition of **32** to **57** presents a scenario in which advantageous physical proximity of alkynes leads to favorable cycloaddition conditions. Intermolecular 2+2 cycloadditions occur readily when the cycloadduct is electron-withdrawing – the reaction with electron-poor isocyanate **59** is a good example of this. Similarly, 1+2 cycloadditions, like the one with isonitrile **61**, occur readily with electron-poor substrates.

Other reactions of strained alkynes include oligomerization and reactions with metal complexes. Oligomerization is a common pathway for the decomposition of many strained alkynes. Cyclooctyne is known to trimerize into **63** at high temperatures. More strained alkynes undergo oligomerizations at lower temperatures. Metal association and subsequent insertions, like the one exhibited by cyclooctyne and $\text{Ni}(\text{CO})_6$, produce cyclobutadienes and cyclopentadienones depending on whether the metal contains CO ligands in its ligand-sphere.

Table 1.9 Noteworthy examples of reactions of strained cyclic alkenes.

Reaction Type	Examples	Reference(s)
Norbornene cycloaddition	 <p>Reaction of norbornene (14) with 4-nitro-2-methoxyazide (60) at 24 °C to form norbornene 14-azide (61).</p>	[68]
Tetrazine ligation	 <p>Reaction of cyclooctene (13) with a 1,3,5-diphenyl-1,2,4,5-tetrazine (67) at 24 °C to form a bicyclic product (68).</p>	[69,70]

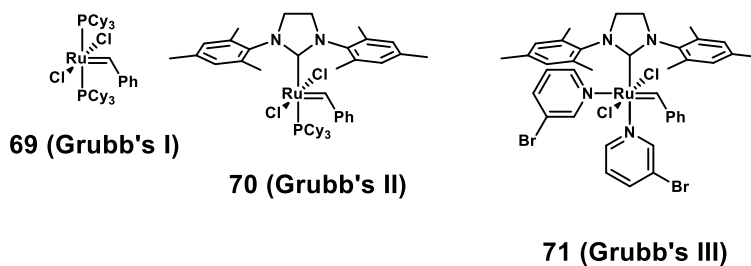
The characteristics of the reactions of strained cycloalkenes are not unlike reactions of strained cycloalkynes; the strained alkene bonds undergo reactions under much milder conditions than unstrained counterparts. Strained alkene reactions are usually limited to only a couple substrates, namely norbornene and trans-cyclooctene, and a couple reactions types besides ROMP: azide cycloaddition and tetrazine ligation (Table 1.9). Both of these are reactions utilized in bioconjugation.

1.3 Progress Toward Controlled, Living ROAMP and ROMP of Strained Conjugated Monomers

1.3.1 Background and defining examples in the development of ROMP and ROAMP

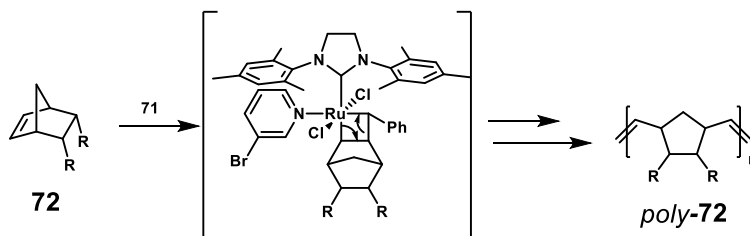
Ring-opening alkene metathesis (ROMP) and ring-opening alkyne metathesis (ROAMP) are two prolific and commercially useful applications of strained alkene or alkyne reactivity. ROMP and ROAMP were both discovered as methods for polymer synthesis in the 1960s.⁷¹ Since then ROMP has taken off and a number of stable well-defined and functional-group tolerant olefin metathesis catalysts have been developed and have made great impact in developing areas such as biomimetic synthetic polymers and self-assembled nanomaterial.⁴ Despite the availability of highly functionalized ring-strained alkynes, outlined in previous sections, awakened interest in ROAMP has only occurred in the last 10 years.^{22-24,72-74} Living polymerization and the synthesis of conjugated polymers via ROMP and ROAMP mechanisms has also been a challenge in recent years. In this section we report some notable recent examples of ROMP and ROAMP that have advanced their respective fields. We then report on subsequent examples that outline the progress toward conjugated polymers synthesized by living ROMP and ROAMP polymerizations.

Robert Grubbs and his group have been well-noted for discovering the first examples of living ring-opening alkene metathesis polymerization.^{75,76} However, these early catalysts such as **69**, usually regarded as Grubb's 1st generation catalysts, still had low functional group tolerance and low activity (slow reaction times). Another series of ruthenium catalysts incorporating N-heterocyclic carbenes, deemed Grubb's 2nd Generation Catalysts, were found to be both more active and functional-group tolerant.⁷⁷ Nevertheless, Grubbs II catalyst, **70**, generally gave polymers with broad PDIs due to high propagation rates and slow initiation rates (or k_p/k_i), and competing chain-transfer reactions.^{78,79} In 2003, Choi and Grubbs discovered that catalyst **71**, known as Grubb's III, allowed for a controlled living ROMP of norbornene derivatives, **72** to create monodisperse polymers (*poly-72*).



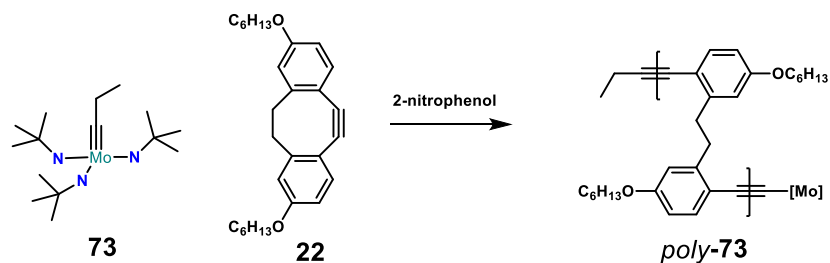
Scheme 1.6 Series of Grubbs's catalyst utilized in ROMP.

Low PDIs were maintained with varying monomer to catalyst ratios, varying concentrations, and varying solvents. However, low temperatures ($-20\text{ }^{\circ}\text{C}$) were required to keep PDIs low. Living polymerization was confirmed by strong agreement between the degree of polymerization, calculated from the integration of protons in the end groups and that of protons in the polymer backbone, and the initial monomer and catalyst feedstock ratios. This was a seminal advancement in ROMP because it allowed for very well controlled, living ROMP utilizing bench stable catalysts at low temperatures – all characteristics desirable for commercial scale-up. However, the substrate scope was not well-established and living ROMP toward conjugated polymers was not yet demonstrated.



Scheme 1.7 ROMP of norbornene **72** with Grubbs's III catalyst **71**.

In **2010**, Fischer et al. reported on the first example of a living ROAMP. In their study, they reported on the synthesis of 3,8-dihexyloxy-5,6-dihydro-11,12-didehydridibenzo[a,e]annulene and its ROAMP reactivity with a molybdenum catalyst activated by the addition of an alcohol.²² The result of the polymerization, with 2-nitrophenol specifically was polymers of high monodispersity (PDI = 1.1).

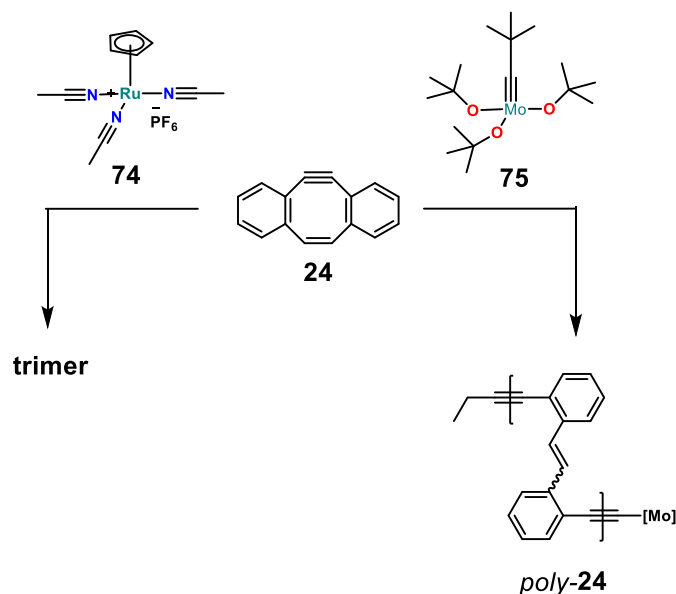


Scheme 1.8 ROAMP of cyclooctyne **22** with Schrock's catalyst **73**.

A living polymerization mechanism was probed by an experiment involving incremental addition of monomer every 40 s, taking aliquots between each addition and characterizing it for its molecular weight and PDI. A decrease in PDI and increase in molecular weight, characteristic of a living system, was observed. No direct correlation between the pK_a of the alcohols and their ability to promote living polymerization was made, but the narrower PDIs were obtained with more acidic, or more electron-withdrawing alcohols. This likely led to a faster initiation, thereby increasing the k_i/k_p of the reaction. Unfortunately, the active species could not be identified and the substrate scope was limited to cyclooctyne **22** and similar derivatives. However, this study provided many clues toward a molecularly-defined catalyst with a well-defined active species and larger substrate scope later identified by Bellone et al.

1.3.2 ROAMP of dibenzocyclooctenyne

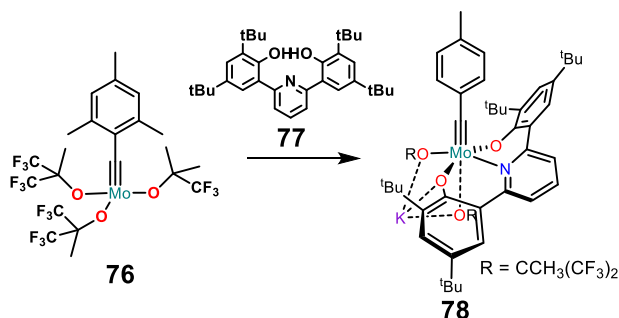
Around the same time, the Nuckolls group was also investigating ROAMP of a conjugated monomer.⁸⁰ This monomer had the potential for both ROMP and ROAMP, containing both strained alkene and alkyne bonds. However, ROMP was unsuccessful in forming polymers – instead, forming the more thermodynamically favorable trimer that is a derivative of benzene, a compound reminiscent of the oligomerization product of cyclooctyne reported previously. Other catalysts, including Grubbs II, resulted in a trimer that is a derivative of Dewar benzene. The ROAMP of **24** was more successful. However, the PDIs were quite large (>2), and there was no evidence of a living mechanism. In just a couple years span, the Nuckolls group published the first example of ROAMP to create conjugated polymers and an example of living ROAMP, but had yet to discover a ROAMP reaction that both generates conjugated polymers and is driven by a living mechanism.



Scheme 1.9 ROAMP and ROMP of cyclooctenyne **24**.

1.3.3 Living ROAMP of Strained Alkynes with a Highly-Selective Molybdenum ONO Pincer Complex

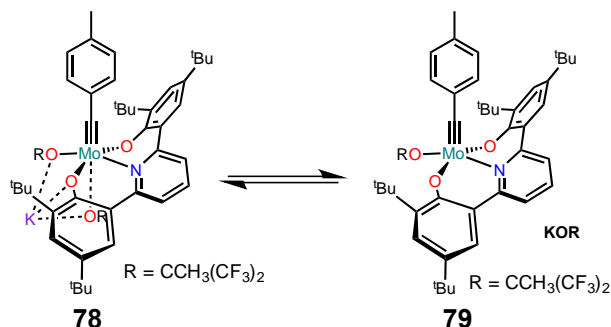
The living polymerization demonstrated by Fischer et al. and subsequent studies by the Nuckolls group provided a blueprint to the first molecularly defined living ROAMP reported by Bellone et al.²³ Fischer et al. showed that the electron-withdrawing nature of ligands allows for faster initiation over propagation.²² There is also evidence that chelating ligand with a sigma donor prevents side reactions such as chain backbiting and decomposition.⁸¹ Thus, Bellone et al. strived to develop a catalyst that incorporated chelating electron-withdrawing alcohols to stabilize the molybdenum propagating species and prevent alkyne cross metathesis. This catalyst was synthesized through the reaction of carbyne **76** with chelating ligand **77** (Scheme 1.10). Crystals of **78** are stable in dry air for hours and can be stored indefinitely under an atmosphere of nitrogen.



Scheme 1.10 Synthesis of -ate complex catalyst **78** from **76**.

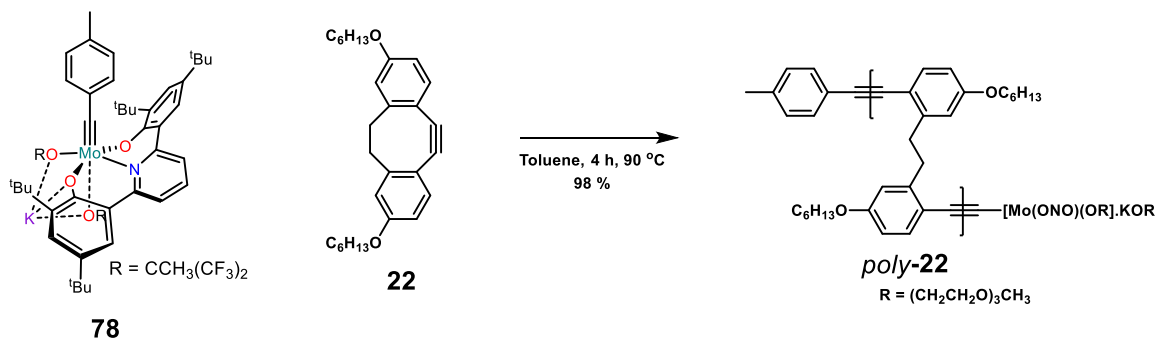
In toluene-*d*₈, the pseudooctahedral -ate complex **78** was found to be in dynamic equilibrium with the dissociated pentacoordinate complex, **79**. This provides the advantage of stability in the solid state, but also allows for appreciable reactivity due to dissociation

of the alkoxide that opens up a free coordination site for a ring-strained monomer (Scheme 1.11)



Scheme 1.11 Equilibrium between pentacoordinate species **79** and pseudooctahedral complex **78**.

After studying the dissociation of complex **78**, Bellone et al. studied the ROAMP of **78** with 3,8-hexyloxy-5,6-dihydro-11,12-didehydridibenzo[*a,e*]annulene (**22**). At 90 °C, the initiation of the reaction is instantaneous and a living ROAMP of monomer **22** (10 equivalents) is completed within 2 h, as determined by ¹H NMR spectroscopy (Scheme 1.12).



Scheme 1.12 ROAMP of cyclooctyne **22** with catalyst **78** to produce PPEs poly-**22**.

GPC analysis after precipitation by methanol showed a PDI of 1.07. For the same polymerization with 50 equivalents of monomer, a PDI of 1.02 was achieved – the lowest PDI value ever reported for ROAMP. As expected for a living ROAMP, PDI decreased with increasing molecular weights and monomer loadings and there was a linear correlation between M_n and % conversion.

Table 1.10 Molecular weight analysis of *poly-22*. ^a calibrated to narrow polydispersity polystyrene standards; ^b degree of polymerization determined by ¹H NMR end-group analysis.

[5a]/[1]	T (°C)	M_n theory	M_n GPC ^a	M_w GPC ^a	X_n^b	PDI GPC ^a
10/1	60	4,000	7,200	7,700	-	1.07
10/1	70	4,000	7,300	7,800	-	1.07
10/1	80	4,000	9,100	9,500	-	1.04
10/1	90	4,000	6,100	6,600	11	1.08
20/1	90	8,100	11,400	11,800	23	1.03
50/1	90	20,200	21,500	22,100	47	1.02
100/1	90	40,400	40,600	41,500	99	1.02

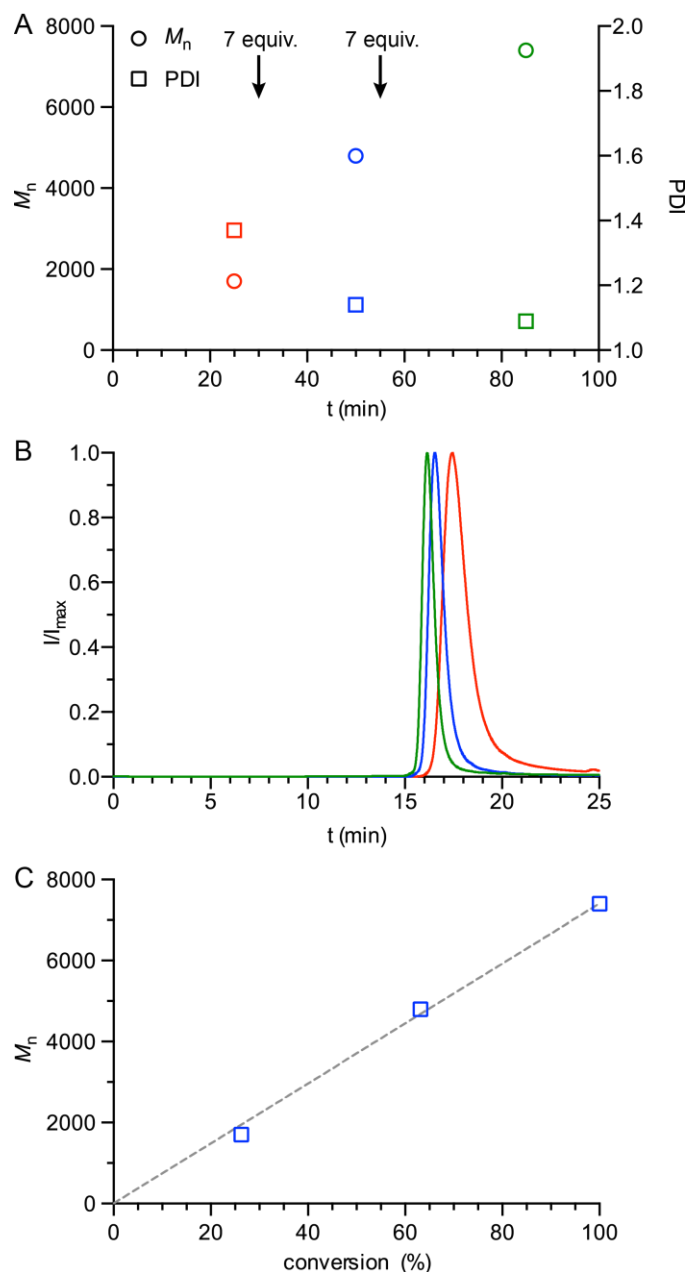


Figure 1.1 A) Sequential addition of equivalents of monomer **22** after consumption of initial monomer loading at 90 °C in Tol- d_8 . Complete consumption of monomer was confirmed by ^1H NMR. B) GPC traces for living polymer samples taken at 25 min (red), 50 min (blue), and 80 min (green). C) Linear correlation between M_n and % conversion.

Although these characteristics suggested living polymerization, in order to meet the stringent criteria for a living polymerization the initiation of the catalyst must be fast and quantitative ($k_i > k_p$), the concentration of propagating species has to remain constant throughout the reaction, all propagating chains have to grow at the same rate, and irreversible termination and chain-transfer processes should be absent. Kinetic studies revealed that the initiation rate was much faster than the propagation rate of the reaction. Additionally, plots of $\ln([M]/[M]_0)$ over time were linear throughout the entire

polymerization, fitting the rate law Bellone et al. derived that is first order in monomer (E2) where $[C]_0$ is the starting concentration of catalyst, $[M]$ is the concentration of monomer over the course of the reaction, $[KOR]$ is the concentration of alkoxy ligand, K_{diss} is the dissociation constant for alkoxide dissociation from the catalyst, k_i is the initiation rate, and $[C_i]$ is the concentration of all initiated species. This linearity over time suggested the concentration of the propagating species is constant throughout the reaction and irreversible termination processes are absent.

$$\frac{d[C_i]}{dt} = \frac{k_i[C]_0[M]}{\left(\frac{[KOR]}{K_{diss}} + 1\right)} = k_{i,obs}[C]_0[M] \quad (E2)$$

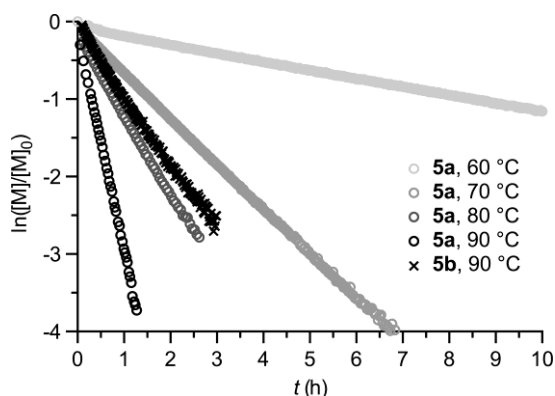
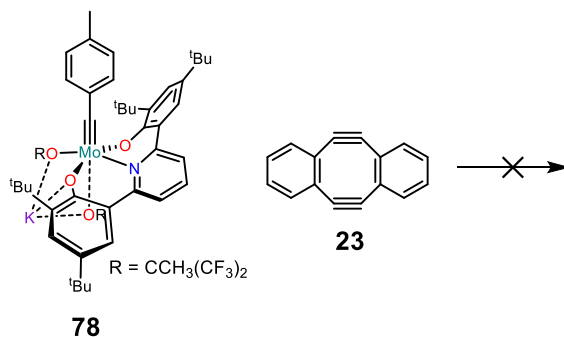


Figure 1.2 Kinetic studies of the rate of polymerization of **5a** and **5b** by **1** at various temperatures.

Further evidence suggested that the equilibrium dissociation of the alkoxide ligand was essential for the performance of ROAMP catalyst **78**. Addition of 2 equiv. of BPh_3 effectively shifted the equilibrium to the pentacoordinate complex **77**. Polymers formed from this pentacoordinate complex featured much broader weight distributions ($PDI > 1.3$) and M_n that do not reflect the initial catalyst and monomer loading. Additional BPh_3 leads to even greater PDIs. Living polymerization also allowed for the ability to form block-copolymers from **22** and a similar monomer with PEG side chains.

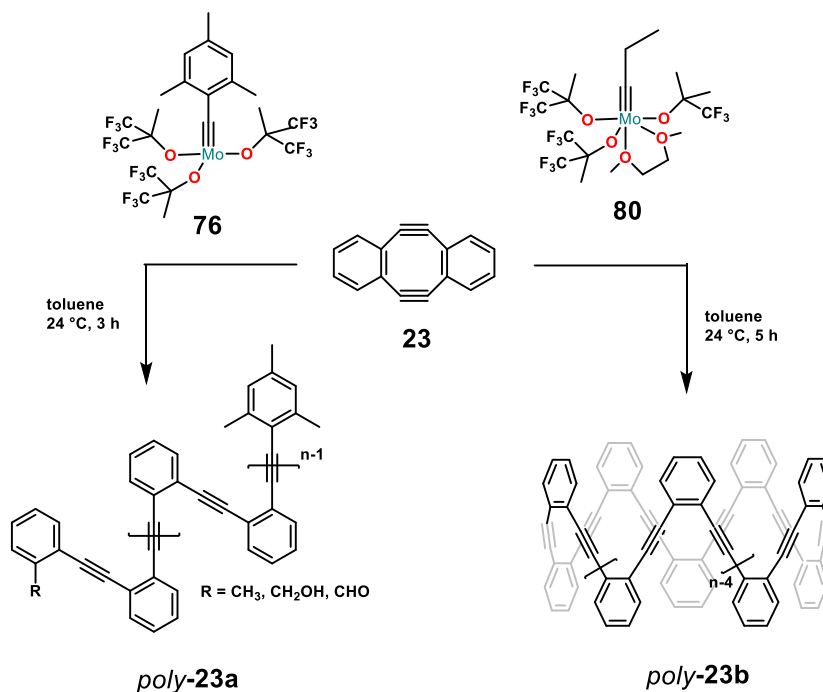
This study was a huge step forward for living ROAMP reactions by demonstrating a catalyst capable of excellent molecular weight-distribution and the ability to create block co-polymers. However, the substrate scope is still limited. Attempts to polymerize 5,6,11,12-tetrahydrobenzo[a,e]annulene **23** at a variety of temperatures results in faster decomposition of **23** than the intended propagation. Ideally, a catalyst would be able to undergo ROAMP at lower temperatures and successfully react with substrates capable of producing conjugated polymers in a living fashion.



Scheme 1.13 Attempt at ROAMP of dibenzocyclooctyne **23** with catalyst **78**.

1.3.4 ROAMP of Dibenzocyclooctadiyne Toward Conjugated Polymers

Although catalyst **78** was unsuccessful in the polymerization of 5,6,11,12-tetrahydrobenzo[*a,e*]annulene **23**, two other catalysts were able to promote the polymerization of **23**. Catalysts **76** and **80** demonstrated the strong dependence of polymer topology on the steric demand of the molybdenum carbyne – more sterically demanding **76** yields strictly linear polymers, whereas **80** yields primarily cyclic polymers.



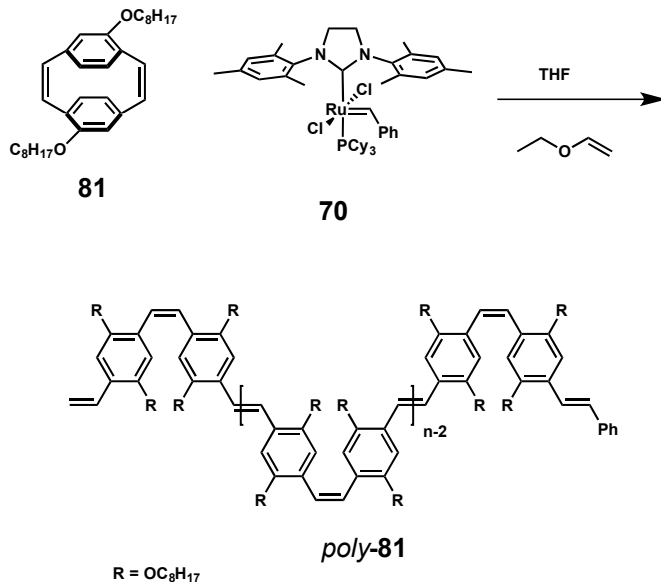
Scheme 1.14 ROAMP of dibenzocyclooctyne **23** with catalysts **76** and **80** to produce PPEs *poly-23a* and *poly-23b*, respectively.

This study presented the exceptional control over polymer structure, sequence and topology from a small change in catalyst structure. However, PDIs were quite large (1.3–1.7) and the actual M_n was larger than the M_n predicted from the starting monomer to catalyst ratios likely due to catalyst decomposition during the reaction. So, although this

study was novel in its utilization of ROAMP to produce conducting polymers of varied topology, living polymerization to yield optimal control and predictability of polymer dispersity was not yet achieved. In order to fully realize living ROAMP polymerization toward conjugated polymers, further study of catalyst decomposition products with **23** are necessary. Otherwise, further changes in catalyst structure or the use of different monomer substrates may be required.

1.3.5 Soluble poly(*p*-phenylenevinylene)s through ring-opening metathesis polymerization

In 2006, Yu et al. reported on the first example of ROMP to produce monodisperse, soluble phenylenevinylene homopolymers.²¹ They accomplished this by adding Grubb's 2nd generation catalyst, **70**, dissolved in THF, to [2.2]paracyclophane-1,9-diene **81** in a THF solution and stirring at 68 °C for 36 h. Though reaction times were slow, there was a strong linear dependence of molecular weight on catalyst to monomer ratio with no change in polydispersity. Additionally, MALDI evidence showed a series of peaks separated by monomer molecular weight and consistent with vinyl and phenyl end-groups, as expected, with no evidence of defect structures characteristic of other PPV synthetic routes. In a subsequent publication, Michael Turner's group investigated the success of this polymerization in creating block-copolymer PPVs.²⁰



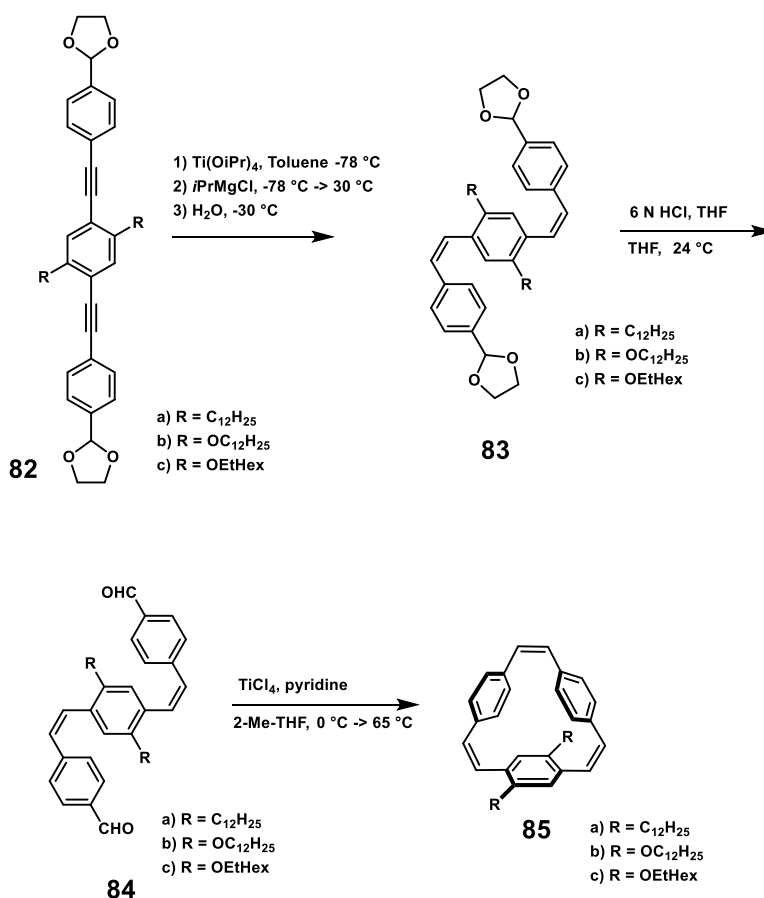
Scheme 1.15 ROMP of cyclodiene **81** with Grubb's II (**70**).

Menk et al., in a 2015 study, extensively investigated the mechanistic aspects of the polymerization.¹⁸ In this study they looked at the potential of the polymerization with five different catalysts and collected data on the initiation and propagation kinetics of each reaction. 3rd generation Grubbs catalyst like **71** were found to promote the fastest initiation rates as well as high propagation rates limiting slow catalyst decomposition and decreasing PDIs. In addition to optimizing the reaction kinetics, Menk et al. also discovered the integral role of the *ortho*-alkoxy groups on the growing polymer chain in limiting catalyst decomposition and increasing selectivity.¹⁸ Although this is useful for certain mechanistic

attributes, it also represents the limited substrate scope of the reaction. The [2.2]paracyclophane-1,9-diene's utilized in this polymerization are also synthetically complex and require several, low-yielding synthetic transformations. Nevertheless, these mechanistic studies provided valuable insight in to future studies of ROMP to create PPVs.

1.3.6 Ring-opening alkene metathesis polymerization of [2.2.2]Paracyclophane-Trienes

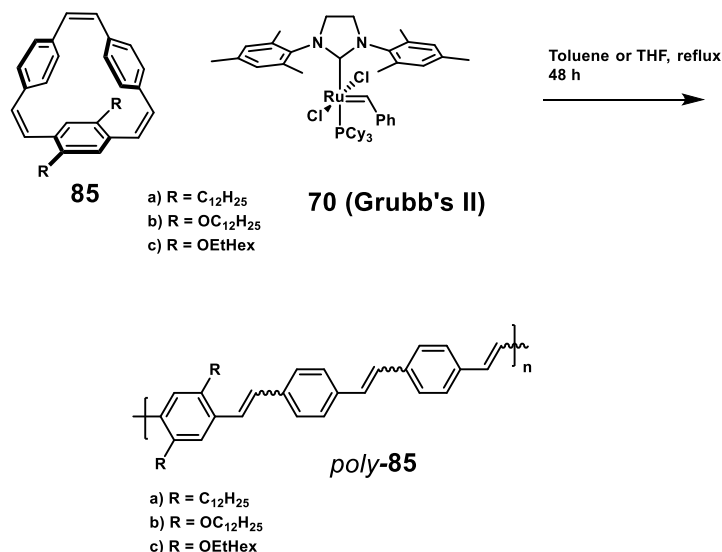
In 2014, Maker et al. addressed the monomer accessibility problem for ROMP toward PPVs by synthesizing [2.2.2]-paracyclophane-trienes.¹⁷ These monomers for ROMP toward PPVs were synthesized in fewer steps and with higher yields than the monomers utilized in previous studies. The key transformations were a double reduction of two internal alkynes, followed by acetal cleavage, and finally a McMurry macrocyclization (Scheme 1.16).



Scheme 1.16 Synthesis of triene **85**.

In the polymerization studies, **85a** initiated at room temperature with Grubbs II catalyst, **70**, but the resulting polymers had a large polydispersity index of 2.8. Increasing the temperature to $65\text{ }^\circ\text{C}$ and allowing the reaction to stir for 2 days resulted in a lower PDI of 1.9, presumably due to improved initiation rates. The alkoxy-substituted monomers **85b** and **85c** both initiated at a higher temperature of $110\text{ }^\circ\text{C}$. This was likely due to the

participation of the alkoxy group in the polymerization first observed in the polymerization of **81**.



Scheme 1.17 ROMP of triene **85** with Grubb's II to produce PPVs *poly-85*.

The polymers produced from **85b** and **85c** also had lower PDIs of 1.4 and 1.7 respectively since the alkoxy groups likely slowed down catalyst decomposition. Unlike the previous ROMP studies of PPV precursors monomers, the authors do not claim a living polymerization or the ability to form block co-polymers. In fact, they do not even include a MALDI mass spectrum for the resulting polymers – an omission that does not rule out the occurrence of back-biting. Additionally, the long reaction times and high temperatures are non-ideal conditions. Perhaps the authors may have had more success using Grubb's third generation catalyst as attempted by Menk et al. in 2015. Regardless of lack of exceptional control and predictability of the polymerization morphology, the authors did innovate a modular synthetic pathway and could likely create a library of monomers and polymers with a variety substitution patterns and properties.

1.4 Conclusion and Outlook

In this chapter we reviewed the origin of strain in organic molecules and more recent efforts to exploit that strain in conjugated cyclic molecules for orthogonal reactivity with an emphasis on ROMP and ROAMP of cyclic alkenes and alkynes, respectively. Even though strained molecules have been known and isolated for over 100 years, only in the last two decades have researchers capitalized on strained conjugated molecule's reactivity toward important applications.

We first explored how researchers have quantified strain in a survey of cyclic alkanes, alkenes and alkynes. Strain has been discussed in terms of bond length, bond angle distortions, torsional interactions and non-bonded interactions, but is typically quantified from the difference in heats of formation of the strained cyclic molecule and its respective open chain molecule. Strained cyclic alkenes are characterized usually by bending and/or

twisting deformations while strained cyclic alkynes can usually be assessed for their strain by the degree of distortion from a normal 180° alkyne bond angle.

We next explored a survey of the reactions to form cyclic alkenes and alkynes. Because strained cyclic alkenes and alkynes are of high energy, reaction pathways are usually low yielding and require favorable kinetics. Strained cyclic alkenes are typically formed from the Wittig or McMurry reactions. Strained cyclic alkynes are generally conceived from a bromination and subsequent elimination of the cyclic alkene; other types of eliminations are also utilized. From this survey we discovered that there are very few electron-withdrawing strained alkynes due to the difficulty in their formation from elimination-type pathways.

Lastly we explored the types of reactions of strained cyclic alkenes and alkynes. First we surveyed the types of cycloaddition possible with these strained systems; cycloadditions, or sometimes called bioconjugations, to strained alkynes and alkenes have been used extensively in biological systems for “clicking” on fluorescent tags (usually an isocyanate or an azide) for monitoring of biological processes. We then detailed historical precedence of the ROMP and ROAMP reactivity of cyclic alkenes and alkynes, respectively. ROMP of cyclic alkenes has been successful in producing PPVs in a living fashion, but an expanded substrate scope is still desired. Historical precedent for ROAMP has shown that the first well-defined and well-behaved living ROAMP with PDIs as low as 1.02 was discovered only within the last year. However, several improvements are still needed: a living ROAMP catalyst that is stable in protic solvents under air conditions at room temperature with low PDIs have yet not been reported. In addition, a living ROAMP toward conjugated PPEs has also not yet been demonstrated.

The juxtaposition of a discussion on the historical precedent of ROMP/ROAMP and the vast research on strained alkenes and alkynes should demonstrate that there are plenty of opportunities to create conjugated polymers from a burgeoning library of potential monomers. The likely barricade to exploration of more monomers for these polymerizations is the synthetic complexity of the monomers. To expand the application and understanding of ROMP and ROAMP, then, these strained monomers will need to be made synthetically accessible and modular.

2 Synthesis and Polymer Studies of an Array of Monomers for Morphologically Well-Controlled Ring Opening Alkyne and Alkene Metathesis Polymerizations *Via* a Single Progenitor Triene Macrocycle

2.1 Background and Motivation

While there have been many recent examples of strained, conjugated organic molecules, the synthetic pathways toward such molecules have not been adequately facile. This lack of synthetic facility in accessing varied strained conjugated cyclic molecules is an especially high barrier to the commercial and technological vitality of PPEs and PPVs derived from ROAMP or ROMP. Limited monomer access also mitigates the expanse in understanding of the mechanistic attributes of ROMP and ROAMP.

In order to probe mechanistic issues of living ROMP and ROAMP of conjugated monomers and synthesize a library of monomers, a modular route toward such monomers could be developed in which manipulation of the structure of monomers is relatively simplistic. One could imagine a template molecule in which the side chains could be readily engineered with desirable solubilizing, electronic or steric properties. This versatility in side-chain structure alone could illuminate critical mechanistic criteria for effective living ROMP and ROAMP.

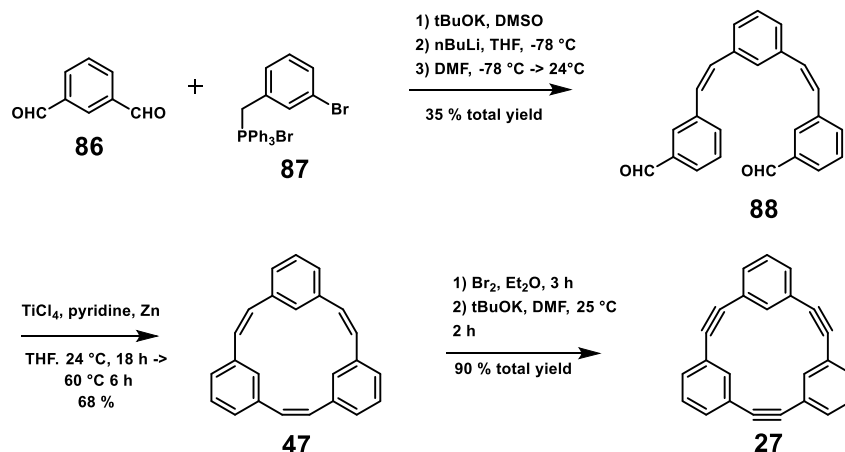
In this chapter, we report on the synthesis of (2Z,5Z,8Z)-15,45,75-tribromo-1,4,7(1,3)-tribenzenacyclononaphane-2,5,8-triene (**89**) as a precursor to a potential library monomers of various substitutions for ROMP and ROAMP. Then, we demonstrate our investigations of the ROMP and ROAMP of synthetic derivatives of **89**. Herein, we demonstrate the first example of near-living ROAMP toward conjugated PPEs and a modular route toward the synthesis of variously substituted PPVs and PPEs. In addition, we demonstrated the ability of such PPEs to undergo a transition to helical foldamer structures, similar to biological polymers, with intercalation of RDX.

2.2 Modular synthesis of substituted conjugated monomers for ROMP and ROAMP

2.2.1 Design of a suitable monomer library for ROMP and ROAMP

The previous section's examples of ROMP and ROAMP reveal that in order to achieve living polymerization toward conjugated PPVs and PPEs, improvements in catalyst structure must be made or the development of a larger library of useful potential monomers must be opened. New monomers for ROMP or ROAMP must have specific design constraints. Synthetic facility is required in order to inspire further study and adoption of ROMP and ROAMP as commercially successful techniques for the production of PPVs and PPEs. The polymers produced from this library of monomers must also be viable for novel and interesting applications. Lastly, polymerization of this library of monomers must allow for new mechanistic insights of ROMP and ROAMP to further the fields toward optimization.

Kawase et al. reported the synthesis of (2Z,5Z,8Z)-1,4,7(1,3)-tribenzenacyclononaphane-2,5,8-triene **89** and [2.2.2]metacyclophane-1,9-17-triyne, **27**.⁴⁶ The synthesis is similar to the synthesis adopted by Maker et al. – the key transformation involves a McMurry coupling for macrocyclization.¹⁷



Scheme 2.1 Synthesis of triene **47** and triyne **27**.

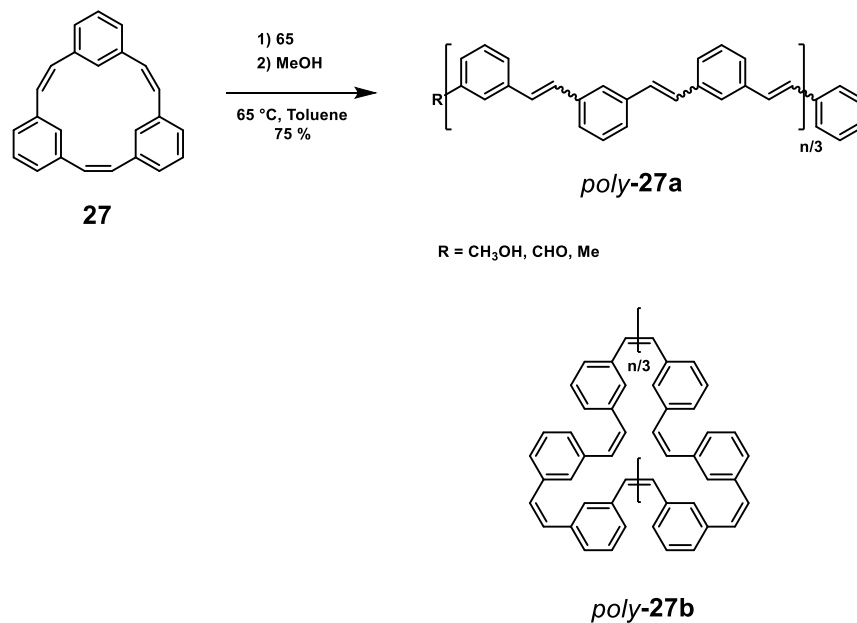
Triene **47** and triyne **27** provide a potential template for a library of monomers for ROMP and ROAMP. They both require only a few synthetic transformations, they are derived from a singular synthetic pathway, and the resulting polymers from the ROMP and ROAMP of **47** and **27**, respectively, have potential for further study and interest. *m*-Substituted PPVs are commonly intercalated into *p*-PPVs as copolymers, thereby reducing the extent of the delocalization of π -electrons, to achieve blue photoluminescence.⁸² Living ROMP would successfully enable well-controlled and predictable synthesis of these highly desirable conductive copolymers. *m*-Substituted PPEs are known for their unique folding characteristics. Oligomeric *m*-PPEs, specifically, have been synthesized and studied extensively.^{4,5} However, longer polymers have not been studied well and ROAMP enables the polymers to be end-capped with functional handles that could expand interest in the helical nature of the polymers.

2.2.2 Initial synthesis of [2.2.2]metacyclophane-1,9-17-triyne and its ROAMP by [TolC≡Mo(ONO)(OR)]•KOR (R = CCH₃(CF₃)₂, ONO = 6,6'-(pyridine-2,6-diyl)bis(2,4-di-*tert*-butylphenolate))

To explore the potential ability of [2.2.2]metacyclophane-1,9-17-triyne for ROAMP, **27** was synthesized by the published synthetic route.⁴⁶ From this synthesis, over 200 mg of **27** was obtained, but the synthesis could easily be upgraded to gram-scale.

Initial attempts at ROAMP were conducted with molybdenum -ate complex **78**. Although ROAMP was unsuccessful with diyne **23**, triyne **27** is less sterically constrained and is stable up to 180 °C in solution. Addition of **78** to a solution of **27** in toluene ([**27**]/[**78**] = 10) at 24 °C resulted in slow initiation, as confirmed by ¹⁹F NMR. After 1 h at 24 °C, the temperature was raised to 90 °C (Scheme 2.2). The reaction toward *poly-27* was complete in less than an hour and an insoluble precipitate formed immediately. MALDI evidence demonstrated that polymerization occurred, but the presence of peaks separated by 1/3 × monomer molecular weight suggested backbiting occurred. Raising the temperature of the reaction at a slower rate may have prevented backbiting. However, general insolubility of

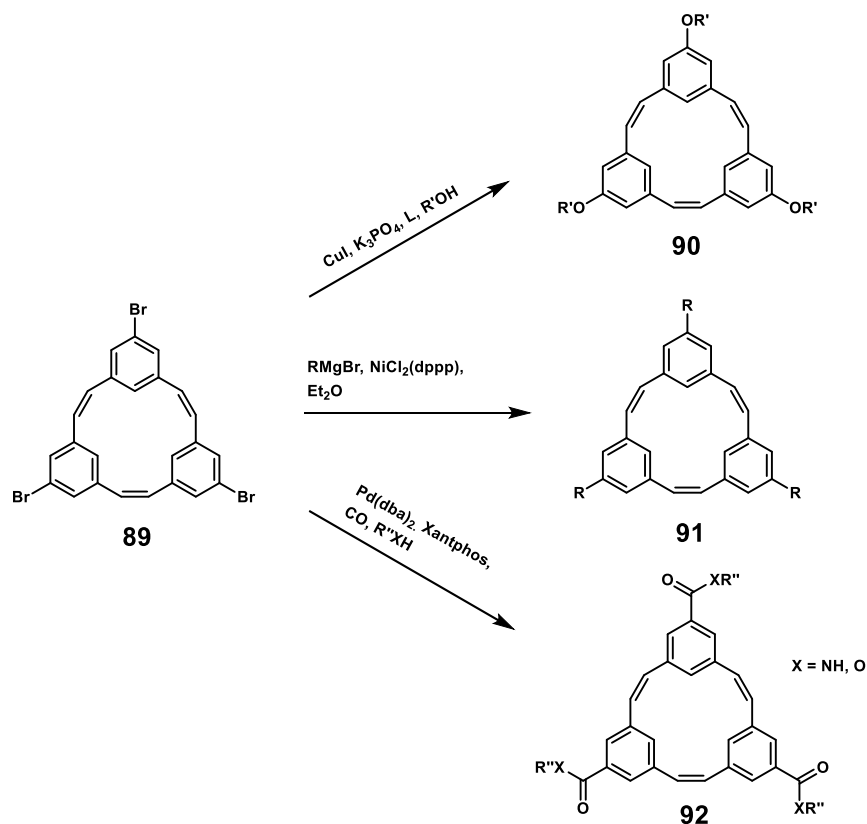
the polymers precluded further studies. In order to continue to study these monomers, substituted variations with solubilizing side chains were required.



Scheme 2.2 Synthesis of *poly-27a* and *poly-27b*.

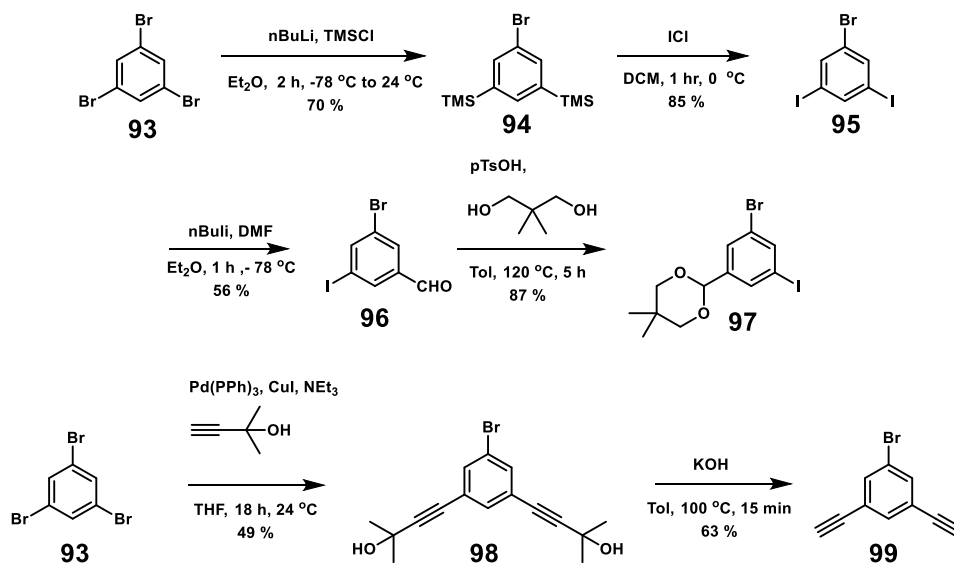
2.2.3 Step-wise synthesis toward (2Z,5Z,8Z)-15,45,75-tribromo-1,4,7(1,3)-tribenzenacyclononaphane-2,5,8-triene for modular synthesis of differently substituted triene and triyne derivatives

A late-stage synthetic installation of sidechains allows for a modular synthetic route by enabling facile variation of the types of side chains. One way to install varied sidechains is by introducing a *m*-substituted bromine; aryl bromides allow for a panoply of synthetic transformations including ones toward alkoxy side chains, alkyl side chains, and carbonyl side chains, among others. Thus, (2Z,5Z,8Z)-15,45,75-tribromo-1,4,7(1,3)-tribenzenacyclononaphane-2,5,8-triene **89** was a desirable synthetic target to facilitate a larger library of monomers for ROMP and ROAMP.



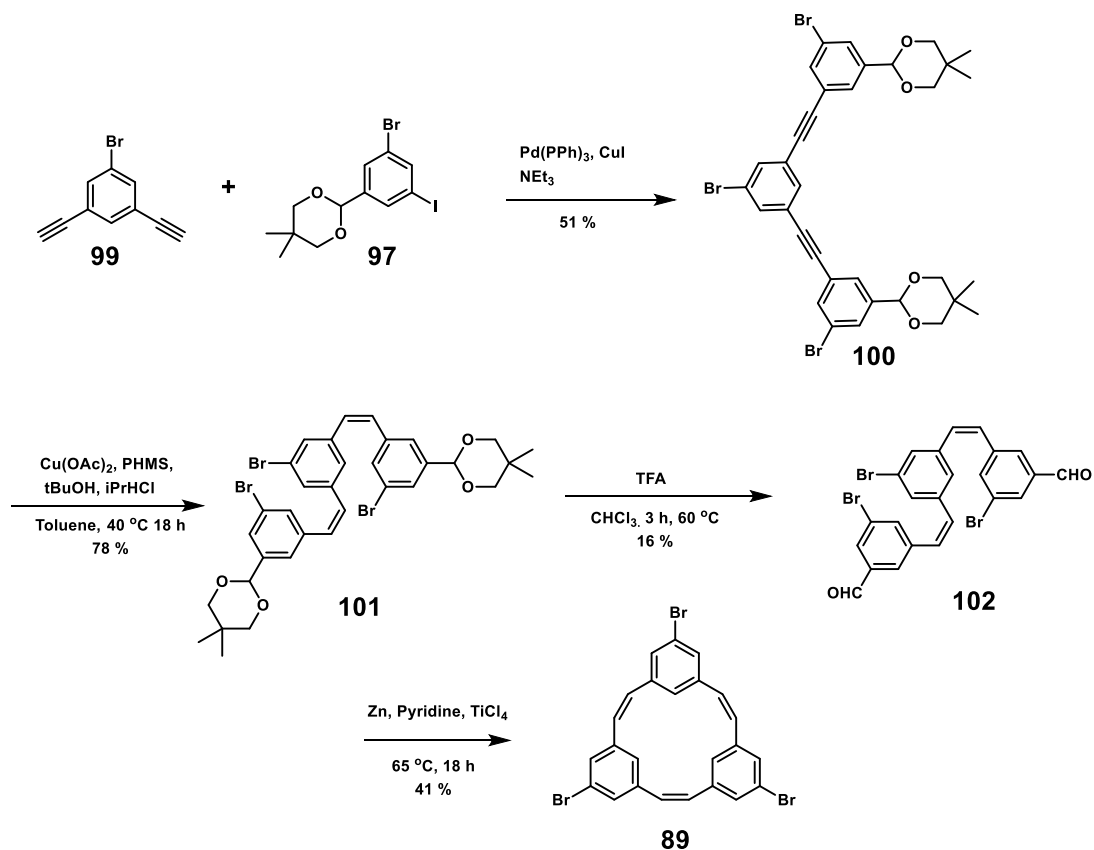
Scheme 2.3 Synthetic transformations possible via an aryl-bromide handle.

The first synthetic route attempted toward triene **89** involved the key macrocyclization step with McMurry coupling utilized in the synthesis of the unsubstituted triene **47**. This synthesis, detailed in Scheme 2.3, began with divergent synthetic pathways from 1,3,5-tribromobenzene (**93**). This synthesis began with a double lithiation followed by subsequent nucleophilic addition to trimethylsilylchloride to form **94**. Successive reaction with iodine monochloride yielded 1-bromo-3,5-diiodobenzene (**95**). Another lithiation and subsequent formylation lead to benzaldehyde **96**. Protection of this aldehyde by reaction with 2,2-dimethylpropanediol yielded **97**. The second synthetic pathway from 1,3,5-bromobenzene involved a double Sonagashira coupling with 2-methyl-3-buten-2-ol to form **98**. Subsequent deprotection resulted in diyne **99** in 63 % yield.



Scheme 2.4 Synthesis of toward diyne **99** and iodoarene **97**.

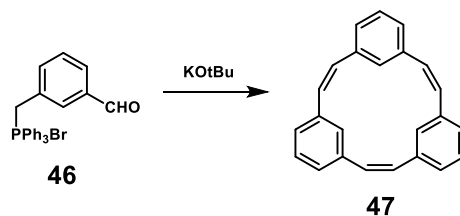
The next steps in this synthetic pathway first required utilizing aryl iodide selective Sonogashira coupling to combine **97** and **99** and form di-yne **100**. Afterwards, a selective reduction approach to obtain *Z*-only alkenes was enacted followed by acetal cleavage to form dialdehyde **102** in only 12.5 % total yield – these two steps presented the main bottleneck to an otherwise high-yielding synthesis. Additionally, AgNO₃-impregnated silica chromatography was necessary to separate any unreduced alkynes.⁸³ The last step toward triene **89** was a relatively high-yielding McMurry coupling (Scheme 1.21). Isolation of **89** was achieved through silica chromatography and its structure was confirmed by ¹³C NMR and ¹H NMR spectroscopy. Although this route was successful in attaining **89**, only 50 mg was isolated from a synthesis that began with over 20 g of 1,3,5-tribromotriene (**93**) starting material. A shorter, more high yielding synthesis was still desired.



Scheme 2.5 Synthesis of tribromo-triene **89** via stepwise coupling of **97** and **99** and subsequent intramolecular McMurry coupling of **102**.

2.2.4 One-pot macrocyclization toward (2Z,5Z,8Z)-15,45,75-tribromo-1,4,7(1,3)-tribenzenacyclononaphane-2,5,8-triene

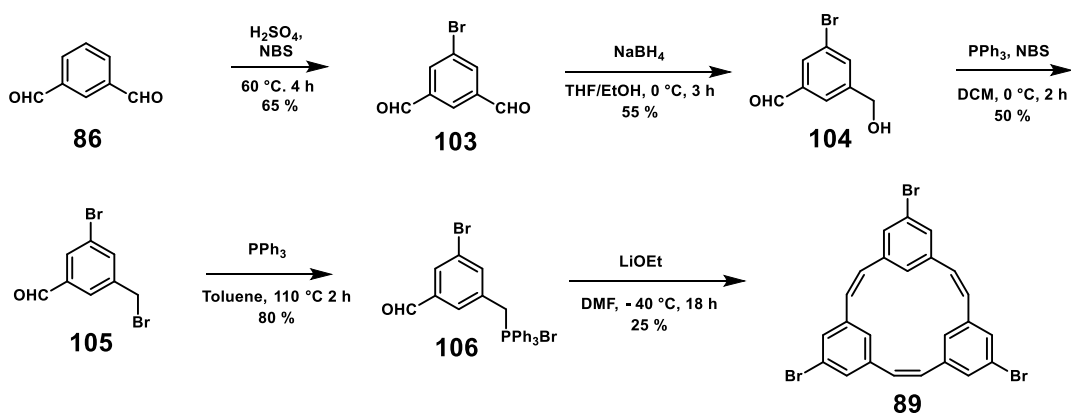
One synthetic pathway that would be potentially shorter and more high-yielding is the one-pot Wittig macrocyclization established by Tanner et al. in the synthesis of unsubstituted triene **47**.⁶³ Tanner et al. reported a remarkably high 28 % yield from the triphenylphosphonium bromide **46**.



Scheme 2.6 Synthesis of triene **47** via triple Wittig macrocyclization.

To undergo a similar triple Wittig macrocyclization, synthesis of bromo-substituted version of **41** was necessary. Triphenylphosphonium bromide **109** was thus synthesized beginning with an NBS bromination of **89** to form 3-bromoisophthalaldehyde (**103**).

Subsequent reduction with sodium borohydride lead to benzyl alcohol **104**. The Appel reaction, utilizing triphenylphosphine and NBS, of **104** yielded **105** in 50% yield. Reaction of **105** in refluxing toluene with triphenylphosphine readily formed the desired triphenylphosphonium bromide salt **106** in high yield as a white powder. Dropwise addition of **106** in DMF to a solution of lithium ethoxide in DMF at $-40\text{ }^{\circ}\text{C}$ resulted in the ZZE and ZZZ isomers of tribromotriene **89**. The ZZE converted to the ZZZ isomer by UV-light exposure for 2 h in THF.⁶¹ This synthetic pathway to tribromotriene **89** was much more efficient – over a gram of **89** was isolated starting from 15 g of **86**.

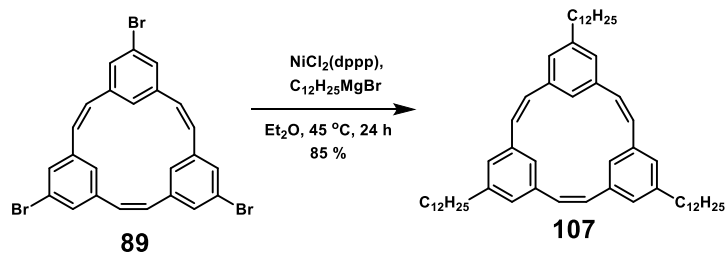


Scheme 2.7 Synthesis of triene **89** via triple Wittig macrocyclization.

2.2.5 Grignard cross-coupling toward tris-alkyl triene **110** and palladium-catalyzed carbonylation toward tris-amide triene **111**

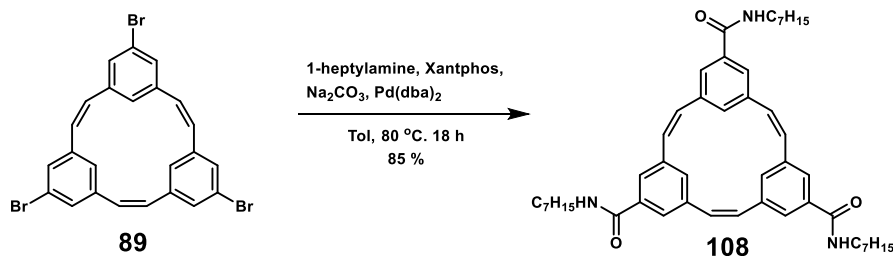
Once tribromo triene **89** was attained, subsequent reactions to install an array of side chains could be achieved. Side-chains of highest priority were ones that were a) solubilizing, b) easy to install, and/or c) would lead to polymers with useful applications. Long-chain amides accomplish all three of these criteria. *m*-Phenyleneethynylene polymers with amide side chains are known to have increased ability to form helical secondary structures due to stabilizing intramolecular hydrogen bonding.⁴ Alkyl side chains also accomplish all three criteria – alkyl-substituted *m*-phenyleneethynylene polymers have not yet been studied for their properties.

The synthesis of alkyl substituted trienes was accomplished by employing a commonly utilized Grignard cross-coupling reaction with an alkyl Grignard and a nickel catalyst.⁸⁴ Specifically, **89** reacted with three equivalents of dodecylmagnesium bromide and $\text{NiCl}_2(\text{dppp})$ to form **107**. After pouring the reaction mixture over a short plug of silica and evaporating the solvent, pure **107** was isolated as flaky white crystals.



Scheme 2.8 Synthesis of substituted triene **107**.

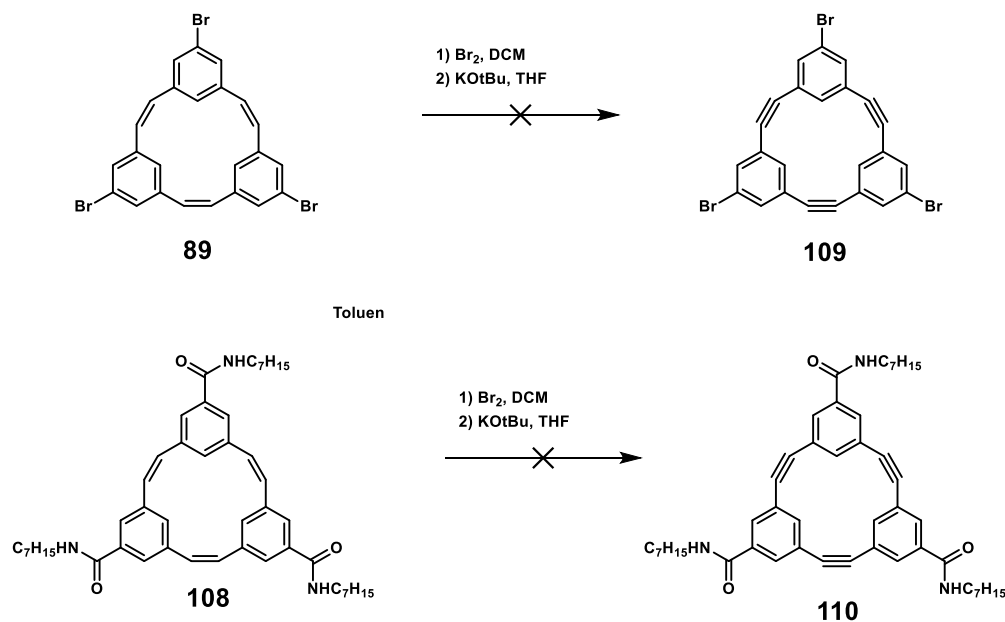
The synthesis of amide substituted trienes was accomplished utilizing a palladium-catalyzed carbonylation reaction with atmospheric pressure CO, an amine, a base and the Xantphos ligand.⁸⁵ Tribromo triene **89** underwent this carbonylation reaction with 1-heptylamine and sodium carbonate efficiently to form **108**. Column chromatography and subsequent crystallization from hexanes yielded pure **108** as flaky white crystals.



Scheme 2.9 Synthesis of substituted triene **108**.

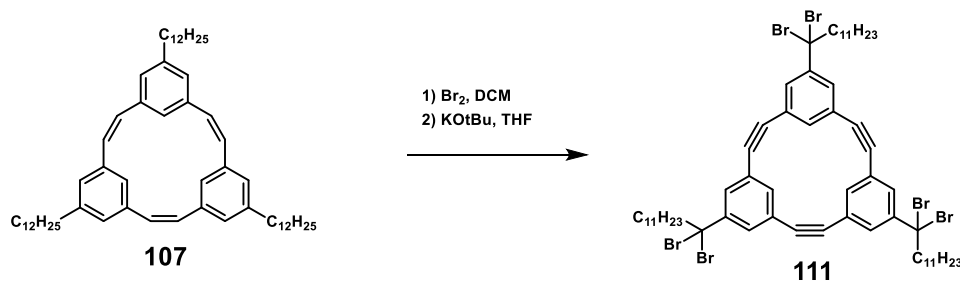
2.2.6 Bromination and elimination of substituted triene macrocycles toward triyne monomers

After synthesizing three different trienes, we then tested their ability to undergo bromination-elimination reactions to form the respective triynes. First, each triene was dissolved in DCM under N_2 and 10 equivalents of bromine was added at 24 °C. The reactions are monitored by TLC and after 3 h sodium thiosulfate was added, the organic layer separated and then evaporated. The resulting residue was then used for the subsequent elimination reaction without further purification or analysis; ^1H NMR spectroscopy was not useful due to the several diastereomers formed that complicated the aromatic region. The residue was dissolved in THF, purged with N_2 , and 12 equivalents of potassium tert-butoxide was added. Typical purification involved an alumina column and subsequent crystallization from ethanol. However, in the case of the reactions of **89** and **108**, the product was not observable from ^1H NMR spectroscopy and there was no molecular weight consistent with each respective triyne by MALDI analysis.



Scheme 2.10 Failed synthetic attempts toward **109** and **110**.

One likely reason for these failed elimination reactions was the presence of electron-withdrawing substituents. In previous sections we reported on numerous examples of other failed elimination reactions toward strained alkynes that were correlated to electron-withdrawing substituents. Thus, the substrate scope of this synthetic pathway may be limited to substrates with substituents less electron-withdrawing than bromine or amide substituents. In the case of alkyl-substituted triene **107**, the failed reaction was likely due to the bromination of the alkyl side chains. ^1H NMR evidence showed a lack of benzylic protons characteristic of the desired triyne, but it did show two clear aromatic peaks. This benzylic bromination was likely a result of excess bromine and exposure to light.



Scheme 2.11 Synthesis of triyne **111** containing undesired benzylic bromine substituents.

In order to mitigate this undesired side reaction, we decide to use a brominating agent less capable of benzylic bromination and avoided exposure to light. This brominating agent was benzyltrimethylammonium tribromide – this reagent slowly releases bromine to the reaction mixture preventing the undesired benzylic bromination. Thus, 1.2 equivalents of benzyltrimethylammonium tribromide was added to DCM and **107**, and fully brominated **112** was formed without benzylic bromination. Subsequent elimination of **112** successfully lead to solubilized ROAMP monomer **113** in 45 % yield (Scheme 2.12).

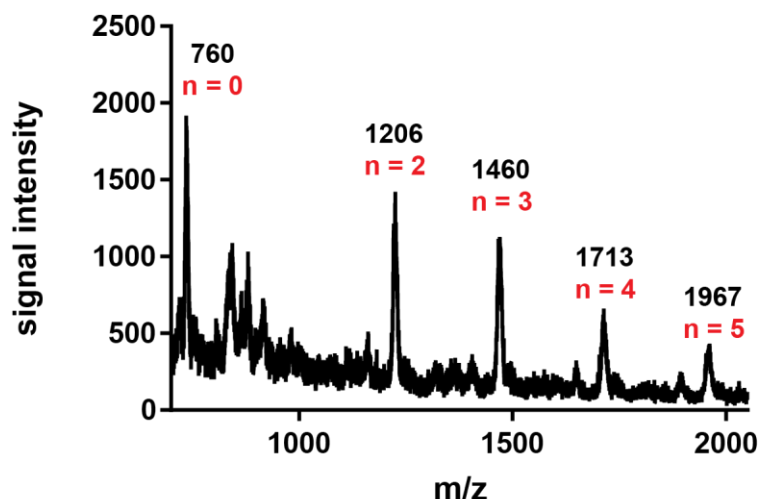


Figure 2.1 MALDI of *poly-108*. The main family of peaks is separated by a mass of 253 Da ($1/3$ the mass of the monomer **108**) and corresponds to molecular ions of [*poly-2a*].

Addition of **70** to a solution of **108** in toluene ($[70]/[108] = 10$) at 24 °C did not lead to the formation of a polymeric species within 24 h. However, ^1H and ^{19}F NMR indicates that ROMP catalyst **70** did initiate quantitatively in less than 1 h. At 65 °C, there was clear conversion of monomer to another species and after 30 min full conversion of monomer was achieved, as determined by ^1H NMR spectroscopy. Precipitation of the resulting polymers in MeOH afforded *poly-108* in greater than 75% isolated yield. GPC analysis of this polymerization showed a few different peaks corresponding to lower molecular weight species as well as a broad peak perhaps corresponding to larger molecular weight species (Figure 2.2). MALDI spectroscopic evidence showed the clear presence of peaks separated by $1/3 \times$ monomer molecular weight. This suggested that unselective backbiting was occurring.

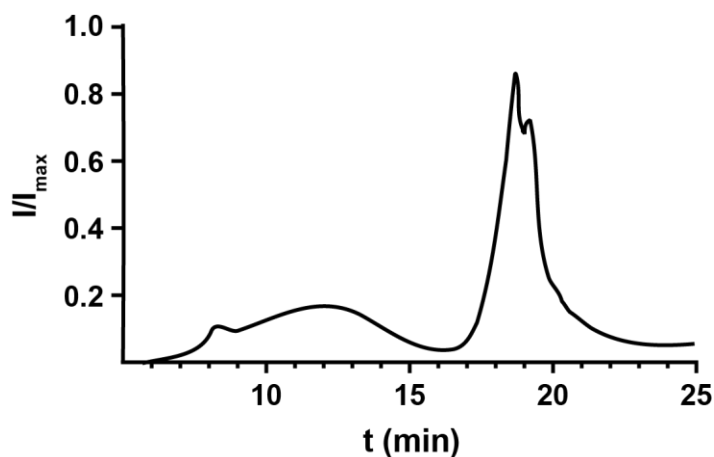
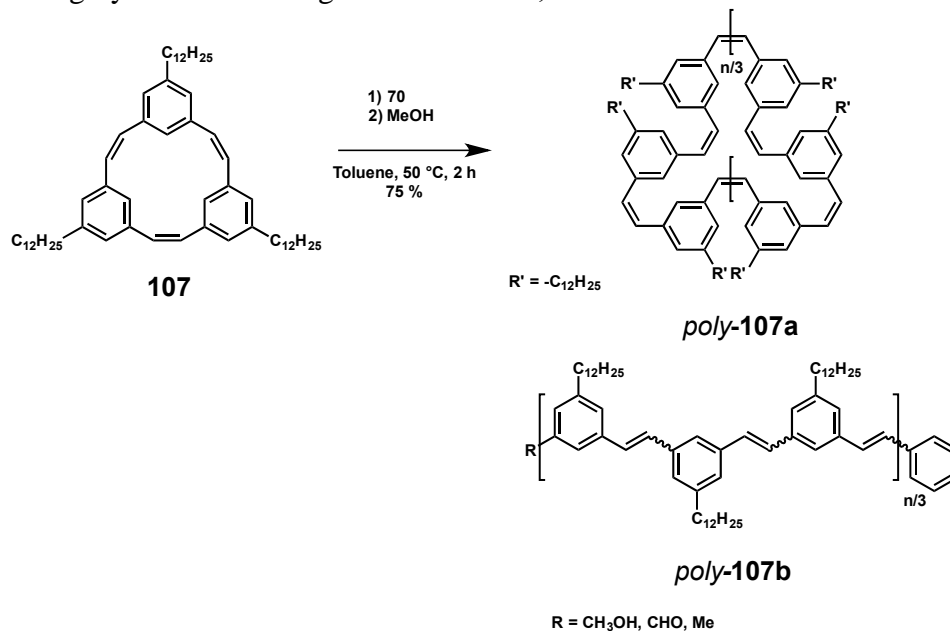


Figure 2.2 GPC traces for *poly-108* produced through ROMP of **108** with catalyst **70** at a loading of $[70]/[108] = 10$ (red) ($T = 65^\circ$); calibrated to polystyrene standards.

2.3.2 ROMP of **107** with Grubbs II Catalyst, **70**

We studied the ROAMP of alkyl substituted (2Z,5Z,8Z)-1,4,7(1,3)-Tribenzenacyclononaphane-2,5,8-triene Monomers (**107**) (Scheme 2.14), an all-carbon accessible highly solubilized ring-strained alkene, with Grubb's 2nd Generation catalyst.



Scheme 2.14 Synthesis of *poly-107a* and *poly-107b* from triene **107**.

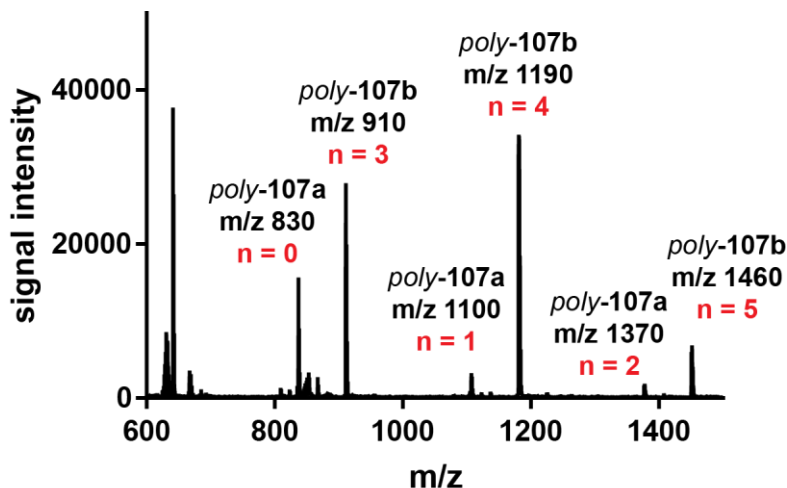


Figure 2.3 MALDI of *poly-107a* and *poly-107b*. The taller family of peaks is separated by a mass of 280 Da (1/3 the mass of the monomer **107**) and corresponds to molecular ions of [*poly-107b*]. The smaller family of peaks is also separated by a mass of 270 DA (1/3 the mass of the monomer **107**) and corresponds to molecular ions of [*poly-107a*].

Addition of **70** to a solution of **107** in toluene ($[\mathbf{70}]/[\mathbf{107}] = 10$) at 24 °C did not lead to the formation of a polymeric species within 24 h. However ¹H and ¹⁹F NMR indicated that ROMP catalyst **70** initiated quantitatively in less than 30 min. At 45 °C, there is clear conversion of monomer to another species and after 2 h full conversion of monomer is

achieved, as determined by ^1H NMR spectroscopy. Precipitation of the resulting polymers in MeOH afforded *poly-107* (mixture of *poly-107a* and *poly-107b*) in greater than 85% isolated yield. GPC analysis of the polymerization this polymerization showed one main peak with a significant shoulder (Figure 2.4). MALDI evidence showed peaks corresponding to both *poly-107a* ($n = 0, 1, 2$) and *poly-107b* ($n = 3, 4, 5$). This suggested that intermolecular and intramolecular termination reactions (chain-transfer and backbiting, respectively) were occurring. NMR spectroscopic evidence also suggested the formation of both linear and cyclic polymers (Figure 2.5)

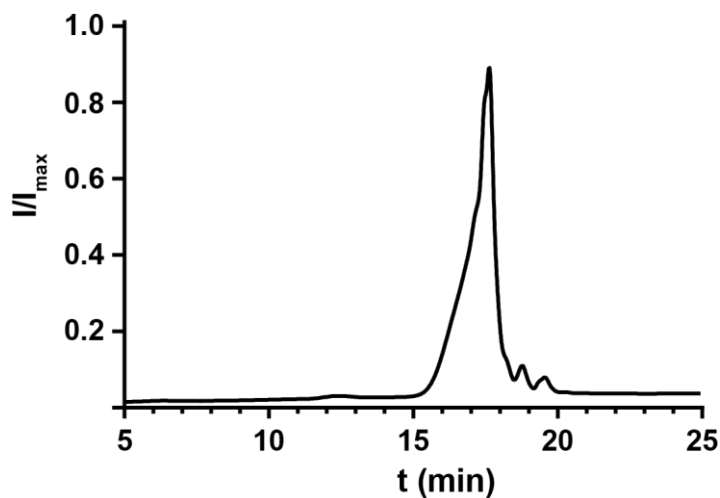


Figure 2.4 GPC traces for *poly-110a* produced through ROMP of **110** with catalyst **70** at a loading of $[\mathbf{65}]/[\mathbf{110}] = 10$ (red) ($T = 65^\circ$); calibrated to polystyrene standards.

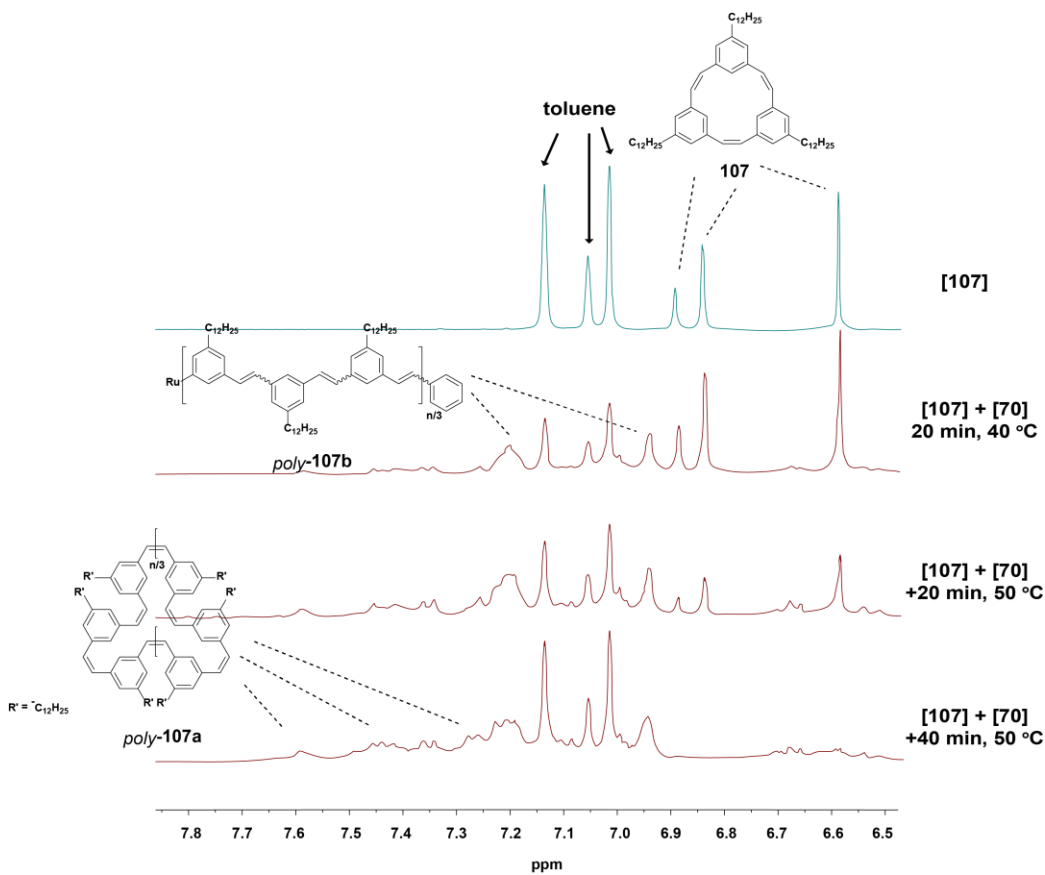
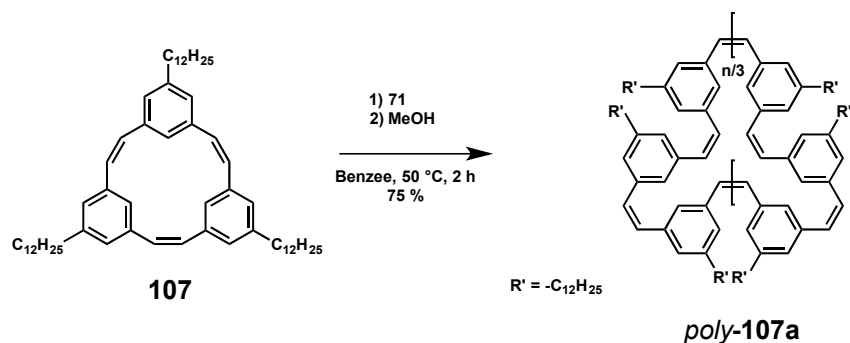


Figure 2.5 Polymerization progress of **107** and **70** evaluated by ^1H NMR spectroscopy shows conversion to species consistent with cyclic and linear polymers.

2.3.3 ROMP of **107** with Grubbs III Catalyst, **71**

Menk et al. demonstrated greater control for ROMP reactions utilizing Grubb's III catalyst (**71**). Despite the lack of selectivity shown for polymerizations with Grubb's II, attempting ROMP with Grubb's III could result in faster initiation and a lower energy requirement for the reaction to occur. This lower energy requirement may allow for a larger differentiation between strained and unstrained alkenes resulting in more linear polymers and less undesired chain-transfer or backbiting.



Scheme 2.15 Synthesis of *poly-107a* and *poly-107b* from triene **107**.

Addition of **71** to a solution of **107** in benzene ($[\mathbf{71}]/[\mathbf{107}] = 10$) at 24 °C did not lead to the formation of a polymeric species within 24 h. However, ^1H and ^{19}F NMR indicated that ROMP catalyst **71** initiated quantitatively in less than 1 h. At 50 °C, there was clear conversion of monomer to another species and after 2 h full conversion of monomer was achieved, as determined by ^1H NMR spectroscopy (Scheme 2.15). Precipitation of the resulting polymers in MeOH afforded *poly-107a* 75% isolated yield. GPC analysis of this polymerization showed three discrete peaks, likely consistent with *poly-107a* ($n = 1, 2, 3$) (Figure 2.6).

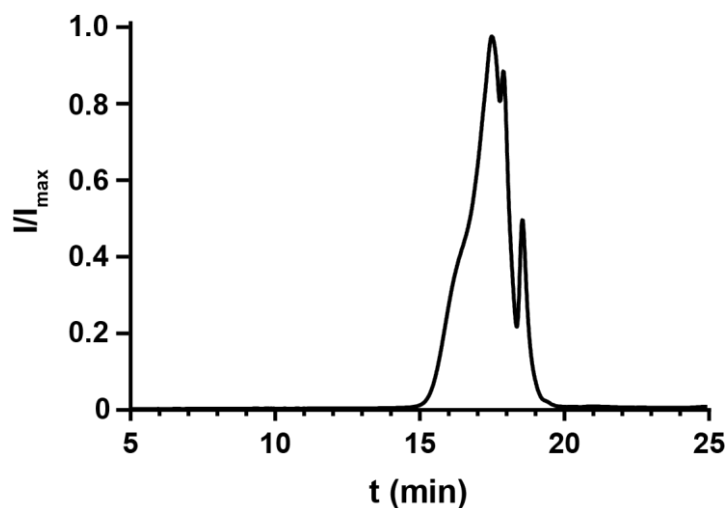


Figure 2.6 GPC traces for *poly-110a* produced through ROMP of **110** with catalyst **66** at a loading of $[\mathbf{110}]/[\mathbf{65}] = 10$ (red) ($T = 50^\circ$); calibrated to polystyrene standards

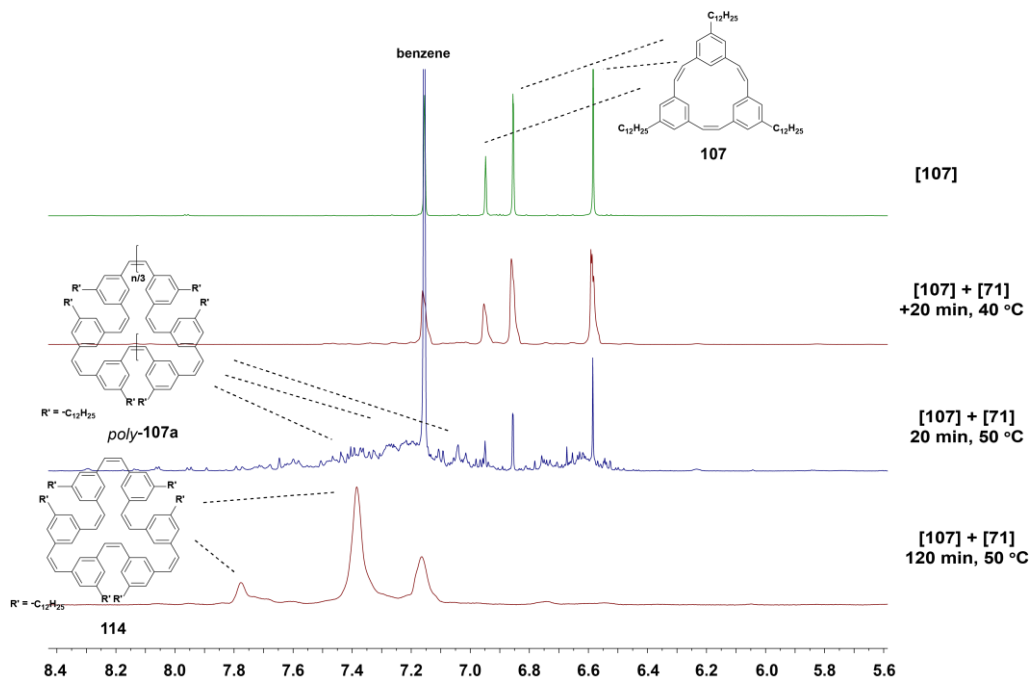
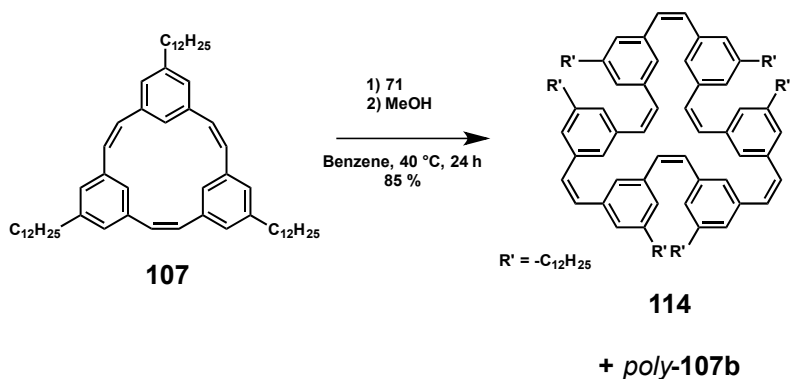


Figure 2.7 Polymerization progress of **107** and **71** evaluated by ^1H NMR spectroscopy shows conversion to species consistent with cyclic oligomers after 2 h at 50 °C.

The same polymerization was also attempted at 40 °C. At this temperature, full conversion was not achieved for 24 h. Precipitation of the resulting polymers in MeOH afforded *poly-107a* and in 85% isolated yield (Scheme 1.30). GPC analysis of this polymerization showed one main peak (Figure 2.8). ^1H NMR also showed one main species – there were three proton peaks integrating 2:2:1. MALDI spectroscopic evidence showed primarily a peak characteristic of 2x the molecular weight of **110** and a small peak corresponding to *poly-107b* ($n = 6$).



Scheme 2.16 Synthesis of **114** and other cyclic oligomers from triene **110**.

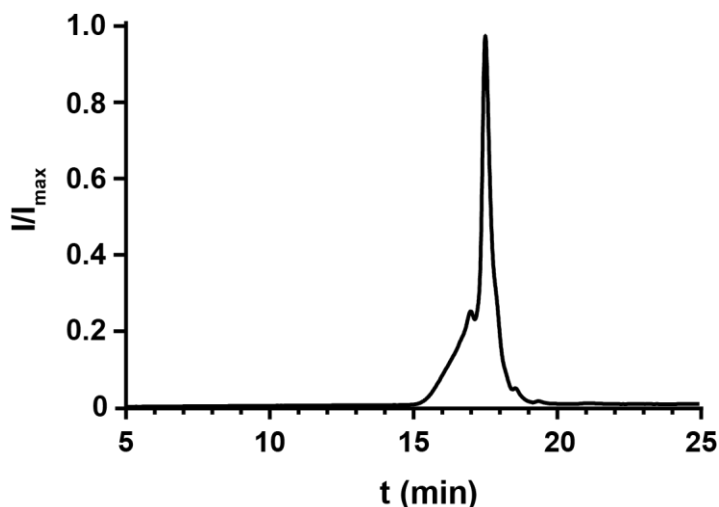


Figure 2.8 GPC traces for *poly-107* and **114** produced through ROMP of **107** with catalyst **71** at a loading of $[110]/[65] = 10$ (red) ($T = 40^\circ$); calibrated to polystyrene standards.

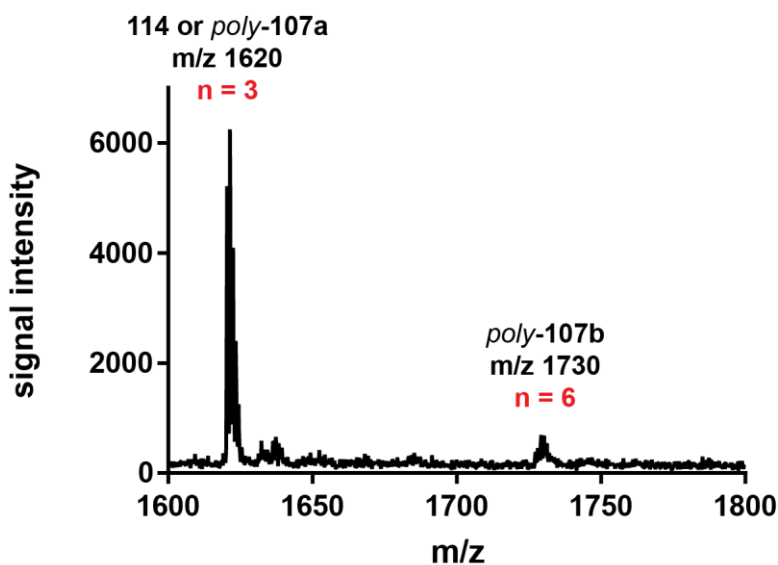
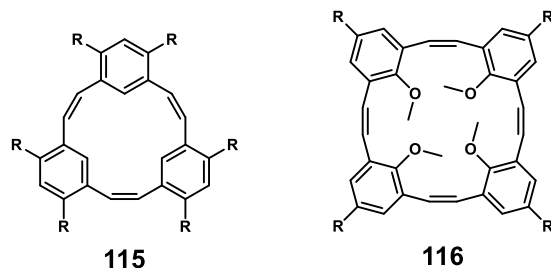


Figure 2.9 MALDI of the polymerization of **107**, showing the formation of mainly **114**.

The weight of evidence of these ROMP reactions demonstrated a lack of selectivity between strained and unstrained alkenes and after long reaction times the polymerization was driven toward the thermodynamic sink (dimer **114**). ROMP with Grubb's Gen II (**70**) was more likely to lead to a mixture of cyclic and linear polymers due to its more sterically hindered ligands, while ROMP with Grubb's Gen III (**71**) generated primarily cyclic polymers. These results differed significantly from past studies of polymerizations utilizing Grubb's catalysts (**70** and **71**) for ROMP with more sterically hindered *o*-substituted monomers that are selective for linear polymers. This difference demonstrated ROMP's high sensitivity to sterics. Another possibility was that the strain energy for these *m*-substituted monomers was not large enough for the propagating catalyst to differentiate between strained and unstrained alkenes.

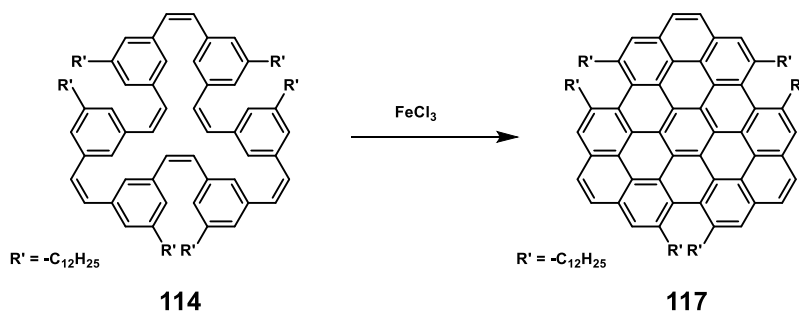
2.3.4 Future Directions

If the lack of enough steric interference dictated the lack of selectivity, the synthesis of monomers with *ortho*-substitutions would be ideal. Two such monomers are **115** and **116**. **116** is an especially attractive monomer target given the potentially stark difference in sterics between the monomer and the hypothetical propagating polymer chain. This difference in sterics may allow for enough differentiation to favor chain-growth over undesirable back-biting.



Scheme 2.17 Potential monomers for ROMP that may result in better selectivity for chain-growth.

The thermodynamic sink for the ROMP of **107** could also be exploited for its structural similarity to nanographenes. If **114** could be purified and isolated, a Scholl oxidation could be employed to access solubilized nanographene **117**. This synthetic pathway would allow for nanographenes of varying substitution due to the highly modular route to the substituted triene precursors.

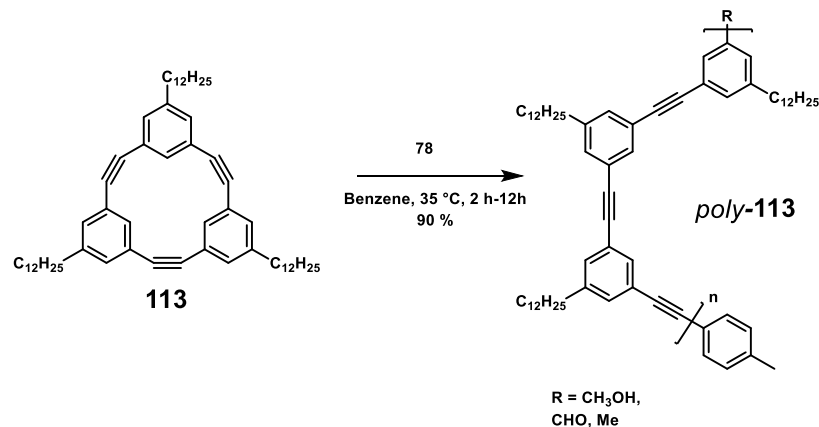


Scheme 2.18 Synthesis of nanographene **117** from cyclic oligomer **115** produced from ROMP.

2.4 Ring-Opening Alkyne Metathesis of Substituted [2.2.2]Metacyclophane-1,9,17-triyne Monomers

2.4.1 ROAMP of **113** by -ate complex, **78**

We studied the ROAMP of **113** (Scheme 1.33), a readily accessible, highly solubilized ring-strained alkyne, with -ate complex **78**.



Scheme 2.19 Synthesis of *poly-113* from ROAMP of **113** by catalyst **78**.

Addition of **78** to a solution of **113** in benzene ($[\mathbf{113}]/[\mathbf{78}] = 10$) at 24 °C did not lead to the formation of polymeric species within 24 h. However, ^1H and ^{19}F NMR indicated that the ROAMP catalyst **78** quantitatively initiated within 1 h. At 35 °C, however, the ROAMP of monomer **113** (10 equiv.) in toluene was completed in less than 2 h, as determined by ^1H NMR spectroscopy. Precipitation of the resulting polymers in MeOH afforded *poly-113* in greater than 90% isolated yield. GPC analysis for various monomer/catalyst loadings at 35 °C in benzene showed a PDI of ~ 1.09 , the lowest value ever reported for ROAMP toward conjugated polymers (Figure 1.7, Table 1.3). The molecular weights of *poly-113* determined by GPC, calibrated to polystyrene standards, were proportional to the initial $[\mathbf{113}]/[\mathbf{78}]$ loading and showed a nearly unimodal distribution (Figure 2.10). No evidence for branching or the formation of cyclic polymers could be observed by ^1H NMR analysis, though the molecular weight distribution of polymers could not be definitively determined from mass spectrometry. ^1H NMR end-group analysis of the tolyl group revealed that GPC overestimated the M_n of *poly-113*. A correction factor $\sim 0.6\text{--}1.0$ correlated well with the degree of polymerization determined by NMR analysis and the expected molecular weight based on the $[\mathbf{113}]/[\mathbf{78}]$ loading.

Table 2.1 Molecular weight analysis of *poly-113*. ^a calibrated to narrow polydispersity polystyrene standards; ^b degree of polymerization determined by ^1H NMR end-group analysis.

$[\mathbf{112}]/[\mathbf{76}]$	T (°C)	M_n theory	M_n GPC ^a	M_w GPC ^a	X_n^b	PDI GPC ^a
10/1	35	8,100	17,500	20,000	11	1.14
20/1	35	16,200	26,800	29,700	22	1.11
30/1	35	24,300	43,000	46,870	33	1.09

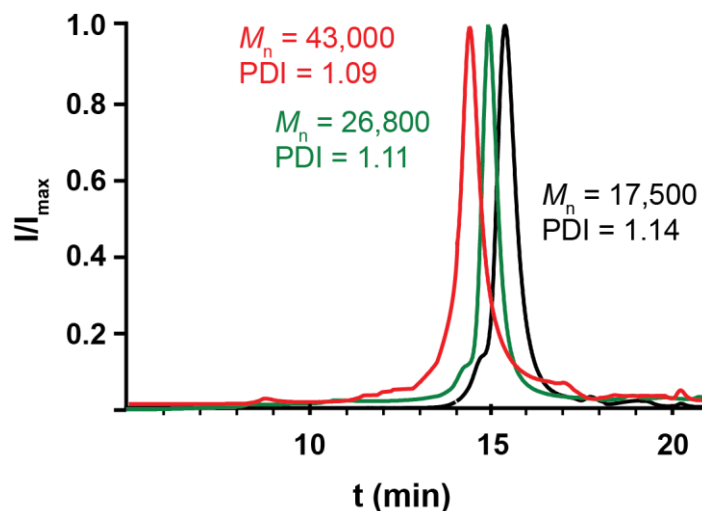
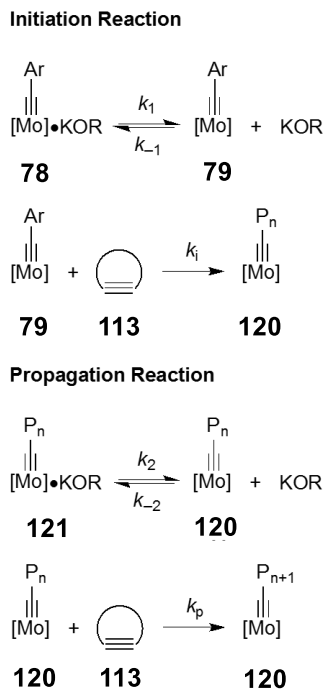


Figure 2.10 GPC traces for *poly-113* produced through ROAMP of **113** with catalyst **78** at a loading of $[113]/[78] = 10$ (black), 20 (green), and 30 (red) ($T = 35^\circ$); calibrated to polystyrene standards.

2.4.2 Kinetic Studies of the Rate of ROAMP Propagation of **113** by **78** Over Time

The proposed kinetic scheme for the polymerization of a ring-strained monomer **113** with catalyst **78** is depicted in Scheme 2.20. This proposed kinetic scheme is consistent with the scheme previously derived by Bellone et al for the ROAMP of **22** by **78**. In a fast initiation reaction, 1 equiv. of **113** reacts with **78** to form the initiated complex **79** ($n = 1$). Binding of KOR to **77** stabilizes the initiated complex and reversibly blocks the active site. Dissociation of KOR from **121** regenerates the active propagating species that undergoes linear chain-growth polymerization with further equivalents of **113** to form extended living polymer chains.



Scheme 2.20 Proposed kinetic scheme for the ROAMP of **113** by **78**.

As mentioned in a previous section the detailed ROAMP study by Bellone et al., to meet the stringent criteria for a living polymerization the initiation of the catalyst must be fast and quantitative ($k_i > k_p$), the concentration of propagating species has to remain constant throughout the reaction, all propagating chains have to grow at the same rate, and irreversible termination and chain-transfer processes should be absent. Bellone et al. derived the overall rate law given this proposed kinetic scheme, previously mentioned in section 1.2, and it applies in this case as well (E2).

$$\frac{d[\text{C}_i]}{dt} = \frac{k_i[\text{C}]_0[\text{M}]}{\left(\frac{[\text{KOR}]}{K_{\text{diss}}} + 1\right)} = k_{i,\text{obs}}[\text{C}]_0[\text{M}] \quad (\text{E2})$$

To probe consistency of experimental data with this proposed rate law, the concentration of monomer over the course of the polymerization was measured by ^1H NMR spectroscopy from the integration of a monomer proton signal (in red in Figure 2.11).

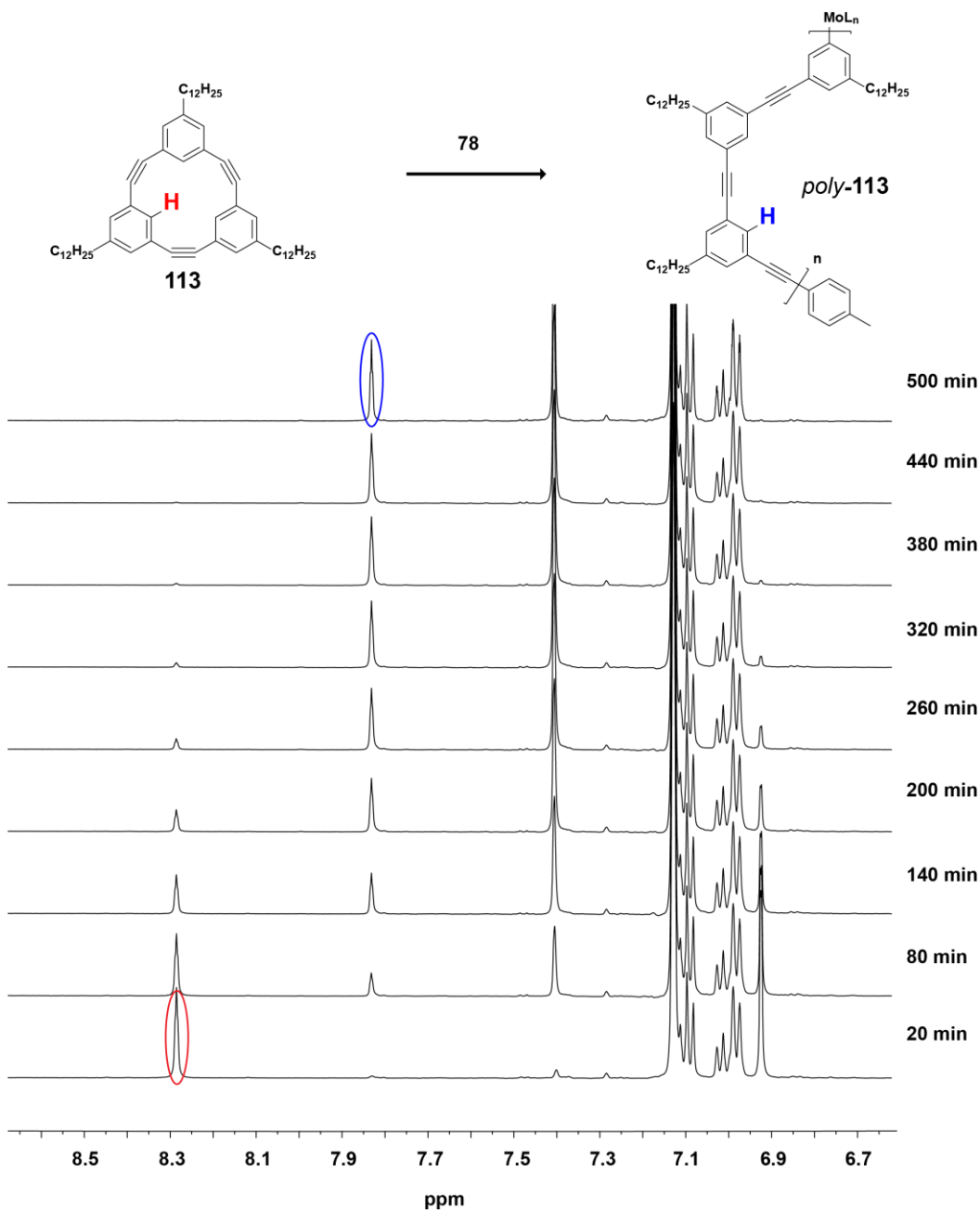
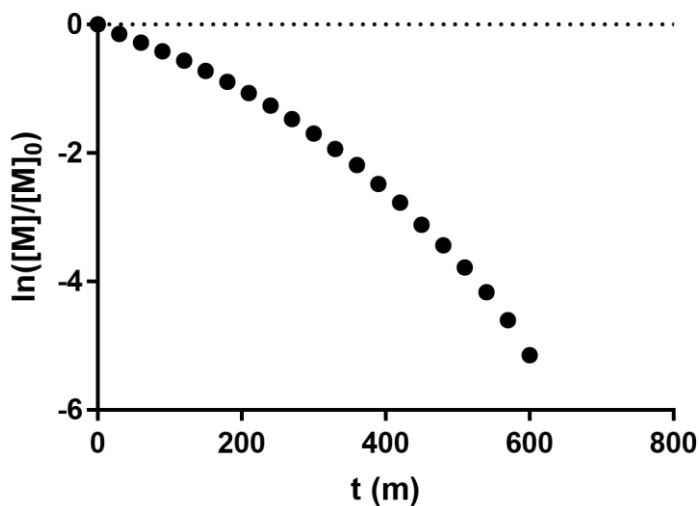


Figure 2.11 ¹H NMR spectra of the reaction of **113** with **78** at various time points demonstrating the conversion of **113** (protons circled in red) in to *poly-113* (protons circled in blue).

A linear plot of $\ln([M]/[M]_0)$ over time throughout the entire polymerization would suggest that the concentration of propagating species is constant throughout the reaction and irreversible termination processes are absent. However, experimental data only showed linearity for the first ~ 50 % of the polymerization for both $[113]/[78] = 10$ and 30 (Figure 2.12). This suggested an irreversible termination process or chain-transfer process occurring as monomer concentrations decrease. This may explain the not-quite unimodal distribution of the GPC traces for each polymerization – higher molecular weight shoulders were apparent and may be characteristic of polymers resulting from these undesired

termination process. However, these undesired side reactions were nowhere near as apparent as those reported in the ROAMP polymerization toward conjugated polymers in Kugelgan et. al. So, although this polymerization is not fully living – it is a significant step forward for living ROAMP toward conjugated polymers.

a)



b)

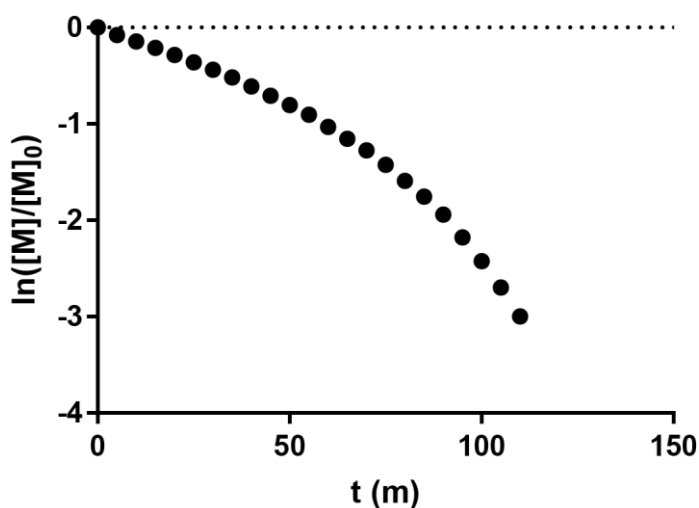


Figure 2.12 Kinetic studies of the rate of polymerization of **113** by **78**. a) $[113]/[78] = 30$ b) and $[112]/[76] = 10$.

2.4.3 Post-Polymerization Addition of Monomer as a Living Polymerization Test

Regardless of these minimal side-reactions, in the absence of monomer, the molybdenum catalyst attached to the propagating polymer chain remained active and continued to incorporate equivalents of monomer added sequentially to the reaction mixture (Figure 2-9). This was demonstrated by conducting a polymerization with catalyst loading of $[113]/[78] = 10$ and then after monomer consumption adding 5 more equivalents

of monomer. GPC data confirmed further incorporation of monomer and suggested a persistently active catalyst (Figure 2.13). This boded well for the potential of these monomer types to form block co-polymers via ROAMP with **78**.

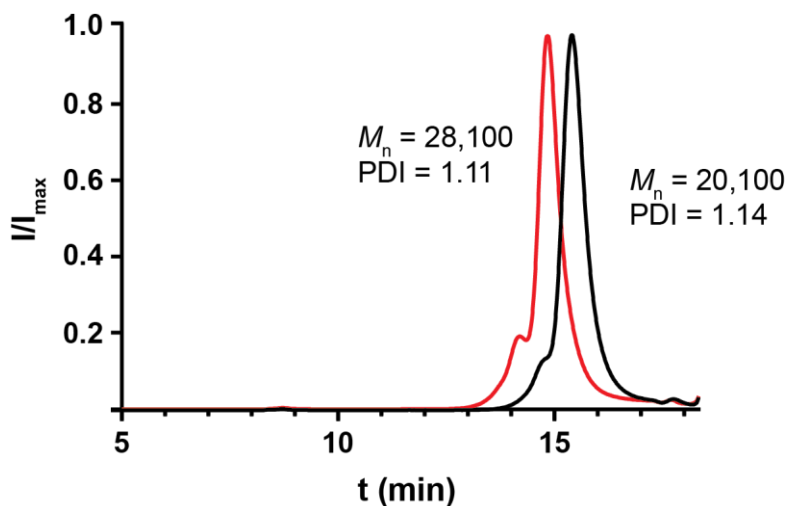
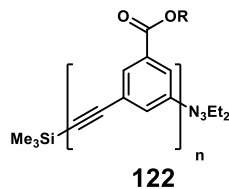


Figure 2.13 GPC traces for *poly-113* produced through ROAMP of **113** with catalyst **78** at a loading of $[113]/[78] = 10$ (black). After full monomer consumption 5 more equiv. of **113** is added resulting polymers represented by the GPC trace in red.

2.4.4 UV-Vis Studies on Solvent and Small-Molecule Guest Dependence on Secondary Structure of *poly-113*.

We studied the folding behavior of *poly-113* in various solvents and in the presence of guest molecules. These experiments were conducted in order to demonstrate similarities to the work first described by Jeffrey Moore's group in 1997 on the folding behavior of substituted *m*-phenyleneethynylene oligomers in solution.⁴ This seminal work was an important demonstration of control and manipulation of secondary-structure of synthetic polymers that was only previously demonstrated by biopolymers. In their study they showed that there was a strong solvent, temperature and chain-length dependence on the ability for *m*-PPEs to form helices and that the driving force of this transition was solvophobic in nature. Their *m*-PPE oligomers were substituted with triglyme mono methyl ether groups in order to solubilize the oligomers in a number of solvents. They were also substituted with these side chains in order to create a difference in solvent interaction between the side-chains and the polymer backbone that help drive helical formation. In Nelson et al., they found that oligomers with greater than 10 phenyl units in acetonitrile readily formed helical structures, although oligomers in chloroform were in the open-chain state.⁴



n - 2, 4, 6, 8, 10, 12, 14, 16, 18

Scheme 2.21 *m*-PPE oligomers capable of folding behavior in certain solvents.

UV-VIS spectroscopy revealed key differences in absorbance peaks for oligomers in their folded and open-chain states. Oligomers in the open chain state demonstrated a ratio in absorbance of the two peaks centered at 303 nm and 298 nm of around 0.9 ($I_{303}/I_{290} = 0.9$). Oligomers in the helical state demonstrated an absorbance ratio of $I_{303}/I_{290} = 0.6$. Nelson et al. showed that by increasing temperature or chloroform concentration that a clear transition from the absorbance ratio for open-chain state to the absorbance ratio for the helical state could be observed and visualized by a neat titration curve.⁴ These findings suggested that *poly-113*, which contains the same polymer backbone, could undergo a similar transition with the right solvent combination. Unlike the *m*-PPE oligomers studied in Nelson et al., the polymers we synthesized contained side chains that are similar in solvent affinity to the polymer backbone. Nonetheless, short polymers (MW ~ 15,000) of *poly-113* were still appreciably soluble in a number of different solvents and no one has yet to investigate *m*-PPEs with the all-carbon alkyl substitution pattern for their secondary structure. We thus sought to first examine the UV-Vis spectroscopy of *poly-113* in a variety of solvents: toluene, chloroform, cyclohexane and acetonitrile (Figure 2.14).

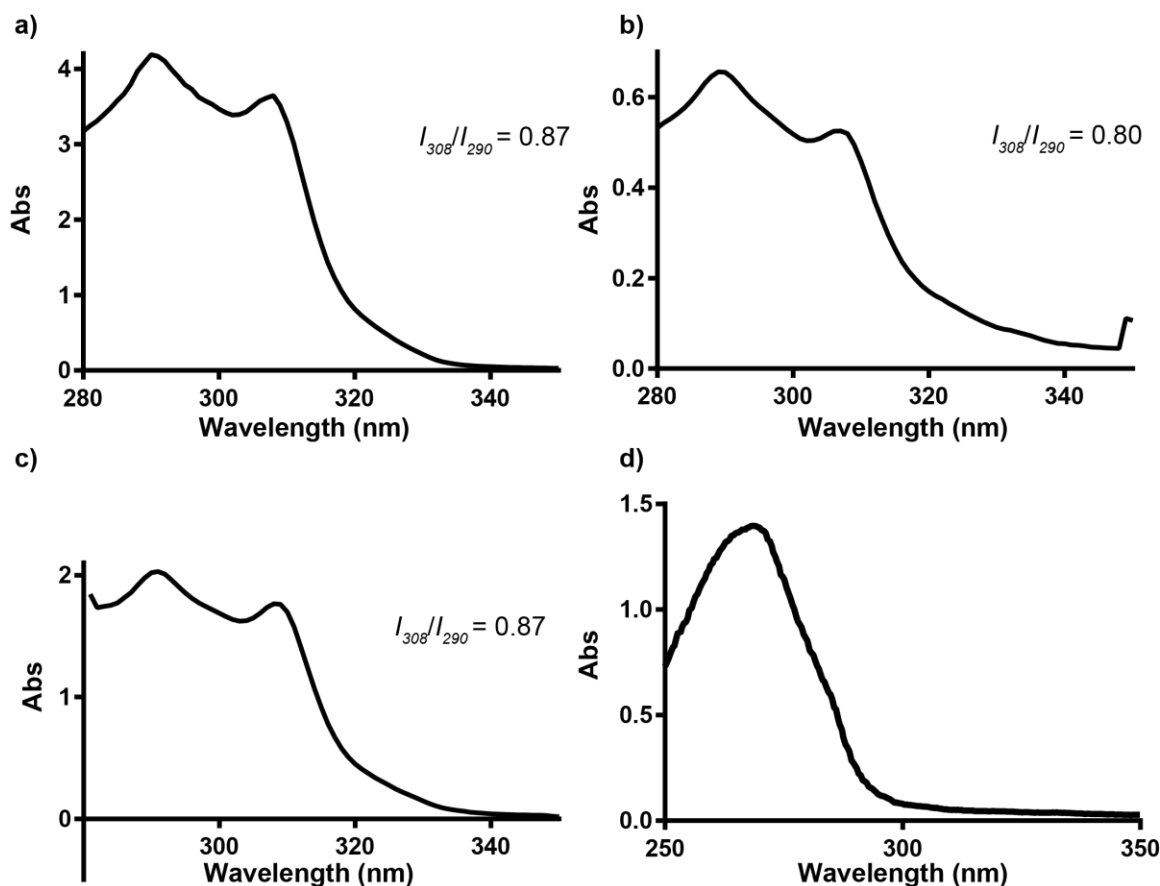


Figure 2.14 UV-Vis spectra for *poly-113* in a) chloroform, b) cyclohexane, c) toluene, d) acetonitrile.

Unlike oligomers **121**, *poly-113* showed a consistent ratio of absorbances in each solvent that is representative of the open-chain state. However, the UV-Vis spectrum was much different in acetonitrile. The two peak absorbances characteristic of *m*-PPEs were not apparent, and instead there was one peak absorbance with $\lambda = 260$ nm. *Poly-113* was barely soluble in acetonitrile; it could be that its absorbance profile in this solvent was thus characteristic of higher order structures of the *m*-PPEs. In order to clarify whether this peak was an artifact or one that is characteristic of *poly-113*, we also looked at the UV-Vis spectrum in 10 % CH₃CN in chloroform (Figure 1.11). In this mixed solvent, the peak absorbances for the *m*-PPE in 100 % chloroform and 100 % acetonitrile were both apparent. This suggested that the peak absorbance at $\lambda = 260$ nm was indeed real and possibly indicative of higher-order structures (Figure 2.15).

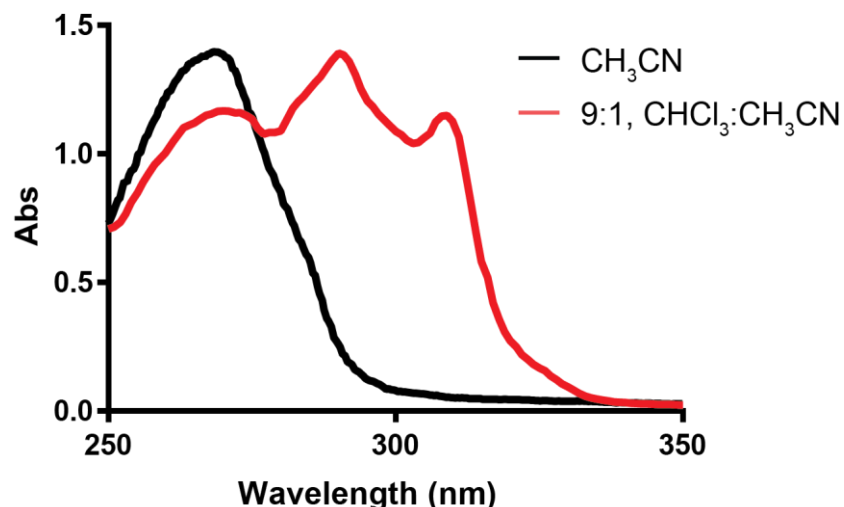


Figure 2.15 UV-Vis spectra for *poly-113* in acetonitrile (black) and 10 % acetonitrile in chloroform (red).

We also studied the temperature dependence of the UV-Vis spectrum, but we were unable to find any strong differences in the spectra in any solvent at a variety of temperatures (-20 to 60 °C). In another study by Jeffrey Moore's group, they found a strong affinity between the helical oligomers and certain guest molecules.⁸⁶ In Stone et. al, specifically, they found a high association between oligomer **122** in solutions with α -pinene. This association was highest ($K_a \sim 10^6$) in solutions containing more water due to the presence of the helical state of the oligomer and the solvophobic effect. This strong association suggested that guest molecules, like α -pinene, may even be able to drive folding of *m*-PPEs. Thus, we studied the effects of increasing concentrations of two guest molecules, α -pinene and RDX, on the UV spectra of *poly-113* in THF. The UV-Vis spectra with various concentrations of α -pinene demonstrated a lack of drive toward the helical state, even at very large concentrations ($[\alpha\text{-pinene}]/[\textit{poly-113}] = 1500$). However, there was a small apparent transition to a more folded state demonstrated by the somewhat larger ratio of I_{303}/I_{290} .

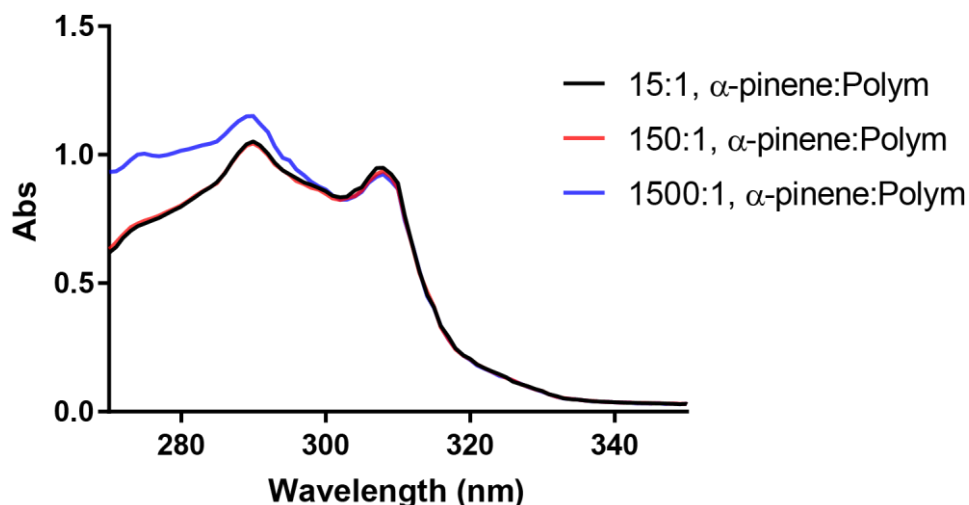


Figure 2.16 UV-Vis spectra for *poly-113* with various concentrations of α -pinene.

Addition of RDX seemed to have a more profound effect on the UV-Vis spectrum of *poly-113*. With 1500 equivalents of RDX, *poly-113* underwent a full transition to the helical state. At this concentration of guest, the ratio of absorbances at 303 and 290 was equal to around 0.6; a ratio consistent with the helical state found in Nelson et. al.⁴

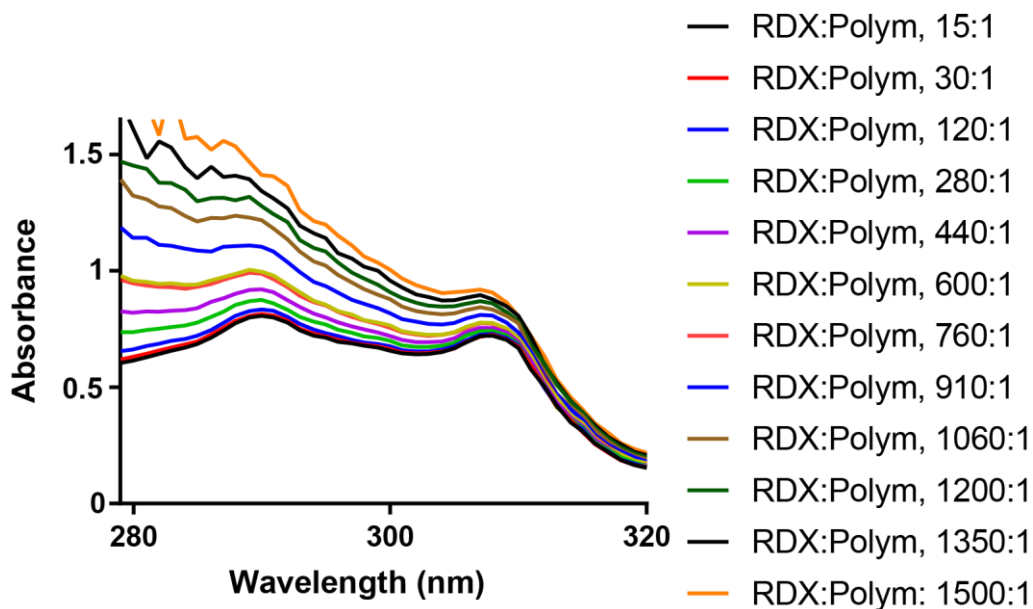


Figure 2.17 UV-Vis spectra for *poly-113* with various concentrations of RDX.

A titration curve suggested a transition from the open chain state to the helical state with increasing concentrations of RDX (Figure 1.14). This transition was similar to that seen for solvent or temperature transitions found in Nelson et al. ⁴ The affinity between nitro-compounds and electron-rich arenes may explain this drive in transition observed toward a helical state.

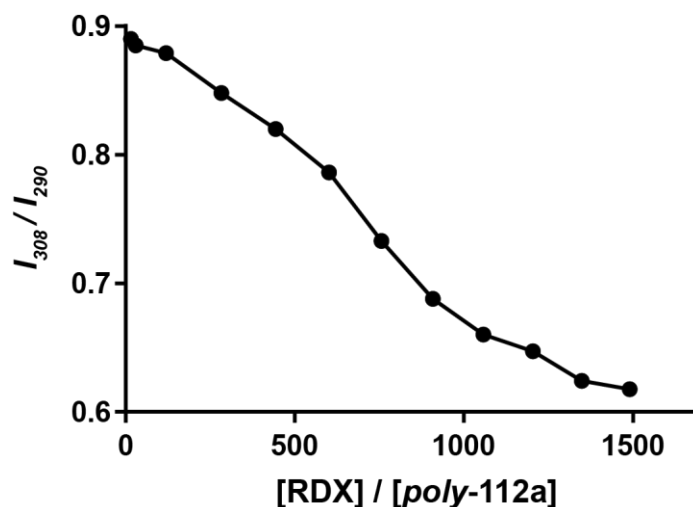
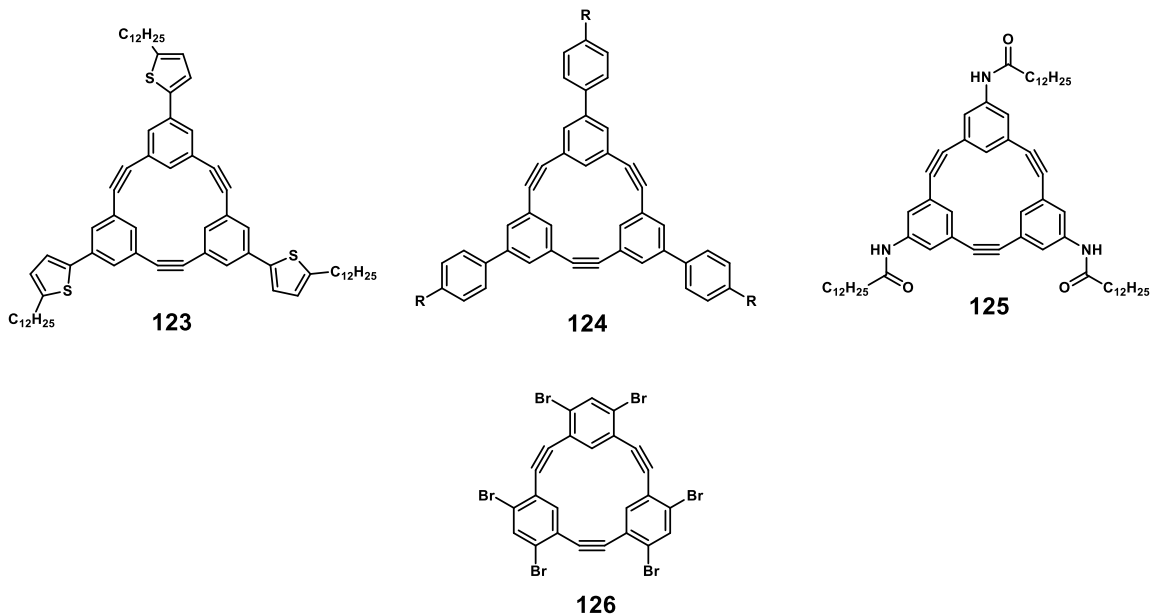


Figure 2.18 Titration curve exhibiting the transition from open-chain to folded state with increasing concentrations of RDX.

2.4.5 Future Directions

Although these experiments are a big step forward for ROAMP toward conjugated polymers, the substrate scope is still limited and fully-living conditions have not yet been established. To expand the substrate scope, monomers such as thiophene substituted **123**, phenyl-substituted **124** and aminocarbonyl-substituted **125** could be synthesized from the precursor tribromo triene **89**. The thiophene substituted monomer could lead to potentially interesting electronic properties in its respective ring-opened polymer. The phenyl substituted monomers are a simple work-around for the electron-withdrawing substituent problem; because of the lack of electronic communication between the phenyl ring and the triyne, a variety of electron-withdrawing substituents may be installed on the phenyl ring without affecting the ability to synthesize the desired respective triyne. The aminocarbonyl substituent is a variation of the amide substituent, except it is much less electron-withdrawing. Accessing this monomer will enable access to polymers with intramolecular hydrogen-bonding ability.



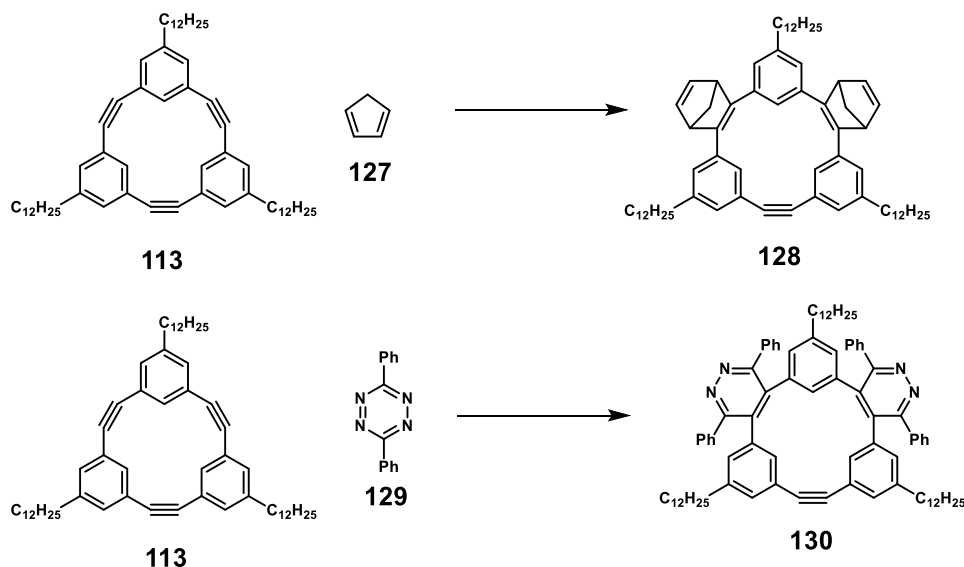
Scheme 2.22 Array of possible monomers that are highly accessible for ROAMP.

Synthesis of **126** and variously substituted monomers that would result from reaction of the aryl-bromides may allow for a fully living polymerization by influencing the sterics of the reaction. The likely reason for why ROAMP of **22** by **78** satisfies living polymerization conditions and the ROAMP of **113** by **78** does not is likely sterics: **22** is more sterically congested than **113** due to *ortho*-substitution on the phenyl rings. Therefore, monomers with *ortho*- rather than *meta*-substitutions would likely lead to fully-living conditions. Of course, a more generalized approach would be ideal. In order for **113** to achieve living ROAMP conditions, the conditions of the reaction (solvent, additives) must change or the catalyst structure must be refined to suit less sterically encumbered substrates.

Future studies might also benefit from synthesizing a variety of conjugated block copolymers from these monomer types. Block copolymers are desirable because they facilitate morphological control of polymer structure at the nanometer scale. Conjugated block copolymers are especially desirable because the performance of OLEDs relies crucially on understanding and controlling the morphology of polymers on the nanometer scale.⁸⁷

Another method to expand the substrate scope and application of this study is by employing cycloaddition in a synthesis with substituted triynes. Cyclopentadiene has been shown to undergo only two cycloadditions to unsubstituted triene **27**; after two additions, a third addition is unfavorable at room temperature (Scheme 2.23). This reactivity could be exploited toward interesting ROAMP applications. The resulting product from cycloaddition still has one strained alkyne intact. These substrates could be ring-opened, opening up an even larger library of new polymers with various applications from ROAMP. For example, polymers formed from ROAMP of **128** could undergo a subsequent ROMP reaction of the norbornene alkenes to form brush polymers. Polymers formed from

ROAMP of tetrazine-ligated **129** would certainly have interesting electronic properties. And ROAMP substrates aren't limited to monomers from the reaction of cyclopentadiene or tetrazine; those are only two of many other substrates that would potentially react *via* cycloaddition with **113** or other substituted triynes.



Scheme 2.23 Proposed synthetic scheme for possible cycloaddition reactions with **113**.

2.5 Conclusion

In summary, we have described the synthesis of a template molecule toward a library of monomers for ROMP and ROAMP. In addition, we have described the near-living ROAMP of one of those monomers toward conjugated polymers and progressed mechanistic insight into ROMP and ROAMP of conjugated monomers. Two triene monomers were effectively ring-opened by Grubb's II (**70**) or Grubb's III (**71**) catalysts. Unfortunately, the polymerizations were not well-controlled leading to non-selective backbiting and an eventual thermodynamic sink in the form of a cyclic dimer. However, these results did lead to mechanistic insights into ROMP toward PPVs. For example, a certain degree of steric encumbrance was likely necessary for effective selectivity of strained alkenes. Additionally, the dimer formed from long-reaction times could be a potential precursor for variously substituted nanographenes.

One triyne monomer, **113**, underwent a near-living polymerization with -ate catalyst **78** to form conjugated PPEs. **78** is capable of selectively ring-opening **113** in a controlled polymerization to yield high molecular weight polymers with low PDIs (1.09). Mechanistic studies revealed that the ROAMP catalyst met most of the criteria for a controlled living polymerization. The concentration of the propagating polymer was not completely constant over time, suggesting a small amount of chain-transfer or termination reactions occurring. However, in the absence of monomer, the molybdenum catalyst attached to the propagating polymer chain remained active and continued to incorporate equivalents of monomer added

sequentially to the reaction mixture, suggesting the potential for synthesis of block copolymers. These polymers showed similar folding ability to other polymers with the same backbone, studied previously, in THF with the introduction of an intercalating guest, RDX. Reactivity toward cycloaddition could also open up an even larger library of potential ROAMP monomers. The synthesis of tribromo triene **89** herein provided a modular route toward conjugated monomers for ROAMP and ROMP, unprecedented control and access to functionalized conjugated PPE polymers, and fruitful mechanistic insight in to ROMP and ROAMP toward conjugated polymers with potential applications in molecular sensing, nano-patterning and advance thin-film electronic/phonics among others.

3 Introduction: Molecular Recognition of Carboxylates and Nitro Compounds Via Hydrogen-Bonding to (Thio)Ureas

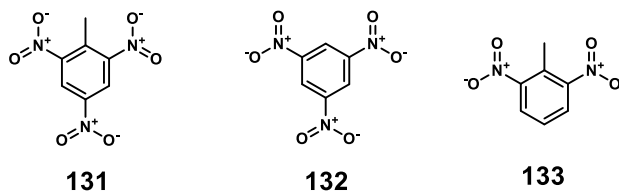
3.1 Background and Motivation

In order to optimize chemical reactivity, chemists have looked toward biological molecules that have mastered orthogonal, selective and efficient processes. These processes go beyond singular chemical interactions – large molecules bind smaller molecules tightly and specifically, and this type of binding is what drives most biological processes.⁸⁸ In the last two chapters, we investigated the orthogonal reactivity of high-energy small molecules – an important facet for expanding our understanding of chemical interaction and accessing a larger a library of materials. However, the types of supramolecular forces that lead to elaborate multi-subunit complexes in biology are still in need of further understanding in order reach similar heights with synthetic chemistry.^{89,90} The tools organic synthetic chemists could multiply if they were able to harness and manipulate small, weak forces toward much more substantial effects the way biology does.

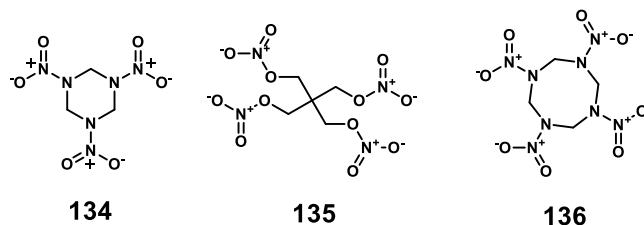
Understanding and manipulating supramolecular forces and molecular recognition has already led to important advances in molecular sensing for industry (pollution and monitoring gaseous processes), medical fields (diagnostic and therapeutic medicine), environmental monitoring and explosives sensing.⁹¹ Considerable effort has recently been directed toward the development of synthetic receptors that rely solely on hydrogen bond arrays for molecular recognition.⁹⁰ Hydrogen bonding arrays are a common feature of protein-sugar complexes, cellular self-assembly and DNA sequence recognition.⁹² In all of these biological features, multiple hydrogen bonds complement each other for a combined selective, strong binding event. Mimicking these strategies by designing hydrogen bonding abiotic receptors will help to unravel the principles of the recognition elements in these biomolecules. For this reason, a large number of receptors have been studied for selective binding of anionic fragments.⁹¹ Specifically, ionic substrates such as carboxylates are important in biological self-assembled systems and often bind in a multidentate fashion.⁹³

Hydrogen bonding arrays have also recently been described with nitro-groups – aryl(thio)ureas are commonly utilized as organocatalysts for organic transformations involving nitro-groups such as the Henry reaction, or reduction of nitroalkenes.^{94,95} Nitro groups are common features in explosive molecules such as trinitrotoluene (TNT, **131**), trinitrobenzene (TNB, **132**), dinitrotoluene (DNT, **133**), 1,3,5-trinitro-1,3,5-triazacyclohexane (**134**, RDX), pentaerythritol tetranitrate (**135**, PETN) and octahydro-1,3,5,7-tetranitro-1,3,5,7-tetrazocine (**136**, HMX) (Scheme 2.1). Catalytic reactivity of hydrogen-bond donors such as (thio)ureas, as seen for the Henry reaction, toward nitro-groups suggests potential as molecular sensors for explosives. Indeed, recent examples of electron-withdrawing (thio)ureas show high affinity for nitro-compounds.⁹⁶

a)



b)



Scheme 3.1 a) Nitro-arene explosives: TNT (**131**), TNB (**132**), DNT (**133**) b) nonaromatic explosives: RDX (**134**), PETN (**135**), HMX (**136**).

This chapter will cover the guiding principles of molecular recognition and supramolecular interaction and detail the experimental methodologies to probe such principles. We will then discuss previous efforts toward molecular recognition of nitro-explosives *via* size-exclusion and/or π - π interactions. Finally, we will detail some important highlights of nitro-group and carboxylate recognition by means of hydrogen-bond interactions with (thio)ureas.

3.2 Introduction: Principles of Molecular Recognition and Supramolecular Interaction

3.2.1 The thermodynamics of binding and the role of cooperativity and complementarity

In order to study and understand molecular recognition phenomena in solution, we need to obtain an understanding of the thermodynamic origin of binding events and how to measure and interpret the thermodynamic parameters (K_a , ΔG° , ΔH° , and ΔS°).⁹⁷ The tenets of strong supramolecular interaction are well established – thermodynamics of binding, cooperativity, preorganization, complementarity.⁹⁸ When discussing the solutes involved in binding we typically refer to the larger molecule as the host and the smaller one as the guest. The host/guest vernacular is interchangeable with biological terms such as enzyme/substrate, antibody/antigen – it is just more generally used to describe synthetic systems.⁹⁹ Solvent interaction are typically not incorporated into the equilibrium binding between host and guest; as such binding constants and related thermodynamic quantities should always be tabulated as being determined in a specific solvent and temperature. The host/guest equilibrium and the association constant, K_a are typically described by the following equations:



$$K_a = \frac{[\mathbf{H} \cdot \mathbf{G}]}{[\mathbf{H}][\mathbf{G}]} \quad (\text{E4})$$

$$\Delta G^\circ = -RT \ln(K_a) \quad (\text{E5})$$

where ΔG° describes the favorability of binding in free energy terms. It should be noted that these values are in their standard states. However in the laboratory setting we are not working with standard states; depending on whether we are working at high concentrations or low concentrations, the dominant species in the flask might be \mathbf{H} and \mathbf{G} or $\mathbf{H} \cdot \mathbf{G}$. Specifically, dilution, which is defined by increased entropy, always increases free \mathbf{H} and \mathbf{G} relative to $\mathbf{H} \cdot \mathbf{G}$.⁹⁹ In other terms, upon dilution a $\mathbf{H} \cdot \mathbf{G}$ complex will continually dissociate to \mathbf{H} and \mathbf{G} due to the favorable entropy of the entire solution.

Positive cooperativity, another thermodynamic concept, sometimes called the chelate effect, is the effect when the Gibbs free energy of binding is more negative than the sum of all Gibbs free energy changes for each individual binding interaction.¹⁰⁰ Central to this concept is relative entropic costs. One could imagine a potential binding interaction between a guest consisting of two binding sites, \mathbf{A} and \mathbf{B} , to a host (\mathbf{H}) (Figure 3.1a).⁹⁹ The entropy required for binding \mathbf{B} while \mathbf{A} is bound is partly paid by linking \mathbf{A} and \mathbf{B} . Additionally, in binding \mathbf{A} and \mathbf{B} separately to the host, the translational/rotational entropy cost is paid twice, while in binding $\mathbf{A} \cdot \mathbf{B}$ to the host it is only paid once (Figure 3.1b). Although entropic considerations are important for positive cooperativity, enthalpic considerations can negate the positive entropic considerations. For example, if \mathbf{A} is connected to \mathbf{B} in a way that once \mathbf{A} binds, conformational adjustment of the host takes place, there may be an enthalpic cost introduced due to strain induced from that conformational adjustment (Figure 3.1c).⁹⁹

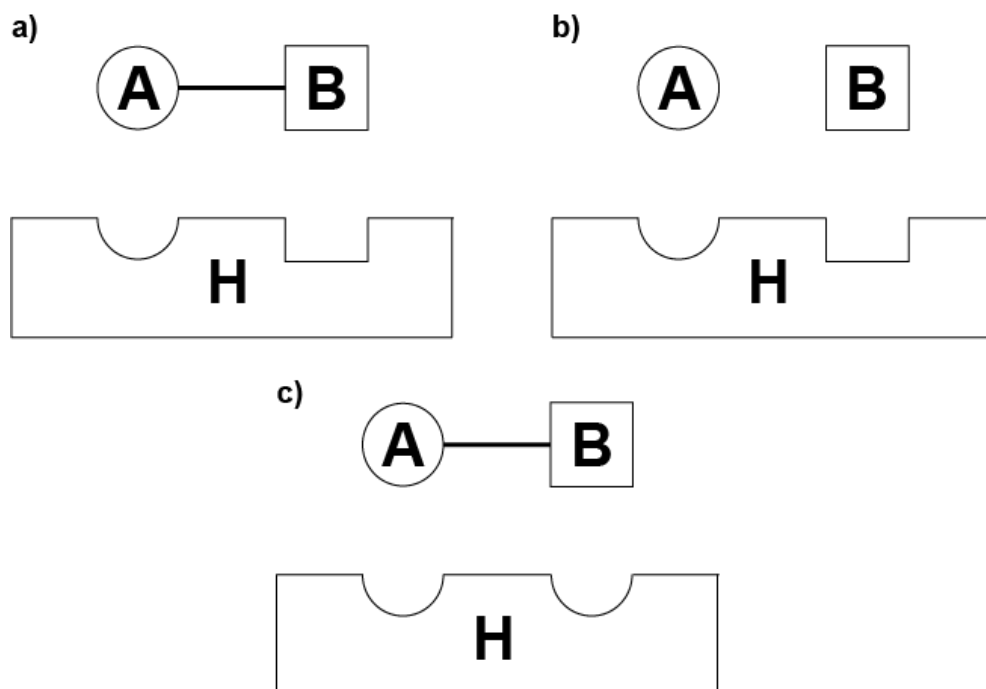


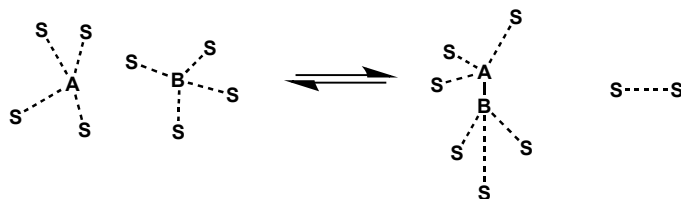
Figure 3.2 Three various ways a host, **H**, could bind to **A** and **B**. a) Preorganized and complementary bidentate, b) preorganized and complementary with no chelate, c) chelate without preorganization of complementarity.

This enthalpic penalty can be explained by the concepts of preorganization and complementarity.^{88,98} Complementarity is the concept of using a host that has proper structure complement to the structure of the “guest”. Preorganization is the notion of having the receptor be complementary prior to the binding event.⁹⁸ If there is complementarity prior to the binding event, enthalpic costs of binding are significantly reduced. In reality, preorganization is imperfect – even with advanced computational structural estimates, it is difficult to predict true complementarity, especially with multidentate interactions. Therefore, having an the ideal binding scenario is an “induced fit”: a balance of flexibility and conformational preorganization.¹⁰¹

One type of binding that allows for the design of an induced fit in molecular recognition is hydrogen-bonding. Because hydrogen-bonds are weaker than ionic bonds or covalent bonds, a certain amount of reversibility is allowed, giving structures with hydrogen-bond components a good degree of conformational flexibility.⁹⁹ Additionally, sensors that engage in hydrogen-bonding rather than ionic bonding are much more soluble in organic solvents. In organic solvents, a hydrophobic environment allows for even stronger hydrogen-bonding than in water.

One last important concept in molecular recognition, especially in regard to binding through hydrogen-bonding motifs, is the solvent. Because hydrogen-bonding is typically weaker than ionic bonding, removing any competition from solvent maximizes the host-guest hydrogen bonding interactions. Even a small amount of DMSO, a potent hydrogen bond acceptor, can be enough to disrupt a hydrogen bonding system. Generally, we can

regard all molecular recognition phenomena as a differential solvation between the reactants and products (Scheme 3.2).⁹⁹ If the solvent makes less favorable interactions with **A** and **B** separately than what is gained when **A** and **B** associate, then complex **A-B** will be preferred over a free **A** and **B**.



Scheme 3.2 Reaction diagram exhibiting the true equilibrium between free **A** and **B** and complex **A-B** that involves a solvation differential.

3.2.2 The binding isotherm and methods for monitoring complexation in supramolecular chemistry and stoichiometry of binding

Although the equations E3-E5 are rather simple, experimentally quantifying $[H]$, $[G]$ and $[HG]$ is not trivial. If the concentration of $[HG]$ is known, then the remaining concentrations can be determined by the mass balance described by equations 6 and 7.

$$[H]_T = [H] + [H \cdot G] \quad (\text{E6})$$

$$[G]_T = [G] + [H \cdot G] \quad (\text{E7})$$

where $[H]_T$ and $[G]_T$ are the concentration of uncomplexed and complexed host and guest, respectively. It is not usually possible to measure $[HG]$ (or $[G]$ and $[H]$) in supramolecular chemistry experiments, but the knowledge of these is required in order to determine K_a , unless the host and guest are in slow enough exchange for monitoring of the signals corresponding to the distinct complex and free species. In order to determine K_a , other accurate methods are available that indirectly determine the complex $[HG]$ from titration experiments. For example, NMR titration studies are typically conducted by preparing a solution of the host and then diluting a flask containing the solid guest with this solution. This produces both a host and a host/guest solution with a fixed host concentration, $[H]_T$. By adding subsequent aliquots of this host/guest stock solution to the NMR tube that initially contains only host, the concentration of the guest, $[G]_T$, is varied while the host concentration stays the same.

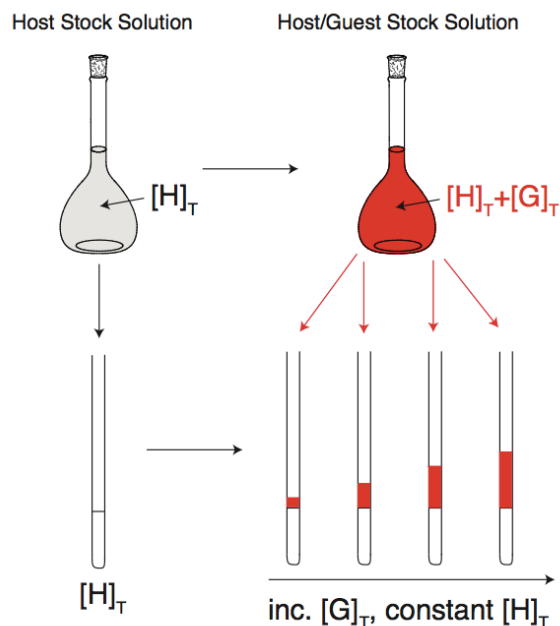


Figure 3.2 Experimental process of titration experiments to determine K_a .

During the course of this titration, the physical changes in the system are monitored by changes in the chemical shift values of protons – these changes in chemical shift value, $\Delta\delta$, can then be plotted as a function of guest added to host. When full complexation is achieved, maximum chemical shift change, $\Delta\delta_{tot}$, between the original host and host/guest complex occurs. The resulting titration curve is known as a *binding isotherm* and can be fitted into a mathematical model that is derived from an assumed equilibrium to obtain the association constant, K_a . This mathematical model used to obtain the K_a is developed from realizing that these chemical shift changes observed are correlated to the concentration of the complex, $[H \cdot G]$, as described by the general binding isotherm, equation 8.

$$\frac{[H \cdot G]}{H_T} = X_{HG} = \frac{\Delta\delta}{\Delta\delta_{tot}} = \frac{K_a[G]}{1 + K_a[G]} \quad (E8)$$

Specifically, the ratio of these two differences in chemical shift values ($\frac{\Delta\delta}{\Delta\delta_{tot}}$), known as the mol fraction of the complex, X_{HG} , is particularly helpful in solving for K_a when we combine it with the mass balance equations 6 and 7. In order to determine K_a , we first estimate a K_a value, calculate $[G]$ values for different $[G]_T$ values, and then iteratively change K_a until the theoretical isotherm matches the experimental data.¹⁰⁰ Although this can be done manually by invoking complex quadratic equations, this process is typically achieved by linear regression methods or other related shortcuts. When it comes to actual data fitting, there are two different types of software available: i) commercial software packages dedicated to fitting data to binding models such as GraphPad and 2) custom written programs that often run as macros or routines with generic data and mathematical programs such as Excel, Matlab or Mathematica.¹⁰² In Chapter 4 we choose to use a custom written program by Thordarson et al. utilizing Matlab in which the only inputs required are

the concentrations of host and guest throughout and the chemical shift values of one or two protons over the course of the titration.¹⁰² What results is a plot of the binding isotherm, which consists of X_{HG} versus changing $[G]_T$, giving a hyperbolic relationship where X_{HG} approaches 1 indicating full complexation, as well as an estimate of K_a (Figure 3.3). The quality of the fit and the estimate of uncertainty is also calculated and represented by the standard error, SE_y , and the % confidence interval, respectively.

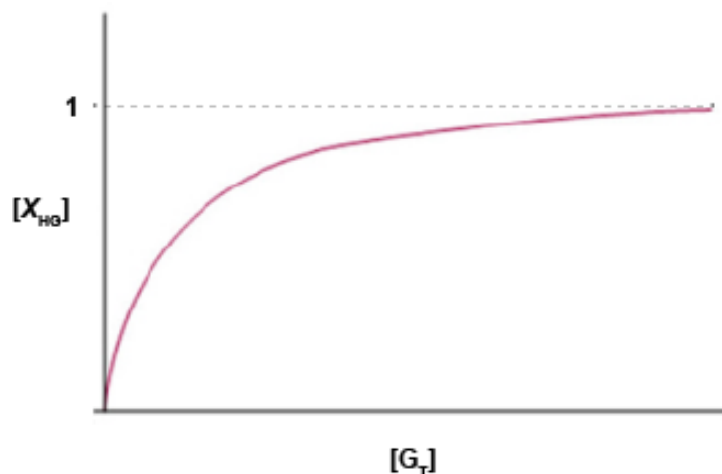


Figure 3.3 Theoretical plot of the binding isotherm.

For this non-linear regression approach in calculating K_a to be accurate, one must obtain a determination of the stoichiometry of binding of the host to guest (i.e. 1 : 1, 1 : 2, 1 : 3, etc.). The most commonly used method for determining the stoichiometry of binding is Job's method.⁹⁹ Job's method is based on the idea that the concentration of a host-guest complex, H_mG_n , is at its maximum when the $[H]/[G]$ ratio is equal to m/n . In order to determine this the mole fraction of the guest, X_G , is varied while keeping the total concentration of the host and guest constant ($[H]_T + [G]_T = \text{constant}$).¹⁰² Then, the concentration of the host-guest complex $[H_mG_n]$ is plotted against the mole fraction X_G yielding a curve where the maxima is located at $X_G = n/(m+n)$. In the case of $m = n$ (e.g. 1 : 1), X_G is equal to 0.5 at the maxima. Although this is the most commonly utilized method to determine stoichiometry, it is not always the most appropriate or reliable, especially in the case of binding stoichiometries of 1 : 2 and 2 : 1.¹⁰² Other methodologies such as 2D NMR, X-ray crystallography, and even molecular modeling are acceptable and often more accurate and reliable methodologies for determining binding stoichiometry.¹⁰²

3.2.3 Important considerations when devising a titration experiment

Before conducting a titration experiment, it must be planned meticulously to avoid common pitfalls. One of the most important considerations is to obtain as much information prior to carrying out the titration experiment on what the expected outcomes are by looking at related systems. In the following sections we will detail some systems in order to illuminate what may be required for the titrations we will conduct.

Once a good idea of the possible outcome of binding experiment is established, the choice of binding experiment, the choice in concentration of host, and which complexation shifts to monitor can be determined. Regardless of the potential binding constant 15-20 titrations is the norm – too many titrations can create uncertainty due to evaporation of solvent.¹⁰² NMR is typically used for experiments in which the K_a is expected to be less than $100,000 \text{ M}^{-1}$. At higher binding constants, the proton peaks can broaden severely thereby creating uncertainty in the complexation shift with each additional titration. In the case of a K_a likely higher than $100,000 \text{ M}^{-1}$, UV/Vis and fluorescence are recommended.

Once an experimental method is chosen, one should determine the concentration of the host most correlated to the predicted association constant. At this point it may be more helpful to introduce the concept of a dissociation constant

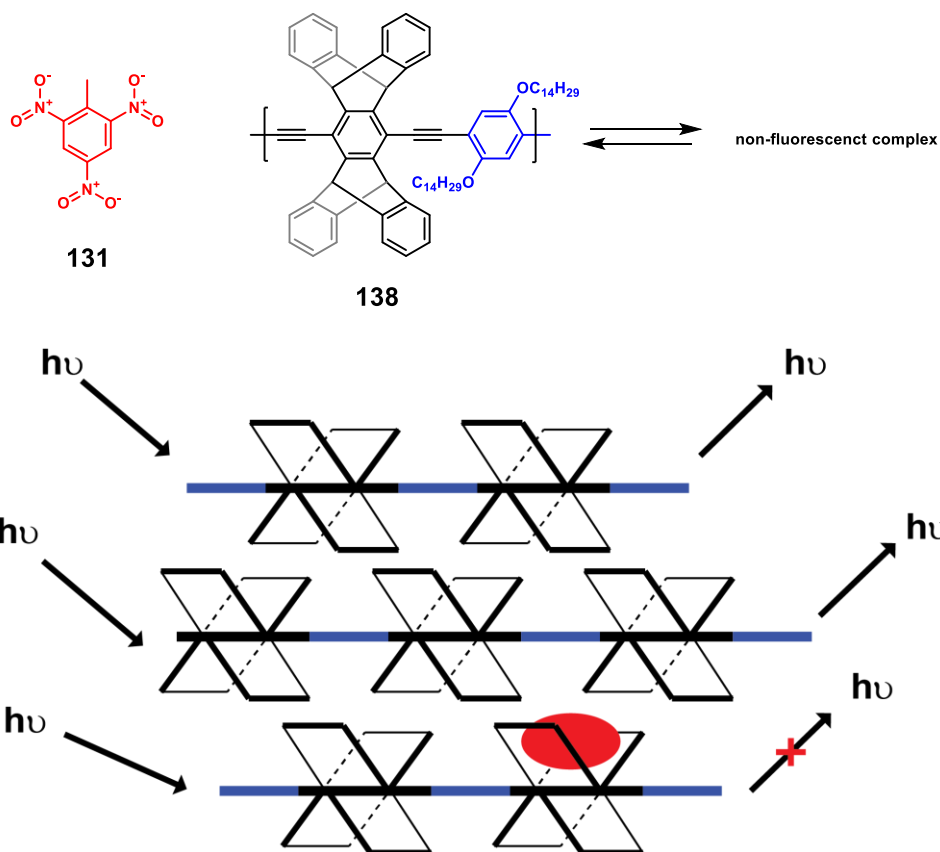
$$K_d = \frac{1}{K_a} \quad (\text{E11})$$

When $[\text{H}]_T/K_d > 100$, the non-linear portion of the resulting binding isotherm is restricted to a very small region around 1 equivalent and when $[\text{H}]_T/K_d > 1000$ there is very little “information” content in the isotherm. That is – there is so much uncertainty, that obtaining an accurate value for K_a would be nearly impossible. This is why NMR experiments are not typically performed for binding in which $K_a > 100,000 \text{ M}^{-1}$. In order to obtain accurate data, a sufficing concentration would be far below the detection limit of NMR instruments.

3.3 Methodologies for the detection of explosives containing nitro-groups

3.3.1 Detection of nitroaromatic compounds by conducting polymers

Conducting polymers, primarily polyarylene(ethylnylene)s (PAEs), have reemerged in last couple decades as viable and practical substrates for selective, observable sensors of aromatic explosive molecules.¹⁰³⁻¹⁰⁵ PAEs are ideal substrates because of their selectivity for electron-withdrawing aromatic analytes, and their ability to amplify the signal of the binding event. In a seminal study published in 1998, the Swager group reported on these sensitive, selective PAEs for nitroaromatic detection. Their substrate was a solubilized pentipycene polymer (**138**) that was chosen for its high porosity, allowing gaseous analytes to diffuse through the polymeric film (Scheme 3.3). The fluorescence of these pentipycene polymers, when spin-cast into films, responds rapidly to vapors of TNT and DNT. They found that electron-rich polymers and larger cavities are pivotal to the fluorescence response.



Scheme 3.3 Intercalation of TNT into Swager's pentipycene polymers and the resulting quenching of fluorescence.

The very high sensitivity of these PAEs is due to their molecular wire properties; excitons generated upon photoexcitations travel through polymer energy bands by Förster or Dexter mechanisms and the emissive properties of conjugated polymers are dominated by this energy migration to and exciton recombination at the local minima of their band structures.¹⁰⁶ Therefore, only a few analytes perturbing the energy migration of the PAE are needed to quench the fluorescence of an entire polymer chain.¹³ Several factors contribute to observed fluorescence quenching. The fluorescence quenching (FQ) per unit time is affected by the vapor pressure of the analytes, the exergonicity ($-\Delta G^\circ$) of electron transfer and the binding strength (K_b) (E9).

$$\text{FQ} \propto (\text{VP})[\exp(-\Delta G^\circ)^2](K_b) \quad (\text{E9})$$

These considerations explain the selectivity of fluorescence quenching: high vapor pressure (VP) substrates with poor electron-acceptors ($-\Delta G^\circ \geq 0$) show no FQ. Substrates like benzoquinone and chloranil with high vapor pressure and good electron-accepting ability did not show great FQ due to low polymer-substrate interaction (K_b). TNT, DNT, chlorodinitrobenzene, and a few other substrates showed similarly high FQ responses due to optimal $-\Delta G^\circ$, K_b , and VP. So although this methodology allows for highly sensitive detection of explosive molecules, it is not entirely selective for these types of molecules.

In later studies, Swager's group addressed this limitation.¹⁰⁴ In Narayanan et al., researchers utilized the additional benefits of non-linear optical methods involving multiphoton excited fluorescence. The technique specifically employs infrared excitation that increase eye-safety application and involves little background noise. Using two or three-photon cross sections allowed for greater sensitivity and a unique profile for TNT garnering optimal selectivity.

3.3.2 Detection of nitroaromatic compounds by molecular cavities, dendrimers, oligomers and small molecules

Nitroaromatics have been detected by various other substrates; many have looked toward smaller molecular substrates since their discrete nature allows for reliability in sensor measurements. Small molecules also have the potential to overcome other limitations with polymeric materials: inefficient, laborious synthetic schemes and non-selectivity toward other electron-poor substrates. Of these smaller molecule substrates, researchers have looked at three different types: oligomers or small molecules, molecular cavities or clefts, and dendrimers.

In 2012 Venkatramaiah et al. reported on a fluoranthene-based fluorescent chemosensor, **139**, for the detection of various explosives (Table 2.1).¹⁰⁷ Its sterically crowded phenyl rings hinder aggregation and excimer formation, and its long chains promote solubilization. They studied its detection of nitroaromatics *via* fluorescence quenching in solution, vapor and contact-mode approaches. *Via* vapor-phase detection, fluoranthene **139** performs comparably to the PPEs developed by Swager's group. Quenching response of fluoranthene is apparent with DNT, 2,5-dinitrophenol (DNP), *p*-nitrophenol (NP), and *p*-nitrotoluene (NT), but there is a very strong response to picric acid (at ppb levels) with over 66% quenching after 180s. An even more sensitive fluorescence quenching response comes from spotting concentrations of TNT or picric acid at 10⁻¹³ M on a plate coated with **139**.

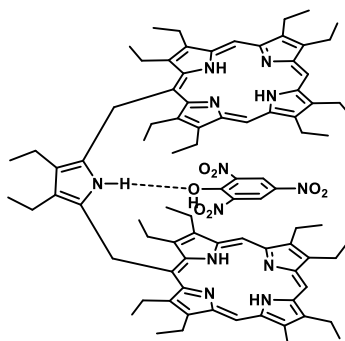
In 2012, Liu et al. developed four aromatic end-capped terthiophenes differing in end-substitutions (**140**). Liu et al. demonstrated that small molecule sensors are advantageous for their modularity – by changing the end-caps of the terthiophene, they were able to modulate the fluorescence emissions of each molecule and their potential responses to different nitro aromatic compounds. To determine the quenching ability of terthiophene by different explosive molecules, the solution quenching data, indicated by K_{SV} , must be determined. K_{SV} is calculated from the Stern-Volmer equation where I_0 and I are the fluorescence intensities of the host in presence and absence of the guest, respectively, and K_{SV} is the Stern-Volmer constant that indicates static quenching ability.

$$\frac{I_0}{I} = 1 + K_{SV}[Guest] \quad (E10)$$

Detailed studies on the doubly-pyrene end-capped terthiophene, showed high quenching ability in chloroform ($K_{SV} = 2 \times 10^4 \text{ M}^{-1}$) with very low detection limit (10⁻⁷ M) for picric acid.

Although small molecules allow for easier synthetic processing and potential modularity of sensor substrates, they are still relatively non-selective toward various nitroaromatics. One way to make sensing more selective is to differentiate guest analytes by size, H-bonding and/or π - π interactions and this requires a greater degree of structural matching in the host. Molecular clefts and cavities have been developed to enhance selectivity based on this structural matching. For example, Feng et al. developed macrocycle **141** derived from tetraphenylethylene (TPE), an organic molecule known for its ability to exhibit a novel aggregation induced emission (AIE) effect (Table 2.1).¹⁰⁸ The AIE fluorescence of TPE has previously been shown to be effectively quenched by TNT or 2,4,6-trinitrophenol (TNP) due to effective aggregate disruption. In order to endow selectivity, Feng et al. incorporated a macrocyclic component into TPE that would be only be size-selective for TNT and DNT due to a specific CH_3 - π interaction. Indeed, macrocycle **141** was selective only for TNT and DNT and showed much higher sensitivity toward TNT due to strong electrostatic interaction. By the contact TLC method, macrocycle **141** was able to detect TNT at 1×10^{-13} with a detection limit of 0.45 pg/cm^2 .

Mondal et al. employed a similar strategy for the selective detection of picric acid. In their study,¹⁰⁹ Mondal et al. synthesized bisporphyrin scaffold **142** to encapsulate explosive molecules. The bisporphyrin they developed formed a strong host-guest complex with picric acid (PA) (Figure 3.4). The strong complexation was facilitated by matching host-guest size, strong π - π interactions and H-bonding between the pyrrole N-H and the oxygen on picric acid. While not particularly sensitive, bisporphyrin **142** was effectively able to select for picric acid over every other nitroaromatic explosive.



142 • PA

Figure 3.4 Bisporphyrin cleft **142** binding to picric acid.

Ponnu and Anslyn exploited the size selectivity and ability of cyclodextrins to extract hydrophobic molecules from aqueous solutions in order to bind explosive molecules.¹¹⁰ Cyclodextrins (CDs) are spectroscopically inactive, but by incorporating a fluorescent molecule such as 9,10-bis(phenylethynyl)anthracene (BPEA), CDs can be transformed into spectroscopically active hosts that signal guest binding. Ponnu and Anslyn found that the fluorescence of the CD-BPEA inclusion complex (**143**) is quenched by TNT and tetryl, but not by non-aromatic explosives (Table 2.1). They also found that the CD-BPEA complex

had a K_{SV} 1.6 times higher than that for BPEA, suggesting that encapsulation by CD increases the quenching ability of TNT.

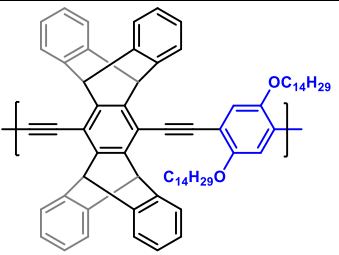
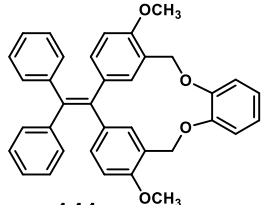
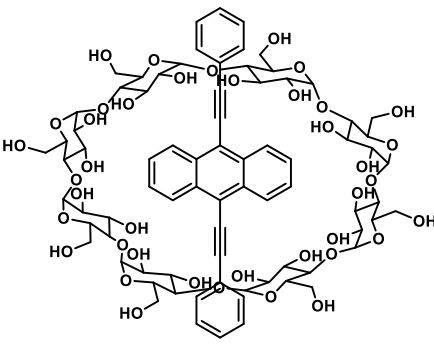
3.3.3 COFs, MOFs and nanoparticle detection of aromatic nitro compounds

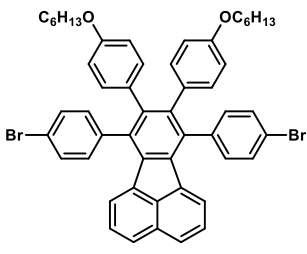
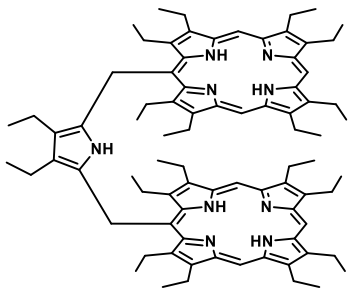
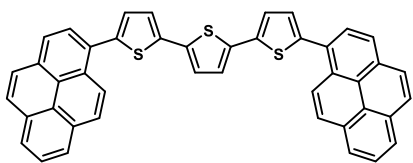
Larger molecular frameworks have also been utilized for explosives sensing. More specifically, researchers have sought to develop 2D and 3D structures such as covalent organic frameworks and metal organic frameworks because of their porous properties and strong fluorescence. These frameworks are also made from simple building blocks and the secondary structure of the framework can be made modular based on the types of building blocks involved. Having a predictable 2D or 3D network such as COFs or MOFs or certain nanoparticles is desirable for selective sensing of specific guests.^{111,112}

Zhang et al. developed one such COF (or nanoparticle) (**144**) from a polycondensation of melamine and terephthaldehyde (Table 2.1). This COF was highly sensitive to nitroaromatics, mainly due to the transfer of photoexcited electrons from the luminescence network donor to the electron-deficient nitroaromatic acceptors and strong π - π interactions between the network and the nitroaromatics. COF **144** is particularly sensitive toward detection of picric acid with a K_{SV} of 94,000 M^{-1} and a detection limit of .05 μM . The authors attribute this to hydrogen-bond formation between the secondary amine of COF and the hydroxyl of picric acid. While this methodology is not particularly selective, it demonstrates the simplicity of synthesis of COFs and their strong relative efficacy to more synthetically difficult substrates.

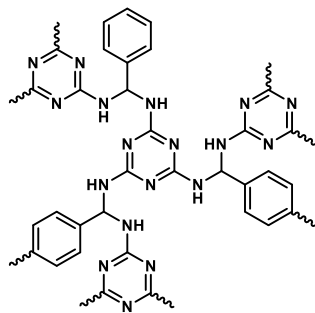
Che et al. developed a methodology that utilizes nanoporous fibers fabricated by the self-assembly of carbazole-based macrocyclic molecule **145**.¹¹³ This methodology differs from other small molecule sensor substrates because the authors were more concerned about higher order nanofiber structures interactions, as opposed to singular molecular interactions, that bestow nanoporosity for effective intercalation of analytes. The authors also tuned the side chains of the carbazole macrocycle in order to diminish oxygen gas binding to the internal surface of the nanofiber. TNT intercalation occurs by slow intercalation, and TNT can be detected at as low as 30 parts per trillion (ppt) over 400 s. DNT vapors led to 90 % fluorescence quenching within 10 s of exposure.

Table 3.1 Examples of substrates for recognition of nitroaromatic explosives.

Sensor Type	Molecule	Ref	Sensitivity by Vapor	Sensitivity by Solution	Sensitivity by Spotting	Selective For
Conjugated polymer	 <p style="text-align: center;">138</p>	[103], [104]	Detection limit 7 ppb, 75 % quenching within 60 s			TNT + 5 other substrates
Macrocyclic Cavity	 <p style="text-align: center;">141</p>	[108]	N/A	$1.37 \times 10^5 \text{ M}^{-1}$ in EtOH	Detection limit 0.45 pg/cm ³ , quenching from 10 ⁻¹³ M solution	TNT only
Cyclodextrin	 <p style="text-align: center;">143</p>	[110]	N/A	$K_{SV} = 3.53 \times 10^3 \text{ M}^{-1}$ in EtOH	N/A	TNT, tetryl

Small molecule	 <p style="text-align: center;">139</p>	[107]	<p>Detection limit – 2 ppb, 66 % quenching after 180s (Picric Acid)</p> <p>Picric acid: $K_{SV} = 1.24 \times 10^5 \text{ M}^{-1}$ in EtOH</p>	<p>Picric Acid: Detection limit 1.15 fg/cm³, 12-17 % quenching for 1×10^{-13} M solution</p>	<p>Picric acid, TNT, DNT, DNP, NP, NT</p>
Molecular cleft	 <p style="text-align: center;">142</p>	[109]	<p>$K_{SV} = 3.4 \times 10^4 \text{ M}^{-1}$ in DCM</p>	<p>Evidence of quenching from a 1×10^{-4} M in water</p>	<p>Picric acid</p>
Oligomer	 <p style="text-align: center;">140</p>	[84]	<p>Detection limit – 8.9×10^{-7} mol/L, $K_{SV} = 2 \times 10^4 \text{ M}^{-1}$ in CHCl₃</p>	<p>Picric acid, 2,5-dinitro-2,6-bis(picryl)amino pyridine</p>	

Covalent
organic
framework
(COF)



144

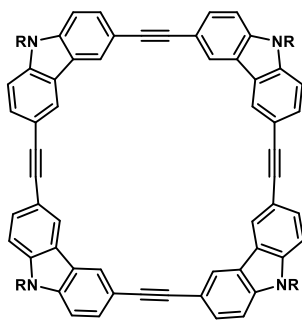
[112]

DNT:
Detection limit
= 9.8 ppb,
50 % in 10 s

Picric acid:
Detection
limit = 5×10^{-7} M, $K_{sv} = 9.4 \times 10^5$ M⁻¹
in DMF

Picric acid,
TNT,
tetryl,
DNT

Nanoporous
nanofibers



145

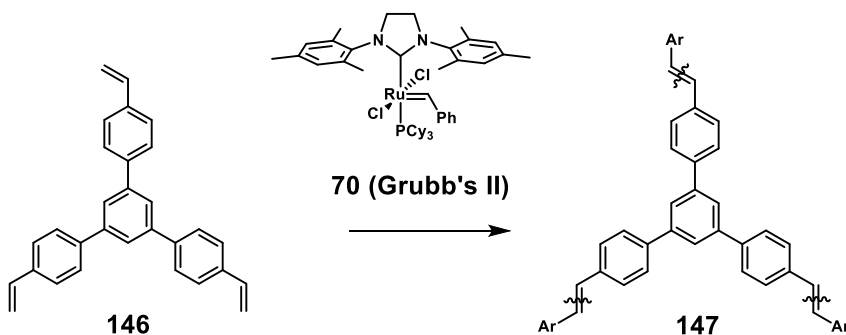
[113]

Detection
limit = 30 ppt
TNT, 15 %
emission
quenching

DNT, TNT

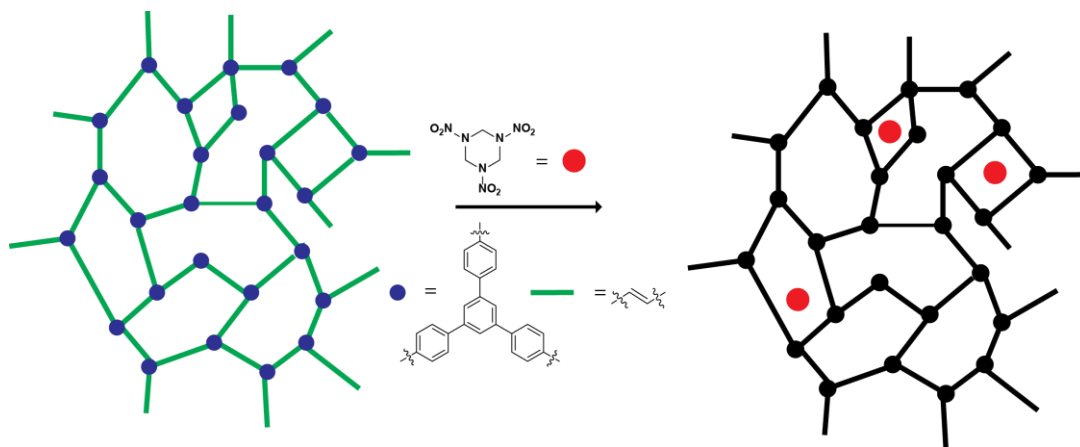
3.3.4 Indirect and “direct” detection methodologies for detection of RDX and other non-aromatic explosives

Non-aromatic explosives have been historically more difficult to detect selectively because they do not have a flat π -surface to enable π - π interactions that are normally exploited to quench fluorescence. In 2013, Dichtel’s group was the first to directly detect RDX by a conjugated polymer network synthesized from ADIMET of tris(phenylene)vinylene (TPV) (Scheme 3.4).¹¹⁴



Scheme 3.4 Formation of a TPV polymer network (**147**) from ADIMET of TPV (**146**).

While the powder formed from this reaction was insoluble, they were able to create thin films of the polymer on fused SiO_2 substrates. Fluorescence of the films decreased with exposure to a small amount of RDX (Scheme 3.5). For solution experiments, a solution of RDX in acetonitrile and MeOH was delivered to the thin films in picogram quantities. Films of TPV network that were developed for over 72 showed the greatest response. In vapor-phase studies, TPV network films showed 22 % quenching within 30 s to RDX vapor at equilibrium or subequilibrium vapor pressures. Although this study demonstrated the first example of direct RDX detection by a fluorescence quenching mechanism, the authors did not demonstrate the network’s selectivity for RDX over other nitro-explosives.

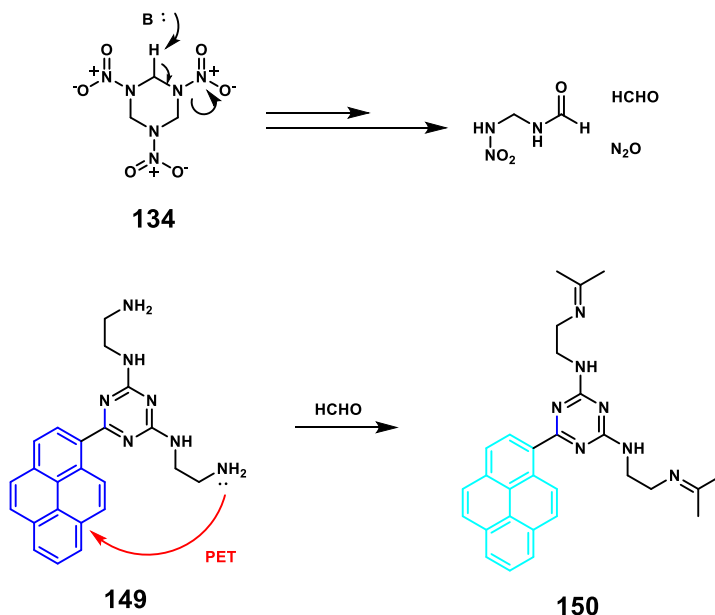


Scheme 3.5 Quenching of the TPV polymer network (**147**) by RDX.

In order to improve on this methodology, Dichtel's group developed a similar TPV network but with enhanced control by employing an allylsilane-functionalized SiO₂ substrate.¹¹⁵ TPV films grown in the presence of allylsilane-functionalized SiO₂ enabled access to more dispersed, thinner films that exhibited superior sensitivity and response rates. Specifically, these films allowed for 10 s response rates to RDX vapor exposure, and only 2-3 ag of RDX required in solution to exhibit fluorescence quenching. However, the authors still do not demonstrate exclusive selectivity over other nitro-explosives (besides HMX).

Other methods for RDX detection rely on indirect methodologies. When RDX or other nitramine explosives are exposed to UV light, they undergo photolysis and give off NO₂[·] radical or NO₂⁺ ions, respectively. Nitroaromatics do not undergo a similar photolysis, thereby allowing for selective detection of nitramine-type explosives if the photolysis byproducts, NO₂[·] radical or NO₂⁺ ions, can be detected. In 2016 Wang et al. reported on a fluorescent molecule (**148**) that when exposed to these byproducts converts into a non-fluorescence species.¹¹⁶ The authors utilized a contact TLC method for detecting nitramine explosives and they found that a thin-layer of sensor **148**, when exposed to UV light, exhibit quenching at a detection limit of 0.2 ng for RDX.

In a similar study, Mosca et al. demonstrated an even more desirable mechanism for detection of RDX (Scheme 3.6).¹¹⁷ They reported on pyrene fluorophore **149** that exhibited greater fluorescence when exposed to RDX. This was enabled by an acid-base reaction that decomposes RDX into NO₂, formaldehyde and another byproduct.

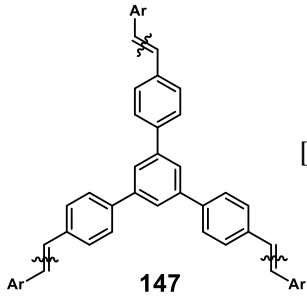
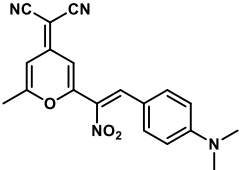
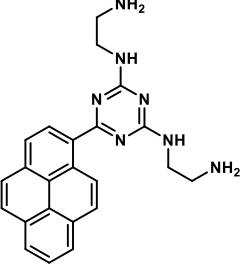


Scheme 3.6 Fluorescence turn-on event from the interaction of base-reaction products of RDX.

The resulting formaldehyde then reacts with the fluorescent substrate to form a product that is even more fluorescent, **150**, due to photo-electron-transfer that is no longer occurring. Although these studies demonstrate excellent selectivity for RDX over other non-aromatic

explosives, the byproducts that lead to the sensing event could come from other sources; formaldehyde is naturally occurring and has significant concentrations in some consumer products, and NO_x species are ubiquitous pollutants. A methodology that is selective for RDX based on its unique structural characteristics is still required for optimal selectivity.

Table 3.2 Examples of substrates for recognition of RDX or other nitramine explosives.

Sensor Type	Molecule	Ref	Sensitiv- ity by Vapor	Sensitiv- ity by Solution	Sensiti- vity by Spotting	Selective For
Polymeric Network	 147	[114]	22 % quenchin g within 30 s to RDX vapor	Detecti- on limit: 2-3 ag of RDX		Nitramines
Small molecule	 148	[116]			Detect- ion limit of 0.2 ng for RDX.	
Small molecule	 149	[117]		$K_{SV} =$ 2000 M ⁻¹ for RDX		Nitra-mines (fluor-escence turn-on), Nitro- explosives (fluo-rescence turn-off)

3.4 Ureas and thioureas as hydrogen bond donors for carboxylate and nitro-groups

3.4.1 Factors dictating the hydrogen-bond donor ability of ureas and thiourea

A developing field that may allow for better structure-based detection relies on the molecular recognition of nitro moieties *via* hydrogen bond donors, such as urea or thiourea. In one of the first examples of this phenomenon, the Jacobsen group developed a thiourea organocatalyst to catalyze the addition of hydrogen cyanide to *N*-allyl aldimines in the absence of a metal ion. Since then, the field of thiourea catalysts has expanded and many researchers have tried to optimize the catalyst for various synthetic applications. For many reactions the tetra(trifluoromethyl)-substituted *N,N'*-diarylthiourea, **151**, is the optimal

catalyst. The trifluoromethyl groups have a rigidifying effect – polarizing the adjacent hydrogen atoms and facilitating the hydrogen-bond interaction with the sulfur.¹¹⁸

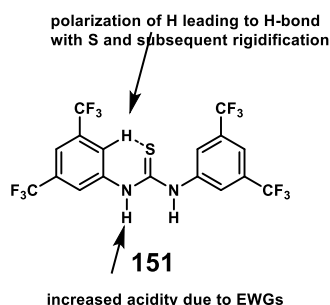
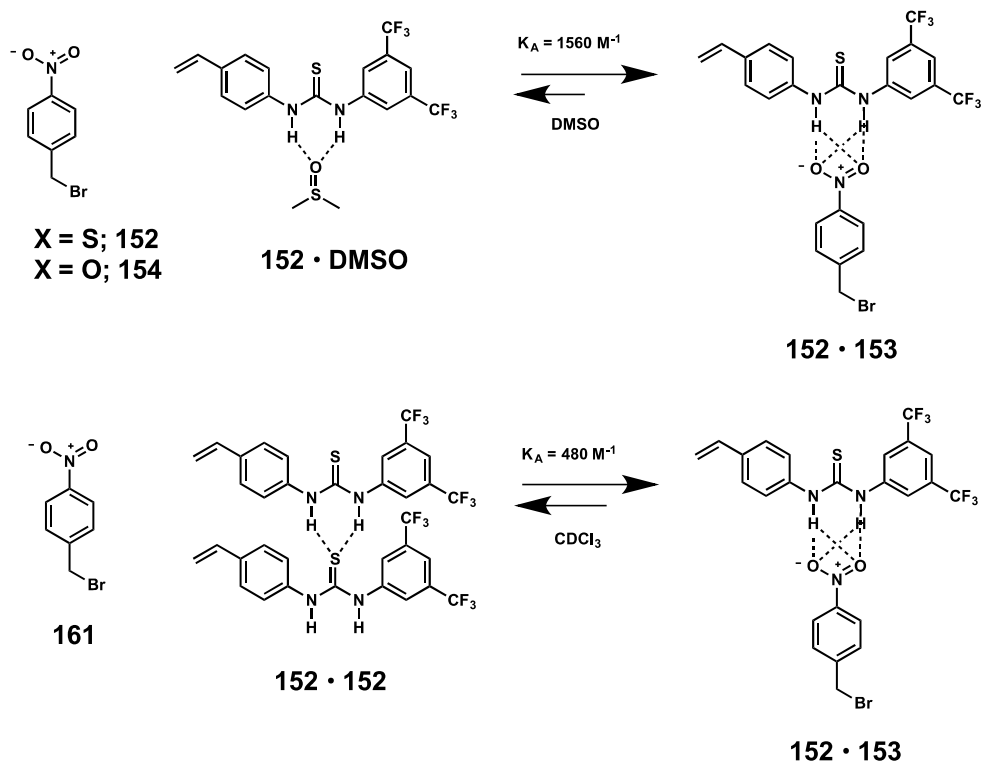


Figure 3.5 Contributions to hydrogen-bonding ability in thiourea **151**.

The rigidification and the increased acidity of the thiourea protons allow for maximum bifurcate binding of the thiourea to the desired substrate. Specifically, they allow for significant binding to isosteric anions and neutral substrates such as the nitro group. For this reason, electron-deficient *N,N'*-diaryl(thio)ureas have been exploited as substrates for nitro-group^{96,119} carboxylate-group^{92,120-123}, and anion recognition^{91,124,125}. Athikomrattankankul et al. was the first to report significant binding of (thio)ureas to nitro-groups via fluorescence binding studies. Thiourea **152** demonstrated a K_a of 1560 M^{-1} with nitroarene **153** in DMSO, while the respective urea **154** demonstrated a K_a of 470 M^{-1} with nitroarene in DMSO. These binding constants for thiourea **152** and urea **154** were actually higher than those in chloroform, a non-polar solvent. This likely has to do with more competitive self-association in non-polar solvents that is absent in polar solvent DMSO (Scheme 3.7, Table 3.3). Additionally, greater electron-withdrawing ability also leads to stronger self-association and with good hydrogen bond-acceptor, DMSO. Thus, solvent effects and self-association cannot be ignored when designing new receptors; if a substrate is too electron-withdrawing, competitive solvent or self-association effects may dominate otherwise stronger binding ability to guests of interest.



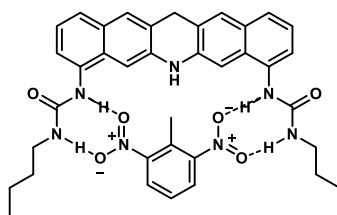
Scheme 3.7 Binding of thiourea **152** to nitrobenzene **161** in DMSO and CDCl_3 .

In 1994, Kelly et. al reported on the hydrogen-bonding ability of a much less electron-withdrawing urea, **155**, from NMR binding studies in chloroform, DMSO, and CCl_4 .¹²² In CCl_4 urea **155** demonstrated a much smaller K_a to nitrobenzene ($K_a = 180 \text{ M}^{-1}$) (**158**) than that of the ureas and thioureas studied in Athikomratankankul et al. and, in CHCl_3 and DMSO no binding was observed. This suggests that the acidity of the H-bond donor is indeed very important for optimal binding as urea **155** is much less acidic due to the lack of electron-withdrawing substituents. Although Kelly et al. did not demonstrate significant binding to nitro-compounds, they were first to suggest that the problem with nitro-groups as hydrogen-bond acceptors, compared to carboxylates, is their relatively weak Brønsted basicity. Kelly et al. also studied the binding ability of urea **155** to other isosteres, including benzoate (**156**).¹²² A complex of urea **155** with benzoate in chloroform gives a K_a of 1300 M^{-1} and 150 M^{-1} in CDCl_3 and DMSO, respectively (Table 3.3). The higher number in CDCl_3 is likely, again due to competitive binding with DMSO solvent. Another benzoate Kelly et al. studied is *m*-nitrosubstituted benzoate **157**. Binding to this benzoate in DMSO was almost $10 \times$ less than that of the unsubstituted benzoate. This is consistent with the proposition that the lower Brønsted basicity of the hydrogen-bond acceptor, the weaker the hydrogen-bond with a hydrogen-bond donor.

3.4.2 Examples and challenges of multi-site binding of compounds containing more than one nitro-group or carboxylate

Although there is copious evidence for strong hydrogen bond interaction between neutral nitro groups and bifurcate hydrogen bond donors such as thioureas, there have been few examples of the incorporation of these donors into a supramolecular system to give a geometrically specific hydrogen bond donor pattern to sense a neutral guest molecule containing NO₂ groups. However, there have been quite a few systems that have demonstrated significant multidentate binding to dicarboxylates. These systems demonstrated the need for balancing two important concepts in molecular recognition: preorganization and complementarity.

Kelly et. al, in addition to reporting on monodentate recognition ability of urea, also reported on bisurea molecule **159** that is capable of bidentate recognition of hydrogen-bond acceptors.¹²² Their motivation in such a bisurea was perceived complementarity from space-filling models of **159** with *meta*-dinitro-substituted compounds. They indicated that this potential complementarity may make **159** a suitable sensor for explosives such as TNT and RDX. Bisurea also had the advantage of having a rigid, preorganized structure that would confer strong binding, given that their inference of complementarity from space-filling models was correct. Bisurea also had the potential to enable illumination of the ability of nitro-groups to act as hydrogen-bond donors through studies of bisurea's binding to *m*-nitrobenzoate (**160**).



159•DNT

Figure 3.5 Contributions to hydrogen-bonding ability in thiourea **151**.

Bisurea **159** is only adequately soluble in DMSO and unfortunately not sufficiently soluble in CDCl₃ and CCl₄. Due to synthetic issues, a solubilized version of bisurea that would allow for binding experiments in less polar solvents could not be accessed. Unfortunately, studies of *m*-dinitrobenzene's binding to bisurea **159** showed no apparent binding in DMSO. The fact that this interaction would have resulted in 4 N–H···O bonds, suggested how poor nitro-groups are as intermolecular hydrogen-bond acceptors in solution. Isophthalate (**161**), however, forms a very strong complex, $K_a = 63,000 \text{ M}^{-1}$, with bisurea **159**. This binding is greater than $2 \times K_a$ for the binding of monourea **155** to benzoate, suggesting a great degree of positive cooperativity endowed by preorganization and complementarity. Therefore, the lack of binding of bisurea **159** to *m*-dinitrobenzene is likely not a result of a complete geometric mismatch. Another hypothesis for the poor-binding ability of *m*-dinitrobenzene was the lower basicity of the hydrogen bond-acceptors due to the conference of inductive electron-withdrawing effects from the *m*-substituted

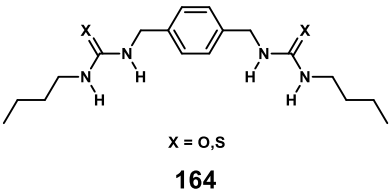
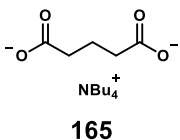
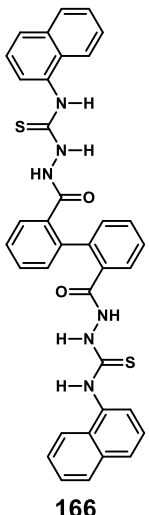
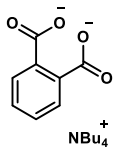
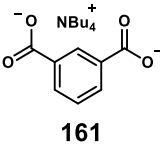
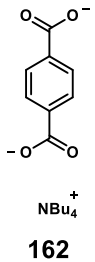
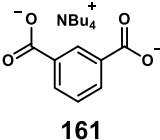
nitro group. This hypothesis was unconfirmed from the DMSO binding study of bisurea with *m*-nitrobenzoate; the binding of *m*-nitrobenzoate is comparable to that of monotopic benzoate ($K_a \sim 100 \text{ M}^{-1}$). Unfortunately, despite recent revelations in increasing the hydrogen-bond donating ability of ureas and thioureas, no one has done additional studies to understand why *m*-nitrobenzenes are such poor hydrogen-bond acceptors.

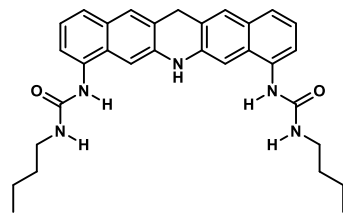
In addition to having flexibility for electron-withdrawing nature of (thio)ureas to manipulate hydrogen-bond donating ability, new sensors should also be flexible in their preorganization and rigidity. In a study that was reported a year before Kelly et al.'s study, Fan et al. proposed a more conformationally flexible bis-thiourea (**164**) for complexation of aliphatic bis-carboxylate, glutarate (**165**). Despite the conformational flexibility of the host and the guest, the K_a in DMSO of such a complex is still comparably high to that of bisurea **159** with isophthalate ($K_a = 1 \times 10^4$). This suggests that some flexibility, or an *induced fit* as proposed by Cram, is necessary for optimal binding – a host or guest that is too rigid may decrease if there is only a slight mismatch in geometry.⁸⁸

Two more recent studies have seemed to confirm this idea of a “goldilocks” zone for preorganization and rigidity. In 2007 Lin et al. proposed a thiourea-based molecular clip (**166**) for fluorescent discrimination of isomeric dicarboxylates.¹²⁶ The backbone of this molecular clip is a biphenylene unit that allows for free rotation of the orientation of the thiourea groups. This free rotation enables an induced fit for the *o*- *m*- or *p*-phthalate ions in varying geometrical fashions with similar binding constants ($K_a \sim 1\text{-}4.6 \times 10^5 \text{ M}^{-1}$). Complexation of *o*-phthalate (**163**) results in a unique complex that leads to an increase in fluorescence from excimer emission of the stacked appending naphthalenes. In 2008 Lowe et al. developed two bithiourea molecular receptors with a fused [*n*]polynorbornane backbone.¹²⁷ These receptors differed in the length of [*n*]polynorbornane to demonstrate how changing the size the cleft dictates complementarity of differing dicarboxylate guests. These receptors also contained short ethylene spacers between the [*n*]polynorbornane backbone and the thioureas to allow for an *induced fit* for optimal binding. By manipulating the backbone and including this ethylene spacer, Lowe et al. achieved a K_a of 10^6 for the complex of **167** with a terephthalate ion.

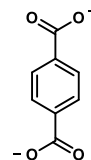
In summary, a comprehensive analysis of these studies suggests the importance of several factors in developing a new, more optimal sensor for *m*-substituted guests like RDX, nitro-explosives or isophthalate: 1) Hydrogen-bond donors should be acidic, which is dictated by the electronic effects of appending moieties or the type of donor (urea or thiourea), but not too acidic in order to mitigate self-association or solvent association, 2) to achieve an optimal *induced fit* a balance between rigidity and flexibility is required, 3) sensors should geometrically complement the guest.

Table 3.3 Array of sensors containing urea or thioureas for molecular recognition of nitro- and carboxylate analytes.

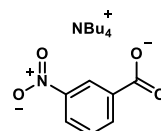
Entry	Year	Ref	Host	Guest	Solvent	Method	K_A
1	1993	[128]	 <p>X = O, S 164</p>	 <p>165</p>	DMSO	NMR	$X=S,$ 1×10^4 $X=O$ 6.4×10^2
2	2007	[126]	 <p>166</p>	 <p>163</p>	CH ₃ CN	Fluor.	1.4×10^5
				 <p>161</p>	CH ₃ CN	Fluor.	4.5×10^5
				 <p>162</p>	CH ₃ CN	Fluor.	4.7×10^5
3	1994	[122]		 <p>161</p>	DMSO	NMR	6.3×10^4



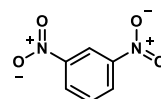
159



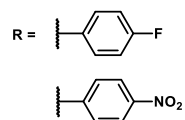
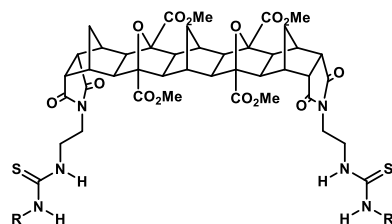
162



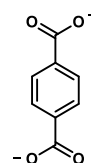
157



160



167a, 167b



162

4 2008 [127]

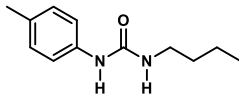
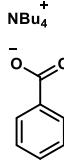
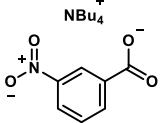
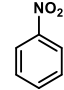
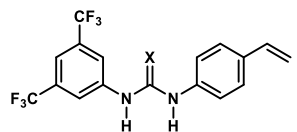
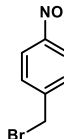
DMSO NMR 745

DMSO NMR 86

DMSO NMR 0

DMSO NMR Ar = $\text{C}_6\text{H}_6\text{F}$
 4.0×10^4

DMSO NMR Ar = $\text{C}_6\text{H}_6\text{NO}_2$
 1×10^6

5	1994	[122]	 155	 156	DMSO	NMR	150
				 157	DMSO	NMR	163
				 158	CCl ₄	NMR	180
6	2009	[96]	 X = O, S X = S; 152 X = O; 154	 153	DMSO	Fluor.	X = O 470
				DMSO	Fluor.	X = S 1.5×10 ³	
				CDCl ₃	Fluor.	X = O 270	
CDCl ₃	Fluor.	X = S 480					

3.5 Conclusion and Outlook

In this chapter, we reviewed the main concepts of molecular recognition, how the strength of binding events between a host and guest are calculated from experimental spectroscopic methods and subsequent computational analysis. We also surveyed important examples of nitro-compound recognition and examples of (thio)ureas receptors with significant binding to carboxylates and nitro-compounds. While there has been significant progress in the detection of nitro-explosives and (thio)ureas as hydrogen bond donors for nitro-groups, the two fields have not been combined effectively to address more selective detection of non-aromatic explosives.

Relevant concepts of molecular recognition, first conceived by Cram et al., include preorganization, positive cooperativity, complementarity and thermodynamics of binding. Finding a good balance of these characteristics of a host, also known as an induced fit, is important for optimal binding. Hydrogen-bonding offers a unique opportunity to exploit an induced fit – hydrogen bonds are not as strong as ionic bonds and when several are employed can often lead to an ideal host for certain guests in non-polar solvents.

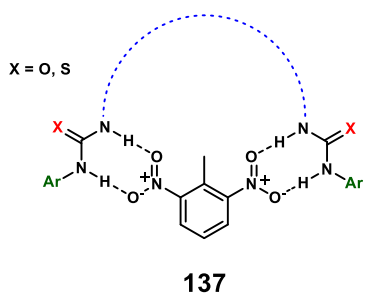
Current sensors for nitroaromatics include conductive polymers, extended polyaromatic hydrocarbons, oligomers, molecular clefts, COFs, and MOFs. Each type of system has benefits over others. Many of these sensors are very sensitive to certain groups of nitroaromatics or for picric acid specifically. Conjugated polymers are especially sensitive to very small vapor concentrations of explosives. Smaller molecules often utilize more specific interactions, but are not typically as sensitive to explosive vapors. COFs and MOFs have the advantage of being synthetically modular, but, similar to polymers, are also not very specific in binding aromatic explosives. Sensors for non-aromatic explosives, like RDX, are even less specific and direct. Because these molecules do not have a π surface, researchers have typically had to rely on byproducts of RDX for sensitive and selective detection. These methods are not sufficient – sensors that detect non-aromatic explosives for their specific structural characteristics are still needed.

Hydrogen-bond donors such as urea or thiourea seem to offer that sort of opportunity. Although, there has not been any cases of direct hydrogen-bonding to any explosive molecule, a few researchers have discovered hosts for significant binding to nitro-groups. Others have also discovered very significant binding of bisurea or bithiourea hosts to bidentate carboxylate molecules with ($K_a = 10^6$) – molecules that are isosteres of nitro-explosives. These reports further corroborate the potential of bisurea or bithiourea receptors for the direct detection of nitro explosives.

4 Modulating the Lock to Fit the Key: Extensible Host Molecular Clefts for Multi-Site Binding of Bidentate Nitro and Carboxylate Compounds

4.1 Background and Motivation

Molecular sensing is a burgeoning field because of increasing security concerns, but current methods for TNT detection rely on π - π interactions.^{13,129} Non-aromatic explosives typically require indirect methods for detection.^{114,129,130} Multidentate hydrogen bonding offers an opportunity for more direct detection of prolific explosives like RDX and PETN.¹²² Recently, Athikomrattanakul et al. demonstrated the first example of significant binding of nitroarenes to aryl(thio)ureas via a bifurcate hydrogen bonding interaction.⁹⁶ A molecular cleft, such as **137**, containing a dual hydrogen bonding array of aryl(thio)ureas, could be utilized as a host for nitro-group bearing explosives such as DNT or RDX in addition to bis-carboxylates such as isophthalate (Scheme 2.2).



Scheme 4.1 Molecular cleft design **137** for multidentate nitro-group or carboxylate recognition.

In this chapter, we report on the design and performance of a modular molecular cleft such as **137** for multidentate molecular recognition of carboxylates and nitro-compounds. This cleft, unlike most synthetic systems, will allow for facile manipulation of the important facets of molecular recognition, preorganization, complementarity, thermodynamics of binding, and cooperativity, via structural tuning of the molecular backbone (blue), hydrogen bond donors (red), and the appending aryl groups (green). After all, in order to optimize the association or “tightness” of the bind between a host and guest, these tenets need to be balanced optimally. In this chapter we will first discuss relevant concepts of molecular recognition, the precedent for detection of explosives, and the viability of (thio)ureas for molecular recognition *via* hydrogen bond interactions. We then, herein demonstrate the superior binding of molecular cleft **137** to isophthalate and the first example of direct hydrogen bonding to RDX.

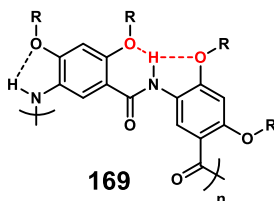
4.2 Design of a molecular cleft for bidentate intercalation of carboxylates and nitro compounds

Based on earlier studies of binding to *m*-substituted nitro or carboxylate compounds, a strategy to optimize binding to such substrates would be to develop sensors that are electronically modular, exchangeable hydrogen-bond donor types (urea or thiourea), and contain a backbone with tunable preorganization and complementarity. Such a theoretical sensor might have the structure of a molecular cleft like **137** (Scheme 4.1).

Appending aryl-groups will allow for tuning of the electronic characteristics of the hydrogen-bond donors in the molecular cleft. Appending aryl groups could also contain moieties that bestow other characteristics to the sensor (such as fluorescence). 3,5-bistrifluoromethylbenzene is a commonly appended electron-withdrawing group for (thio)ureas in catalysis. Styrene appendages have also been utilized in previously studied sensors for their ability to endow fluorescent characteristics, thereby creating the opportunity for monitoring binding by quenched fluorescence.

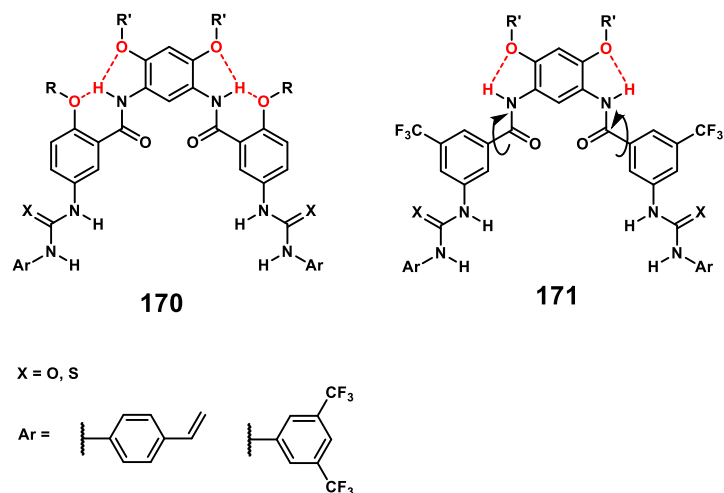
Varying the hydrogen-bond donor could also illuminate potentially important characteristics of binding. Thiourea (X=S) is more acidic than urea (X=O) and thus has been shown to have stronger binding to substrates (as well as solvent molecules).¹²⁸ Thioureas are also known to undergo weaker self-association because of the molecular orbital size mismatch between sulfur and hydrogen (at least compared to oxygen and hydrogen). This suggests that enabling variation of hydrogen bond donors could allow for tuning of their binding ability toward guests.

Implementing modularity of the preorganization, or rigidity, of the backbone of the sensor is a less intuitive problem. Although, insights might be incurred from synthetic helical foldamers.^{3,131} Helical foldamers are conformationally ordered synthetic oligomers and have been used to mimic the structure and function of biopolymers for sensing guest molecules.^{89,132} In 2005, Yuan et al. proposed a class of oligomers with backbones that adopt well-defined, crescent conformations resulting in synthetic helical foldamers.^{3,131} These oligomers are comprised of an aromatic oligoamide backbone containing benzene rings that are *meta*-linked by secondary amide groups (Scheme 4.2). Characteristic of these oligoamides is a three-center H-bond between two alkoxy groups and the amide H that results in an immutable conformation (Scheme 4.2).^{3,131}



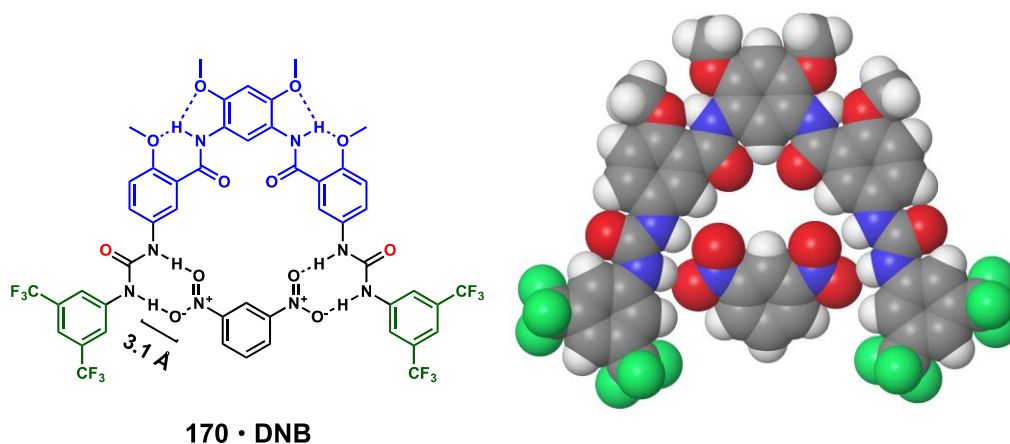
Scheme 4.2 *m*-Linked oligoamide demonstrating the rigidifying three-center H-bond (red).

This three-center hydrogen bond could be exploited to confer the desired conformational modularity to the backbone of molecular cleft **137**. Two variations of **137** employing either the aforementioned three-center hydrogen bond (**170**) or only a two-center hydrogen bond (**171**) would result in differing rigidity. Without the additional alkoxy substituent, **171** could have an *m*-CF₃ installed to increase the electron-withdrawing nature and thereby the hydrogen-bond donating abilities of the (thio)ureas in the molecular cleft. Another advantage of these amide structures is that the alkoxy groups allow for the inclusion of solubilizing R groups; solubilization is required in order to conduct binding studies in non-polar solvents.



Scheme 4.3 *m*-Linked oligoamide demonstrating the rigidifying three-center H-bond (red).

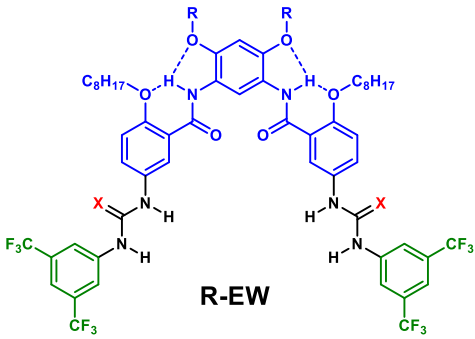
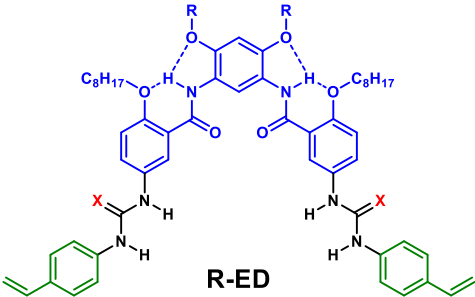
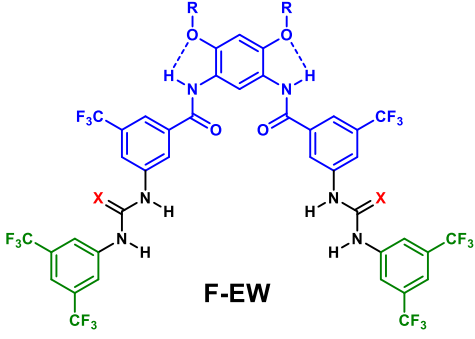
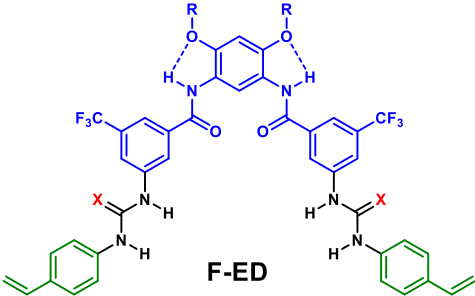
These molecular cleft receptors are similar to bisurea **159** in their geometrical distribution of the (thio)ureas. We calculated a B3LYP/6-31G* optimized structure of **170**·DNB ($X = S$, $Ar = C_8H_3F_6$, $R = Me$) in order to check for complementarity (Scheme 4.4).



Scheme 4.4 B3LYP/6-31G* optimized structure of a complex of **170** with 1,3-dinitrobenzene.

The B3LYP/6-31G* indicates very good complementarity; a typical N–H···O total bond length (combined N–H and H···O bond lengths) found in protein secondary structures is ~ 3.0 Å and the N–H···O total bond lengths in the optimized structure is 3.1 Å. Given this conclusion, we sought out to synthesize derivatives of **170** and **171** with two variations in hydrogen bond donors ($X = O$ and S) and two variations in aryl groups ($Ar = C_8H_3F_6$, and $Ar = C_8H_8$) for a total of 8 different sensors.

Table 4.1 Array of sensors for molecular recognition with varied aryl groups, H-bond donors and backbones. **R** indicates a rigid backbone, **F** indicates a flexible backbone, **EW** indicates electron-withdrawing appending aryl groups, **ED** indicates electron-donating appending aryl groups. **O** indicates urea and **S** indicates thiourea.

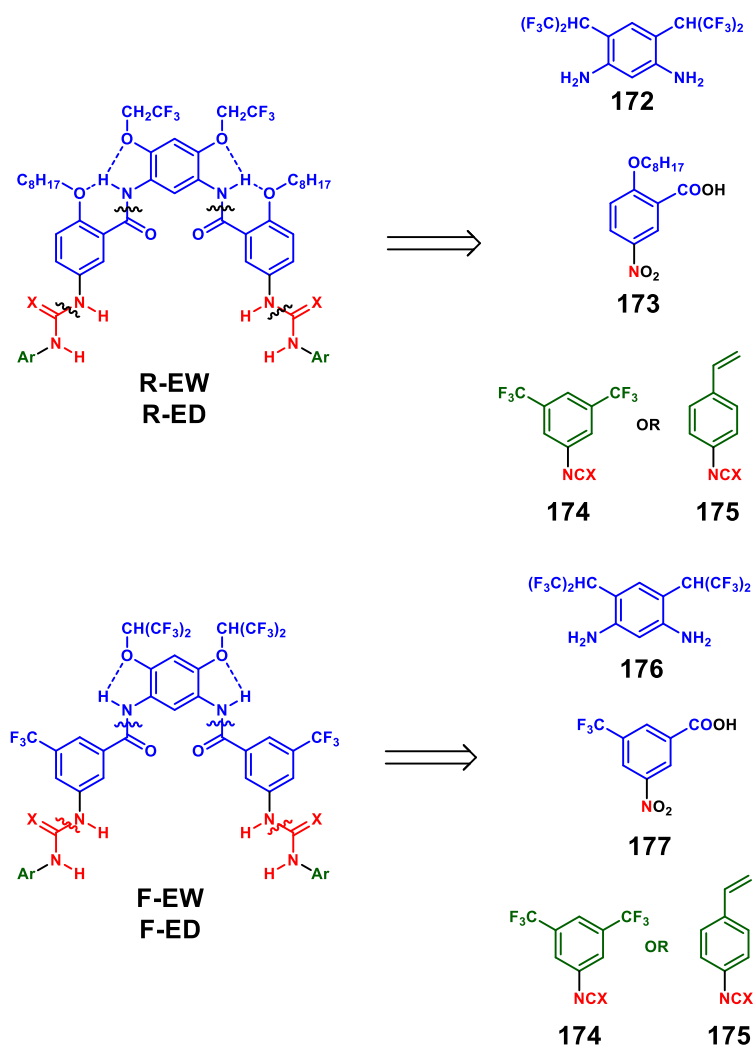
Molecule Receptor	Sensor Type	Substituents
 <p style="text-align: center;">R-EW</p>	Rigid, electron-withdrawing	X = O,S R = CH ₂ CF ₃
 <p style="text-align: center;">R-ED</p>	Rigid, electron-donating	X = O,S R = CH ₂ CF ₃
 <p style="text-align: center;">F-EW</p>	Flexible, electron-withdrawing	X = O,S R = CH(CF ₃) ₂
 <p style="text-align: center;">F-ED</p>	Flexible, electron-donating	X = O,S R = CH(CF ₃) ₂

The choice in R groups between the **R** (rigid) sensors and the **F** (flexible) sensors is justified by synthetic ease – long all-carbon alkoxy groups in the diamino precursors lead

to high susceptibility to oxidation in air. Adding trifluoromethyl groups to the alkoxy chains makes the diamino precursors much more stable in air at room temperature. The **F** sensors have an additional CF₃ in their R groups for added solubility since they do not have the other long-chain alkoxy group the **R** sensors have. These variations in flexibility, hydrogen-bond type, and hydrogen-bond ability allow for deeper insight into the characteristics of molecular recognition of ditopic *m*-substituted analytes.

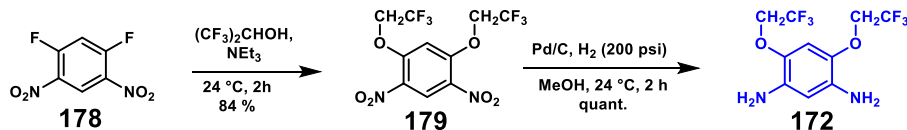
4.2.1 Modular synthesis of molecular clefts for recognition of nitro- and carboxylate-analytes

The rigid (**R**) and flexible (**F**) molecular clefts have reasonable synthetic disconnections that result in two similar, modular synthetic pathways with differing components (Scheme 4.5).



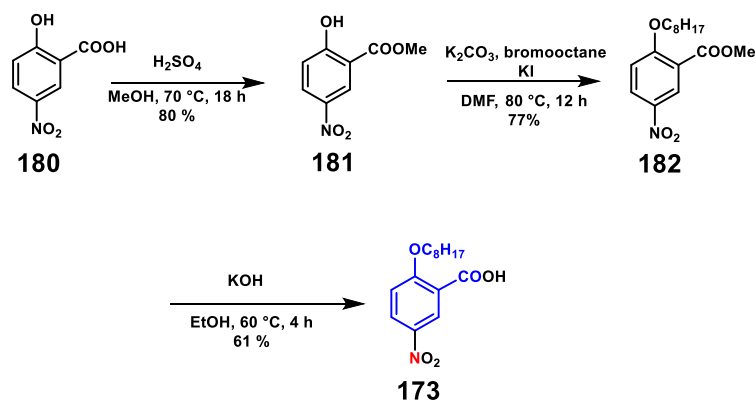
Scheme 4.5 Retrosynthetic disconnections for the **R** and **F** molecular clefts.

The synthesis of **R-EW** and **R-ED** began with a nucleophilic aromatic substitution; 2,2,2-trifluoroethanol underwent two nucleophilic attacks, with the addition of triethylamine, on 1,5-difluoro-2,4-dinitrobenzene (**178**) to give alkoxy-substituted arene **179**. High pressure hydrogenation of **179** in the presence of Pd/C at room temperature then lead to diamine **172** as a stable light-purple solid in quantitative yield (Scheme 4.6).



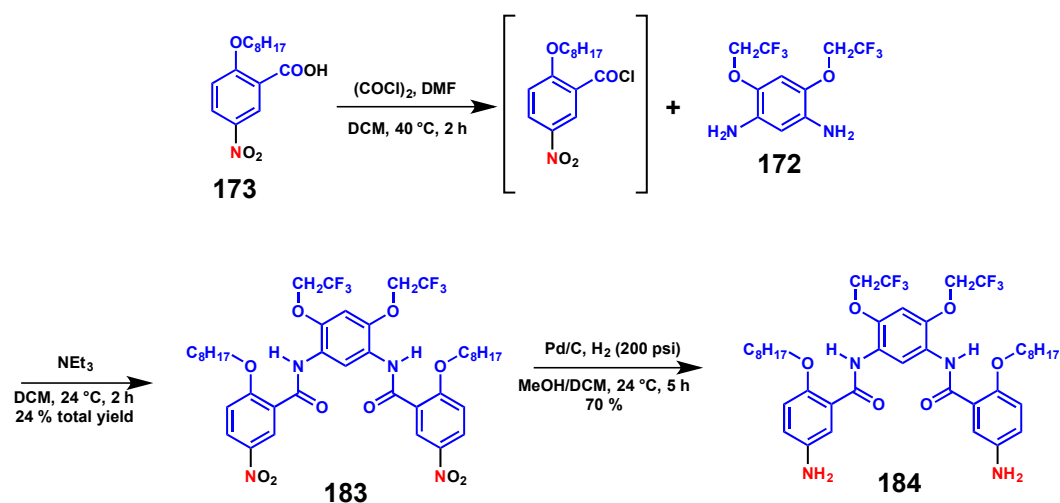
Scheme 4.6 Synthesis of backbone component **172**.

The synthesis of the second component of the backbone of **R-EW** and **R-ED** began with methyl esterification of 5-nitrosalicylic acid (**180**) in the presence of sulfuric acid and methanol to form methyl-ester (**181**). Subsequent nucleophilic attack of **5** in the presence of K_2CO_3 on 1-bromooctane resulted in ester **182**. Lastly, saponification of **182** with KOH in EtOH at 60 °C gave backbone component **173** (Scheme 4.7)



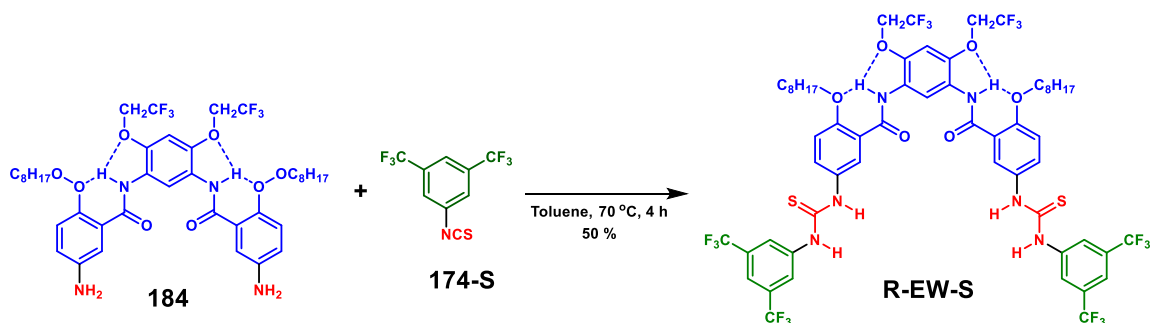
Scheme 4.7 Synthesis of backbone component **173**.

The next reactions combined both component **172** and **173** to form the backbone of molecular receptors **R-EW** and **R-ED**. To create the pivotal amide linkages, **173** was converted to its acid chloride *via* reaction with oxalyl chloride and DMF. The acid chloride was then used without purification and added to diamine **172** in DCM with triethylamine to form rigidified bisamide **183**. **183** was subsequently reduced *via* high pressure hydrogenation in the presence of Pd/C to give diamine **184** (Scheme 4.8).



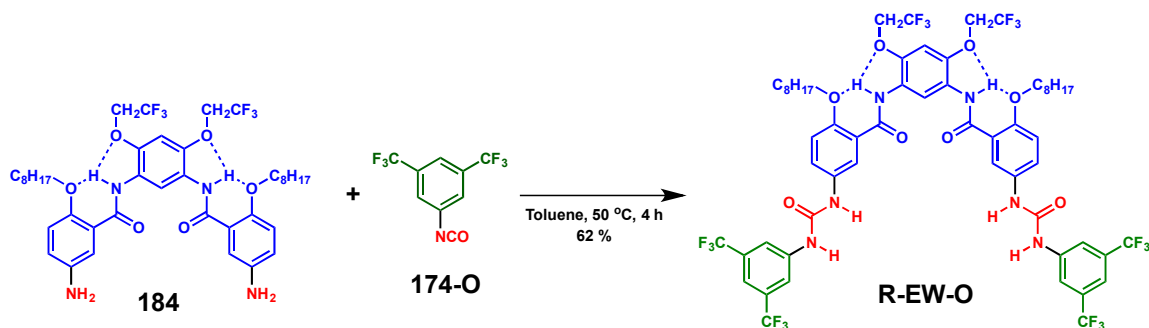
Scheme 4.8 Synthesis of the backbone of R-EW and R-ED (**184**)

The last step involved reaction with either an aryl thioisocyanate or aryl isocyanate to generate the respective thioureas or ureas. To synthesize **R-EW-S**, **184** was heated to 70 °C in toluene with 3,5-bistrifluoromethylphenyl isothiocyanate (**174-S** [X = S]). Bis-thiourea molecular cleft **R-EW-S** was then formed in 50% yield and isolated as a grey solid (Scheme 4.9).



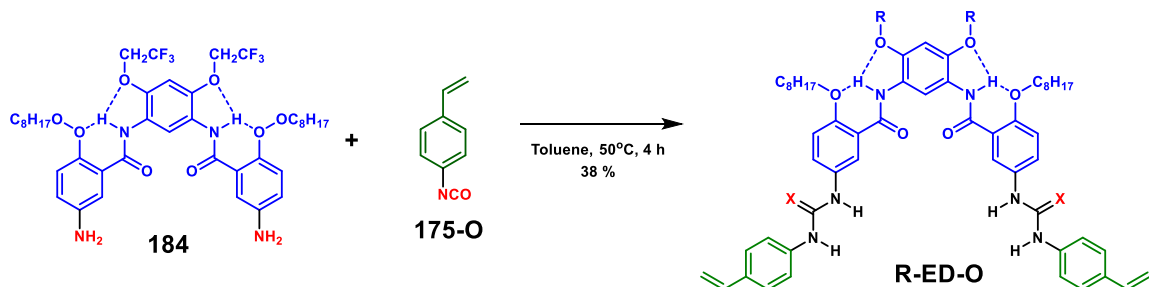
Scheme 4.9 Synthesis of rigid, electron-withdrawing, bis-thiourea molecular receptor **R-EW-S**.

To synthesize **R-EW-O**, **184** was added to 3,5-bistrifluoromethylphenyl isocyanate (**174-O** [X = O]) in toluene at room temperature. After stirring at 50 °C for 4 h, bis-urea molecular cleft **R-EW-O** was formed in 62% yield and isolated as a colorless solid (Scheme 4.10).



Scheme 4.10 Synthesis of rigid, electron-withdrawing, bis-urea molecular receptor **R-EW-O**.

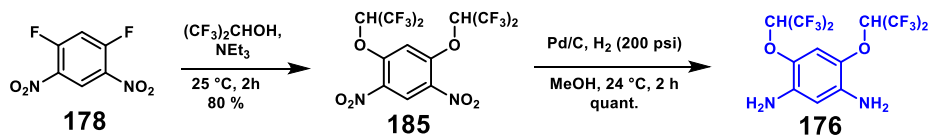
To synthesize **R-ED-O**, **184** was added to 4-vinylphenyl isocyanate (**175-O** [X = O]) in toluene at room temperature. After stirring at 50 °C for 4 h, bis-urea molecular cleft **R-ED-O** was formed in 62% yield and isolated as a red-orange solid (Scheme 4.11)



Scheme 4.11 Synthesis of rigid, electron-donating, bis-urea molecular receptor **R-ED-O**.

Unfortunately, attempts to synthesize **R-ED-S** were unsuccessful. **175-S** could not be accessed; all attempts at synthesizing **175-S** from 4-aminostyrene did not result in the desired isothiocyanate.

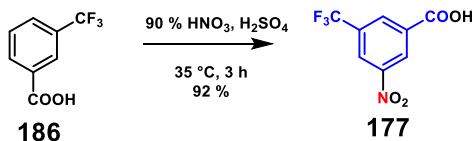
The synthesis of the **F-EW** and **F-ED** sensors began with a nucleophilic aromatic substitution; 1,1,1,3,3,3-hexafluoro-2-propanol underwent two nucleophilic attacks, with the addition of triethylamine, on 1,5-difluoro-2,4-dinitrobenzene (**178**) to give alkoxy-substituted arene **185**. High-pressure hydrogenation of **185** in the presence of Pd/C at room temperature then lead to diamine **176** as a stable light-purple solid in quantitative yield (Scheme 4.12).



Scheme 4.12 Synthesis of backbone component **176**.

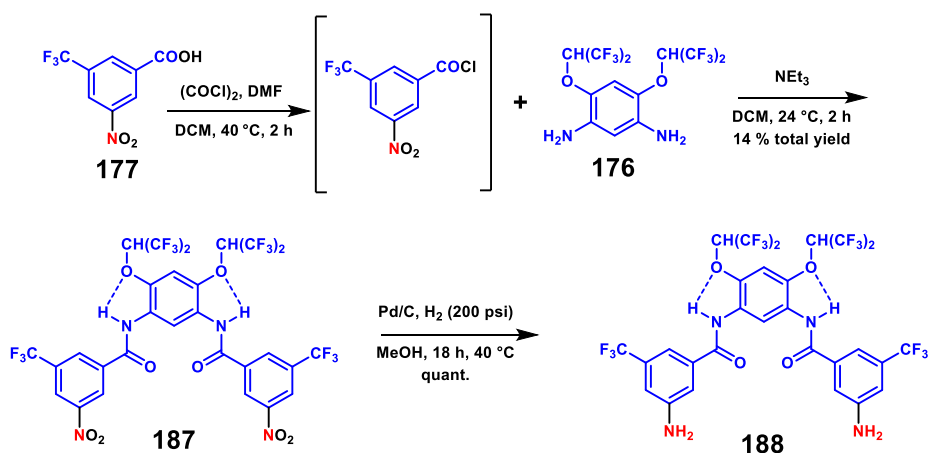
To synthesize the second component of the backbone of the **F-EW** and **F-ED** sensors, **177**, nitration of benzoic acid **186** was conducted. **186** was added to a cooled solution of

fuming nitric acid and sulfuric acid and then stirred at 35 °C for 3 h to form **177** (Scheme 4.13).



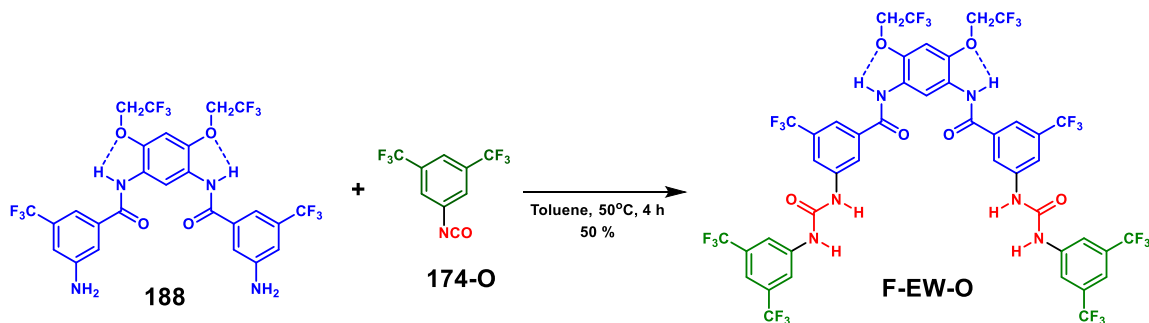
Scheme 4.13 Synthesis of second backbone component **177**.

The next reactions combined both component **177** and **176** to form the backbone of molecular receptors **F-EW** and **F-ED**. To create the pivotal amide linkages, **177** was converted to its respective acid chloride *via* reaction with oxalyl chloride and DMF. The acid chloride was then used without purification and added to diamine **176** in DCM with triethylamine to form bisamide **187**. **187** was subsequently reduced *via* high pressure hydrogenation in the presence of Pd/C to give diamine **188** (Scheme 4.14).



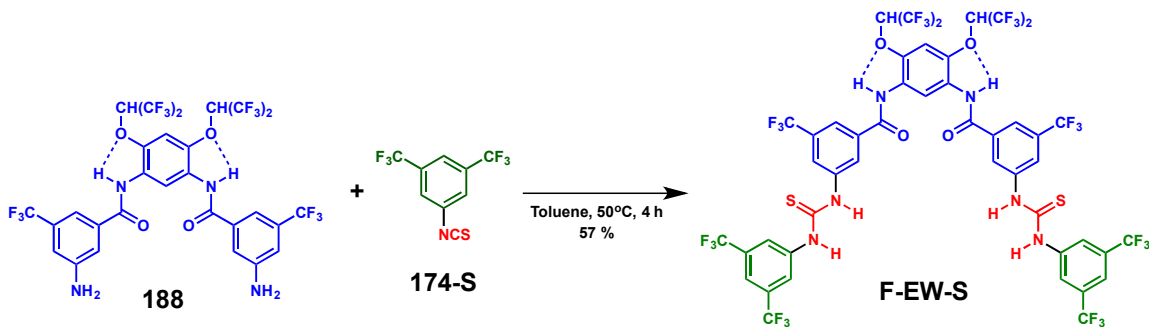
Scheme 4.14 Synthesis of the backbone of **F-EW** and **F-ED** (**188**)

To synthesize **F-EW-O**, **188** was heated to 50 °C in toluene with 3,5-bistrifluorophenyl isocyanate (**174-O** [X = O]) for 4 h. Bis-urea molecular cleft **F-EW-O** was then formed in 50% yield and isolated as a grey solid (Scheme 4.15).



Scheme 4.15 Synthesis of conformationally flexible, electron-withdrawing, bis-urea molecular receptor **F-EW-O**.

To synthesize **F-EW-O**, **188** was heated to 50 °C in toluene with 3,5-bistrifluorophenyl isothiocyanate (**174-S** [X = S]) for 4 h. Bis-thiourea molecular cleft **F-EW-S** was then formed in 57% yield and isolated as a light-brown solid.



Scheme 4.16 Synthesis of conformationally flexible, electron-withdrawing, bis-thiourea molecular receptor **F-EW-O**.

Unfortunately, attempts to synthesize both **F-ED-S** and **F-ED-O** were unsuccessful. Synthesis of **F-ED-S** was not accomplished because access to isothiocyanate **175-S** was not feasible. **F-ED-O** was not synthesized because no reaction occurred between **175-O** and **188** when attempting similar reaction conditions to those in the synthesis of the other molecular clefts. This is likely because isocyanate **175-O**, the electrophile in the reaction, is too electron-rich and **188**, the nucleophile, too electron-poor for an energetically favorable reaction to occur between them.

4.2.2 Determination and comparison of binding of receptors with isophthalate

With five sensors synthesized, we first sought to conduct NMR binding studies with isophthalate (**161**) because of its much stronger binding ability compared to that of nitro-compounds; stronger binding association will give a better signal toward any emerging patterns of the molecular recognition of *m*-substituted ditopic analytes. NMR studies were conducted by preparing a solution of the host, which is one of five of the sensors, with known concentration (usually around 0.5×10^{-3}) and then diluting a flask containing the solid guest, tetrabutylammonium isophthalate (**161**), with this solution. This produced both a host and a host/guest solution with the same concentration of host. By adding subsequent aliquots of this host/guest stock solution to the NMR tube that initially contains only host, the concentration of the guest, $[G]_T$, was increased while the total host concentration, $[H]_T$ stayed the same, as dictated from section 3.2.

We first conducted the experiment outlined above with sensor **R-EW-O** and tetrabutylammonium isophthalate in DMSO and analyzed the data accordingly using the nonlinear regression approach outlined above with the aid of MATLAB and a custom written program developed by Thordarson.¹⁰² Likely because of the strong binding event, the urea protons (in blue and red) in **R-EW-O** broadened with the first addition of guest to

the extent that they are no longer observable. This suggested a slow exchange phenomenon which is characteristic of a strong binding association. Additionally, the red urea proton signal underwent more broadening and shifts more significantly, indicating a stronger electrostatic interaction due to its proximity to the 3,5-bistrifluoromethylbenzene appendage (Figure 4.1). Protons not involved in the binding event (in green) underwent faster exchange and their change in chemical shift could be observed in the spectrum from each successive addition of guest. For this reason, these are the protons that we analyzed for the determination of binding.

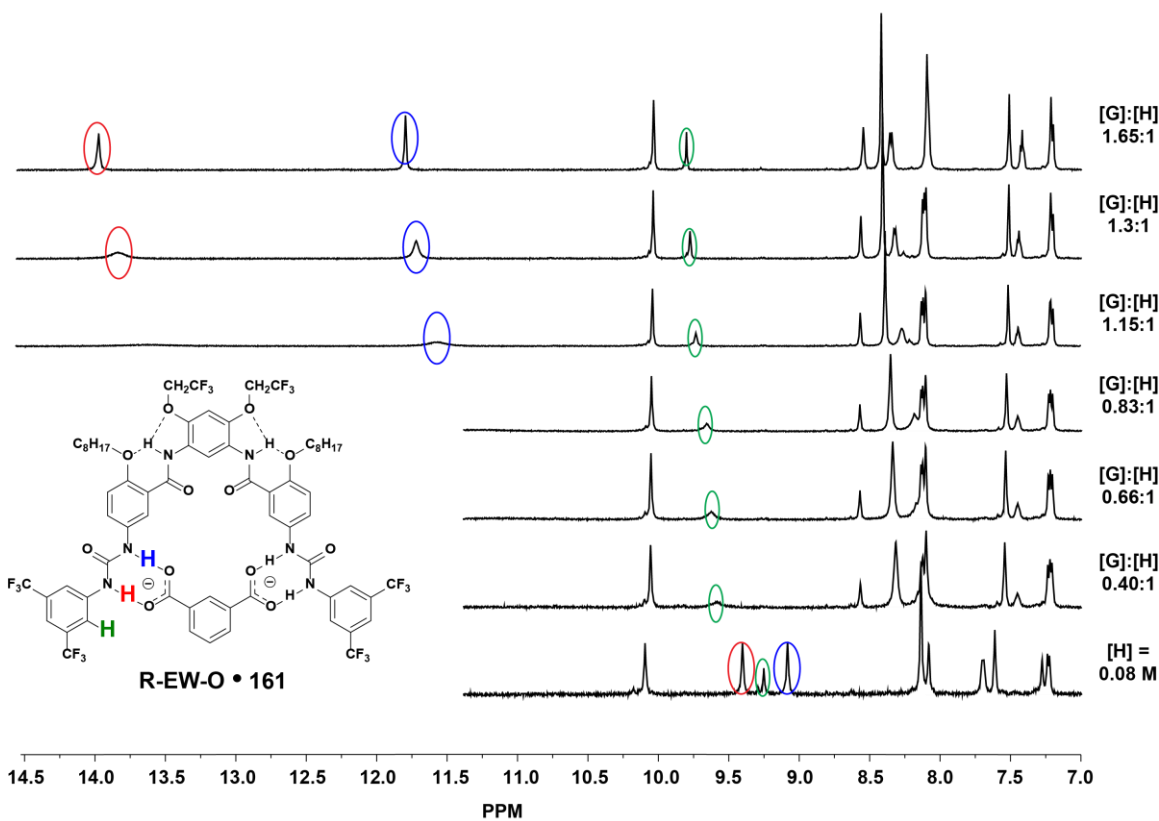


Figure 4.1 Change in chemical shifts of protons in **R-EW-O** due to increase complexation with **161** in DMSO.

After conducting the experiment above and running analysis through MATLAB, the estimated K_a of binding was calculated to be $18,000 \text{ M}^{-1} (\pm 24 \%)$, which is similar to that of isophthalate and sensor **159** in Kelly et. al (Figure 4.2).

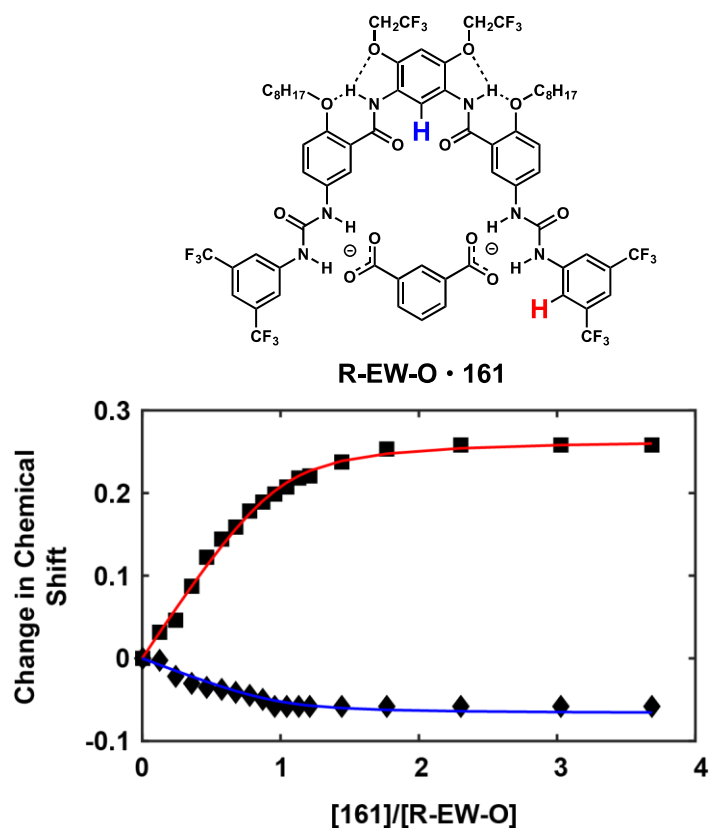


Figure 4.2 Non-linear regression model determined binding isotherm for binding of **R-EW-O** to **161** in DMSO.

A similar binding experiment was conducted in chloroform, and the results from this experiment indicated a much higher K_a , albeit with a greater error in the measurement, of $88,000 M^{-1}$ (Figure 4.3). This was also apparent from the sharper binding isotherm; the non-linear portion of the binding isotherm was restricted to a much smaller area right around 1 equivalent of guest added, typical of stronger associations. Unfortunately, because of broadening of the signals in chloroform (likely due to self-association), obtaining the correct integrations made data analysis imperfect – this was likely the largest contribution to the experimental uncertainty (Figure 4.4).

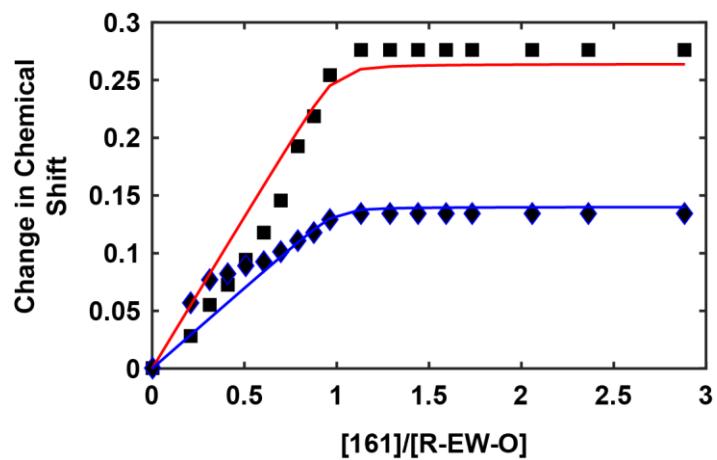
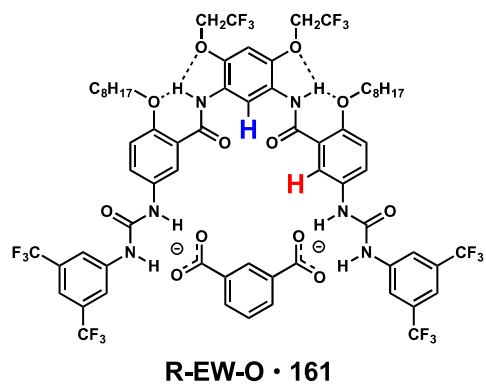


Figure 4.3 Non-linear regression model determined binding isotherm for binding of **R-EW-O** to **161** in chloroform.

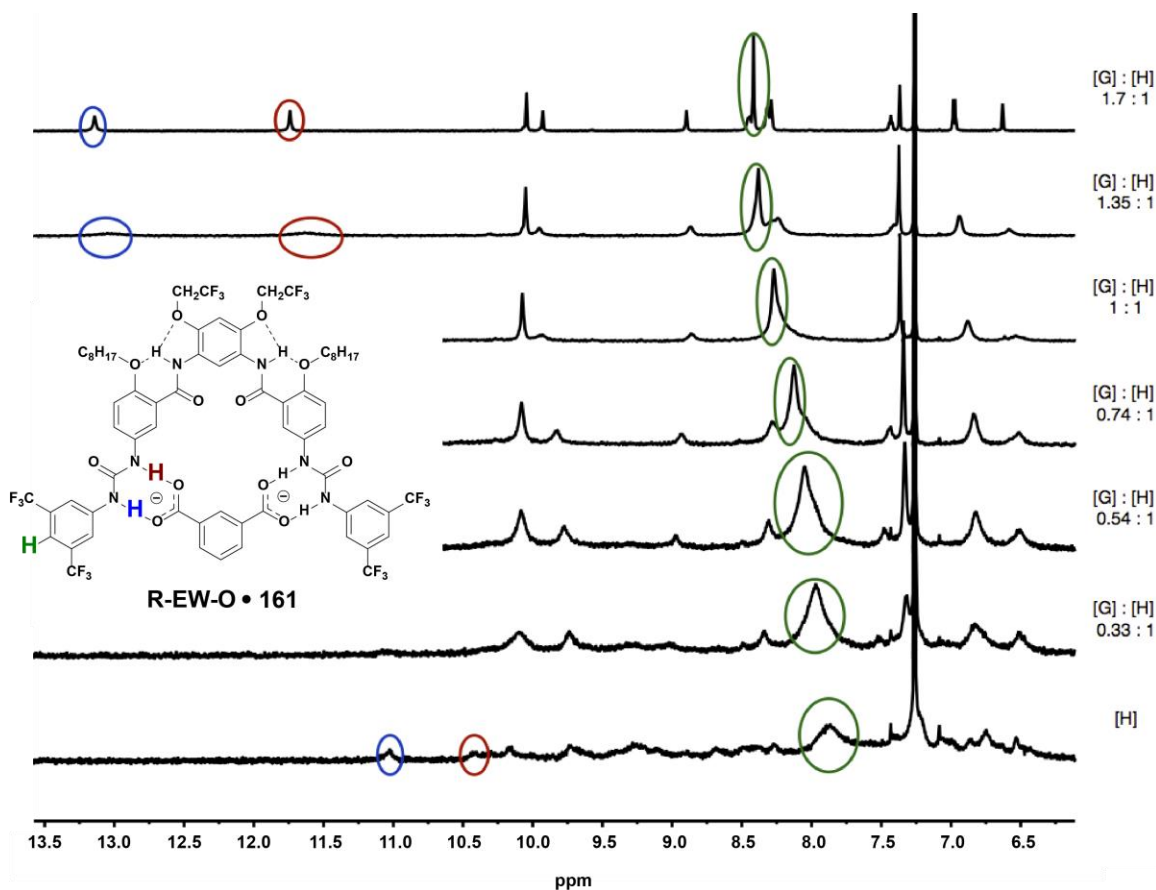


Figure 4.4 Change in chemical shifts of protons in **R-EW-O** due to increase complexation with **161** in chloroform.

To understand the role of hydrogen-bond donor in binding of these substrates, we also conducted binding studies with **R-EW-S** in DMSO and CDCl_3 . **R-EW-S** showed significantly higher binding in DMSO compared to **R-EW-O**. A K_a of $112,000 \text{ M}^{-1}$ is as large as some of the most significant sensors to isophthalate (Figure 4.5). The stronger binding of **R-EW-S** in DMSO likely has to do with the increased H-bonding donating ability of thioureas, as predicted.

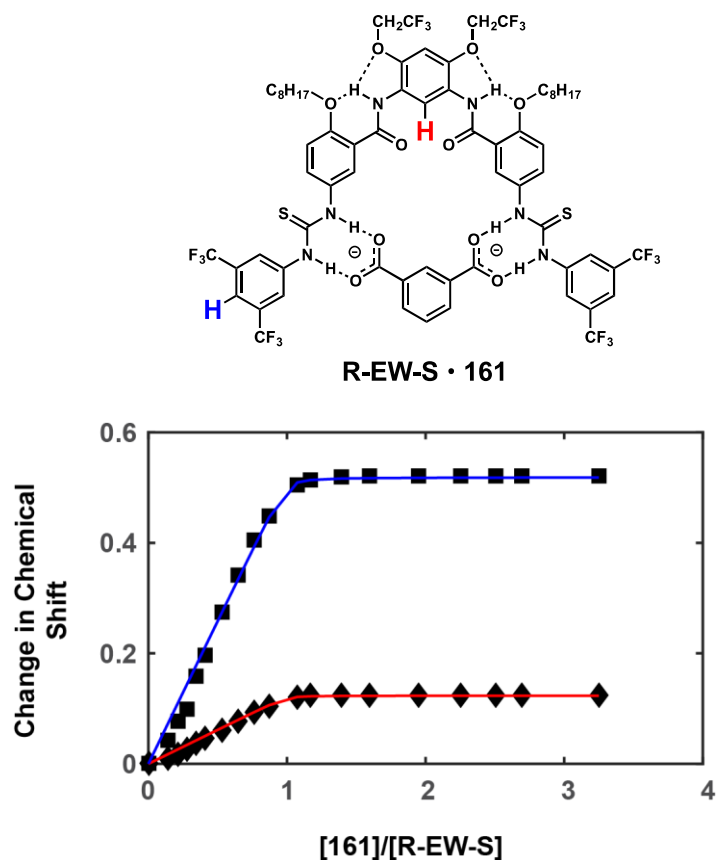


Figure 4.5 Non-linear regression model determined binding isotherm for binding of **R-EW-S** to **161** in DMSO.

In chloroform, the difference in binding of isophthalate between the respective urea sensor **R-EW-O** and the **R-EW-S** sensor was even more drastic. NMR binding studies to isophthalate (**161**) indicated an extremely strong binding with a K_a greater than $300,000 \text{ M}^{-1}$ (Figure 4.6). It could be even higher given the large uncertainty characteristic of NMR studies of strong binding associations. This likely has to do with not only the increased hydrogen-bonding ability of thioureas, but also the relatively lower instances of self-association of thioureas compared to ureas; self-association likely hindered the binding event of isophthalate and **R-EW-O** to a certain degree.

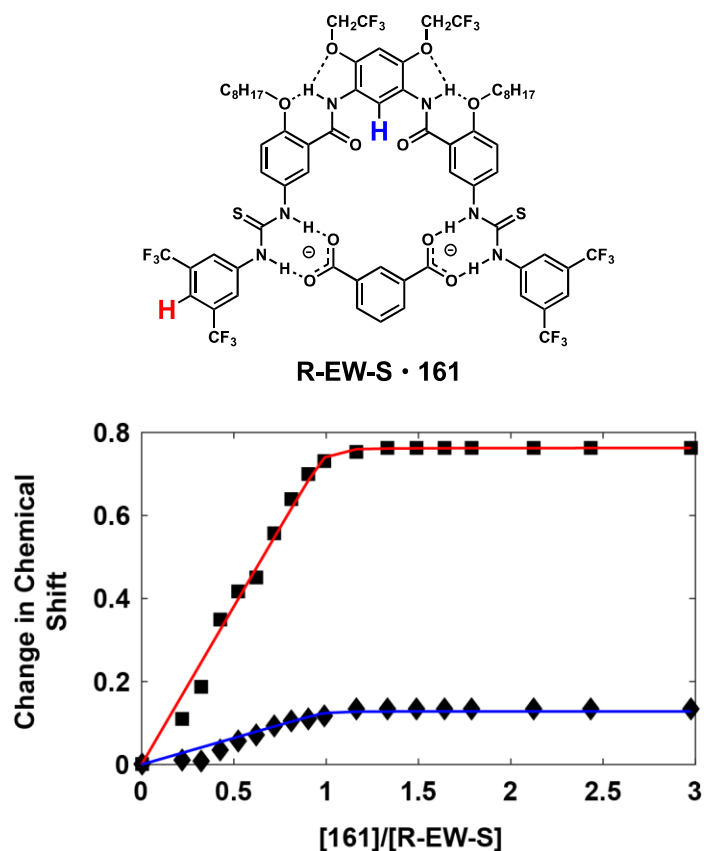


Figure 4.5 Non-linear regression model determined binding isotherm for binding of **R-EW-S** to **161** in chloroform.

To understand the role of the rigidity or preorganization, we also analyzed the **F** receptors. **F-EW-O** and **F-EW-S** exhibited weaker binding with isophthalate in DMSO compared to that of their rigid counterparts. **F-EW-O** exhibited binding with a K_a of 4,700 M^{-1} and **F-EW-S** exhibited binding with a K_a – relatively low numbers considering the greater electron-withdrawing nature of the sensors compared to more conformationally rigid **R-EW-O** and **R-EW-S** (Figure 4.6, Figure 4.7). This result suggested that these sensors may be *too* conformationally flexible for a strong binding event. Unfortunately, neither sensor was soluble enough in chloroform to conduct binding studies in that solvent.

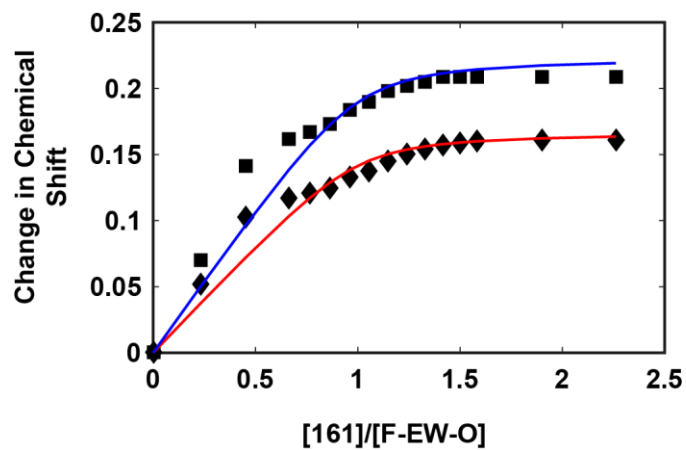
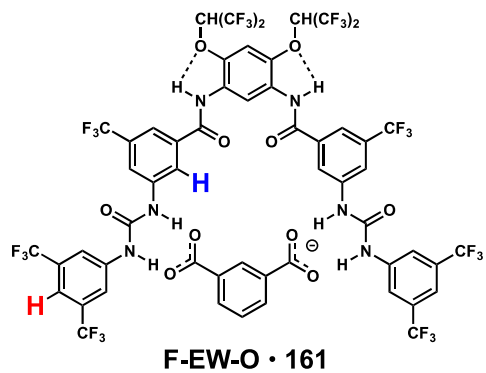


Figure 4.6 Non-linear regression model determined binding isotherm for binding of **F-EW-O** to **161** in DMSO.

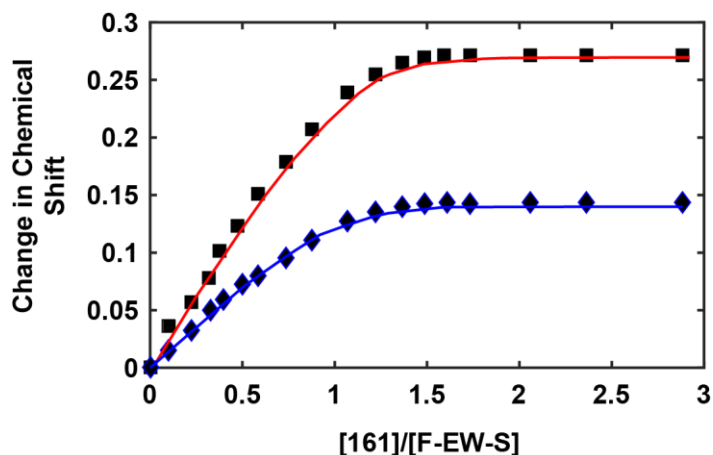
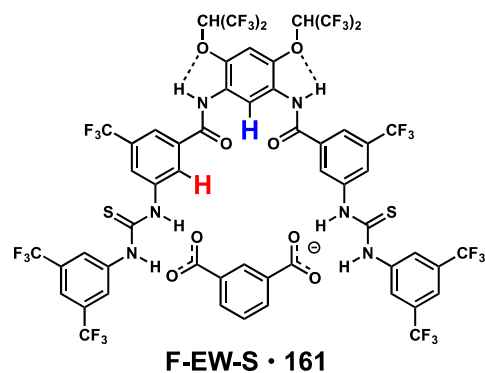


Figure 4.7 Non-linear regression model determined binding isotherm for binding of **F-EW-S** to **161** in DMSO.

To understand the role of electronics in binding, we lastly conducted experiments with **R-ED-O**. Unsurprisingly, **R-ED-O** exhibited weaker binding than **R-EW-O** in both chloroform and DMSO with K_a 's of $2,100 \text{ M}^{-1}$ and $2,500 \text{ M}^{-1}$ respectively (Figure 4.8, 4.9). These binding constants are even lower than that of receptor **159** proposed by Kelly et. al (which also contained a lack of electron-withdrawing groups on the sensor). **R-ED-O** is particularly electron-rich. Styrene's are much more electron-rich than even benzene, and the other phenyl ring attached to the urea contains a *p*-alkoxy group known for its electron-donating ability through resonance.

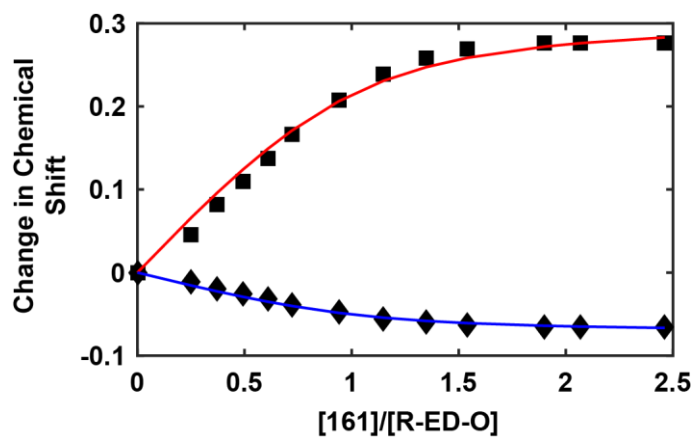
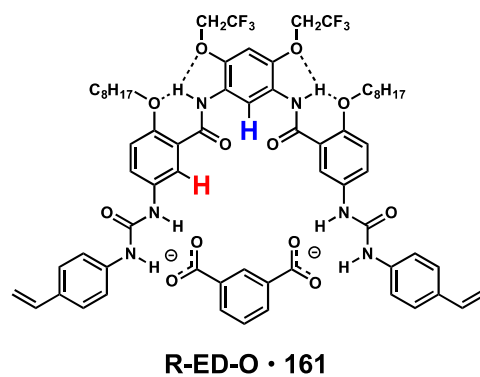


Figure 4.8 Non-linear regression model determined binding isotherm for binding of **R-ED-O** to **161** in DMSO.

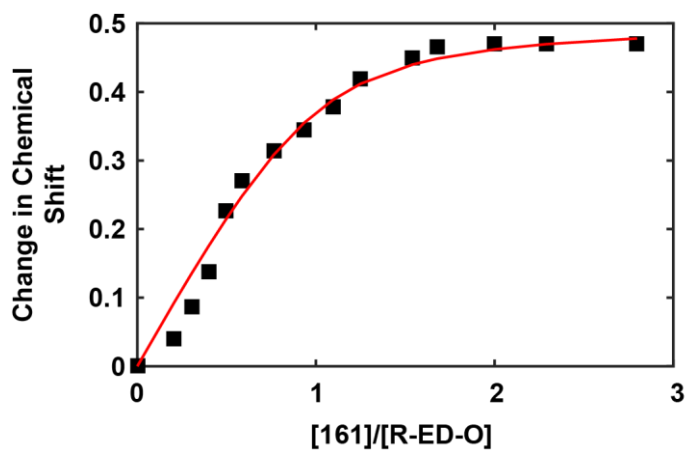
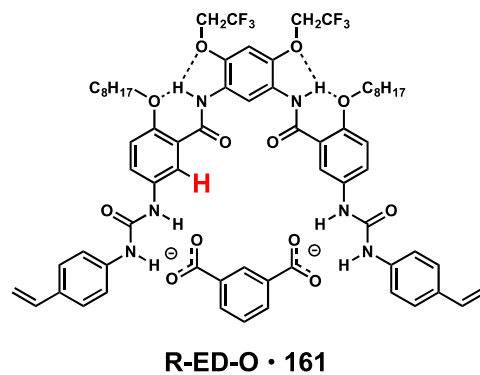


Figure 4.9 Non-linear regression model determined binding isotherm for binding of **R-ED-O** to **161** in CDCl_3 .

Table 4.2 Summary of binding data between receptors and **161**.

Host	Exp. Method	Solvent	Chemical Shift of (Thio)urea Protons in Fully Complexed Sensor	Change in Urea/Thiourea Proton Shift	K_a	Fit and Uncertainty
R-EW-O	NMR	DMSO	14.00, 11.81	4.58, 2.738	18,000	$\pm 24 \%$, $SE_Y = 5 \times 10^{-3}$
		CDCl ₃	13.13, 11.78	Undetermined	81,000	$\pm 54 \%$, $SE_Y = 2 \times 10^{-2}$
R-EW-S	NMR	DMSO	14.81, 13.12	4.54, 2.95	112,000	$\pm 31 \%$, $SE_Y = 1 \times 10^{-2}$
		CDCl ₃	13.93, 13.33	Undetermined	> 300,000	$\pm 41 \%$, $SE_Y = 2 \times 10^{-2}$
R-ED-O	NMR	DMSO	12.73, 11.61	3.99, 2.90	2,500	$\pm 27 \%$, $SE_Y = 7 \times 10^{-3}$
		CDCl ₃	12.11, 11.67	Undetermined	2,100	$\pm 42 \%$, $SE_Y = 2 \times 10^{-2}$
F-EW-O	NMR	DMSO	14.11, 12.5	4.40, 2.79	4,700	$\pm 40 \%$, $SE_Y = 1 \times 10^{-2}$
F-EW-S	NMR	DMSO	15.12, 13.39	4.50, 2.86	25,000	$\pm 35 \%$, $SE_Y = 1 \times 10^{-2}$

4.2.3 Determination and comparison of binding of receptors with RDX

With a better understanding of how the array of sensors performed in their binding with isophthalate, the same binding studies were also conducted with RDX. Because sensor **R-EW-S** performed the best with isophthalate, it seemed like the best place to start with titrations with RDX. Preliminary NMR binding studies of RDX with **R-EW-S** in both DMSO and CDCl₃ were unsuccessful – no change in the chemical shift values of any protons occurred with excess RDX. If any binding was occurring, it was not apparent in any structural changes in the receptor. This result suggested that either: a) the nitro group in RDX are not good enough hydrogen-bond acceptors to bind appreciably with the thiourea protons, or b) the receptor geometry was not complementary enough to the distribution of nitro-groups in RDX. Because other research groups have successfully reported ureas and thioureas with significant binding to nitro groups, the latter explanation seemed more likely. Thus, we looked toward our more conformationally flexible sensors to undergo binding experiments with RDX. Both **F-EW-O** and **F-EW-S** showed small changes in proton chemical shifts with exposure to excess RDX in DMSO (but not in chloroform). This led us to conduct a binding experiment of **F-EW-S** in DMSO with RDX.

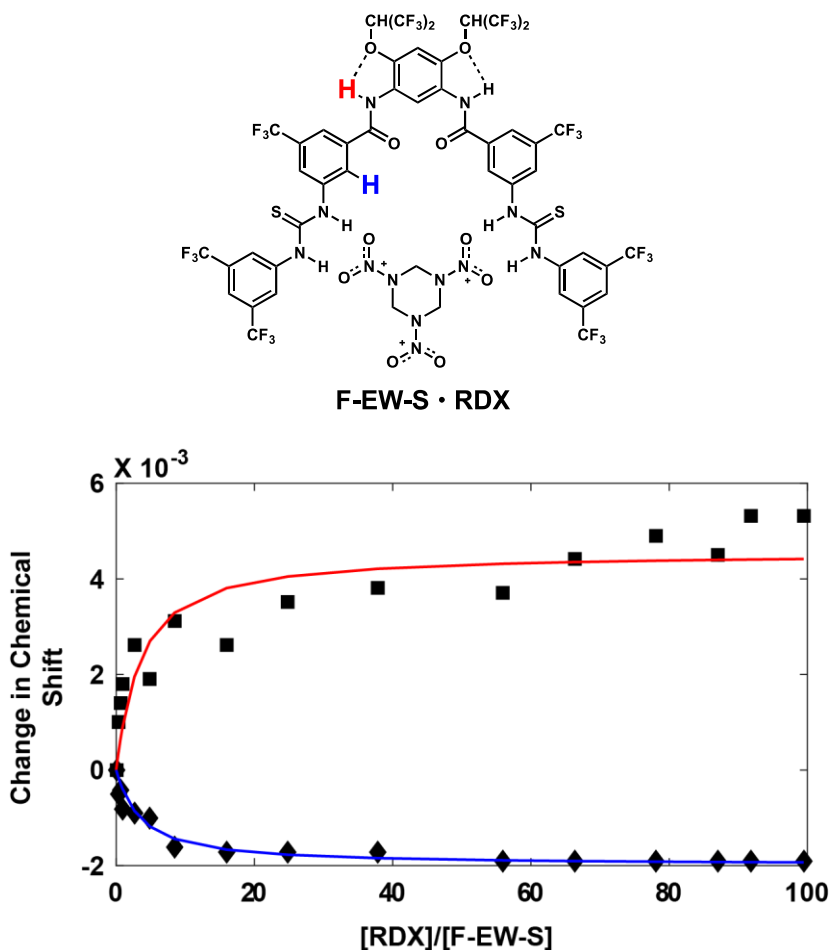


Figure 4.10 Non-linear regression model determined binding isotherm for binding of **F-EW-S** to RDX in DMSO.

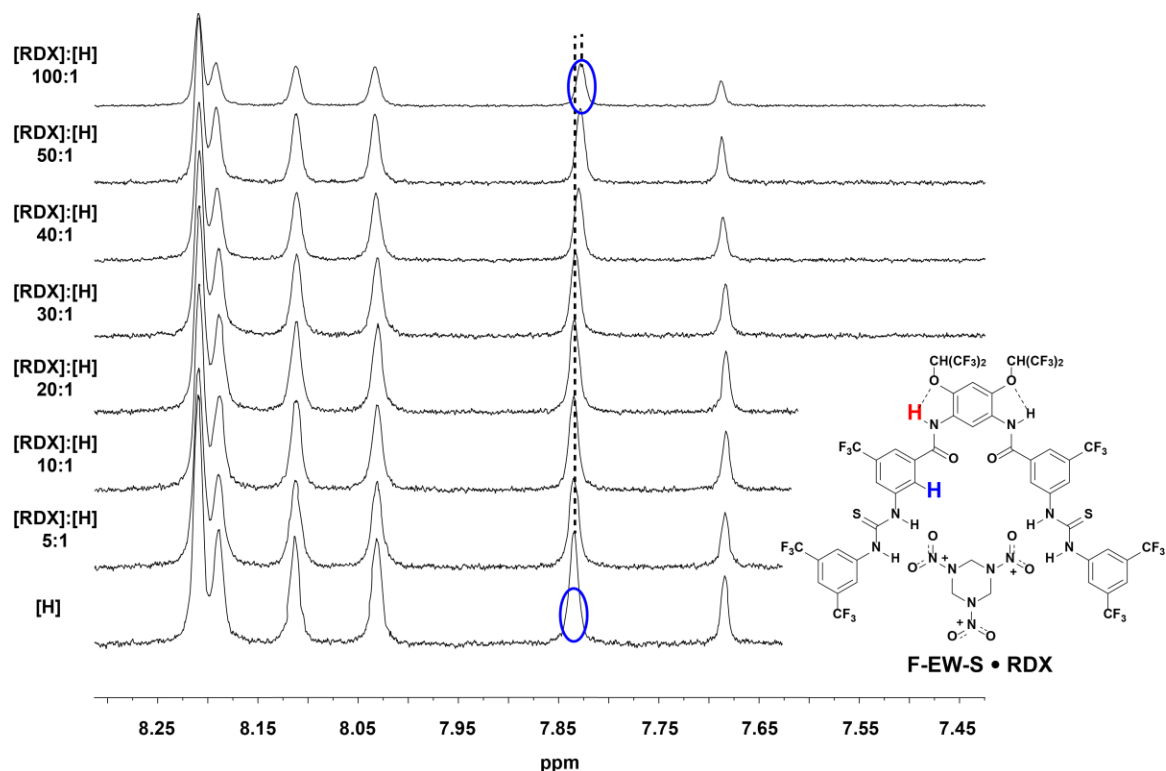


Figure 4.11 Change in chemical shifts of protons in **F-EW-S** due to increased complexation with RDX in chloroform.

Analysis of the binding data resulted in a K_a of around 430 M^{-1} . Although this is not a very significant binding constant, it is the first reported appreciable binding of a substrate to RDX *via* a hydrogen bonding mechanism. Because one of the sensors, **R-ED-O**, also has fluorescent properties, it was also pertinent to examine the fluorescence quenching ability of RDX. For this experiment, we prepared a 10^{-5} M solution of **R-ED-O** and then diluted a flask containing **RDX** with this solution. We then added sequential additions of the solution containing **R-ED-O** and RDX to a fluorescence cuvette and obtained a spectrum after each addition.

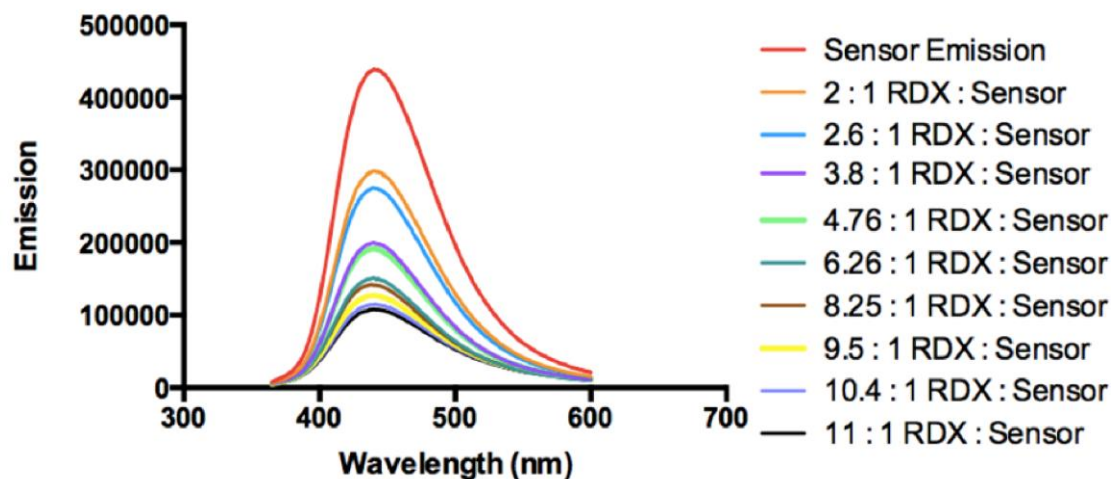


Figure 4.12 Fluorescence titration plot demonstrated the quenching ability of RDX on sensor **R-ED-O**.

These fluorescent experiments exhibited significant quenching from RDX. The mechanism of quenching was likely not from exciplex formation – there was no significant bathochromic shift with quenching activity typical of such phenomena. The mechanism, then, was likely from photoinduced electron transfer. Previous fluorescence studies of (thio)ureas binding to nitro-groups demonstrated the role of nitro-groups in the quenching of the fluorescent host (thio)urea; direct binding to the fluorescent host was important and correlated to quenching ability due to the requirement for intimate contact between the excited state molecule and the quencher. Given that RDX is non-aromatic, π - π interaction was prohibited. Thus, this “intimate” interaction could only come from N-H•••O bonding between the nitro-groups and the urea. By analyzing the data *via* the Stern Volmer relationship, the $K_a = K_{SV}$ was determined to be $3,600 \text{ M}^{-1}$. Such a high association constant determined from fluorescence studies conflicted with NMR studies that show a lack of change in urea proton chemical shifts. Given the high sensitivity of fluorescence measurements compared to the others spectroscopic measurements, the fluorescence measurement should be a better reflection of the experimental value of K_a , but more research is necessary to amend this discrepancy.

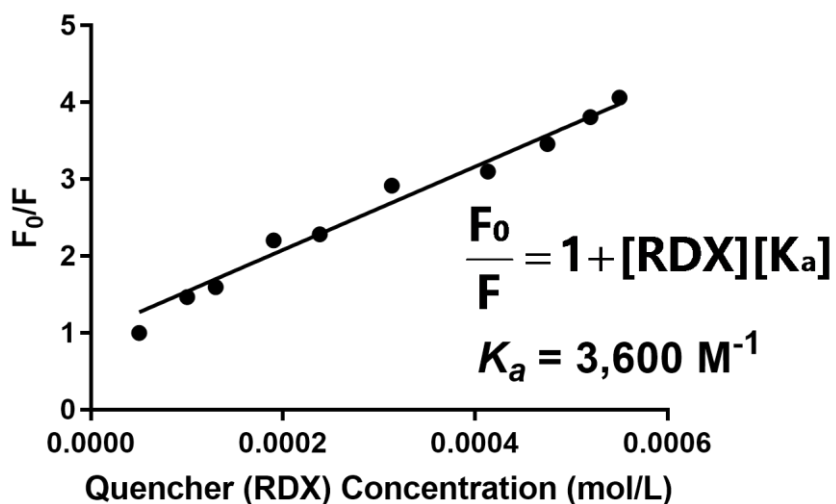


Figure 4.12 Stern-Volmer graph demonstrating significant binding of R-ED-O to RDX.

Given the possibility for RDX to bind in a different stoichiometry than 1 : 1 with the bisurea and bistiourea hosts (RDX contains three nitro groups), we decided to conduct a Job's titration experiment with F-EW-S to determine if the stoichiometry was consistent with the isophthalate guests. The data showed that at peak $[H]_T$ concentration, $[H]_T / ([H]_T + [G]_T)$ is = to 0.5 which is consistent with a 1:1 stoichiometric binding event (Figure 4.13).

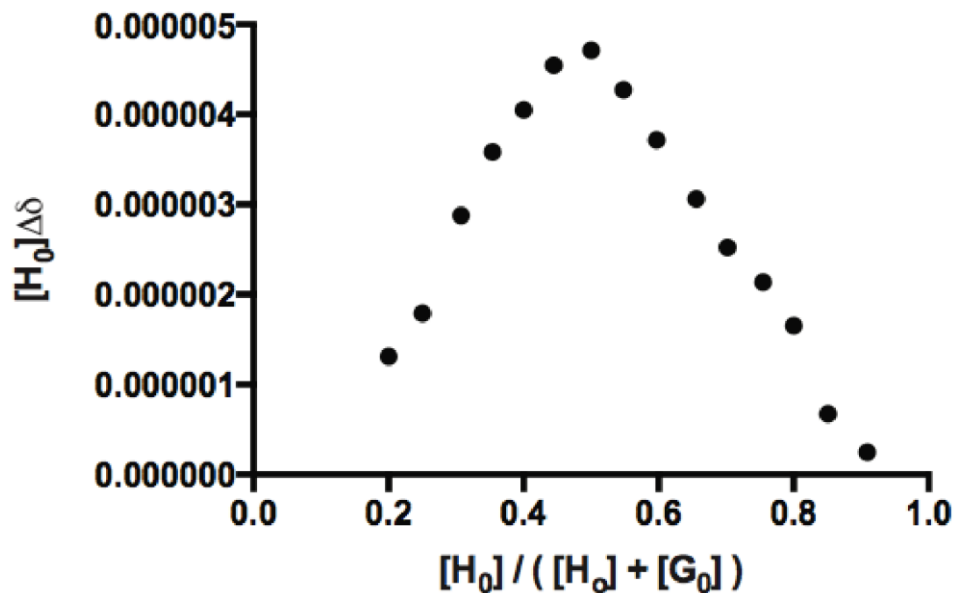


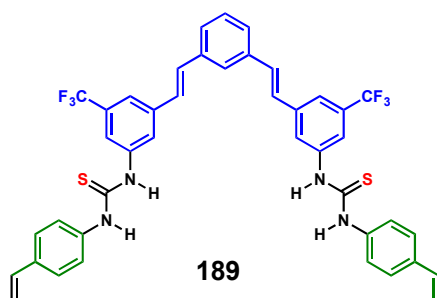
Figure 4.13 Job's titration plot of RDX with sensor F-EW-S.

Table 4.3 Summary of binding data between receptors and RDX.

Sensor	Exp. Method	Solvent	(Thio)Urea Proton Chemical Shift	Chemical Shift Change or % Change in Fluorescence	K_a	Fit and Uncertainty
R-EW-O	NMR	DMSO	N/A	0	No binding	
		CDCl ₃	N/A	0	No binding	
R-EW-S	NMR	DMSO	N/A	0	No binding	
		CDCl ₃	N/A	0	No binding	
R-ED-O	NMR	DMSO	N/A	0	No binding	
		CDCl ₃	N/A	0	No binding	
	Fluorescence	Acetone	N/A	50 % quenched with 4 equiv. of RDX	3,600	
F-EW-O	NMR	DMSO	N/A	0	No binding	
F-EW-S	NMR	DMSO	10.622, 10.530	0.003, 0.003	430	$\pm 61 \%$, $SE_Y = 5 \times 10^{-4}$
		CDCl ₃	N/A	0	No binding	

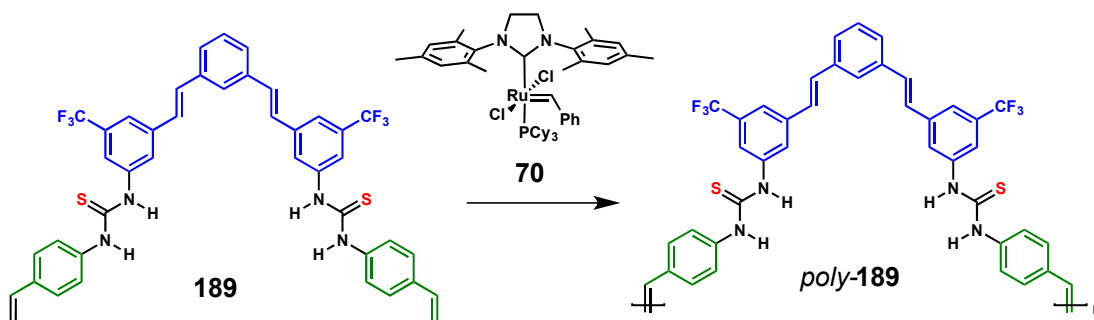
4.2.4 Future Directions

Conclusions from the binding studies of these five molecules with isophthalate and RDX suggest a few directions to go in order to a) optimize binding further, b) create a sensitive binding signal. It seems like the flexible sensors we synthesized were too conformationally flexible to exhibit optimal binding. However, it is possible that the rigid sensors are too rigid. It would be ideal to have a sensor that is flexible, but still somewhat rigid to allow for a better induced fit. Sensor **189** might be able to exhibit these qualities. *trans*-Stilbenes have some conformational rigidity, but also have a certain amount of rotation freedom pertaining to the single bonds between the internal double bond and the phenyl rings.



Scheme 4.17 Sensor with conductive backbone and moderate flexibility for potentially optimal binding of RDX or isophthalate.

A sensor like **189** also has the benefit of having a conductive backbone that would produce additional signals for a binding event. Lastly, **189** has the benefit of being a precursor to a conductive polymer incorporating this bis-thiourea. A polymer such as *poly-189* would have the selectivity benefit of the hydrogen-bonding event to molecules like RDX and additionally have the benefit of sensitivity typical of conductive polymers first exhibited by Swager's group.



Scheme 4.17 Polymerization of sensor **189** to form *poly-189*.

4.3 Conclusion

In this chapter, we reported on the synthesis of five synthetically modular bis-urea and bis-thiourea sensors varied in their hydrogen bond ability, electron-withdrawing nature, and conformational flexibility. We studied these five receptors for their ability to detect isophthalate and RDX in DMSO and chloroform *via* NMR studies. One sensor was also studied by fluorescence spectroscopy.

For the detection of isophthalate, one sensor stood above the rest: **R-EW-S** in chloroform (Table 4.2). The reason for this, when comparing to the binding of the other receptors, is likely because of 1) its highly electron-withdrawing nature that allows for tighter binding to the substrate, 2) its rigidity and preorganization, and 3) the use of thioureas, instead of ureas, that increase hydrogen bond ability and diminish competing self-association in non-polar solvents. With **R-EW-S** we were able to achieve binding comparable to the highest K_a 's known for dicarboxylates ($\sim 10^6$). In addition, the chemical shift difference between the thiourea protons in the complex and the unbound host, 4.95 ppm, is among the greatest complexation shifts for binding of isophthalate. And, because

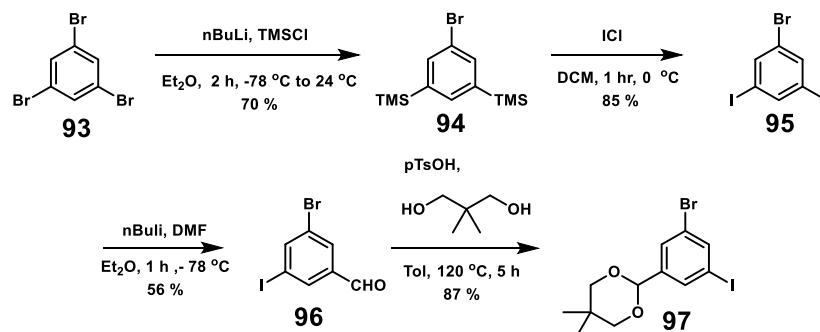
of the modular synthesis of such receptors, we were also able to aptly compare **R-EW-S** to other sensors based on individual tenets of molecular recognition to understand how a sensor may be optimized toward stronger binding.

For the detection of RDX, two sensors demonstrate the first documented cases of significant binding to a nitro-explosive: **F-EW-S** and **R-ED-O**. NMR experiments show a lack of response by urea or thiourea protons to the rigid sensors; however, **F-EW-S** demonstrates significant binding to RDX in 1 : 1 stoichiometry according to Job's Plot titration (480 M^{-1}). By fluorescence studies, **R-ED-O** shows even more significant binding, $3,600 \text{ M}^{-1}$, to RDX – this is conflicting with NMR studies, but given the greater sensitivity of fluorescence studies the stronger binding may be more indicative of the true binding of these sensors. Because of the moderate binding exhibited by these sensors, and this apparent discrepancy, more studies are required to understand the potential of these types of receptors for recognition of non-aromatic explosives. Future sensors should incorporate a more moderately flexible backbone and also be able to create a sensitive signal for isophthalate or RDX detection.

5 Experimental

5.1 Synthetic Details

Materials and General Methods. Unless otherwise stated, all manipulations of air and/or moisture sensitive compounds were carried out in oven-dried glassware, under an atmosphere of Ar or N₂. All solvents and reagents were purchased from Alfa Aesar, Spectrum Chemicals, Acros Organics, TCI America, and Sigma-Aldrich and were used as received unless otherwise noted. Organic solvents were dried by passing through a column of alumina and were degassed by vigorous bubbling of N₂ or Ar through the solvent for 20 min. Flash column chromatography was performed on SiliCycle silica gel (particle size 40–63 μm). Thin layer chromatography was carried out using SiliCycle silica gel 60 Å F-254 pre-coated plates (0.25 mm thick) and visualized by UV absorption. All ¹H, {¹H}¹³C, and ¹⁹F NMR spectra were recorded on Bruker AVQ-400 and are referenced to residual solvent peaks (CDCl₃ ¹H NMR δ = 7.26 ppm, ¹³C NMR δ = 77.16 ppm; C₆D₆ ¹H NMR δ = 7.16 ppm, ¹³C NMR δ = 128.06 ppm; Tol-*d*₈ ¹H NMR δ = 2.08 ppm; THF-*d*₈ ¹H NMR δ = 1.78 ppm, ¹³C NMR δ = 67.21 ppm). The temperature in all VT NMR experiments is calibrated to ethylene glycol or MeOH standards. ESI mass spectrometry was performed on a Finnigan LTQFT (Thermo) spectrometer in positive ionization mode. MALDI mass spectrometry was performed on a Voyager-DE PRO (Applied Biosystems Voyager System 6322) in positive mode using a matrix of dithranol with AgNO₃. Gel permeation chromatography (GPC) was carried out on a LC/MS Agilent 1260 Infinity set up with a guard and two Agilent Polypore 300 x 7.5 mm columns at 35 °C. All GPC analyses were performed on a 0.2 mg/mL solution of polymer in chloroform. An injection volume of 25 μL and a flow rate of 1 mL/min were used. Calibration was based on narrow polydispersity polystyrene standards ranging from *M*_w = 100 to 4,068,981.



Scheme 5.1 Synthesis of **97**.

(5-bromo-1,3-phenylene)bis(trimethylsilane) (**94**) A 1 L round bottom flask was charged under N₂ with 1,3,5-tribromobenzene (20.0 g, 63.7 mmol) and diethyl ether (280 mL). The reaction was cooled to -78 °C and a 2.5 M solution of n-Butyllithium in hexanes (27 ml,

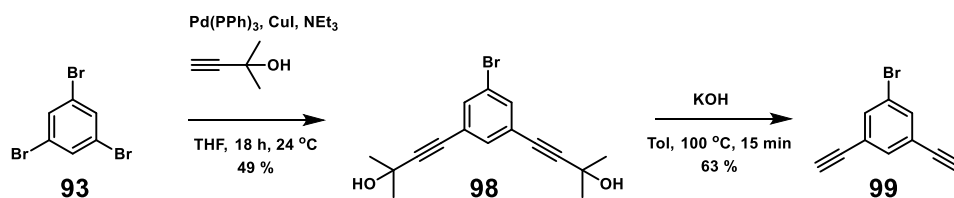
67.5 mmol) was added dropwise and the reaction mixture was stirred for 30 min at -50 °C. The reaction mixture was then brought back to -78 °C and trimethylsilylchloride (10 ml, 78.8 mmol) was added dropwise. The reaction was then brought to room temperature and stirred for 30 min. The reaction was cooled to -78 °C and a second portion of n-Butyllithium (32 ml, 2.5 M in Hexanes, 73 mmol) was added dropwise and the reaction was stirred for 30 min. A second portion of trimethylsilylchloride (12 ml, 94.5 mmol) was then added dropwise and the reaction was stirred at 24 °C for 10 minutes. The reaction mixture was then diluted with saturated NaHCO₃ (300 mL) and extracted with three portions of diethyl ether (200 mL). The organic phases were combined and dried over MgSO₄ and concentrated on a rotary evaporator. The residue was distilled under vacuum at 120 °C. Recrystallization from ethanol (35 mL) yielded 1-bromo-3,5-diiodobenzene (12.9 g, 42.8 mmol, 70 %) as brilliant white crystals. ¹H NMR (600 MHz, CDCl₃) δ = 7.60–7.57 (m, 2H), 7.54–7.50 (m, 1H), 0.30–0.24 (m, 18H) ppm. ¹³C NMR (68 MHz, CDCl₃) δ = 143.0, 136.2, 123.4, -1.2 ppm. EI-HRMS (m/z): [C₁₂H₂₁BrSi₂]⁺, calcd for [¹²C₁₂H₂₁BrSi₂] 301.374; found 301.3745.

1-bromo-3,5-diiodobenzene (95) A 250 ml round bottom flask was charged under N₂ with (5-bromo-1,3-phenylene)bis(trimethylsilane) (12.9 g, 42.8 mmol) and dichloromethane (100 mL). The reaction was cooled to 0 °C and iodine monochloride (16.29 g, 100.33 mmol) in dichloromethane (50 mL) was added dropwise. The reaction mixture was stirred at this temperature for 1 h. The reaction mixture was then diluted with sat. NaOH (30 mL) and sat. Na₂S₂O₃ (30 mL) and stirred for 30 min. The organic layer was separated, and the aqueous layer was extracted with two portions of dichloromethane (50 mL). The organic phases were combined, dried over MgSO₄, and concentrated on a rotary evaporator to yield 1-bromo-3,5-diiodobenzene (14.8 g, 36.2 mmol, 85 %). ¹H NMR (600 MHz, CDCl₃) δ = 7.80 (t, 1H) and 7.96 (d, 2H) ppm. ¹³C NMR (126 MHz, C₆D₆) δ = 143.8, 139.1, 123.5, 95.2 ppm. GC-MS (m/z): [C₆H₃BrI₂]⁺, calcd for [C₆H₃BrI₂] 407.7507; found 407.80 ([M⁺]).

3-bromo-5-iodobenzaldehyde (96) A 250 ml round bottom flask was charged under N₂ with 1-bromo-3,5-diiodobenzene (5.0 g, 12.2 mmol) dry, degassed diethyl ether (50 mL). The reaction was cooled to -3-bromo-5-iodobenzaldehyde 78 °C and a 2.5 M solution of n-Butyllithium in hexanes (5.23 ml, 13.08 mmol) was added dropwise and the reaction mixture was stirred for 20 min. Dimethylformamide (1.16 g, 15.89 mmol) was added and the reaction mixture was brought to 24 °C. The reaction mixture was quenched with sat. NH₄Cl and extracted with three portions of ethyl acetate (25 mL). The organic phases were combined, dried over MgSO₄, and concentrated on a rotary evaporator. The residue was diluted with hexanes and the solid filtered off and dried to yield 3-bromo-5-iodobenzaldehyde (2.14 g, 6.9 mmol, 56 %) as an off-white solid. ¹H NMR (400 MHz, CDCl₃) δ = 9.91 (s, 1H), 7.89 – 7.79 (m, 1H), 7.74 – 7.66 (m, 1H), 7.53 (d, *J* = 3.3 Hz, 1H) ppm. ¹³C NMR (126 MHz, C₆D₆) δ = 95.2, 123.5, 139.1, and 143.8 ppm. GC-MS (m/z): [C₇H₄BrIO]⁺, calcd for [C₇H₄BrIO] 310.91; found 310.90 ([M⁺]).

2-(3-bromo-5-iodophenyl)-5,5-dimethyl-1,3-dioxane (97) A 100 ml round bottom flask

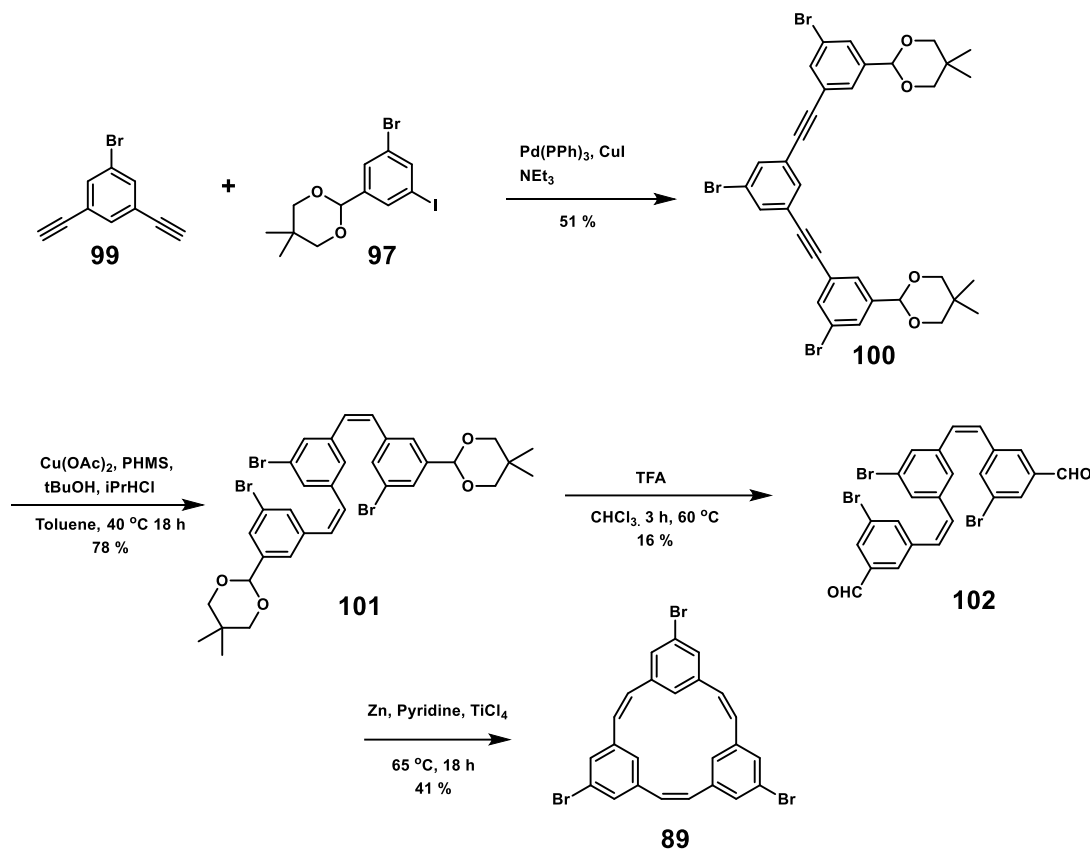
fitted with a Dean-Stark trap was charged under N₂ with 3-bromo-5-iodobenzaldehyde (2.14 g, 6.9 mmol), 2,2-dimethyl-1,3-propanediol (0.86 g, 8.3 mmol), *p*-toluenesulfonic acid (0.1 g, 0.5 mmol) and toluene (50 mL). The reaction mixture was stirred at 120 °C for 5 h. The reaction mixture was then diluted with sat. NaHCO₃ (30 mL), and extracted with three portions of ethyl acetate (30 mL). The organic phases were combined, dried over MgSO₄, and concentrated on a rotary evaporator. Column chromatography (SiO₂; 9:1 hexanes:EtOAc) yielded 2-(3-bromo-5-iodophenyl)-5,5-dimethyl-1,3-dioxane (2.4 g, 6.04 mmol, 87 %) as a pale-yellow waxy solid. ¹H NMR (600 MHz, CDCl₃) δ = 7.82 (t, *J* = 1.7 Hz, 1H), 7.78 (d, *J* = 1.6 Hz, 1H), 7.62 (t, *J* = 1.7 Hz, 1H), 5.29 (s, 1H), 3.76 (dt, *J* = 11.2, 1.4 Hz, 2H), 3.69 – 3.57 (m, 2H), 1.26 (s, 3H), 0.80 (s, 3H) ppm. GC-MS (*m/z*): [C₁₂H₁₄BrIO₂]⁺, calcd for [C₁₂H₁₄BrIO₂] 397.05; found 397.10 ([M⁺]).



Scheme 5.2 Synthesis of **99**.

4,4'-(5-bromo-1,3-phenylene)bis(2-methylbut-3-yn-2-ol) (**98**) A 250 ml round bottom flask was charged with N₂ and 1,3,5-tribromobenzene (9.44 g, 30 mmol), triethylamine (6.17 g, 61 mmol), 3-methyl butynol (5.12 g, 61 mmol) and tetrahydrofuran (100 mL). Copper (I) iodide (0.14 g, 0.75 mmol) and bis(triphenylphosphine)palladium(II) dichloride (0.21 g, 0.30 mmol) were then added and the reaction mixture was stirred at 24 °C for 18 h. The reaction mixture was concentrated on a rotary evaporator. Column chromatography (SiO₂; 4:1 hexane/EtOAc to 1:1 hexane/EtOAc) followed by dilution with hexane and filtering yielded **98** (4.7 g, 14.6 mmol, 49 %) as an off-white solid. ¹H NMR (600 MHz, CDCl₃) δ = 7.49 (d, *J* = 1.5 Hz, 2H), 7.39 (t, *J* = 1.5 Hz, 1H), 2.04 (d, *J* = 2.8 Hz, 6H) ppm. Previously reported by Juricek et al.¹³³

1-bromo-3,5-diethynylbenzene (**99**) A 500 ml round bottom flask was charged under N₂ with 4,4'-(5-bromo-1,3-phenylene)bis(2-methylbut-3-yn-2-ol) (4.7 g, 14.63 mmol), and dry, degassed toluene (200 mL). Powdered potassium hydroxide (12 g, 58.5) was added and the reaction mixture was stirred at 100 °C for 15 min. The reaction mixture was then poured over SiO₂ and concentrated on a rotary evaporator yielding **99** (1.9 g, 9.26 mmol, 63 %) as an off-white solid. ¹H NMR (500 MHz, CDCl₃) δ = 7.62 (d, *J* = 1.4 Hz, 2H), 7.54 (t, *J* = 1.5 Hz, 1H), 3.15 (s, 2H) ppm. Previously reported by Constable et al.¹³⁴



Scheme 5.3 Synthesis of **89**.

2,2'-(((5-bromo-1,3-phenylene)bis(ethyne-2,1-diyl))bis(5-bromo-3,1-phenylene))bis(5,5-dimethyl-1,3-dioxane) (**100**) A 100 ml round bottom flask was charged under N₂ with **97** (2.38 g, 6.0 mmol), **99** (0.6 g, 2.92 mmol), tetrakis(triphenylphosphine)palladium(0) (0.2106 g, 0.3 mmol), copper (I) iodide (0.114 g, 0.6 mmol), triethylamine (10 mL), and tetrahydrofuran (20 mL). The reaction mixture was stirred at 24 °C for 12 h. The reaction mixture was then diluted with sat. NH₄Cl and extracted with three portions of ethyl acetate (20 mL). The organic phases were combined, washed with H₂O (30 mL) and concentrated on a rotary evaporator. Column chromatography (SiO₂; 5:1 hexanes:EtOAc) yielded **100** (2.5 g, 6.17 mmol, 51 %) as a clear oil. ¹H NMR (600 MHz, CDCl₃) δ = 7.66 – 7.65 (m, 2H), 7.64 (t, *J* = 1.8 Hz, 2H), 7.61 (d, *J* = 1.4 Hz, 2H), 7.60 (d, *J* = 1.6 Hz, 2H), 7.56 (t, *J* = 1.5 Hz, 1H), 5.30 (s, 2H), 3.84 – 3.72 (m, 4H), 3.65 (d, *J* = 10.9 Hz, 4H), 1.28 (s, 6H),

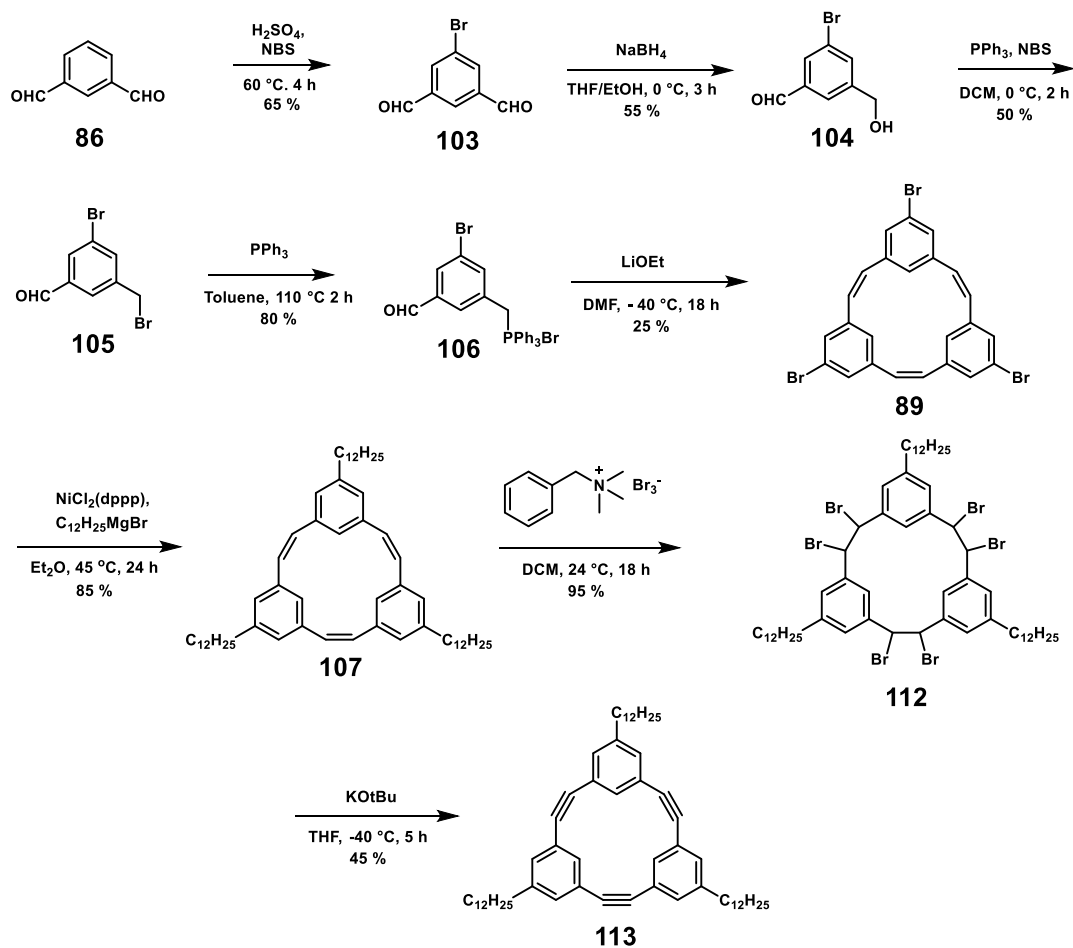
0.81 (s, 6H) ppm. FTMS (MALDI) m/z: [C₃₁H₃₄Br₃O₄+H]⁺, calcd. [C₃₁H₃₄Br₃O₄+H] 743.33; found 743.99.

5,5'-((1Z,1'Z)-(5-bromo-1,3-phenylene)bis(ethene-2,1-diyl))bis(3-bromobenzaldehyde)
(102) A 200 ml roundbottom flask fitted with a reflux condenser was charged under N₂ with 2,2'-(((5-bromo-1,3-phenylene)bis(ethyne-2,1-diyl))bis(5-bromo-3,1-phenylene))bis(5,5-dimethyl-1,3-dioxane) (1.89 g, 2.48 mmol), 1,3-bis(2,6-diisopropylphenyl)imidazolium chloride (0.211 g, 0.5 mmol), Copper (II) acetate (0.0988 g, 0.5 mmol), potassium tertbutoxide (0.11 g, 0.993 mmol), and dry, degassed toluene (40 mL). The reaction mixture was then stirred at 50 °C for 1 h at which point the mixture turned green. The reaction mixture was cooled to 40 °C, polyhydroxymethylsilane (1.19 g, 20 mmol) was added dropwise and the mixture was stirred for 30 min. t-Butanol (0.74 g, 10 mmol) was then added and the reaction mixture was stirred at 40 °C for 18 h. The reaction mixture was diluted with sat. NaOH (100 mL) and allowed to stir for 4 h at 24 °C. The mixture was extracted with three portions of ethyl acetate (40 mL). The organic phases were combined, dried over MgSO₄ and concentrated by a rotary evaporator to yield a crude mixture of 2,2'-(((1Z,1'Z)-(5-bromo-1,3-phenylene)bis(ethene-2,1-diyl))bis(5-bromo-3,1-phenylene))bis(5,5-dimethyl-1,3-dioxane) (1.5 g, 2.0 mmol, 78 %). **101** was used without further purification.

A 100 ml round bottom flask fitted with a reflux condenser was charged under N₂ with 2,2'-(((1Z,1'Z)-(5-bromo-1,3-phenylene)bis(ethene-2,1-diyl))bis(5-bromo-3,1-phenylene))bis(5,5-dimethyl-1,3-dioxane) (1.5 g, 2.0 mmol), trifluoroacetic acid (20 mL), chloroform (20 mL) and a few drops of water. The reaction mixture was stirred at 60 °C for 4 h. The reaction mixture was concentrated on a rotary evaporator. Column chromatography (SiO₂ impregnated with AgNO₃; 6:1 hexanes:EtOAc) resulted in a waxy solid which was diluted with 3:1 hexanes:EtOAc. The resulting solid was filtered off and the filtrate was concentrated on a rotary evaporator yielding **102** (0.18 g, 0.3 mmol, 16 %) as a yellow oil. ¹H NMR (600 MHz, CDCl₃) δ = 9.85 (d, *J* = 0.9 Hz, 2H), 7.84 (t, *J* = 1.4 Hz, 2H), 7.61 (q, *J* = 1.2 Hz, 2H), 7.59 (d, *J* = 1.8 Hz, 2H), 7.26 (d, *J* = 0.9 Hz, 1H), 7.24 – 7.21 (m, 2H), 6.56 (s, 4H) ppm. FTMS (MALDI) m/z: [C₃₁H₃₄Br₃O₄+H]⁺, calcd. [C₃₁H₃₄Br₃O₄+H] 745.01; found 745.03.

(2Z,5Z,8Z)-1⁵,4⁵,7⁵-tribromo-1,4,7(1,3)-tribenzenacyclononaphane-2,5,8-triene (**89**) A 500 round bottom flask fitted with a reflux condenser was charged under N₂ with titanium tetrachloride (0.363 g, 2 mmol), zinc (0.135 g, 2.1 mmol) and tetrahydrofuran (70 mL) at 0 °C. The reaction mixture was stirred at 65 °C for 2 h. Pyridine (0.226 g, 2.8 mmol) and **102** (0.18 g, 0.174 mmol) in tetrahydrofuran (30 mL) was then added dropwise over several hours at 65 °C. The reaction mixture was stirred at 65 °C for 18 h. The reaction mixture was slowly diluted with isopropanol (20 mL) and then sat. NaOH (20 mL) and extracted with three portions of ethyl acetate (50 mL). The organic phases were combined, dried over MgSO₄, and concentrated on a rotary evaporator. Column chromatography (SiO₂; 19:1 hexanes:EtOAc) yielded **89** (0.07 g, 0.124 mmol, 41 %) as a white solid. ¹H NMR (500 MHz, CDCl₃) δ = 7.15 (d, *J* = 1.5 Hz, 6H), 6.62 (t, *J* = 1.5 Hz, 3H), 6.57 (s, 6H) ppm. ¹³C

NMR (600 MHz, CDCl₃) δ = 138.9, 130.5, 130.3, 127.9, 122.5 ppm. FTMS (MALDI) m/z: [C₂₄H₁₅Br₃+H]⁺, calcd. [C₂₄H₁₅Br₃+H] 543.10; found 543.57.



Scheme 5.4 Synthesis of **113**.

5-bromoisophthalaldehyde (103) A 500 ml two-neck roundbottom flask was charged under N₂ with isophthalaldehyde (40 g, 298.21 mmol), N-bromosuccinimide (61 g, 342.70 mmol), and H₂SO₄ (160 mL). The reaction mixture was stirred for 3.5 h at 65 °C. At this time the reaction mixture was poured in to ice water (500 mL) and the precipitate was isolated by vacuum filtration. After being washed with water (3 x 500 mL), the solid was allowed to dry for 3 h. The solid was then taken up in 5 % EtOAc in Hexanes and stirred at 75 °C for 30 min. The precipitate was isolated hot by vacuum filtration. This process was repeated two more times to yield **103** (46.36 g, 217.62 mmol, 73 %). ¹H NMR (400 MHz, CDCl₃) δ = 7.35 (dd, *J* = 5.2, 1.3 Hz, 2H), 10.06 (s, 1H) ppm; ¹³C NMR (151 MHz, CDCl₃) δ = 129.0, 137.0, 138.2, 189.3 ppm; LRMS (ES⁺) calculated for C₈H₅BrO₂ [M+H] 212.95. Found 212.95.

3-bromo-5-(hydroxymethyl)benzaldehyde (104) A two-neck 1000 mL round-bottom was charged under N₂ with **103** (46.36 g, 217.62 mmol), THF (230 mL) and ethanol (400 mL). The reaction mixture was cooled to 0 °C and sodium borohydride (2.28 g, 60.46 mmol)

was added in small portions. The reaction mixture was then stirred at 0 °C for 1 h. After this time the reaction mixture was poured in two water (500 mL) and extracted with ethyl acetate (300 mL) three times. The combined organic extracts were washed with water (300 mL), dried over MgSO₄, and concentrated on a rotary evaporator. Column chromatography (SiO₂; 1:3 ethyl acetate:hexanes) yielded **23** (25.54 g, 118.8 mmol, 55 %) as a colorless solid. ¹H NMR (600 MHz, CDCl₃) δ = 9.90 (d, *J* = 1.2 Hz, 1H), 7.86 (d, *J* = 1.8 Hz, 1H), 7.75 (s, 1H), 7.74 (s, 1H), 4.73 (s, 2H) ppm. Previously reported by Strunk et al.¹³⁵

3-bromo-5-(bromomethyl)benzaldehyde (105) A two-neck 1000 ml round-bottom was charged under N₂ with **104** (20.16 g, 93.7 mmol), triphenylphosphine (49.63 g, 189.36 mmol) and dry DCM (400 mL). The reaction mixture was cooled to 0 °C and N-bromosuccinimide (33.7 g, 189.36 mmol) was added in small portions over 30 min. The reaction mixture was then stirred for 3 h at 24 °C, poured into water and extracted with DCM (300 mL) three times. The combined organic extracts were washed with brine (200 mL), dried over MgSO₄ and concentrated on a rotary evaporator. Column chromatography (SiO₂; 1:10 ethyl acetate:hexanes) yielded **105** (15.39 g, 55.36 mmol, 59 %) as a colorless solid. ¹H NMR (400 MHz, Acetone-*d*₆) δ 10.02 (s, 1H), 8.01 – 7.99 (m, 2H), 7.98 (t, *J* = 1.8 Hz, 1H), 4.75 (s, 2H) ppm. ¹³C NMR (150 MHz, Acetone-*d*₆) δ = 192.0, 141.5, 138.8, 138.2, 131.3, 129.1, 122.5, 33.2 ppm. ESI-HR-MS (*m/z*): [C₈H₆Br₂O]⁺, calcd for [C₈H₆Br₂O] 275.8785; found 275.8787

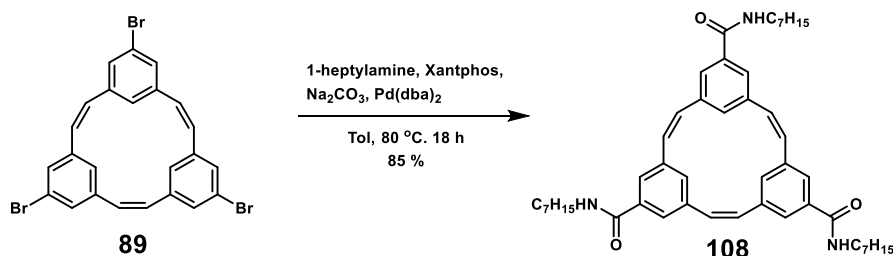
3-bromo-5-((bromotriphenyl-λ⁵-phosphanyl)methyl)benzaldehyde (106) A 250 ml two-neck round-bottom flask was charged under N₂ with **105** (4.7 g, 17.00 mmol), triphenylphosphine (4.7 g, 18.00 mmol) and dry toluene (80 mL). The reaction mixture was stirred for 2 h at 110 °C. The resulting precipitate was isolated and dried by vacuum filtration to yield **25** (8.26 g, 14.00 mmol, 82 %). ¹H NMR (400 MHz, DMSO-*d*₆) δ = 9.82 (s, 1H), 8.08 (q, *J* = 1.8 Hz, 1H), 8.01 – 7.86 (m, 3H), 7.83 – 7.63 (m, 12H), 7.50 (s, 1H), 7.37 (m, 1H), 5.31 (s, 1H), 5.27 (s, 1H) ppm. FTMS (MALDI) *m/z*: [C₂₄H₁₅Br₃+H]⁺, calcd. [C₂₄H₁₅Br₃+H] 544.10; found 544.57.

(2Z,5Z,8Z)-1⁵,4⁵,7⁵-tribromo-1,4,7(1,3)-tribenzenacyclononaphane-2,5,8-triene (89) A two-neck 1000 mL round-bottom was charged under N₂ with **106** (8.26 g, 14.00 mmol) and dimethylformamide (300 mL). The reaction was cooled to –40 °C and 1 M lithium ethoxide in ethanol (20 ml, 18.35 mmol) was added by dropwise addition over 5 hours at –40 °C. The reaction mixture was stirred at –40 °C and warmed up gradually to 24 °C over 18 h. The reaction mixture was then concentrated by rotary evaporator. Column chromatography (SiO₂; 1:20 ethyl acetate:hexanes) yielded **89** (0.70 g, 1.29 mmol, 25 %) as a colorless solid. ¹H NMR (500 MHz, CDCl₃) δ = 7.15 (d, *J* = 1.5 Hz, 6H), 6.62 (t, *J* = 1.5 Hz, 3H), 6.57 (s, 6H) ppm; ¹³C NMR (150 MHz, CDCl₃) δ = 138.9, 130.5, 130.3, 127.9, 122.5 ppm; FTMS (MALDI) *m/z*: [C₂₄H₁₅Br₃+H]⁺, calcd. [C₂₄H₁₅Br₃+H] 544.10; found 544.57.

(2Z,5Z,8Z)-1⁵,4⁵,7⁵-tridodecyl-1,4,7(1,3)-tribenzenacyclononaphane-2,5,8-triene (107) A two-neck 25 ml round-bottom flask was charged under N₂ with **89** (0.135 g, 0.25 mmol),

NiCl₂(dppp) (0.008 g, 0.015 mmol), and dry diethyl ether (5 mL). 1 M Dodecylmagnesium bromide in diethyl ether (0.9 ml, 0.9 mmol) was then added by dropwise addition over 1 h. The reaction mixture was stirred for 24 h at 40 °C. Hexanes (5 mL) was added to the mixture and the mixture was filtered over a short plug of silica gel. Additional solvent (2:1 hexanes:diethyl ether) was poured over the plug. The filtrate was concentrated by rotary evaporator. Column chromatography (SiO₂; hexanes) yielded **107** (0.148 g, 0.182 mmol, 74 %). ¹H NMR (400 MHz, CDCl₃) δ = 6.78 – 6.73 (m, 3H), 6.54 (d, *J* = 4.9 Hz, 6H), 2.49 (t, *J* = 7.7 Hz, 6H), 1.60 (s, 6H), 1.51 (s, 6H), 1.25 (d, *J* = 6.8 Hz, 48H), 0.89 (t, *J* = 6.7 Hz, 9H) ppm; ¹³C NMR (150 MHz, CDCl₃) δ = 142.8, 137.4, 131.1, 127.3, 126.7, 35.6, 31.9, 31.3, 29.7, 29.7, 29.6, 29.6, 29.5, 29.4, 29.3, 22.7, 14.1 ppm; FTMS (MALDI) *m/z*: [C₆₀H₉₀+H]⁺, calcd. [C₆₀H₉₀+H] 812.38; found 812.87.

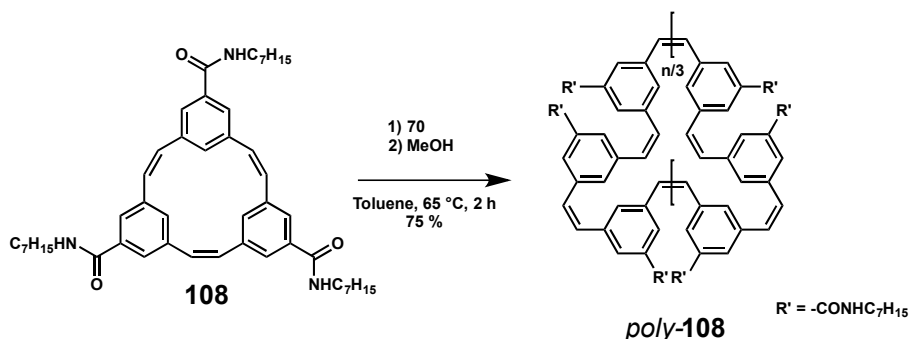
1⁵,4⁵,7⁵-tridodecyl-1,4,7(1,3)-tribenzenacyclononaphane-2,5,8-triylne (**113**) A two-neck 25 ml round-bottom flask was charged under N₂ with **27** (0.10 g, 0.123 mmol) and benzyltrimethylammonium tribromide (0.40 g, 1.03 mmol), and dry, degassed DCM (10 mL). The reaction was stirred for 24 h at 25 °C. The mixture was filtered over a short plug of silica gel and the filtrate was concentrated by rotary evaporator. Column chromatography (SiO₂; 20:1 hexanes:ethyl acetate) yielded the brominated compound, **112**, as a yellow solid which was used in the next reaction without further purification. A two-neck 25 ml round-bottom was charged under N₂ with **112** and dry, degassed THF (7 mL). The mixture was cooled to –30 °C and stirred for 20 min. A 0.44 M solution of potassium tertbutoxide in THF (3.4 mL) was then added dropwise over 1 h. The reaction mixture was stirred at –30 °C for 4 more hours. The mixture was then concentrated by rotary evaporator. Column chromatography (Al₂O₃, basic; 50:1 hexanes: ethyl acetate) yielded crude **113**. Crude **113** was dissolved in ethyl acetate (2 mL) and crystallized with MeOH (3 mL) to yield **113** as an off-white solid (0.05 g, 0.062 mmol, 48 %). ¹H NMR (600 MHz, CDCl₃) δ = 8.19 (s, 3H), 7.04 (d, *J* = 1.6 Hz, 6H), 2.61 (t, *J* = 7.7 Hz, 6H), 1.61 (s, 6H), 1.37–1.29 (m, 6H), 1.25 (s, 48H), 0.87 (t, *J* = 6.9 Hz, 9H) ppm. ¹³C NMR (151 MHz, C₆D₆) δ = 13.9, 22.7, 29.1, 29.4, 29.5, 29.6, 29.7, 29.7, 31.2, 31.9, 35.9, 100.5, 125.1, 125.8, 127.5, 127.7, 127.9, 143.2, 144.5 ppm; FTMS (MALDI) *m/z*: [C₆₀H₈₄+H]⁺, calcd. [C₆₀H₈₄+H] 806.33; found 806.77.



Scheme 5.5 Synthesis of **108**.

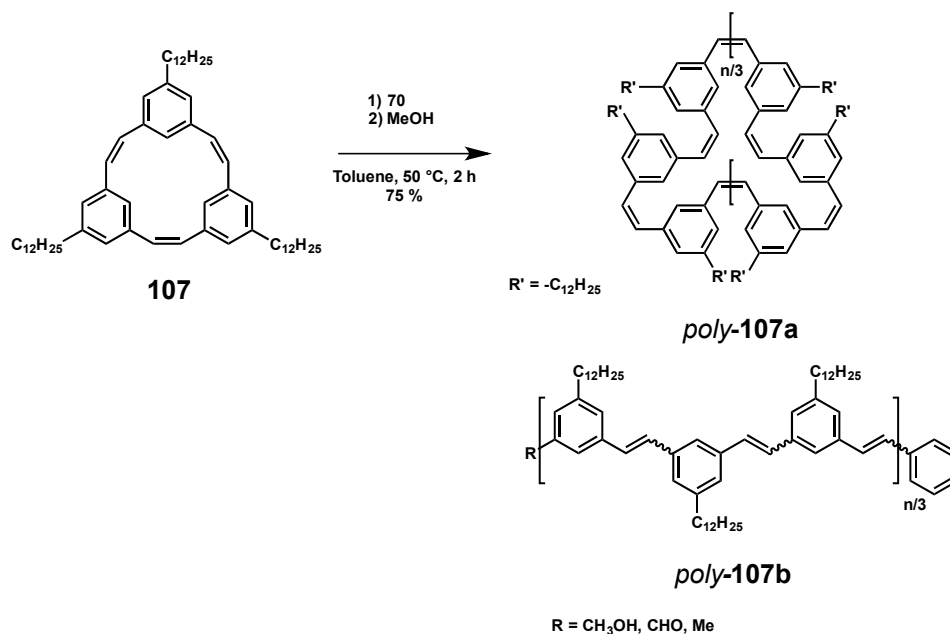
(2Z,5Z,8Z)-1⁵,4⁵,7⁵-tri-heptacarbamoyl-1,4,7(1,3)-tribenzenacyclononaphane-2,5,8-triene (**108**) A 5 ml Schlenk flask was charged under N₂ with *(2Z,5Z,8Z)-1⁵,4⁵,7⁵-tribromo-*

1,4,7(1,3)-tribenzenacyclononaphane-2,5,8-triene (**89**, 0.035 g, 0.064 mmol), 1-heptylamine (0.015 ml, 0.290 mmol), 4,5-Bis(diphenylphosphino)-9,9-dimethylxanthene (0.002 g, 0.003 mmol), Palladium(0) bis(dibenzylideneacetone) (0.001 g, 0.004 mmol), and sodium carbonate (0.022 g, 0.290 mmol) and toluene (0.5 mL). After three freeze-pump-thaw cycles, the atmosphere was evacuated and then charged with CO. The reaction mixture was then stirred at 80 °C for 18 h. The reaction mixture was concentrated on a rotary evaporator. Column chromatography (SiO₂; hexanes:EtOAc 1:1) yielded **108** (0.04 g, 0.055 mmol, 85 %) as a colorless solid. ¹H NMR (400 MHz, CDCl₃) δ = 7.40 (d, *J* = 1.6 Hz, 6H), 6.84 (s, 3H), 6.67 (s, 6H), 6.11 (s, 3H), 3.43 (t, *J* = 6.8 Hz, 6H), 1.38 (s, 20H), 0.93 (d, *J* = 6.0 Hz, 9H) ppm; FTMS (MALDI) *m/z*: [C₄₈H₆₃N₃O₃+H]⁺, calcd. [C₄₈H₆₃N₃O₃+H] 730.49; found 730.75.



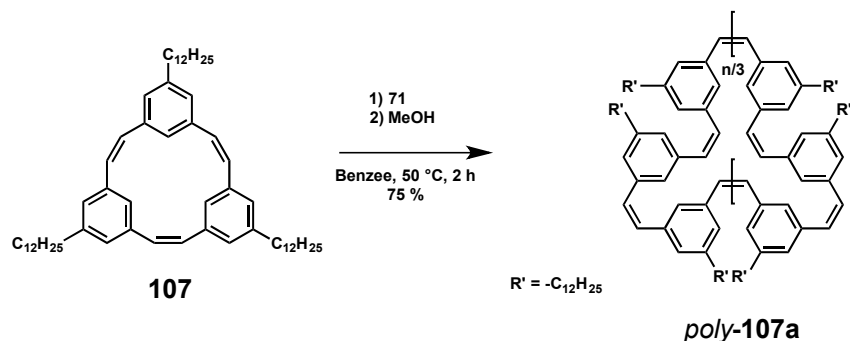
Scheme 5.6 Synthesis of *poly-108* by reaction of **108** with **70**.

Preparation of cyclic heptacarbomoyl substituted poly-(m-phenylene vinylene (poly-108)
 A J. Young tube was charged under N₂ with **108** (0.010 g, 13.7 μmol) in toluene-d₈ (0.45 mL). **70** (1.15 mg, 1.37 μmol) in toluene-d₈ (27 μL) was added at 24 °C and the mixture was warmed to 65 °C and stirred for 2 h. The reaction mixture was quenched with MeOH (10 mL). The solid precipitate was isolated by filtration and washed with MeOH (3 mL) yielding *poly-108* (0.075 g, 75%) as a colorless solid.



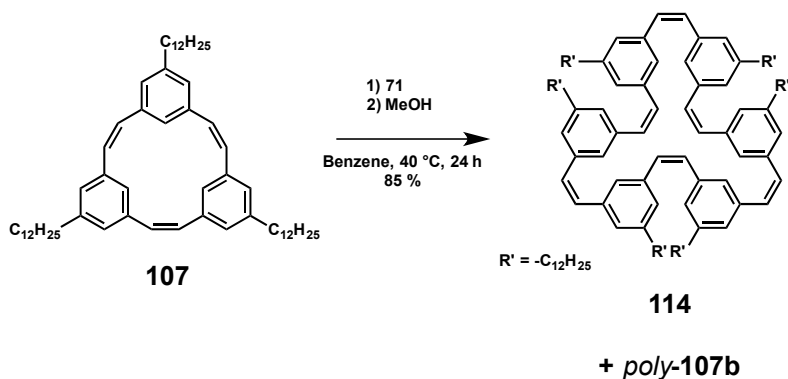
Scheme 5.7 Synthesis of *poly-107a* and *poly-107b* by reaction of **107** with **70**.

Preparation of linear and cyclic dodecyl substituted poly-(m-phenylene vinylene) (poly-107a, poly-107b) A J. Young tube was charged under N_2 with **107** (0.010 g, 12.3 μmol) in toluene (0.45 mL). **70** (1.03 mg, 1.23 μmol) in toluene (24 μL) was added at 24 $^\circ\text{C}$ and the mixture was warmed to 55 $^\circ\text{C}$ and stirred for 2 h. The reaction mixture was quenched with MeOH (2 mL). The solid precipitate was isolated by filtration and washed with MeOH (30 mL) yielding a mixture of *poly-107a* and *poly-107b* (0.075 g, 75%) as a light yellow solid.



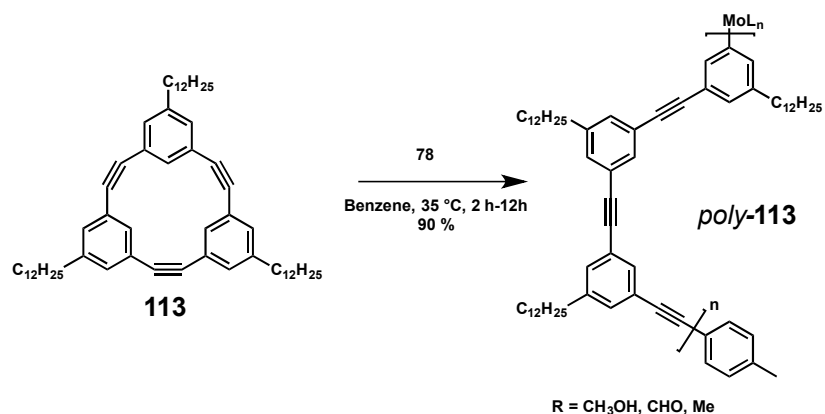
Scheme 5.8 Synthesis of *poly-107a* by reaction of **107** with **71** at 50 $^\circ\text{C}$ for 2 h.

Preparation of cyclic dodecyl substituted poly-(m-phenylene vinylene) (poly-107a) A J. Young tube was charged under N_2 with **107** (0.010 g, 12.3 μmol) in toluene (0.45 mL). **71** (1.11 mg, 1.23 μmol) in C_6D_6 (24 μL) was added at 24 $^\circ\text{C}$ and the mixture was warmed to 50 $^\circ\text{C}$ and stirred for 2 h. The reaction mixture was quenched with MeOH (2 mL). The solid precipitate was isolated by filtration and washed with MeOH (30 mL) yielding a mixture of *poly-107a* and *poly-107b* (0.075 g, 75%) as a light yellow solid.



Scheme 5.9 Synthesis of **114** by reaction of **107** with **71** at 40 °C for 24 h.

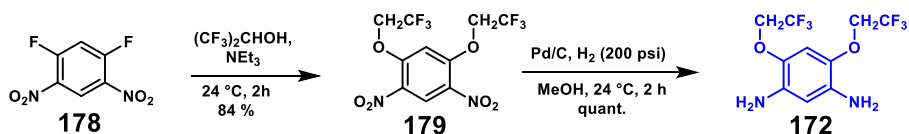
(2*Z*,5*Z*,8*Z*,11*Z*,14*Z*,17*Z*)-1⁵,4⁵,7⁵,10⁵,13⁵,16⁵-hexadecyl-1,4,7,10,13,16(1,3)-hexabenzencyclooctadecaphane-2,5,8,11,14,17-hexaene (**114**) A J. Young tube was charged under N₂ with **107** (0.010 g, 12.3 μmol) in toluene (0.45 mL). **71** (1.11 mg, 1.23 μmol) in C₆D₆ (24 μL) was added at 24 °C and the mixture was warmed to 40 °C and stirred for 24 h. The reaction mixture was quenched with MeOH (2 mL). The solid precipitate was isolated by filtration and washed with MeOH (30 mL) yielding a mixture of a crude mixture of **114** and *poly-107b* (0.085 g, 85%) as a light yellow solid. ¹H NMR (600 MHz, CDCl₃, 22 °C) δ = 7.62 (s, 1H), 7.29 (s, 2H), 7.22 (s, 2H), 2.66 (t, *J* = 6.8 Hz, 2H), 1.68 (m, 2H), 1.36 (m, 2H), 1.21–1.30 (m, 16H), 0.88 (t, *J* = 6.8 Hz, 3H) ppm. FTMS (MALDI) *m/z*: [C₁₂₀H₁₈₀–H]⁺ calcd. [C₁₂₀H₁₈₀–H] 1620.408; found 1620.370



Scheme 5.10 Synthesis of *poly-113* by reaction of **113** with **78**.

Preparation of dodecyl substituted poly-(m-phenyleneethynylene) (poly-113) A J. Young tube was charged under N₂ with **113** (0.0045 g, 5.60 μmol) in C₆D₆ (0.45 mL). **78** (1.51 mg, 1.68 μmol) in C₆D₆ (30 μL) was added at 24 °C and the mixture was warmed to 35 °C and stirred for 2 h. The reaction mixture was quenched with MeOH (1 mL). The solid precipitate was isolated by filtration and washed with MeOH (10 mL) yielding *poly-3b* (0.0041 g, 90 %) as a colorless solid. ¹H NMR (600 MHz, CDCl₃, 22 °C) δ = 7.53 (s, 1H),

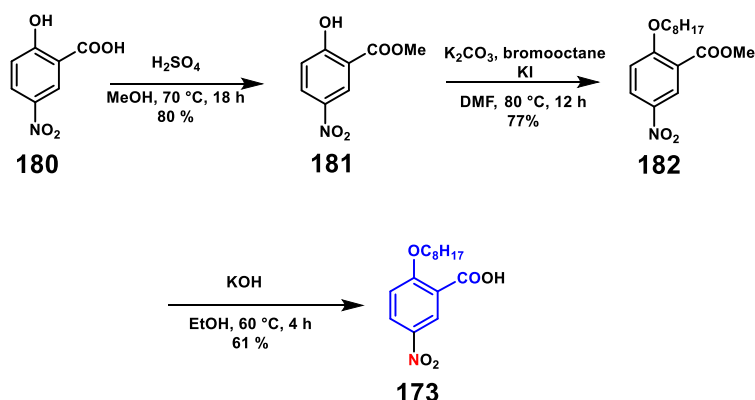
7.32 (s, 1H), 2.6 (t, $J = 6.8$ Hz, 2H), 1.85 (t, $J = 6.8$ Hz, 2H), 1.32 (t, $J = 6.8$ Hz, 2H), 1.21–1.28 (m, 16H), 0.86 (t, $J = 6.8$ Hz, 3H) ppm.



Scheme 5.11 Synthesis of **172**.

1,5-dinitro-2,4-bis(2,2,2-trifluoroethoxy)benzene (179) A 50 mL round bottom flask was charged under N_2 with 1,5-difluoro-2,4-dinitrobenzene (**1**) (3.00 g, 14.70 mmol) and triethylamine (3.27 g, 32.34 mmol). 2,2,2-Trifluoroethanol (3.08 g, 30.87 mmol) was added and the reaction mixture was stirred for 2 h at 24 °C. The reaction mixture was diluted with 50 mL of water and the precipitated solid was isolated by vacuum filtration and washed with three portions of water (20 mL). The filtered material was air dried for 3 hours to yield **179** (5.35 g, 14.69 mmol, quant.) as a yellow solid. 1H NMR (500 MHz, Acetone- d_6) $\delta = 8.75$ (s, 1H), 7.51 (s, 1H), 5.10 (q, $J = 8.2$ Hz, 4H) ppm. Previously reported by Kovalevksy et al.¹³⁶

4,6-bis(2,2,2-trifluoroethoxy)benzene-1,3-diamine (172) A 50 mL pressure bomb was charged under 200 psi H_2 with **2** (6.00 g, 16.48 mmol) and 10 % Pd/C (0.6 g) in methanol (20 mL). The reaction mixture was stirred for 2 h at 24 °C. The reaction mixture was filtered via vacuum filtration and the precipitate was triturated with three portions of methanol (20 mL). The filtrate was then diluted with 50 mL of water and the precipitate was isolated by vacuum filtration. The filtered material was washed with three portion of water (20 mL) and allowed to dry for 3 h to yield **172** (5.0 g, 16.48 mmol, quant.) as a light purple solid. 1H NMR (500 MHz, $CDCl_3$) $\delta = 6.50$ (s, 1H), 6.19 (s, 1H), 4.80 (s, $J = 5.1$ Hz, 2H), 4.25 (q, $J = 8.3$ Hz, 4H) ppm. Previously reported by Kovalevksy et al.¹³⁶



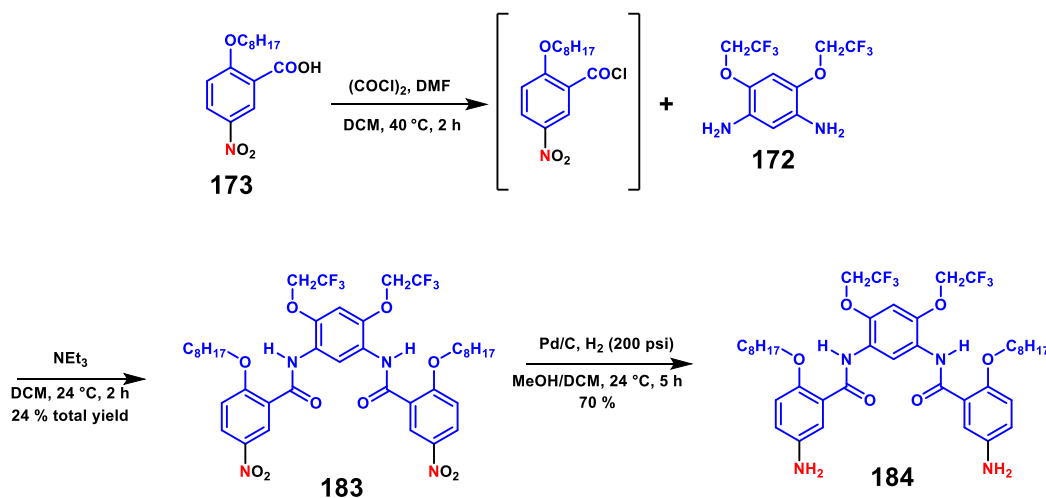
Scheme 5.12 Synthesis of **173**.

Methyl 2-hydroxy-5-nitrobenzoate (181) A two neck 500 mL round bottom was charged under N_2 with 2-hydroxy-5-nitrobenzoic acid (**180**) (30 g, 163.83 mmol), H_2SO_4 (6.6 mL),

and methanol (100 mL). The reaction mixture was stirred for 18 h at 70 °C. After this time, the mixture was diluted with water (250 mL) and the resulting precipitate was isolated by vacuum filtration and washed with three portions of water (100 mL). After drying for 12 h, **181** (26 g, 131.25 mmol, 80 %) was isolated as a pale yellow solid. Previously reported by Ng et al.¹³⁷

Methyl 5-nitro-2-(octyloxy)benzoate (182) A two-neck 250 mL round bottom flask was charged under N₂ with methyl 2-hydroxy-5-nitrobenzoate (**181**) (7.00 g, 35.5 mmol) and K₂CO₃ (7.36 g, 53.25 mmol) and dry DMF (50 mL). The reaction mixture was stirred for 1 h at 60 °C at which point 1-bromooctane (7.2 g, 37.28 mmol) and KI (0.7 g, 4.2 mmol) were added. The reaction mixture was then stirred for 3 h at 90 °C. After this time, the reaction mixture was poured in to water (100 mL) and extracted with three portions of diethyl ether (100 mL). The combined organic phases were washed with water (100 mL), dried over MgSO₄ and concentrated on a rotary evaporator. Recrystallization from ethanol (100 mL) yielded **182** (8.50 g, 27.47 mmol, 77 %) as a colorless solid. ¹H NMR (500 MHz, CDCl₃) δ = 8.71 (d, *J* = 2.9 Hz, 1H), 8.35 (dd, *J* = 9.2, 2.9 Hz, 1H), 7.05 (d, *J* = 9.3 Hz, 1H), 4.16 (t, *J* = 6.5 Hz, 2H), 3.94 (s, 3H), 1.89 (dt, *J* = 15.0, 6.7 Hz, 2H), 1.62–1.47 (m, 2H), 1.43–1.26 (m, 8H), 0.94–0.86 (m, 3H) ppm. Previously reported by Zeng et al.¹³⁸

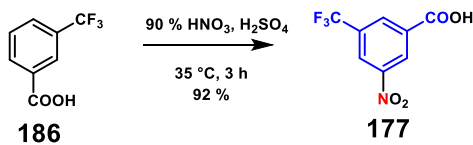
5-nitro-2-(octyloxy)benzoic acid (173) A two-neck 100 mL round bottom flask was charged under N₂ with *methyl 5-nitro-2-(octyloxy)benzoate (182)* (2.59 g, 8.38 mmol), KOH (4.63 g, 82.5 mmol) in water (10 mL), and ethanol (20 mL). The reaction mixture was stirred for 3 h at 85 °C. The reaction mixture was then poured in to water (100 mL) and acidified with to pH 3 with 37 % HCl in water. The resulting precipitate was isolated by vacuum filtration and washed with three portions of water (25 mL). The solid was allowed to dry for 3 h yielding **7** (1.50 g, 5.07 mmol, 60.7 %) as a colorless solid. ¹H NMR (400 MHz, CDCl₃) δ = 0.87 (t, *J* = 6.8, 3H), 1.33 (m, 8H), 1.51 (d, *J* = 6.9, 2H), 1.95 (d, *J* = 6.6, 2H), 4.32 (t, *J* = 6.6, 2H), 7.16 (d, *J* = 9.2, 1H), 8.41 (dd, *J* = 9.2, 2.9, 1H), 8.97 (d, *J* = 2.9, 1H). Previously reported by Zeng et al.¹³⁸



Scheme 5.13 Synthesis of **184**.

5-nitro-N-(5-(5-nitro-2-(octyloxy)benzamido)-2,4-bis(2,2,2-trifluoroethoxy)phenyl)-2-octylbenzamide (183) A 50 mL round bottom flask was charged under N₂ with *5-nitro-2-(octyloxy)benzoic acid (7)* (1.50 g, 5.07 mmol), oxalyl chloride (0.839 g, 6.6 mmol), and dry DCM (15 mL). After these were combined, a drop of DMF was added to the mixture. The reaction mixture was stirred for 2 h at 40 °C and then concentrated on a rotary evaporator. The residue was then dissolved in dry DCM (15 mL) and added dropwise to a two-neck 50 mL round bottom flask charged under N₂ with **3** (0.709 g, 2.33 mmol) and triethylamine (0.52 g, 2.3 mmol) at 0 °C. The reaction mixture was stirred for 2 h at 24 °C. After this time, the reaction mixture was poured in to water (50 mL) and extracted with three portions of ethyl acetate (30 mL). The combined organic phases were washed with water (100 mL), dried over MgSO₄ and concentrated on a rotary evaporator. Recrystallization from DCM (30 mL) yielded **8** (0.5 g, 5.6 mmol, 24 %) as a yellow solid. ¹H NMR (500 MHz, CDCl₃) δ = 9.85 (s, 2H), 9.52 (s, 1H), 9.19 (d, *J* = 2.9 Hz, 2H), 8.29 (dd, *J* = 9.2, 3.0 Hz, 2H), 7.14 (d, *J* = 9.2 Hz, 2H), 6.67 (s, 1H), 4.49 (q, *J* = 8.1 Hz, 4H), 4.38 (t, *J* = 7.2 Hz, 2H), 1.96 (t, *J* = 7.4 Hz, 2H), 1.45 (t, *J* = 7.8 Hz, 2H), 1.36 (t, *J* = 7.6 Hz, 2H), 1.35–1.19 (m, 8H), 0.86 (t, *J* = 6.8 Hz, 3H) ppm; ¹³C NMR (150 MHz, Acetone-d₆) δ = 161.3, 160.6, 144.3, 141.6, 128.2, 127.5, 124.8, 122.9, 114.1, 111.3, 109.2, 70.8, 66.8, 31.5, 29.3, 28.9, 28.5, 28.3, 25.5, 22.3, 13.3 ppm; FTMS (MALDI) (*m/z*): [C₄₀H₄₈F₆N₄O₁₀+H]⁺ calcd for [C₄₀H₄₈F₆N₄O₁₀], 859.33; found, 859.61.

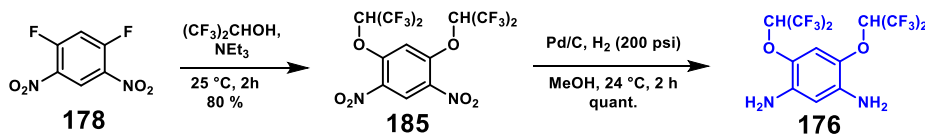
N,N'-(4,6-bis(2,2,2-trifluoroethoxy)-1,3-phenylene)bis(5-amino-2-(octyloxy)benzamide (9) A 25 mL pressure bomb was charged under 200 psi H₂ with **8** (0.4 g, 0.45 mmol) and 10 % Pd/C (0.04 g) in methanol (5 mL). The reaction mixture was stirred for 18 h at 40 °C. The reaction mixture was filtered via vacuum filtration and the precipitate was triturated with three portions of ethyl acetate (10 mL). The filtrate was then concentrated by rotary evaporator to yield **9** (0.26 g, 0.31 mmol, 70 %) as a grey solid. ¹H NMR (600 MHz, CDCl₃) δ = 10.21 (s, 2H), 9.35 (s, 1H), 7.67 (s, 2H), 6.86 (m, 2H), 6.82 (m, 2H), 6.70 (s, 1H), 4.39 (q, *J* = 8.2 Hz, 4H), 4.12 (t, *J* = 7.0 Hz, 2H), 1.82 (t, *J* = 7.3 Hz, 2H), 1.39 (t, *J* = 7.4 Hz, 2H), 1.16–1.33 (m, 8H), 0.84 (t, *J* = 6.8 Hz, 3H) ppm; ¹³C NMR (166 MHz, Acetone-d₆) δ = 158.5, 146.6, 145.5, 141.2, 122.9, 119.3, 118.6, 117.2, 114.1, 112.4, 111.3, 109.2, 70.8, 66.8, 31.5, 29.3, 28.5, 28.3, 25.5, 22.3, 13.3 ppm; FTMS (MALDI) (*m/z*): [C₄₀H₅₂F₆N₄O₆+H]⁺ calcd for [C₄₀H₅₂F₆N₄O₆+H], 799.97; found, 800.03.



Scheme 5.14 Synthesis of **177**.

3-nitro-5-(trifluoromethyl)benzoic acid (13) To a 100 mL roundbottom flask was added 3-trifluoromethylbenzoic acid (**12**) (5.00 g, 26.30 mmol), concentrated sulfuric acid (21.63 mL). The reaction mixture was cooled to 0 °C and 90 % fuming nitric acid (5.16 mL) was added slowly over 1 h. The reaction mixture was stirred for 3 h at 35 °C and then slowly poured over ice (100 g). The resulting precipitate was isolated by vacuum filtration, washed

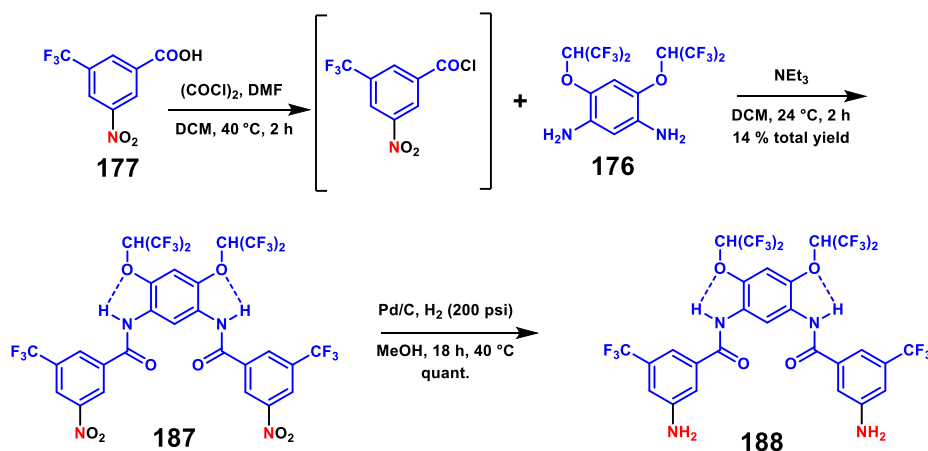
with water (100 mL), then re-dissolved in ethyl acetate (50 mL). The ethyl acetate solution was washed with water (100 mL), dried over MgSO₄ and concentrated on a rotary evaporator to yield 3-nitro-5-(trifluoromethyl)benzoic acid (5.69 g, 24.20 mmol, 92 %) as a colorless solid. ¹H-NMR (300 MHz, CDCl₃) δ = 8.69 (1H, s), 8.74 (1H, s), 9.1 (1H, s) ppm. Previously reported by Takemoto et al.¹³⁹



Scheme 5.15 Synthesis of **176**.

1,5-bis((1,1,1,3,3,3-hexafluoropropan-2-yl)oxy)-2,4-dinitrobenzene (185) A 50 mL round bottom flask was charged under N₂ with *1,5-difluoro-2,4-dinitrobenzene* (5.00 g, 24.50 mmol) and triethylamine (5.45 g, 53.90 mmol). 1,1,1,3,3,3-hexafluoro-2-propanol (8.49 g, 51.45 mmol) was added and the reaction mixture was stirred for 2 h at 24 °C. The reaction mixture was diluted with 50 mL of water and the precipitated solid was isolated by vacuum filtration and washed with three portions of water (20 mL). The filtered material was air dried to yield **185** (7.5 g, 20.60 mmol, 84 %) as a yellow solid. ¹H NMR (500 MHz, Acetone-*d*₆) δ = 8.75 (s, 1H), 7.51 (s, 1H), 5.10 (q, *J* = 8.2 Hz, 4H) ppm; ¹³C NMR (150 MHz, Acetone-*d*₆) δ = 157.4, 131.2, 121.2, 118.7, 105.7, 74.6 ppm; ESI-HR-MS (*m/z*): [C₁₂H₄F₁₂N₂O₆]⁺, calcd for [C₁₂H₄F₁₂N₂O₆] 500.1528; found, 500.1534.

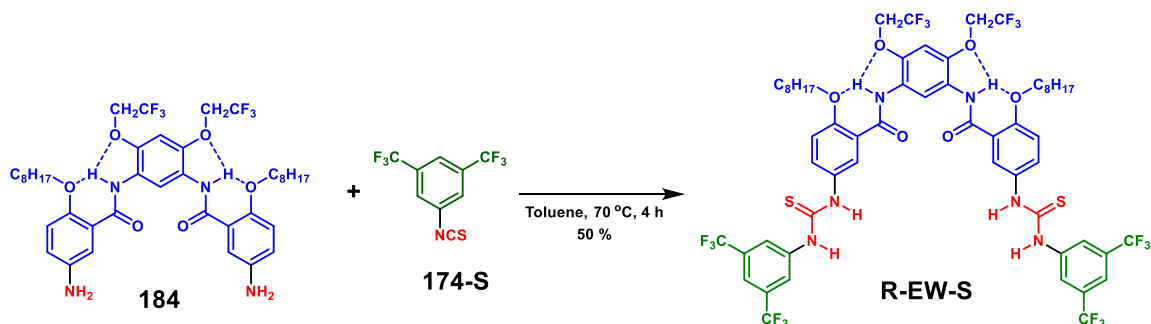
4,6-bis(2,2,2-trifluoroethoxy)benzene-1,3-diamine (176) A 50 mL pressure bomb was charged under 200 psi H₂ with **185** (4.00 g, 8.00 mmol) and 10 % Pd/C (0.4 g) in methanol (20 mL). The reaction mixture was stirred for 2 h at 24 °C. The reaction mixture was filtered via vacuum filtration and the precipitate was triturated with three portions of methanol (20 mL). The filtrate was then diluted with 50 mL of water and the precipitate was isolated by vacuum filtration. The filtered material was washed with three portions of water (20 mL) and allowed to dry for 3 h to yield **176** (3.51 g, 7.99 mmol, quant.) as a light purple solid. ¹H NMR (500 MHz, CDCl₃) δ = 6.50 (s, 1H), 6.19 (s, 1H), 4.80 (s, *J* = 5.1 Hz, 2H), 4.25 (q, *J* = 8.3 Hz, 4H) ppm; ¹³C NMR (150 MHz, Acetone-*d*₆) δ = 135.7, 129.9, 116.9, 102.5, 101.1, 74.6 ppm; ESI-HR-MS (*m/z*): [C₁₂H₈F₁₂N₂O₂]⁺, calcd for [C₁₂H₈F₁₂N₂O₂] 440.0394; found, 440.0395.



Scheme 5.16 Synthesis of **188**.

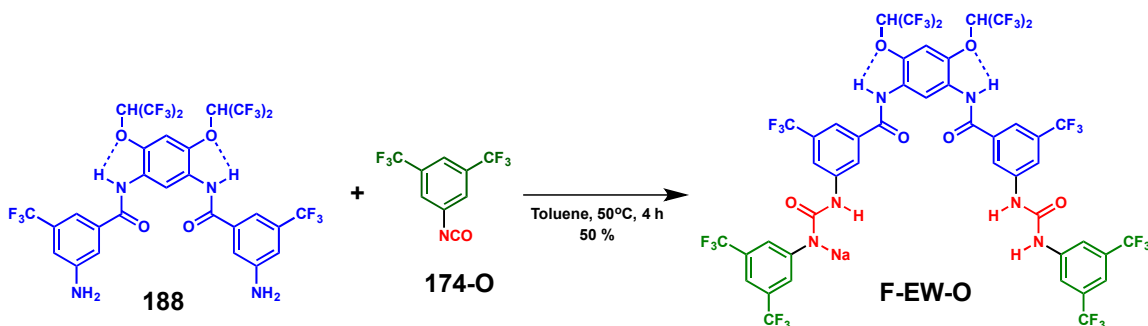
N,N'-(4,6-bis((1,1,1,3,3,3-hexafluoropropan-2-yl)oxy)-1,3-phenylene)bis(3-nitro-5-(trifluoromethyl)benzamide) (**187**) A 50 mL round bottom flask was charged under N_2 with 3-nitro-5-(trifluoromethyl)benzoic acid (**177**) (2.00 g, 8.51 mmol), oxalyl chloride (1.29 g, 10.20 mmol), and dry DCM (10 mL). After these were combined, a drop of DMF was added to the mixture. The reaction mixture was stirred for 2 h at $40\text{ }^\circ\text{C}$ and then concentrated on a rotary evaporator. The residue was then dissolved in dry DCM (10 mL) and added dropwise to a two-neck 50 mL round bottom flask charged under N_2 with **176** (1.61 g, 3.66 mmol) and triethylamine (1.11 g, 10.97 mmol) at $0\text{ }^\circ\text{C}$. The reaction mixture was stirred for 2 h at $24\text{ }^\circ\text{C}$. The precipitated material from the reaction mixture was isolated by vacuum filtration and washed with three portions of water (20 mL). This solid was allowed to dry under vacuum for 3 h to yield **187** (1.00 g, 1.14 mmol, 13.4 %) as an off-white solid. ^1H NMR (500 MHz, CDCl_3) δ = 8.98 (s, 2H), 8.65 (s, 2H), 8.54 (s, 2H), 8.42 (s, 1H), 7.35 (s, 2H), 7.16 (s, 1H), 5.65 (m, 2H) ppm; ^{13}C NMR (150 MHz, Acetone- d_6) δ = 166.7, 145.7, 135.2, 132.7, 128.7, 126.5, 124.3, 122.4, 119.9, 118.5, 116.9, 115.5, 104.1, 74.6 ppm; ESI-HR-MS (m/z): $[\text{C}_{28}\text{H}_{12}\text{F}_{18}\text{N}_4\text{O}_8]^+$, calcd for $[\text{C}_{28}\text{H}_{12}\text{F}_{18}\text{N}_4\text{O}_8]$ 874.0368; found, 874.0372.

N,N'-(4,6-bis((1,1,1,3,3,3-hexafluoropropan-2-yl)oxy)-1,3-phenylene)bis(3-amino-5-(trifluoromethyl)benzamide) (**188**) A 100 mL pressure bomb was charged under 200 psi H_2 with **187** (1.0 g, 1.14 mmol) and 10 % Pd/C (0.12 g) in methanol (10 mL) and ethyl acetate (5 mL). The reaction mixture was stirred for 18 h at $40\text{ }^\circ\text{C}$. The reaction mixture was filtered and the precipitate was triturated with three portions of ethyl acetate (10 mL). The filtrate was then concentrated by rotary evaporator to yield **188** (0.9 g, 1.10 mmol, 96 %) as a grey solid. ^1H NMR (600 MHz, DMSO- d_6) δ = 9.97 (s, 2H), 7.56 (s, 1H), 7.24 (s, 1H), 7.23 (s, 2H), 7.23 (s, 2H), 7.02 (s, 2H), 6.20 (m, 2H), 5.7 (s, 4H) ppm; ^{13}C NMR (150 MHz, Acetone- d_6) δ = 164.5, 149.8, 145.5, 136.5, 131.2, 126.9, 125.2, 123.3, 120.4, 116.3, 112.9, 110.7, 105.2, 75.5 ppm; FTMS (MALDI) (m/z): $[\text{C}_{28}\text{H}_{16}\text{F}_{18}\text{N}_4\text{O}_4+\text{H}]^+$ calcd for $[\text{C}_{28}\text{H}_{16}\text{F}_{18}\text{N}_4\text{O}_4+\text{H}]$, 815.08; found, 815.23.



Scheme 5.17 Synthesis of **R-EW-S**.

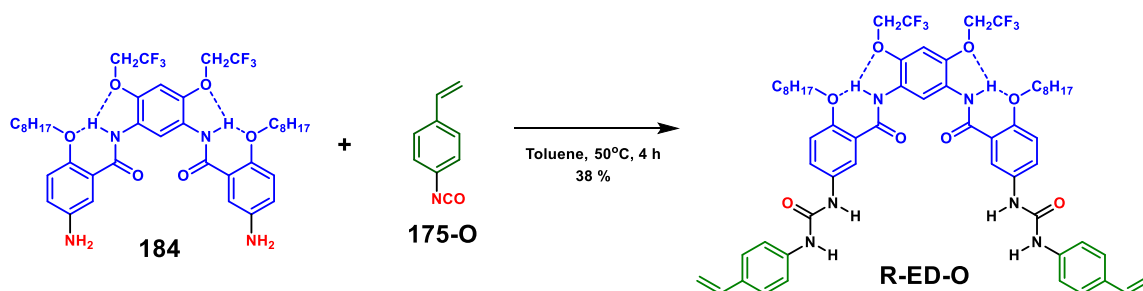
N,N'-(4,6-bis(2,2,2-trifluoroethoxy)-1,3-phenylene)bis(5-(3-(3,5-bis(trifluoromethyl)phenyl)thioureido)-2-(octyloxy)benzamide) (**R-EW-S**) A two-neck 25 mL round bottom charged under N₂ with 3,5-bistrifluoromethyl isothiocyanate (0.18 g, 0.64 mmol), **174-S** (0.25 g, 0.313 mmol), and toluene (10 mL). The reaction mixture was stirred for 4 h at 50 °C. After this time the reaction mixture was concentrated on a rotary evaporator. Column chromatography (SiO₂; 20:1 DCM/MeOH) yielded **R-EW-S** (0.2 g, 0.15 mmol, 47.7 %) as a grey solid. ¹H NMR (600 MHz, DMSO-*d*₆) δ = 10.28 (s, 2H), 10.16 (s, 2H), 10.05 (s, 2H), 9.24 (d, *J* = 2.7 Hz, 1H), 8.22 (s, 4H), 7.98 (t, *J* = 2.7 Hz, 2H), 7.77 (s, 2H), 7.62 (d, *J* = 8.7 Hz, 2H), 7.28 (m, *J* = 2.7 Hz, 3H), 4.91 (q, *J* = 8.9 Hz, 4H), 4.27 (t, *J* = 15.2 Hz, 4H), 1.79 (d, *J* = 8.4 Hz, 4H), 1.35 (t, *J* = 7.8 Hz, 4H), 1.25 (s, 4H), 1.19 – 1.10 (m, 12H), 0.75 (td, *J* = 7.1, 2.6 Hz, 6H) ppm; ¹³C NMR (166 MHz, Acetone-*d*₆) δ = 179.7, 162.6, 152.3, 144.0, 142.4, 132.9, 131.8 (q, 32.7 Hz), 131.3, 126.2, 124.6, 124.6 (q, 272 Hz), 122.8, 122.6, 122.1, 118.3, 114.4, 107.5, 100.8, 69.8, 66.9, 31.5, 29.3, 28.5, 28.3, 25.5, 22.3, 13.3 ppm; FTMS (MALDI) (*m/z*): [C₅₈H₅₈F₁₈N₆O₆S₂+H]⁺ calcd for [C₅₈H₅₈F₁₈N₆O₆S₂-H+Na], 1362.34; found, 1362.42



Scheme 5.18 Synthesis of **F-EW-O**.

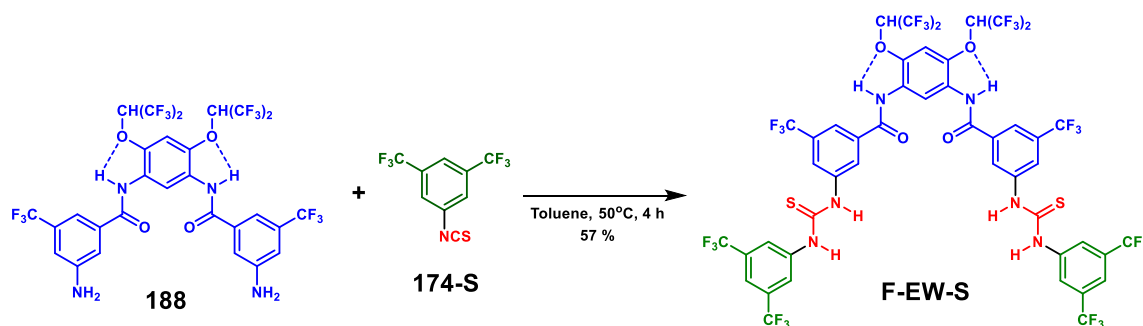
2-trifluoroethoxy)-1,3-phenylene)bis(5-(3-(3,5-bis(trifluoromethyl)phenyl)ureido)-2-(octyloxy)benzamide) (**R-EW-O**) A two-neck 25 mL round bottom charged under N₂ with 3,5-bistrifluoromethyl isocyanate (0.177 g, 0.63 mmol), **174-O** (0.25 g, 0.31 mmol), and toluene (10 mL). The reaction mixture was stirred for 4 h at 50 °C. After this times the reaction mixture was concentrated on a rotary evaporator. Recrystallization from ethanol (5 mL) yielded **R-EW-O** (0.25 g, 0.19 mmol, 61.6 %) as a colorless solid. ¹H NMR (600 MHz, DMSO-*d*₆) δ = 10.10 (s, 2H), 9.37 (s, 2H), 9.26 (s, 1H), 9.06 (s, 2H), 8.14 (s, 4H),

8.09 (d, $J = 2.8$ Hz, 2H), 7.70 (dd, $J = 9.3, 2.7$ Hz, 2H), 7.61 (s, 2H), 7.28 (s, 1H), 7.23 (d, $J = 9.0$ Hz, 2H), 4.91 (q, $J = 8.8$ Hz, 4H), 4.23 (t, $J = 6.7$ Hz, 4H), 1.76 (q, $J = 7.2$ Hz, 4H), 1.34 (t, $J = 7.8$ Hz, 4H), 1.28–1.22 (m, 4H), 1.14 (m, $J = 16.9, 10.4, 8.7$ Hz, 12H), 0.75 (t, $J = 6.9$ Hz, 6H) ppm; ^{13}C NMR (166 MHz, Acetone- d_6) $\delta = 162.6, 152.7, 152.3, 144.0, 142.1, 132.9, 131.6$ (q, 32.7 Hz), 131.3, 126.2, 124.6, 124.4 (q, 272 Hz), 122.8, 122.6, 122.1, 118.0, 114.4, 107.5, 100.8, 69.8, 66.9, 31.5, 29.3, 28.5, 28.3, 25.5, 22.3, 13.3 ppm. FTMS (MALDI) (m/z): $[\text{C}_{58}\text{H}_{58}\text{F}_{18}\text{N}_6\text{O}_8+\text{H}]^+$ calcd for $[\text{C}_{58}\text{H}_{58}\text{F}_{18}\text{N}_6\text{O}_8-\text{H}+\text{Na}]$, 1330.38; found, 1330.43.



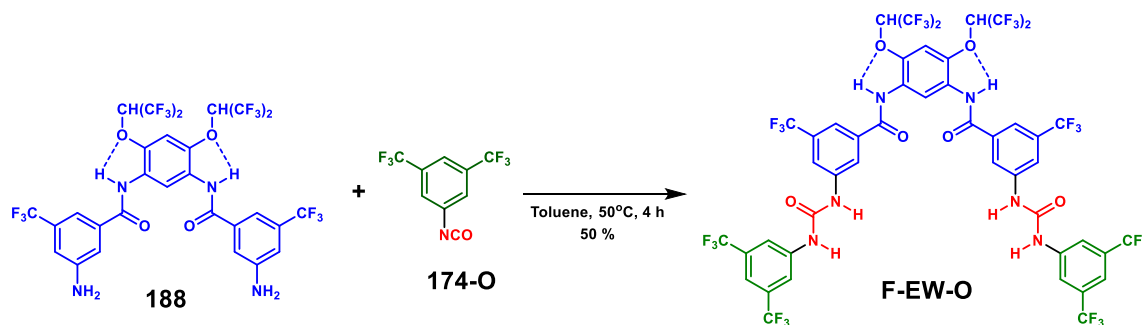
Scheme 5.19 Synthesis of **R-ED-O**.

N,N'-(4,6-bis(2,2,2-trifluoroethoxy)-1,3-phenylene)bis(5-(3-(,5-bis(trifluoromethyl)phenyl)ureido)-2-(octyloxy)benzamide) (**R-ED-O**) A two-neck 25 mL round bottom charged under N_2 with **9** (0.5 g, .63 mmol), 4-vinylisocyanate (**175-O**, 0.186 g, 1.29 mmol), and toluene (10 mL). The reaction mixture was stirred for 4 h at 50 °C. After this times the reaction mixture was concentrated on a rotary evaporator. Column chromatography (SiO_2 ; 10:1 DCM/MeOH) yielded **R-ED-O** (0.6 g, 0.17 mmol, 38 %) as red-orange crystals. ^1H NMR (600 MHz, $\text{DMSO}-d_6$) $\delta = 10.11$ (s, 2H), 9.26 (s, 1H), 8.75 (s, 2H), 8.71 (s, 2H), 8.00 (d, $J = 2.8$ Hz, 2H), 7.72 (dd, $J = 8.9, 2.8$ Hz, 4H), 7.44 (d, $J = 8.6$ Hz, 4H), 7.37 (d, $J = 8.6$ Hz, 4H), 7.28 (s, 1H), 7.22 (d, $J = 9.1$ Hz, 2H), 6.64 (dd, $J = 17.6, 11.0$ Hz, 2H), 5.68 (d, $J = 17.7$ Hz, 2H), 5.11 (d, $J = 11.2$ Hz, 2H), 4.91 (q, $J = 8.7$ Hz, 4H), 4.22 (t, $J = 6.6$ Hz, 4H), 1.79–1.73 (m, 4H), 1.36–1.30 (m, 4H), 1.26–1.19 (m, 4H), 1.14 (dd, $J = 15.1, 7.7$ Hz, 12H), 0.75 (t, $J = 7.0$ Hz, 6H) ppm. ^{13}C NMR (166 MHz, Acetone- d_6) $\delta = 163.1, 152.8, 152.3, 144.2, 139.7, 136.5, 133.5, 131.4, 126.5, 124.8, 124.4, 122.9, 122.5, 121.8, 118.4, 113.8, 110.9, 107.5, 100.8, 69.8, 66.6, 31.5, 29.3, 28.5, 28.3, 25.5, 22.3, 13.4$ ppm; FTMS (MALDI) (m/z): $[\text{C}_{58}\text{H}_{66}\text{F}_6\text{N}_6\text{O}_8+\text{H}]^+$ calcd for $[\text{C}_{58}\text{H}_{66}\text{F}_6\text{N}_6\text{O}_8+\text{H}+\text{Na}]$, 1112.18; found, 1112.71.



Scheme 5.20 Synthesis of F-EW-S.

N,N'-(4,6-bis((1,1,1,3,3,3-hexafluoropropan-2-yl)oxy)-1,3-phenylene)bis(3-(3-(3,5-bis(trifluoromethyl)phenyl)thioureido)-5-(trifluoromethyl)benzamide) (**F-EW-S**) A two-neck 100 mL round bottom charged under N₂ with 3,5-bistrifluoromethyl isothiocyanate (1.66 g, 6.125 mmol), **174-S** (1.25 g, 1.54 mmol), and toluene (25 mL). The reaction mixture was stirred for 4 h at 50 °C. After this times the reaction mixture was concentrated on a rotary evaporator. The residue was taken up in DCM (5 mL) and precipitated with the addition of hexanes (10 mL). The precipitate was isolated by vacuum filtration, washed with water, and dried over 3 h to yield **F-EW-S** (1.2 g, 0.88 mmol, 57%) as a light brown solid. ¹H NMR (600 MHz, DMSO-*d*₆) δ = 10.62 (s, 2H), 10.53 (s, 2H), 10.29 (s, 2H), 8.21 (s, 4H), 8.19 (s, 3H), 8.11 (s, 2H), 8.03 (s, 2H), 7.83 (s, 2H), 7.68 (s, 1H), 7.29 (s, 1H), 6.33 (s, 2H) ppm; ¹³C NMR (150 MHz, Acetone-*d*₆) δ = 181.2, 164.0, 146.2, 142.2, 140.9, 136.3, 131.9 (q, 32.7 Hz), 131.3, 130.9 (q, 32.7), 125.5, 123.9 (q, 270 Hz), 123.5 (q, 270 Hz), 121.3, 118.4, 118.1, 117.5, 115.1, 105.0, 75.6 ppm; FTMS (MALDI) (*m/z*): [C₄₆H₂₂F₃₀N₆O₄S₂+H]⁺ calcd for [C₄₆H₂₂F₃₀N₆O₄S₂-H+Na], 1378.05; found, 1378.05.



Scheme 5.21 Synthesis of F-EW-O.

N,N'-(4,6-bis((1,1,1,3,3,3-hexafluoropropan-2-yl)oxy)-1,3-phenylene)bis(3-(3-(3,5-bis(trifluoromethyl)phenyl)ureido)-5-(trifluoromethyl)benzamide) (**F-EW-O**) A two-neck 25 mL round bottom charged under N₂ with **174-O** (0.25 g, 0.31 mmol), 3,5-bistrifluoromethyl isocyanate (0.156 g, 0.63 mmol), and toluene (10 mL). The reaction mixture was stirred for 4 h at 50 °C. After this time the reaction mixture was concentrated on a rotary evaporator. Column chromatography (SiO₂; 10:1 DCM/MeOH) yielded **F-EW-O** (0.24 g, 0.18 mmol, 58.4 %) as grey crystals. ¹H NMR (400 MHz, DMSO-*d*₆) δ = 10.26 (s, 2H), 9.66 (d, *J* = 5.4 Hz, 4H), 8.23 (s, 2H), 8.20 (s, 4H), 7.91 (s, 2H), 7.76 (s, 1H), 7.69 (s, 2H), 7.34 (s, 1H), 6.38 (q, *J* = 5.9 Hz, 2H) ppm; ¹³C NMR (150 MHz, Acetone-*d*₆) δ = 164.1, 152.3, 146.2, 141.6, 140.9, 136.3, 131.6 (q, 32.7 Hz), 131.3, 130.9 (q, 32.7 Hz), 125.1, 123.9 (q, 270 Hz), 123.5 (q, 270 Hz), 121.3, 118.4, 118.1, 117.5, 115.1, 105.0, 75.6 ppm; FTMS (MALDI) (*m/z*): [C₄₆H₂₂F₃₀N₆O₆+H]⁺ calcd for [C₄₆H₂₂F₃₀N₆O₆-H+Na], 1346.09; found, 1346.35.

5.2 Kinetics Experiment Set-Up

A typical kinetic polymerization experiment of **113** consisted of the following: stock solution of **133** (12.3 mM) in C₆D₆ stored over molecular sieves

- Stock solution of **78** (400 mM) in C₆D₆

A J. Young NMR tube was charged with 450 μ L aliquot of monomer **2b** and 27 or 81 μ L, respectively, aliquot of catalyst **78**. The ¹H NMR spectra were recorded at a calibrated temperature (35 during regular intervals. The disappearance of the resonance for internal benzene proton in the ring-strained monomer **113** at 8.19 ppm was monitored and integrated with respect to an external ERETIC standard.

The data was analyzed by fitting a line to $\ln([M]/[M]_0)$ vs. t . Dividing the slope by $[C]_0$, as determined by ERETIC, provides k_p .

6 References

- (1) Bunz, U. H. F. *Macromol. Rapid Commun.* **2009**, *30* (9-10), 772.
- (2) Zhao, X.; Pinto, M. R.; Hardison, L. M.; Mwaura, J.; Müller, J.; Jiang, H.; Witker, D.; Kleiman, V. D.; Reynolds, J. R.; Schanze, K. S. *Macromolecules* **2006**, *39* (19), 6355.
- (3) Yuan, L.; Zeng, H.; Yamato, K.; Sanford, A. R.; Feng, W.; Atreya, H. S.; Sukumaran, D. K.; Szyperski, T.; Gong, B. *J. Am. Chem. Soc.* **2004**, *126* (50), 16528.
- (4) Nelson, J. C.; Saven, J. G.; Moore, J. S.; Wolynes, P. G. *Science* **1997**, *277* (5333), 1793.
- (5) Kübel, C.; Mio, M. J.; Moore, J. S.; Martin, D. C. *J. Am. Chem. Soc.* **2002**, *124* (29), 8605.
- (6) Bielawski, C. W.; Grubbs, R. H. *Progress in Polymer Science* **2007**, *32* (1), 1.
- (7) Dieck, H. A.; Heck, F. R. *Journal of Organometallic Chemistry* **1975**, *93* (2), 259.
- (8) Sonogashira, K.; Tohda, Y.; Hagihara, N. *Tetrahedron Letters* **1975**, *16* (50), 4467.
- (9) Cassar, L. *Journal of Organometallic Chemistry* **1975**, *93* (2), 253.
- (10) Koch, F.; Heitz, W. *Macromolecular Chemistry and Physics* **1997**, *198* (5), 1531.
- (11) Klingelhöfer, S.; Schellenberg, C. *Macromolecular ...* **1997**.
- (12) McDonald, R. N.; Campbell, T. W. *Journal of the American Chemical ...* **1960**.
- (13) Swager, T. M.; Zheng, J. *Poly(arylene ethynylene)s in Chemosensing and Biosensing*; 2005.
- (14) Zhang, W.; Moore, J. S. *Adv. Synth. Catal.* **2007**, *349* (1-2), 93.
- (15) Weiss, K.; Michel, A.; Auth, E.-M.; Bunz, U. H. F.; Mangel, T.; Müllen, K. *Angewandte Chemie International Edition in English* **1997**, *36* (5), 506.
- (16) Bunz, U. H. F. *Acc. Chem. Res.* **2001**, *34* (12), 998.
- (17) Mäker, D.; Maier, C.; Brödner, K.; Bunz, U. H. F. *ACS Macro Lett.* **2014**, *3* (5), 415.
- (18) Menk, F.; Mondeshki, M.; Dudenko, D.; Shin, S.; Schollmeyer, D.; Ceyhun, O.; Choi, T.-L.; Zentel, R. *Macromolecules* **2015**, *48* (20), 7435.

- (19) Yu, C.-Y.; Horie, M.; Spring, A. M.; Tremel, K.; Turner, M. L. *Macromolecules* **2010**, *43* (1), 222.
- (20) Yu, C.-Y.; Kingsley, J. W.; Lidzey, D. G.; Turner, M. L. *Macromol. Rapid Commun.* **2009**, *30* (22), 1889.
- (21) Yu, C.-Y.; Turner, M. L. *Angew. Chem. Int. Ed. Engl.* **2006**, *45* (46), 7797.
- (22) Fischer, F. R.; Nuckolls, C. *Angew. Chem. Int. Ed. Engl.* **2010**, *49* (40), 7257.
- (23) Bellone, D. E.; Bours, J.; Menke, E. H.; Fischer, F. R. *J. Am. Chem. Soc.* **2015**, 150106063549007.
- (24) Kugelgen, von, S.; Bellone, D. E.; Cloke, R. R.; Perkins, W. S.; Fischer, F. R. *J. Am. Chem. Soc.* **2016**, *138* (19), 6234.
- (25) Liu, S.; Dicker, K. T.; Jia, X. **2015**, *51* (25), 5218.
- (26) Perkin, W. H. *Berichte der deutschen chemischen Gesellschaft* **1884**, *17* (1), 323.
- (27) Baeyer, A. *Berichte der deutschen chemischen Gesellschaft* **1885**, *18* (2), 2269.
- (28) Wiberg, K. B. *Angewandte Chemie International Edition in English* **1986**, *25* (4), 312.
- (29) Franklin, J. L. *Industrial & Engineering Chemistry* **1949**, *41* (5), 1070.
- (30) Maier, W. F.; Rague Schleyer, Von, P. *J. Am. Chem. Soc.* **1981**, *103* (8), 1891.
- (31) Cope, A. C.; Moore, P. T.; Moore, W. R. *Journal of the American ...* **1960**.
- (32) Trætteberg, M. *Chemischer Informationsdienst* **1975**, *6* (22), no.
- (33) Buchanan, G. L. *Chem. Soc. Rev.* **1974**, *3* (1), 41.
- (34) Nokami, J.; Nishiuchi, K.; Wakabayashi, S.; Okawara, R. *Tetrahedron Letters* **1980**, *21* (46), 4455.
- (35) Lonsdale, D. K.; Milledge, H. J.; Rao, K. V. K. *Proceedings of the Royal Society A: Mathematical, Physical and Engineering Sciences* **1960**, *255* (1280), 82.
- (36) Boyd, R. H. *Tetrahedron* **1966**, *22* (1), 119.
- (37) Shieh, C.-F.; McNally, D.; Boyd, R. H. *Tetrahedron* **1969**, *25* (17), 3653.
- (38) Gantzel, P. K.; Trueblood, K. N. *Acta Crystallographica* **1965**.
- (39) Liebman, J. F.; Greenberg, A. *Chem. Rev.* **1976**, *76* (3), 311.
- (40) Bennett, M. A.; Robertson, G. B.; Whimp, P. O.; Yoshida, T. *J. Am. Chem. Soc.* **1971**, *93* (15), 3797.
- (41) Trætteberg, M.; Lüttke, W.; Machinek, R.; Krebs, A.; Hohlt, H. J. *Journal of Molecular Structure* **1985**, *128* (1-3), 217.
- (42) Kloster-Jensen, E.; Wirz, J. *Angewandte Chemie International Edition in English* **1973**, *12* (8), 671.
- (43) Wong, H.; Garratt, P. J. *Journal of the American ...* **1974**.
- (44) Gordon, C. G.; Mackey, J. L.; Jewett, J. C.; Sletten, E. M.; Houk, K. N.; Bertozzi, C. R. *J. Am. Chem. Soc.* **2012**, *134* (22), 9199.
- (45) Agard, N. J.; Prescher, J. A.; Bertozzi, C. R. *J. Am. Chem. Soc.* **2004**, *126* (46), 15046.
- (46) Kawase, T.; Ueda, N.; Oda, M. *Tetrahedron Letters* **1997**, *38* (38), 6681.
- (47) Kawase, T. *Synlett* **2007**, *2007* (17), 2609.
- (48) Kawase, T.; Hosokawa, Y.; Kurata, H.; Oda, M. *Chemistry Letters* **1999**, *28* (8), 745.

- (49) Kawase, T.; Daifuku, Y.; Hirao, Y.; Matsumoto, K.; Kurata, H.; Kubo, T. *Comptes rendus - Chimie* **2009**, *12* (3-4), 403.
- (50) Utsumi, K.; Kawase, T.; Oda, M. *Chemistry Letters* **2003**, *32* (4), 412.
- (51) Kawase, T.; Nishiyama, Y.; Nakamura, T.; Ebi, T.; Matsumoto, K.; Kurata, H.; Oda, M. *Angew. Chem. Int. Ed.* **2007**, *46* (7), 1086.
- (52) Kawase, T.; Darabi, H. R.; Oda, M. ... *Chemie International Edition in ...* **1996**.
- (53) Toyota, S.; Kawai, K.; Iwanaga, T.; Wakamatsu, K. *Eur. J. Org. Chem.* **2012**, *2012* (29), 5679.
- (54) Fukazawa, A.; Oshima, H.; Shiota, Y.; Takahashi, S.; Yoshizawa, K.; Yamaguchi, S. *J. Am. Chem. Soc.* **2013**, *135* (5), 1731.
- (55) Debets, M. F.; Prins, J. S.; Merckx, D.; van Berkel, S. S.; van Delft, F. L.; van Hest, J. C. M.; Rutjes, F. P. J. T. *Organic & Biomolecular Chemistry* **2014**, *12* (27), 5031.
- (56) Debets, M. F.; van Berkel, S. S.; Dommerholt, J.; Dirks, A. T. J.; Rutjes, F. P. J. T.; van Delft, F. L. *Acc. Chem. Res.* **2011**, *44* (9), 805.
- (57) Xu, F.; Peng, L.; Shinohara, K.; Morita, T.; Yoshida, S.; Hosoya, T.; Orita, A.; Otera, J. *J. Org. Chem.* **2014**, *79* (23), 11592.
- (58) MEIER, H. *Synthesis* **1972**, *1972* (05), 235.
- (59) Orita, A.; Otera, J. *Chem. Rev.* **2006**, *106* (12), 5387.
- (60) Gleiter, R. *Angewandte Chemie International Edition in English* **1992**, *31* (1), 27.
- (61) Esser, B.; Rominger, F.; Gleiter, R. *J. Am. Chem. Soc.* **2008**, *130* (21), 6716.
- (62) Bodwell, G. J.; Nandaluru, P. R. *Isr. J. Chem.* **2012**, *52* (1-2), 105.
- (63) Tanner, D.; Wennerström, O.; Chattopadhyaya, J.; Carlberg, G. E.; Sterner, O.; Wickberg, B. *Acta Chemica Scandinavica* **1983**, *37b*, 693.
- (64) Montanari, M.; Bugana, A.; Sharma, A. K.; Pasini, D. *Organic & Biomolecular Chemistry* **2011**, *9* (14), 5018.
- (65) Dommerholt, J.; Rutjes, F. P. J. T.; van Delft, F. L. *Top Curr Chem (J)* **2016**, *374* (2), 16.
- (66) MacKenzie, D. A.; Sherratt, A. R.; Chigrinova, M.; Cheung, L. L. W.; Pezacki, J. P. *Curr Opin Chem Biol* **2014**, *21*, 81.
- (67) Krebs, A.; Wilke, J. In *Wittig Chemistry; Topics in Current Chemistry*; Springer Berlin Heidelberg: Berlin/Heidelberg, 1983; Vol. 109, pp 189–233.
- (68) Bräse, S.; Gil, C.; Knepper, K.; Zimmermann, V. *Angew. Chem. Int. Ed.* **2005**, *44* (33), 5188.
- (69) Blackman, M. L.; Royzen, M.; Fox, J. M. *J. Am. Chem. Soc.* **2008**, *130* (41), 13518.
- (70) Taylor, M. T.; Blackman, M. L.; Dmitrenko, O.; Fox, J. M. *J. Am. Chem. Soc.* **2011**, *133* (25), 9646.
- (71) Pennella, F.; Banks, R. L.; Bailey, G. C. *Chemical Communications (London)* **1968**, No. 23, 1548.
- (72) Sedbrook, D. F.; Paley, D. W.; Steigerwald, M. L.; Nuckolls, C.; Fischer, F. R. *Macromolecules* **2012**, *45* (12), 5040.

- (73) Paley, D. W.; Sedbrook, D. F.; Decatur, J.; Fischer, F. R.; Steigerwald, M. L.; Nuckolls, C. *Angew. Chem. Int. Ed. Engl.* **2013**, *52* (17), 4591.
- (74) Lysenko, S.; Haberlag, B.; Wu, X.; Tamm, M. *Macromolecular Symposia* **2010**, *293* (1), 20.
- (75) Novak, B. M.; Risse, W.; Grubbs, R. H. *The development of well-defined catalysts for ring-opening olefin metathesis polymerizations (ROMP)*; 1992.
- (76) Schrock, R. R. *Acc. Chem. Res.* **1990**, *23* (5), 158.
- (77) Scholl, M.; Ding, S.; Lee, C. W.; Grubbs, R. H. *Org. Lett.* **1999**, *1* (6), 953.
- (78) Bielawski, C. W.; Benitez, D.; Morita, T.; Grubbs, R. H. *Macromolecules* **2001**, *34* (25), 8610.
- (79) Sanford, M. S.; Love, J. A.; Grubbs, R. H. *Organometallics* **2001**, *20* (25), 5314.
- (80) Carnes, M.; Buccella, D.; Siegrist, T.; Steigerwald, M. L.; Nuckolls, C. *J. Am. Chem. Soc.* **2008**, *130* (43), 14078.
- (81) O'Reilly, M. E.; Ghiviriga, I.; Abboud, K. A.; Veige, A. S. *J. Am. Chem. Soc.* **2012**, *134* (27), 11185.
- (82) Manaa, H.; Henari, F. Z.; Al-Saie, A.; Drury, A.; Kobayashi, T.; Blau, W. J. *Journal of Applied Physics* **2003**, *93* (4), 1871.
- (83) Mohamed, Y. M. A.; Hansen, T. V. *Tetrahedron* **2013**, *69* (19), 3872.
- (84) Liu, T.; Zhao, K.; Liu, K.; Ding, L.; Yin, S.; Fang, Y. *J. Hazard. Mater.* **2013**, *246-247*, 52.
- (85) Martinelli, J. R.; Watson, D. A.; Freckmann, D. M. M.; Barder, T. E.; Buchwald, S. L. *J. Org. Chem.* **2008**, *73* (18), 7102.
- (86) Stone, M. T.; Moore, J. S. *Org. Lett.* **2004**, *6* (4), 469.
- (87) Segalman, R. A.; McCulloch, B.; Kirmayer, S.; Urban, J. J. *Macromolecules* **2009**, *42* (23), 9205.
- (88) Cram, D. J. *Angewandte Chemie International Edition in English* **1986**, *25* (12), 1039.
- (89) Horne, W. S.; Gellman, S. H. *Acc. Chem. Res.* **2008**, *41* (10), 1399.
- (90) Benito, J. M.; Gómez-García, M.; Jiménez Blanco, J. L.; Ortiz Mellet, C.; García Fernández, J. M. *J. Org. Chem.* **2001**, *66* (4), 1366.
- (91) Gunnlaugsson, T.; Glynn, M.; Tocci née Hussey, G. M.; Kruger, P. E.; Pfeffer, F. M. *Coordination Chemistry Reviews* **2006**, *250* (23-24), 3094.
- (92) Fitzmaurice, R. J.; Kyne, G. M.; Douheret, D.; Kilburn, J. D. *Journal of the Chemical Society, Perkin Transactions 1* **2002**, No. 7, 841.
- (93) Hamann, B. C.; Branda, N. R.; Rebek, J. *Tetrahedron Letters* **1993**, *34* (43), 6837.
- (94) Marcelli, T.; van der Haas, R. N. S.; van Maarseveen, J. H.; Hiemstra, H. *Angew. Chem. Int. Ed.* **2006**, *45* (6), 929.
- (95) Zhang, Z.; Schreiner, P. *Synthesis* **2007**, *2007* (16), 2559.
- (96) Athikomrattanakul, U.; Promptmas, C.; Katterle, M. *Tetrahedron Letters* **2009**, *50* (3), 359.
- (97) Fielding, L. *Tetrahedron* **2000**, *56* (34), 6151.
- (98) CRAM, D. J. *Science* **1988**, *240* (4853), 760.
- (99) Anslyn, E. V.; Dougherty, D. A. *Modern physical organic chemistry*; 2006.

- (100) Hirose, K. *Journal of Inclusion Phenomena and Macrocyclic Chemistry* **2001**, 39 (3-4), 193.
- (101) Lledó, A.; Rebek, J., Jr. *Chem. Commun.* **2010**, 46 (10), 1637.
- (102) Thordarson, P. *Chem. Soc. Rev.* **2011**, 40 (3), 1305.
- (103) Yang, J.-S.; Swager, T. M. *J. Am. Chem. Soc.* **1998**, 120 (46), 11864.
- (104) Narayanan, A.; Varnavski, O. P.; Swager, T. M.; Goodson, T. *The Journal of Physical Chemistry C* **2008**, 112 (4), 881.
- (105) Yang, J.-S.; Swager, T. M. *J. Am. Chem. Soc.* **1998**, 120 (21), 5321.
- (106) Bunz, U. H. F. *Chem. Rev.* **2000**, 100 (4), 1605.
- (107) Venkatramiah, N.; Kumar, S.; Patil, S. *Chem. Eur. J.* **2012**, 18 (46), 14745.
- (108) Feng, H.-T.; Wang, J.-H.; Zheng, Y.-S. *ACS Applied Materials & Interfaces* **2014**, 6 (22), 20067.
- (109) Mondal, P.; Rath, S. P. *European Journal of Inorganic Chemistry* **2015**, 2015 (29), 4956.
- (110) Ponnu, A.; Anslyn, E. V. *Supramolecular Chemistry* **2010**, 22 (1), 65.
- (111) Chaudhari, A. K.; Nagarkar, S. S.; Joarder, B.; Ghosh, S. K. *Crystal Growth & Design* **2013**, 13 (8), 3716.
- (112) Zhang, W.; Qiu, L.-G.; Yuan, Y.-P.; Xie, A.-J.; Shen, Y.-H.; Zhu, J.-F. *J. Hazard. Mater.* **2012**, 221-222, 147.
- (113) Che, Y.; Gross, D. E.; Huang, H.; Yang, D.; Yang, X.; Discekici, E.; Xue, Z.; Zhao, H.; Moore, J. S.; Zang, L. *J. Am. Chem. Soc.* **2012**, 134 (10), 4978.
- (114) Gopalakrishnan, D.; Dichtel, W. R. *J. Am. Chem. Soc.* **2013**, 135 (22), 8357.
- (115) Gopalakrishnan, D.; Dichtel, W. R. *Chem. Mater.* **2015**, 27 (11), 3813.
- (116) Wang, C.; Huang, H.; Bunes, B. R.; Wu, N.; Xu, M.; Yang, X.; Yu, L.; Zang, L. *Sci Rep* **2016**, 6, 25015.
- (117) Mosca, L.; Karimi Behzad, S.; Anzenbacher, P., Jr. *J. Am. Chem. Soc.* **2015**, 137 (25), 7967.
- (118) Takemoto, Y. *Organic & Biomolecular Chemistry* **2005**, 3 (24), 4299.
- (119) Zheng, W. R.; Xu, J. L.; Huang, T.; Yang, Q.; Chen, Z. C. *Res Chem Intermed* **2011**, 37 (1), 31.
- (120) Gunnlaugsson, T.; Davis, A. P.; O'Brien, J. E.; Glynn, M. *Organic & Biomolecular Chemistry* **2005**, 3 (1), 48.
- (121) Brooks, S. J.; Gale, P. A.; Light, M. E. *Chem. Commun.* **2005**, No. 37, 4696.
- (122) Kelly, T. R.; Kim, M. H. *J. Am. Chem. Soc.* **1994**, 116 (16), 7072.
- (123) Schiebl, P.; Schmidchen, F. P. *Tetrahedron Letters* **1993**, 34 (15), 2449.
- (124) Bregović, V. B.; Basarić, N.; Mlinarić-Majerski, K. *Coordination Chemistry Reviews* **2015**, 295, 80.
- (125) Duke, R. M.; Veale, E. B.; Pfeffer, F. M.; Kruger, P. E.; Gunnlaugsson, T. *Chem. Soc. Rev.* **2010**, 39 (10), 3936.
- (126) Lin, Z.-H.; Xie, L.-X.; Zhao, Y.-G.; Duan, C.-Y.; Qu, J.-P. *Organic & Biomolecular Chemistry* **2007**, 5 (21), 3535.
- (127) Lowe, A. J.; Pfeffer, F. M. *Chem. Commun.* **2008**, No. 16, 1871.
- (128) Fan, E.; Van Arman, S. A.; Kincaid, S. *J. Am. Chem. Soc.* **1993**, 115 (1), 369.

- (129) Meaney, M. S.; McGuffin, V. L. *Anal Bioanal Chem* **2008**, 391 (7), 2557.
- (130) Goodpaster, J. V.; McGuffin, V. L. *Anal. Chem.* **2001**, 73 (9), 2004.
- (131) Yuan, L.; Sanford, A. R.; Feng, W.; Zhang, A.; Zhu, J.; Zeng, H.; Yamato, K.; Li, M.; Ferguson, J. S.; Gong, B. *J. Org. Chem.* **2005**, 70 (26), 10660.
- (132) Prabhakaran, P.; Priya, G.; Sanjayan, G. J. *Angew. Chem. Int. Ed.* **2012**, 51 (17), 4006.
- (133) Juríček, M.; Felici, M.; Contreras-Carballada, P.; Lauko, J.; Bou, S. R.; Kouwer, P. H. J.; Brouwer, A. M.; Rowan, A. E. *J. Mater. Chem.* **2011**, 21 (7), 2104.
- (134) Constable, E. C.; Housecroft, C. E.; Neuburger, M.; Reymann, S.; Schaffner, S. *Eur. J. Org. Chem.* **2008**, 2008 (9), 1597.
- (135) Strunk, R. J.; Bell, A. R. US Patent Office 1992.
- (136) Kovalevsky, A. Y.; Shishkin, O. V.; Ponomarev, I. I. *Russian Chemical Bulletin* **1998**, 47 (6), 1122.
- (137) Ng, C.-F.; Chow, H.-F. *Chem. Commun.* **2015**, 51 (12), 2349.
- (138) Zeng, H.; Miller, R. S.; Flowers, R. A.; Gong, B. *J. Am. Chem. Soc.* **2000**, 122 (11), 2635.
- (139) Miyabe, H.; Tuchida, S.; Yamauchi, M.; Takemoto, Y. *Synthesis* **2006**, 2006 (19), 3295.